SYNTHESIS AND EVALUATION OF TRANSVALENCIN ANALOGUES AND ADENYLATION INHIBITORS AS ANTITUBERCULAR AGENTS AND CHEMICAL PROBES

A DISSERTATION
SUBMITTED TO THE FACULTY OF THE GRADUATE SCHOOL
OF THE UNIVERSITY OF MINNESOTA
BY

KATHRYN MARIE NELSON

IN PARTIAL FULFILLMENT OF THE REQUIREMENTS
FOR THE DEGREE OF
DOCTOR OF PHILOSOPHY

ADVISOR: DR. COURTNEY C. ALDRICH

JUNE, 2013

Acknowledgements

There are many people I would like to thank for their guidance and support throughout my career as a graduate student. First, I would like to thank my advisor, Dr. Courtney Aldrich. His enthusiasm and passion for research have been an unending source of encouragement for me, even when projects have gone awry. As his first PhD student, I am especially grateful that Courtney focused not only on my technical training but on developing my ability to lead and take complete ownership of my projects. I believe I am only the first of many PhD students who will be successful due to Courtney's mentorship. I hope I have helped him become a better advisor as well. I would also like to thank all the past and present members of the Aldrich research group. In particular, I would like to thank Curtis Engelhart, Dr. Ce Shi, Daniel Wilson, Dr. Kimberly Grimes, Dr. Anja Rubenstein, Dr. Benjamin Duckworth, and Dr. Kishore Viswanathan for their collaboration and camaraderie. Dr. Rohit Singh and Dr. Kristal Jackson are thanked for their time and advice during the preparation of this thesis. I would also like to thank other members of the department of medicinal chemistry for their support, including Amy Doan, Adam Benoit, Dr. Martin Phillips, and Dr. Aaron Teitelbaum.

I would like to thank Dr. Rory Remmel for both his collaboration and helpful advice throughout my classroom and laboratory training.

I would like to thank Dr. Robert Fecik and Dr. Mark Distefano for their advice and guidance.

I especially would like to thank my parents, Jeffrey and Virginia Michalski, and my brothers, Brian and David Michalski. Their unending support has helped make all of this work possible.

Most importantly, I would like to thank my husband, Nick. His support has been constant and selfless. His council through both frustration and success kept me focused on my ultimate goals, which could not have been achieved without him.

Dedication

This dissertation is dedicated to my grandmothers, Loretta Kosel and Fern Michalski, who taught me there is no goal you can set that you cannot achieve.

To my parents, Jeffrey and Virginia Michalski, who gave me the passion and ambition to pursue my goals.

And to my husband, Nick, for achieving those goals with me.

Abstract

Mycobacterium tuberculosis (*Mtb*), the etiological agent of pulmonary tuberculosis, is the leading cause of death due to infectious disease worldwide. Due to a lack of new drug development, poor fidelity, and repeated exposure to currently available therapeutics, *Mtb* has become multidrug resistant, extensively drug resistant, and even totally drug resistant in some patients. With nearly 9 million deaths and 1.4 million new cases reported by the World Health Organization (WHO) in 2011, new therapies that act via novel mechanisms of action are desperately needed to fight this global health threat.

Herein we describe our efforts to develop new antitubercular agents by attacking the bacteria's need for iron. This approach involves the inhibition of the biosynthetic pathway to produce siderophores, small molecule iron chelators responsible for acquiring iron in limiting conditions, such as those in a human host. A prototypical inhibitor of the initiating enzyme in this pathway, MbtA, had been previously developed by our lab, and was used to develop a small set of analogues for *in vivo* evaluation. We employed Sprague-Dawley rats to evaluate the oral bioavailability of our compounds, revealing that the pK_a of the linker nitrogen of the scaffold had a large effect on compound permeability.

In addition, we studied the mechanism of action of our parent inhibitor, Sal-AMS, through the development of a photoaffinity probe to label and pull down proteins for target identification. A probe containing a benzophenone moiety for photo-crosslinking and a small alkyne handle for attachment of an imaging or enrichment tag was synthesized. This probe was successful in identifying the intended enzyme of interest

(MbtA) as a binding partner, but did not yield any additional hits, suggesting Sal-AMS is a highly specific inhibitor.

Studies were also done on the natural product transvalencin Z that had been reported as selective against mycobacteria. This compound was very similar in structure to the mycobactin siderophores from *Mtb*. The 4 possible diastereomers of the reported structure were synthesized in an attempt to elucidate the absolute stereochemistry of the natural product, however, spectroscopic data obtained did not match with the literature report. The activity of the diastereomers was tested against a panel of 14 pathogens, but our results were observed in stark contrast to those reported by the discovery group.

Finally, we aided a collaborator in the development and synthesis of a probe against DhbE in *Bacillus subtilis*. Dr. Jun Yin of the University of Chicago was studying the substrate specificity of adenylation domains, and chose an enzyme highly homologous to our target MbtA. We designed a probe that incorporated a similar inhibitor, DHB-AMS, and a long flexible linker with a biotin attached for Dr. Yin's unique yeast cell display assay. Dr. Yin was able to utilize these probes to successfully identify mutant adenylation enzymes with altered specificity towards nonnative substrates. This technique is an exciting new way to potentially access analogues of natural products through manipulation of the biosynthetic machinery, instead of through often cumbersome organic chemistry.

These studies have continued to advance our understanding of a new mechanism of action against *Mtb*, and have brought us one step closer to a preclinical candidate.

Table of Contents

Acknowledgements i

Dedication ii

Abstract iii

Table of Contents v

List of Tables xv

List of Figures and Schemes xvi

Preface xx

Chapter 1: Challenges in Tuberculosis Drug Discovery 1

1.1 Introduction 1

1.2 Challenge 1: Heterogeneity in tuberculosis pathology 11

1.3 Challenge 2: Target validation and vulnerability 15

1.4 Challenge 3: Lead compound and inhibitor design 19

1.5 Challenge 4: Mechanisms of action 27

1.6 Challenge 5: Modeling activity against *Mycobacterium tuberculosis* 37

1.7 Challenge 6: Monetary challenge 41

1.8 Conclusions 43

1.9 References 44

Chapter 2: Synthesis of Adenylation Inhibitors as Antitubercular Agents and Evaluation of Their Oral Bioavailability in a Rodent Model 56

2.1 Introduction 56

2.1.1 Siderophore inhibitors as antitubercular agents 56

2.1.2 Initial evaluation of lead compound Sal-AMS 60

2.2 Research Objectives 66

2.3 Results 67

2.3.1 Synthesis of Sal-AMS (**2-1**) and sulfamide linked analogue (**2-6**) 67

2.3.2 Synthesis of 5′-Amino-5′-deoxy-5′-*N*-[(4-amino-2-hydroxybenzoyl)sulfamoyl]-adenosine (**2-34**) 70

2.3.3 Synthesis of 5′-Amino-N^6-cyclopropyl-5′-deoxy-5′-*N*-[*N*-(2-hydroxybenzoyl)sulfamoyl]adenosine (**2-41**) 71

2.3.4 Synthesis of 2-Phenyl-N^6-cyclopropyl-5′-*O*-[*N*-(2-hydroxyl)sulfamoyl]adenosine (**2-50**) 73

2.3.5 Synthesis of acetate prodrugs of Sal-AMS (**2-51** and **2-52**) 74

2.3.6 Oral bioavailability of siderophore biosynthesis inhibitors 76

2.4 Discussion 91

2.4.1 Strategies for increasing oral bioavailability 91

2.4.2 Anomalous high oral bioavailability of compound **2-50** 92

2.4.3 Prodrugs of nucleosides 94

2.4.4 Trends in oral bioavailability for siderophore inhibitors 96

2.5 Conclusions 96

2.6 Experimental details 97

2.6.1 General procedures for the synthesis of siderophore biosynthesis inhibitors 97

2.6.2 Synthesis of N^6,N^6-bis(*tert*-Butoxycarbonyl)-2′,3′-*O*-isopropylidene-5′-*O*-(sulfamoyl)adenosine (**2-25**) 99

2.6.3 Synthesis of N^6,N^6-bis(*tert*-Butoxycarbonyl)-2′,3′-*O*-isopropylidene-5′-*O*-{*N*-[2-(methoxymethoxy)benzoyl]sulfamoyl}adenosine triethylammonium salt (**2-27**) 99

2.6.4 Synthesis of N^6,N^6-bis(*tert*-Butoxycarbonyl)-5′-{*N*-[(*tert*-butoxycarbonyl)sulfamoyl]amino}-5′-deoxy-2′, 3′-*O*-isopropylideneadenosine (**2-29**) 100

2.6.5 Synthesis of N^6,N^6-bis(*tert*-Butoxycarbonyl)-5′-(*N*-*tert*-butoxycarbonyl-*N*-{[(2-methoxymethoxy)benzoyl]sulfamoyl})amino-5′-deoxy-2′,3′-*O*-isopropylideneadenosine triethylammonium salt (**2-30**) 101

2.6.6 Synthesis of N^6,N^6-bis(*tert*-Butoxycarbonyl)-5′-(*N*-*tert*-butoxycarbonyl-*N*-{*N*-[(4-benzyloxycarboxyamino-2-hydroxy)benzoyl]sulfamoyl})amino-5′-deoxy-2′,3′-*O*-isopropylideneadenosine triethylammonium salt (**2-33**) 102

2.6.7 Synthesis of Synthesis of 5′-Deoxy-5′-({*N*-[(2-hydroxy-4-amino)benzoyl]sulfamoyl}amino)adenosine (**2-34**) 103

2.6.8 Synthesis of 5′-Amino-N^6-cyclopropyl-5′-deoxy-2′,3′-*O*-isopropylideneadenosine (**2-37**) 104

2.6.9 Synthesis of N^6-Cyclopropyl-5′-deoxy-2′,3′-*O*-isopropylidene-5′-[(sulfamoyl)amino]adenosine (**2-39**) 105

2.6.10 Synthesis of N^6-Cyclopropyl-5′-deoxy-2′,3′-*O*-isopropylidene-5′-({*N*-[(2-methoxymethoxy)benzoyl]sulfamoyl}amino)adenosine triethylammonium salt (**2-40**) 106

2.6.11 Synthesis of 5′-*N*-[*N*-(2-Hydroxybenzoyl)sulfamoylamino]-N^6-cyclopropyl-5′-deoxyadenosine triethylammonium salt (**2-41**) 107

2.6.12 Synthesis of N^6-Cyclopropyl-2′,3′-*O*-isopropylidene-2-phenyl-5′-*O*-(sulfamoyl)adenosine (**2-48**) 108

2.6.13 Synthesis of 2′,3′-*O*-Di-acetyl-5′-*O*-{*N*-[(2-acetyloxy)benzoyl]sulfamoyl}adenosine triethylammonium salt (**2-51**) 108

2.6.14 Synthesis of 5′-*O*-[*N*-(2-Benzyloxybenzoyl)sulfamoyl]-N^6, N^6-bis(*tert*-butoxycarbonyl)-2′, 3′-*O*-isopropylideneadenosine triethylammonium salt (**2-54**) 109

2.6.15 Synthesis of 2′,3′-*O*-Di-acetyl-5′-*O*-[*N*-(2-hydroxybenzoyl)sulfamoyl]adenosine triethylammonium salt (**2-52**) 110

2.6.16 Procedures for the measurement of oral bioavailability of siderophore inhibitors in Sprague-Dawley rats 112

2.6.17 Procedure for the measurement of stability of prodrugs **2-51** and **2-52** in simulated gastric fluid (SGF) 117

2.7 References 118

Chapter 3: A Light-Activated Probe for the Study of Adenylation Domains in *Mycobacterium tuberculosis* 123

3.1 Introduction 123

3.1.1 Chemical probes for investigation of target enzymes 123

3.1.2 Investigating a secondary target of Sal-AMS (**3-1**) in *Mtb* 126

3.1.3 Design of a clickable photoaffinity probe for the study of MbtA 128

3.2 Research Objectives 131

3.3 Results 132

3.3.1 Synthesis of a clickable photoaffinity probe for the study of MbtA 132

3.3.2 Control experiments with photoaffinity probe **3-2** and recombinant MbtA 135

3.3.3 Photoaffinity probe **3-2** labeling MbtA from cell lysates in expression and native systems 138

3.4 Discussion 145

3.5 Conclusions 147

3.6 Experimental Data 148

3.6.1 General procedures for the synthesis of a photoaffinity probe against MbtA 148

3.6.2 Synthesis of 5-(Triisopropylsilyl)pent-4-ynoic acid (**3-3**) 149

3.6.3 Synthesis of *N*-[4-(4-Aminobenzoyl)phenyl]-5-(triisopropylsilyl)pent-4-ynamide (**3-6**) 149

3.6.4 Synthesis of 2′,3′-*O*-Isopropylidene-2-{*N*-[4-(4-{*N*-[5-(triisopropylsilyl)pent-4-ynoyl]amino}benzoyl)phenyl]amino}adenosine (**3-8**) 150

3.6.5 Synthesis of 2′,3′-*O*-Isopropylidene-2-[*N*-(4-{4-[*N*-(pent-4-ynoyl)amino]benzoyl}phenyl)amino]adenosine (**3-9**) 151

3.6.6 Synthesis of 2′,3′-*O*-Isopropylidene-2-[*N*-(4-{4-[*N*-(pent-4-ynoyl)amino]benzoyl}phenyl)amino]-5′-*O*-(sulfamoyl)adenosine (**3-10**) 152

3.6.7 Synthesis of 5′-*O*-[*N*-(2-Hydroxybenzoyl)sulfamoyl]-2-[*N*-(4-{4-[*N*-(pent-4-ynoyl)amino]benzoyl}phenyl)amino]adenosine triethylammonium salt (**3-2**) 153

3.7 References 154

Chapter 4: Total Synthesis and Biological Evaluation of Four Diastereomers of the Natural Product Transvalencin Z 158

4.1 Introduction 158

4.2 Research Objectives 163

4.3 Results 164

4.3.1 Synthesis of transvalencin Z diastereomers 164

4.3.2 Biological evaluation of transvalencin Z diastereomers 170

4.3.3 Characterization of transvalencin Z diastereomers 171

4.4 Discussion 174

4.5 Conclusions 175

4.6 Experimental Data 176

4.6.1 General procedures for the synthesis of transvalencin Z diastereomers 176

4.6.2 General procedures for microbiological evaluation of transvalencin Z diastereomers 177

4.6.3 General procedures for mammalian cell toxicity measurements 179

4.6.4 Synthesis of 2-(Benzyloxy)benzoic acid (**4-10**) and *N*-[2-(Benzyloxy)benzoyl]-L/D-serine benzyl esters (**4-12a** and **4-12b**) 180

4.6.5 Synthesis of (4*S*) and (4*R*)-Benzyl-2-[2-(benzyloxy)phenyl]-Δ^2-1,3-oxazoline-4-carboxylate (**4-13a** and **4-13b**) 180

4.6.6 Synthesis of (4*S*) and (4*R*)-2-[2-Hydroxyphenyl]-Δ^2-1,3-oxazoline-4-carboxylic acid (**4-5a** and **4-5b**) 181

4.6.7 Synthesis of (2*S*) and (2*R*)-({[(9H-Fluoren-9-yl)methyloxy]carbonyl}amino)-6-formamidohexanoic acid (**4-16a** and **4-16b**) 182

4.6.8 Synthesis of (2*S*) and (2*R*)-Benzyl-2-({[(9H-fluoren-9-yl)methyloxy]carbonyl}amino)-6-formamidohexanoate (**4-17a** and **4-17b**) 182

4.6.9 Synthesis of (2*S*) and (2*R*)-Benzyl-2-amino-6-formamidohexanoate (**4-6a** and **4-6b**) 183

4.6.10 Synthesis of (2*S*, 9*S*) and (2*R*, 9*R*)-Benzyl-6-formamido-2-[(2-hydroxyphenyl)-Δ^2-1,3-oxazoline-4-carboxamido]hexanoate (**4-18a** and **4-18b**) 184

4.6.11 Synthesis of (2*S*, 9*R*) and (2*R*, 9*S*)-Benzyl-6-formamido-2-[(2-

hydroxyphenyl)-Δ^2-1,3-oxazoline-4-carboxamido]hexanoate (**4-18c** and **4-18d**) 185

4.6.12 Synthesis of (2*S*, 9*S*) and (2*R*, 9*R*)-6-Formamido-2-[(2-hydroxyphenyl)-Δ^2-1,3-oxazoline-4-carboxamido]hexanoic acid (**4-4a** and **4-4b**) 186

4.6.13 Synthesis of (2*S*, 9*R*) and (2*R*, 9*S*)-6-Formamido-2-[(2-hydroxyphenyl)-Δ^2-1,3-oxazoline-4-carboxamido]hexanoic acid (**4-4c** and **4-4d**) 187

4.7 References 188

Chapter 5: Biotinylated Probes for the Study of Adenylation Domains in *Bacillus subtilis* 192

5.1 Introduction 192

5.1.1 Nonribosomal peptide synthetases (NRPS) 193

5.1.2 Adenylation domains 194

5.1.3 Analogues of natural products through native synthetases 195

5.1.4 DhbE as a model system 196

5.2 Research Objectives 197

5.3 Results 198

5.3.1 Synthesis of chemical probes for the study of DhbE 198

5.3.2 Construction of an adenylation domain library of DhbE displayed on yeast cells 202

5.3.3 Identification of DhbE mutants with altered specificity for 3-HBA and 2-

ABA 204

5.4 Discussion 206

5.5 Conclusions 208

5.6 Experimental Data 209

5.6.1 General procedures for the synthesis of biotinylated probes against DhbE 209

5.6.2 Synthesis of *N*-Hydroxysuccinimidyl 3-(methoxymethyloxy)benzoate (**5-12**) 210

5.6.3 Synthesis of 2-[3-(2-{2-[2-(*tert*-Butoxycarbonylamino)ethoxy]ethoxy}ethoxy)prop-1-ynyl]-2′,3′-*O*-isopropylidene-5′-*O*-{*N*-[3-(methoxymethoxy)benzoyl]sulfamoyl}adenosine (**5-13**) 211

5.6.4 Synthesis of 2-[3-(2-{2-[2-({dPEG®$_4$-biotinyl}amino)ethoxy]ethoxy}ethoxy)prop-1-ynyl]-5′-*O*-{*N*-[3-(hydroxy)benzoyl]sulfamoyl}adenosine triethylammonium salt (**5-2**) 212

5.6.5 Synthesis of 2-[3-(2-{2-[2-(*tert*-Butoxycarbonylamino)ethoxy]ethoxy}ethoxy)prop-1-ynyl]-2′,3′-*O*-isopropylidene-5′-*O*-{*N*-[2-(amino)benzoyl]sulfamoyl}adenosine triethylammonium salt (**5-15**) 213

5.6.6 Synthesis of 2-[3-(2-{2-[2-({dPEG®$_4$-biotinyl}amino)ethoxy]ethoxy}ethoxy)prop-1-ynyl]-5′-*O*-{*N*-[2-(amino)benzoyl]sulfamoyl}adenosine triethylammonium salt (**5-3**) 214

5.7 References 215

Chapter 6: Conclusions and Future Directions 218

Chapter 7: Bibliography 223

List of Tables

Table 2.1: Properties of Sal-AMS 60

Table 2.2: Enzymatic activity of siderophore inhibitors against MbtA 76

Table 2.3: Bioavailability of INH and MbtA inhibitors in Sprague-Dawley rats 78

Table 3.1: Inhibition of MbtA and *Mtb* by Sal-AMS and a photoaffinity probe 136

Table 3.2: LC–MS/MS identification of proteins labeled by photoaffinity probe **3-2** 141

Table 4.1: MIC data for isolated transvalencin Z and synthetic diastereomers 171

Table 4.2: ^{1}H and ^{13}C NMR data for transvalencin Z and synthetic diastereomers 173

Table 5.1: Alignment of DhbE mutants selected with probes **5-2** and **5-3** by yeast cell surface display. 205

Table 5.2: Pyrophosphate (PPi) release rate of the aryl acid adenylation reaction catalyzed by wtDhbE and mutants 206

List of Figures and Schemes

Figure 1.1: First line antibiotics against *Mycobacterium tuberculosis* 4

Figure 1.2: INH activation by KatG 5

Figure 1.3: Activation of PZA to POA 8

Figure 1.4: Structure of bedaquiline 8

Figure 1.5: Life cycle of *Mtb* 12

Figure 1.6: Spectrum of pulmonary tubercular infections 13

Figure 1.7: Estimated timeline for development of new *Mtb* therapeutics 20

Figure 1.8: General steps to fragment-based drug design 24

Figure 1.9: Internal hydroxyl radical formation via the Fenton reaction 28

Figure 1.10: Bioactivation of ETA 33

Figure 1.11: Structures of investigational compounds PA-824 and BTZ038 35

Figure 1.12: Hollow fiber infection model 41

Figure 2.1: Structure of mycobactins and carboxymycobactins from *Mtb* 57

Figure 2.2: Role of MbtA in mycobactin biosynthesis 58

Figure 2.3: Design of prototypical inhibitor Sal-AMS 59

Figure 2.4: SAR domains for the study of Sal-AMS 62

Figure 2.5: Summary of SAR results from previous work 64

Figure 2.6: Sal-AMS analogue design to improve pharmacokinetic properties 66

Figure 2.7: Concentration-time profiles for dosing of INH 79

Figure 2.8: Concentration-time profiles for dosing of Sal-AMS 80

Figure 2.9: Concentration-time profiles for dosing of compound **2-6** 81

Figure 2.10: Concentration-time profiles for dosing of compound **2-34** 82

Figure 2.11: Concentration-time profiles for dosing of compound **2-41** 83

Figure 2.12: Concentration-time profiles for dosing of compound **2-50** (N=2) 84

Figure 2.13: Concentration-time profiles for oral dosing of compound **2-50** (N=1) 85

Figure 2.14: Concentration-time profiles for dosing of prodrug **2-51** 86

Figure 2.15: Stability of prodrug **2-51** in pooled rat plasma 87

Figure 2.16: Stability of prodrug **2-51** in simulated gastric fluid (SGF) 88

Figure 2.17: Concentration-time profiles for dosing of prodrug **2-52** 89

Figure 2.18: Stability of prodrug **2-52** in pooled rat plasma 90

Figure 2.19: Stability of prodrug **2-52** in simulated gastric fluid (SGF) 91

Figure 3.1: Design of chemical probes 125

Figure 3.2: Design of prototypical inhibitor Sal-AMS 127

Figure 3.3: Design of a photoaffinity probe based on Sal-AMS 129

Figure 3.4: Design of a photoaffinity probe pulldown experiment 131

Figure 3.5: *In vitro* labeling of MbtA using probe **3-2** 137

Figure 3.6: Dose-response of Sal-AMS competition with probe **3-2** 138

Figure 3.7: Photoaffinity probe labeling of adenylating enzymes in crude cell lysates 139

Figure 3.8: Proposed pathways for iron uptake by *Mtb* 146

Figure 4.1: Natural products and derivatives as antitubercular agents 160

Figure 4.2: Reported structure of transvalencin Z 161

Figure 4.3: Structural differences between Mycobactin S and T 162

Figure 4.4: HPLC trace of epimerized product from EDC coupling of **4-5a** and **4-6a** 168

Figure 4.5: HPLC stack plot of synthetic transvalencins **4-4a–d** 172

Figure 5.1: The NRPS pathway for synthesis of bacillibactin in *Bacillus subtilis* 194

Figure 5.2: Chemical probes **5-1**, **5-2**, and **5-3** targeted against DhbE 198

Figure 5.3: Yeast cell display 203

Figure 5.4: Co-crystal structure of wtDhbE and DHB-AMP 204

Scheme 2.1: Synthesis of Sal-AMS (**2-1**) 68

Scheme 2.2: Synthesis of a sulfamide linked analogue of Sal-AMS (**2-6**) 70

Scheme 2.3 Synthesis of Sal-AMS analogue **2-34** 71

Scheme 2.4: Synthesis of Sal-AMS analogue **2-41** 72

Scheme 2.5: Synthesis of Sal-AMS analogue **2-50** 73

Scheme 2.6: Synthesis of a tri-acetate prodrug of Sal-AMS 75

Scheme 2.7: Synthesis of a di-acetate prodrug of Sal-AMS 76

Scheme 3.1: Improved coupling conditions for step 1 of the synthesis of a photoaffinity probe **3-2** 133

Scheme 3.2: First steps in an improved synthesis of a photoaffinity probe **3-2** 134

Scheme 3.3: Completed improved synthesis of a photoaffinity probe **3-2** 135

Scheme 4.1: Retrosynthetic analysis of transvalencin Z 164

Scheme 4.2: Synthesis of oxazoline building blocks for transvalencin Z 165

Scheme 4.3: Mechanism for dehydrative cyclization using Burgess' reagent 166

Scheme 4.4: Proposed mechanism for molybdenum catalyzed cyclization 167

Scheme 4.5: Synthesis of lysine building blocks for transvalencin Z 168

Scheme 4.6: Penultimate DEPBT coupling for transvalencin Z 169

Scheme 5.1: Synthesis of DhbE probe **5-1** 199

Scheme 5.2: Synthesis of building block **5-12** for synthesis of DhbE probe **5-2** 200

Scheme 5.3: Synthesis of 3-hydroxybenzoic acid (3-HBA) probe **5-2** 201

Scheme 5.4: Synthesis of 2-aminobenzoic acid (2-ABA) probe **5-3** 202

Preface

Please note the following:

Chapter 1: Reproduced in part with permission from Nelson, K. M., Aldrich, C. C. Challenges in Tuberculosis Drug Discovery. Manuscript in progress for submission to *J. Med. Chem.* Please see supplementary page for full citation.

Chapter 3: Reproduced in part with permission from Duckworth, B. P., Wilson, D. J., Nelson, K. M., Boshoff, H. I., Barry, C. E. 3rd, Aldrich, C. C. Development of a Selective Activity-Based Probe for Adenylating Enzymes: Profiling MbtA Involved in Siderophore Biosynthesis from *Mycobacterium tuberculosis*. *ACS Chem. Biol.* **2012**, *7*, 1653–1658. © 2012 American Chemical Society

Chapter 4: Reproduced in part with permission from Nelson, K. M., Salomon, C. E., and Aldrich, C. C. Total Synthesis and Biological Evaluation of Transvalencin Z. *J. Nat. Prod.* **2012**, *75*, 1037–1043. © 2012 American Chemical Society

Chapter 5: Reprinted in part from *Chemistry and Biology*, *20*, Zhang, K.; Nelson, K. M.; Bhuripanyo, K.; Grimes, K. D.; Zhao, B.; Aldrich, C. C.; Yin, J. Engineering the Substrate Specificity of the DhbE Adenylation Domain by Yeast Cell Surface Display, 92–101, **2013**, with permission from Elsevier

Chapter 1. Challenges in Tuberculosis Drug Development

The following chapter is an original review by Kathryn M. Nelson regarding the challenges in tuberculosis drug development. Figure 1.5 is reproduced from *Science* with permission (see caption).

1.1 Introduction

The development of antibiotics in the middle of the twentieth century revolutionized the way we treat bacterial infections. The boom of antibiotic drug discovery and development began with the discovery of penicillin and sulphonamides during the 1920s and 1930s. Intense decades of research followed which produced many new drug classes and derivatives through the 1970s: aminoglycosides (1944), tetracyclines (1945), cephalosporins (1948), macrolides (1949), glycopeptides (1956), quinolones (1961), and carbapenems (1976), among others. These agents have become a standard part of our medical regimen both for the treatment and prevention of infection that has increased our global health and life expectancy over the past five generations.[1] Since the 1980s however, there has been a stark decline in the output of new antibacterial compounds, and an even bigger drop in the introduction of new chemical classes or compounds acting through novel mechanisms of action.[2] This narrowing of the antibacterial pipeline plus the continuing rise in bacterial drug resistance has led to a critical need for new drugs.[1,3,4] While multidrug-resistant (MDR) bacteria were previously limited to secondary

infections in healthcare institutions, these pathogens are more frequently being found in community environments.[4,5] The list of especially concerning pathogens continues to grow, with outbreaks of highly drug resistant pathogens continuing to emerge among not only the ESKAPE pathogens (*Enterococcus faecium*, *Staphylococcus aureus*, *Klebsiella pneumoniae*, *Acinetobacter baumannii*, *Pseudomonas aeruginosa*, and *Enterobacter* species), but also *Escherichia coli*, *Salmonella* (in cases of typhoid fever), *Clostridium difficile*, *Neisseria gonorrhea*, and *Mycobacterium tuberculosis* (*Mtb*).[4] Methicillin-resistant *Staphylococcus aureus* (MRSA) infections are especially illustrative of the high health and financial burden that this increase of drug resistance plays on our economy. MRSA is estimated to cause approximately 19,000 deaths and upwards of $9.7 billion in additional healthcare costs per year in the United States alone.[5,6] Alarming as these numbers are, no other infection presents a greater global health threat than the rise of multidrug-resistant and extensively drug-resistant tuberculosis (MDR-TB and XDR-TB).

Tuberculosis (TB), caused by the acid-fast bacillus *Mycobacterium tuberculosis* (*Mtb*), is the leading cause of infectious disease mortality worldwide due to a bacterial pathogen.[7–9] According to the World Health Organization (WHO), there were 1.4 million deaths attributed to TB, and 8.7 million new cases reported in 2011.[7] *Mtb* is readily transmitted by aerosolized droplets from the coughing or sneezing of an actively infected individual. Innate and adaptive immune responses often physically contain the infection, causing *Mtb* to switch to a nearly non-replicative state that is considered noninfectious. Roughly one-third of the world's population is estimated to be infected with this quiescent form of *Mtb*, which can be triggered to an active infection through stress on the immune system,

malnutrition, or other dietary factors. Even more alarming, co-infection of TB and HIV/AIDS is now responsible for the majority of HIV-related deaths.[7] The ease of bacterial transmission, slow growth of the pathogen during infection, its ability to survive in a latent state, and its unique and highly lipophilic cell wall have all limited the usefulness of many otherwise broad spectrum antibiotics. The current recommended drug therapy is known as DOTS (directly observed therapy short-course), and requires 6–9 months of drug treatment involving a drug cocktail of four first-line antitubercular agents, namely isoniazid, rifampin, ethambutol, and pyrazinamide. This extended period of chemotherapy increases the chances for non-compliance to therapy, greatly contributing to the rise of MDR and XDR-TB. Most recently, reports of totally drug-resistant TB (TDR-TB) have been recorded where strains were unresponsive to all the currently approved therapeutics.[10,11] MDR-TB is any strain that shows resistance to isoniazid and rifampin, the two most powerful of the four first-line agents. XDR-TB strains are resistant to isoniazid, rifampin, at least one fluoroquinoline, and at least one of three injectable second-line agents (capreomycin, amikacin, or streptomycin).[12] In 2012, 84 countries had reported cases of XDR-TB, with approximately 9% of MDR-TB cases actually proving to be XDR.[7] The emergence of these highly drug-resistant strains, coupled with the severe shortage in new antitubercular agents over the past four decades, provides clear motivation for the development of new TB drugs with shortened periods of treatment that are effective against drug-resistant strains, preferably active through novel mechanisms of action.

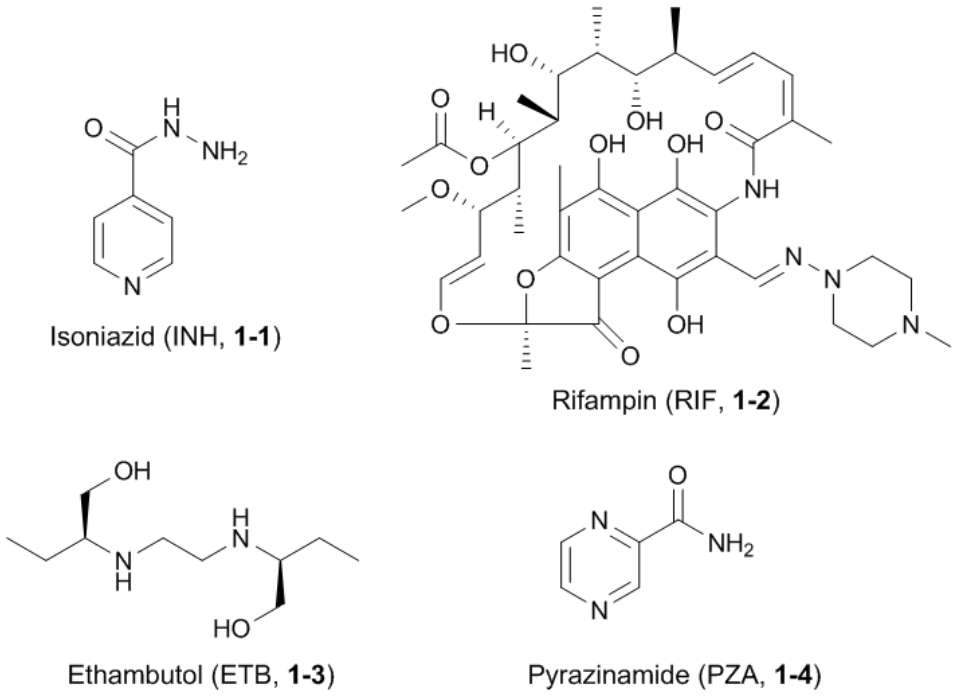

Figure 1.1. First line antibiotics against *Mycobacterium tuberculosis.*

The first line of anti-TB agents includes isoniazid (INH, **1-1**), rifampin (RIF, **1-2**), ethambutol (ETB, **1-3**), and pyrazinamide (PZA, **1-4**) (**Figure 1.1**).[13] First reported as an anti-TB agent in 1952, INH is still one of the most potent anti-TB compounds in use today.[14] Isoniazid is bactericidal for rapidly growing *Mtb*, but is bacteriostatic for nonreplicating bacilli with a minimum inhibitory concentration (MIC) of 0.025–0.050 μg/mL. INH activity requires bioactivation by KatG, a catalase/peroxidase, to give an isonicotinoyl radical (**1-5**) that reacts nonenzymatically with cellular pyridine nucleotides to give INH-NAD adducts (**1-6**, **Figure 1.2**).[15,16] The INH-NAD adducts are slow, tight-binding, reversible inhibitors of InhA, an NADH-dependent enoyl-acyl carrier protein (enoyl-ACP) reductase that ultimately block mycolic acid synthesis, a necessary process for *Mtb* cell wall biosynthesis.[17] Resistance to INH is conferred through selection of

bacilli with spontaneous mutations to the genes *katG* or *inhA*.[18] While INH is usually well tolerated for a long period of treatment, it does show inhibition of several cytochrome P450s, the most clinically relevant being CYP2C19 and CYP3A4.[19] Because of this activity, INH can slow the elimination of co-administered drugs such as the HIV type 1 protease inhibitors, making this therapy more dangerous for co-infected HIV/AIDS patients.[20]

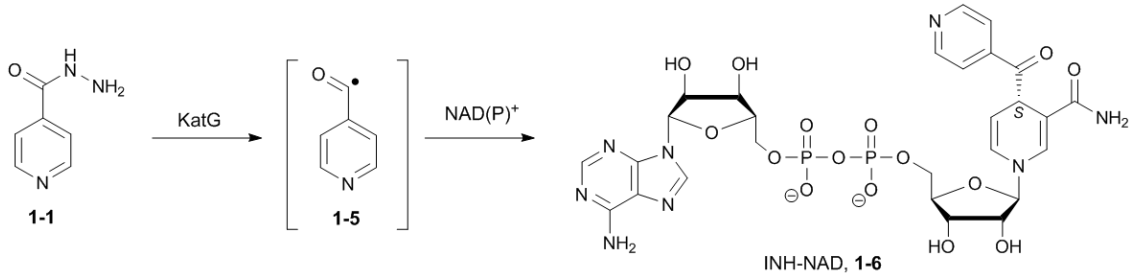

Figure 1.2. INH activation by KatG to the bioactive form INH-NAD.

Rifampin (**1-2**, **Figure 1.1**), was first reported in 1959, approved for use as an anti-TB agent in Italy in 1968, and received FDA approval in 1971.[21,22] It is produced semi-synthetically in 5 steps from the natural product rifamycin B, and shows bactericidal activity against *Mtb* with an MIC of 0.03–0.125 μg/mL.[23,24] The mechanism of action for RIF-mediated bacterial killing is through inhibition of bacterial DNA-dependent RNA polymerase (RNAP), thereby preventing the necessary RNA transcription process. In binding to one of the β-subunits of RNAP, RIF blocks the growing RNA transcript as it is extruded out of the active site, leading to premature transcript truncation.[25,26] Resistance to RIF occurs through random point mutations or short insertions/deletions to the RNAP β-subunit gene (*rpoB*), lowering the affinity for the drug.[27] While RIF is generally well tolerated in most patients, it can have drastic effects on HIV protease inhibitor levels via

inhibition of drug-metabolizine enzymes, especially CYP3A4. The antiretroviral level of protease inhibitors are reduced by greater than 90%, limiting the usefulness for this drug in HIV/AIDS patients.[28,29] Consequently, rifabutin, a less potent pregnane-X-receptor (PXR) activator is recommened for patients on antiretroviral therapy.

Ethambutol (**1-3**, **Figure 1.1**) was synthesized and first described in 1961 as a moderately active anti-TB compound.[30] With a bacteriostatic MIC of less than 2 μM, the benefit of EMB is its low toxicity and highly favorable synergy with other first-line agents.[31,32] The synergistic properties of EMB are readily understood through its mechanism of action. Ethambutol inhibits arabinogalactan biosynthesis, an integral part of the mycobacterial cell wall, which enhances the membrane permeability of other drugs.[33] Monoresistance to EMB is rarely seen, with resistance usually only occurring in MDR-TB strains. About 70% of these resistant strains show a mutation in the glycosyltransferase *embB*, which suggests this to be the primary cellular target.[34] Since monoresistance is so rarely seen, some have suggested using mutations in the *embB* gene as biomarkers of MDR- and XDR-TB.[35] Ethambutol is generally well tolerated and the main side effect is ocular toxicity causing reduced visual acuity, constriction of visual fields, and color blindness. All of these effects are usually reversible if the therapy is discontinued, and intermittent visual testing is highly recommended while on EMB therapy.[36]

Finally, pyrazinamide (**1-4**, **Figures 1.1** and **1.3**) is a largely bacteriostatic agent whose antitubercular activity was first described in 1952.[37,38] Still the most mysterious of the first-line agents against TB, PZA is only active *in vivo* under acidic conditions, with a reported MIC of 16–50 μg/mL at pH 5.5.[39] The acidic environment in macrophages

allows PZA to inhibit non-replicating *Mtb* during active inflammation, which is only observed during initial infection (dosed only in the first 2 months of therapy). The currently accepted mechanism of action for PZA suggests that it is passively uptaken by *Mtb*, then hydrolyzed by a promiscuous amidase (PncA) to release pyrazinoic acid (POA, **1-7**) (**Figure 1.3**).[40]

Accumulation of POA lowers the intracellular pH and disrupts the transmembrane proton gradient and consequently the proton motive force required for the biosynthesis of ATP.[41] This nonspecific mode of action for PZA is supported by the inability to isolate any mutant strains resistant to POA, only to PZA. Mutants that are resistant to PZA show mutations almost exclusively in *pncA*, a cytosolic metalloenzyme.[42] Recently, additional evidence for action of POA against the ribosomala protein S1 (RpsA) has been reported by Shi and co-workers.[43] Their study identified RpsA as a binding partner of POA, and identified clinical isolates of resistant bacteria that contain mutations to the gene for RpsA expression. Their work suggests that POA inhibits the bacteria's ability to manage stalled ribosomes under stressful conditions such as acidic pH, starvation, and hypoxia– all of which are hallmarks of initial *Mtb* infection.[43] Ultimately, mutation to pncA would also eliminate the ability of PZA to act via this mechanism of action also, and seems to be more common for conferring resistance. Pyrazinamide is reported to be nontoxic, with the most prominent side effect being arthralgia (non-inflammatory joint pain) due to increases in uric acid levels in serum.[44] These effects are usually not severe enough to stop treatment. It should also be noted that combination antitubercular therapy shows an increased risk of hepatotoxicity (2% for INH + RIF + PZA versus 0.8% for INH + RIF),

however the mechanism by which this toxicity is increased is unknown.[45]

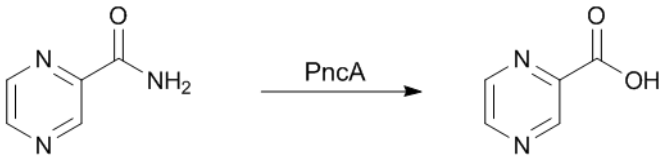

1-4 **1-7**

Figure 1.3. Activation of PZA **1-4** to POA **1-7** by the action of *Mtb* amidase PncA.

On December 31st, 2012, the Food and Drug Administration (FDA) approved the first new antitubercular agent in over 40 years. The compound is Janssen Therapeutics' (owned by parent Johnson & Johnson) bedaquiline **1-8** (**Figure 1.4**). First reported in 2005, bedaquiline acts by inhibiting ATP synthase function, leading to ATP depletion and imbalance of pH homeostasis.[46,47]

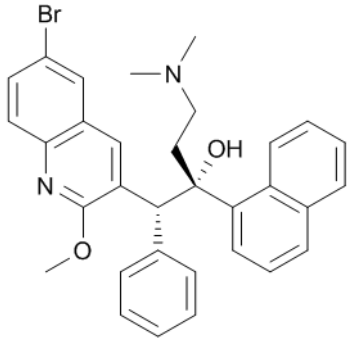

1-8

Figure 1.4. Structure of bedaquiline.

Some of the exciting characteristics of this new compound include its ability to be bactericidal over long periods of treatment, and its broad spectrum of activity against

MDR-TB strains.[46] Preclinical development showed little to no adverse effects in healthy individuals, however irregular heart rhythms and an increased incidence in deaths was noted during studies with MDR-TB infected patients (11.4% vs. 2.5% on placebo). This increase in deaths did not seem to correlate to the abnormal heart rhythms as most deaths occurred a year after patients stopped therapy, with a variety of causes of death.[48] Bacteria did develop resistance to bedaquiline when used as a monotherapy during preclinical development, so it was only administered along with standard MDR-TB therapy regimens. Resistance in most strains was identified as mutations to the *atpE* gene, which encodes the C subunit of ATP synthase.[47] This membrane-bound subunit has been suggested as the binding partner to bedaquiline, mutation of which leads to significantly lowered binding affinities.[49] In two separate tests, patients given bedaquiline became sputum negative for bacilli in 83 days and 57 days versus 125 days for patients taking a placebo. Due to the favorable results from these studies, the FDA fast-tracked the approval of bedaquiline for use in MDR-TB cases in the U.S., and only as part of a combination therapy.[48,50] Part of the challenge now for bedaquiline is to properly administer it so as to prevent the emergence of resistant bacteria for as long as possible. Many patients in areas where TB is endemic do not have access to facilities that can diagnose the drug-sensitivity of their infection, often resulting in the administration of drugs to which they are already resistant. If bedaquiline were added to this type of regimen, it would be like giving it as a monotherapy, encouraging the development of resistance. If sensitivity-testing can become more accessible for regions where MDR-TB has a high impact, bedaquiline has a good chance of having a major impact on the ability

to cure MDR patients. This new therapy is only the beginning of a new fight against TB, and hopefully more new therapies will follow to replace those whose efficacy has been diminished due to resistance development.

The challenges posed to those bold enough to work towards novel anti-TB therapeutics are daunting. To some extent, TB drug discovery faces the same challenges as any other therapeutic area: the identification and validation of an essential target to act upon, and the ability to find and develop useful lead compounds for *in vitro* and *in vivo* evaluation. In other ways, however, treatment of MDR-TB presents unique challenges that have stymied researchers for years. Firstly, *Mtb* displays a unique pathology that is still not well understood, and hinders research on chemotherapeutic efficacy *in vivo*. The target identification and lead compound discovery process has also proved more cumbersome than with other diseases, especially in comparison to other bacteria due to latency and slow growth of the organism. Our understanding of how antimycobacterial agents work continues to evolve, and with it our ability to assess through structural biology and metabolomics how investigational compounds produce bactericidal effects. Validation of essential gene targets in *Mtb* has proved more challenging due to the unique, naturally more resistant cell wall and membrane of mycobacteria. Consequently, the traditional strategies for inhibitor design, e.g. high-throughput screening (HTS), virtual screening, substrate mimics, etc., have not produced successful lead compounds on a timeline that can keep up with bacterial drug resistance. Furthermore, our ability to assess compounds in animal models is limited as there are few predictive *in vitro* models, and we continue to discover shortcomings in experimental models of tuberculosis in lower species animal

models. Other important considerations in TB drug development include an increased scrutiny on bioactivation and drug-drug interactions, especially with antiretrovirals, due to the large population of TB infected individuals co-infected with HIV. Finally, there are many monetary challenges to TB drug discovery. Governmental and special interest groups have donated large sums of money to TB drug development in the last ten years, with a large portion of that money landing in academic institutions. Big pharmaceutical companies have largely removed themselves from antimycobacterial drug discovery, limiting the ability of researchers to fund the clinical trials required for regulatory approval. Herein, we highlight six major challenges to the TB drug researcher, the current state of research in those areas, and hope to draw some conclusions about future directions for antitubercular drug development.

1.2 Challenge 1: Heterogeneity in tuberculosis pathology

A continuing challenge in TB drug development is therapeutic efficacy across strains and stages of the bacterial life-cycle.[51] Not only do medicinal chemists face the challenge of overcoming drug resistance, but a heterogeneous mixture of disease states must be targeted simultaneously. One of the most unique challenges in TB drug development is the spectrum of cell types that must be susceptible to a drug for successful therapy. Inhaled active bacilli are first phagocytosed by alveolar macrophages leading to either development of active granuloma lesions, or trafficking to the lymph nodes where T cell responses are initiated in an immune-suppressed infection (**Figure 1.5**).[52,53]

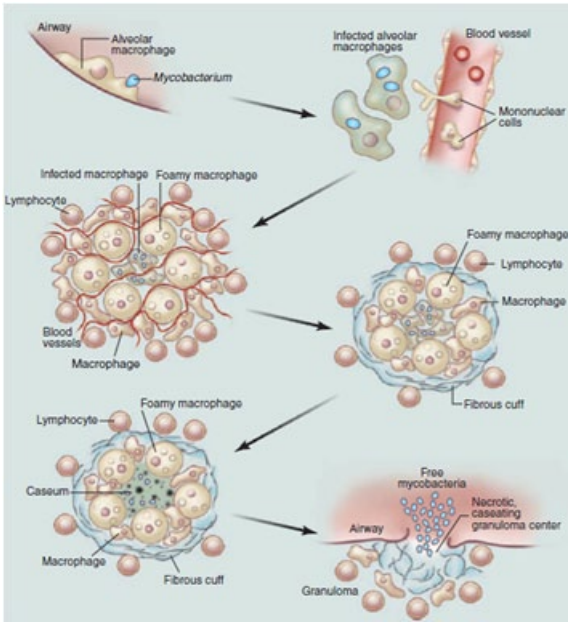

Figure 1.5. Reprinted with permission from Russell, D. G.; Barry, C. E., 3rd; and Flynn, J. L. Tuberculosis: what we don't know can, and does, hurt us. *Science* **2010**, *328*, 852–856 Reprinted with permision from the author, © AAAS publishing.[51] The life cycle of *Mtb*. The infection begins when *Mtb* bacilli are inhaled and phagocytosed by alveolar macrophages. The infected cells invade the subtending epithelium, which leads to the recruitment of monocytes and extensive neovascularization of the infection site. The macrophages in the granulomas differentiate to form epithelioid cells, multinucleate giant cells, and foam cells filled with lipid droplets. Lymphocytes appear to be restricted primarily to this peripheral area. Disease progression is characterized by the loss of vascularization, increased necrosis, and the accumulation of caseum in the granuloma center. Bacilli are released into the airways when the granuloma cavitates and collapses into the lungs.

Active infection results in a high bacterial burden producing high levels of lesions and acute pulmonary distress. The time and frequency of exposure, innate drug resistance of the inoculum, and the presence of co-infections or other complications all contribute to the severity of active infection.[53] Alternatively, host immune responses may suppress bacterial replication leading to persistence through adaptive nonreplicating conditions; previously defined here as latent infection. Our ability to define latency relies solely on

immunosensitization in the absence of clinical signs and symptoms, and more recently has been illustrated to be more complicated than originally thought due to the dynamic nature of the organism even during latency (**Figure 1.6**).[53,54]

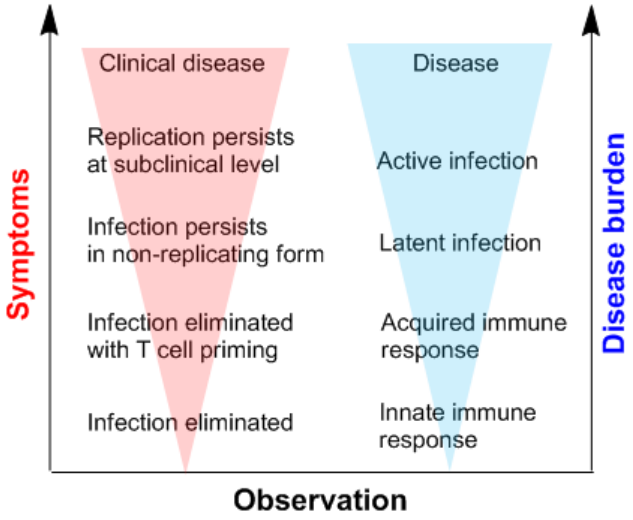

Figure 1.6. Generalized spectrum of pulmonary tubercular infections. Adapted from Barry, et. al.[53]

The pathology of active infection presents a complex mixture of lesions ranging from areas of swelling of aveoli to highly organized granulomas, some of which have intimate contact with host airways. Upon initial invasion by *Mtb* bacilli, a pro-inflammatory response leads to invasion of the epithelium and recruitment of monocytes from circulation. Vascularization of the infection site allows for conglomerated macrophages to differentiate forming the beginnings of a variety of granulomatous lesions. Epithelioid cells, multinucleated giant cells, and foam cells filled with liquid droplets are all common to active infection. Further diversification is achieved through the development of a fibrous extracellular matrix surrounding the macrophages that resists penetration by foreign bodies. Progression of the disease state is enhanced by increased necrosis and

accumulation of cells, forming a caseum in the center of the granuloma. The progression of granulomas to this necrotic state leads to the transmission of *Mtb*. Granulomas excised from active TB patients show rapid bacterial growth in macrophages located both at the surface as well as within the liquefied center.[55,56] Erosion of airways by these granulomas then allows the release of free mycobacteria via cavitation within the bronchus that can be aerosolized through coughing up of sputum (**Figure 1.5**).[51] This complex cycle of pulmonary disease pathology is dynamic and constantly changing throughout the timeline of infection.

Due to the innate human immune response, upwards of 90% of *Mtb* exposed individuals can suppress active infection resulting in latency of infection, with a 5–10% chance for these individuals to reactivate later in life. Factors leading to latency are not well understood, but it is hypothesized to evolve from the bacterial response to the host organism. Lesions in latent infection are much less frequent, and bacterial load and replication is much lower in latent lesions.[53] Host defenses activated through IFN-γ-mediated signaling result in reactive oxygen and nitric oxide release, which are cidal for *Mtb* at low levels.[57] However, higher levels of these reactive species seem to activate adaptive pathways through a key transcriptional regulator, DosR, allowing many key metabolic processes in *Mtb* to be shutdown.[58] Other mechanisms normally initiated by a host upon infection have also been implicated in triggering this latent stage of the bacteria, including ubiquitin-mediated proteolysis and intracellular autophagy.[59,60] In addition, some granulomas developed during latent infection form hypoxic microenvironments that halt the replication and spread of the bacteria.[61] It is

hypothesized that these granulomas containing nonreplicating bacilli serve as a reservoir to harbor cells for release during times of immunosuppresion, e.g. contraction of HIV, or TNF-α suppression.[62,63] The absolute mechanism of reactivation is unclear, since the constant release of mycobacterial antigens (detectable by immunosensitization) by latent infection illustrates the interplay between host and pathogen even in a nonreplicative phase.[64] These highly variable phenotypes demonstrate the vast heterogeneity of the clinical manifestation of TB that we are only now beginning to understand. Therapeutics must overcome multiple obstacles in order to effectively treat such a multi-faceted disease. First, they must be able to cross macrophage membranes without being modified or shuttled back out by the host cell. Second, latency offers an additional layer of complexity as it changes the bacterial metabolic pathways resulting in variable gene expression levels that can severely reduce efficacy or eliminate potency. And third, the heterogeneity between the granuloma lesions–e.g. fibrous coating, necrotic lesions, cavitary lesions–results in differential responses to treatment.[54] This laundry list of challenges facing TB drug development may be an explanation for the continued lack of a single anti-TB agent and reliance on a frontline combination therapy. Challenges that exist in our understanding of TB pathology contribute to our inability to effectively identify new target pathways/enzymes, as well as develop potent bactericidal compounds.

1.3 Challenge 2: Target validation and vulnerability

The advances in genomic sequencing and recombinant protein techniques have increased

the popularity of a strictly rational, target-based approach to new therapy design. While this approach has been successful for a number of indications (HIV, cancer, cardiovascular disease, diabetes), there has been a lack of success for antibacterial drug development.[3,65,66] Part of this is likely due to the fact that a few well-established targets have been exhausted by development of iterative generations of therapeutics to combat growing resistance. New targets and new chemical scaffolds have been left largely unexplored. One very neglected area of target-based approaches is the validation of a gene/gene product/molecular mechanism as essential, vulnerable, and sensitive to modulation by an external stimulus. The essentiality of a target is often improperly determined in an *in vitro* manner, which will not determine if bacterial growth and virulence will be attenuated in the *in vivo* setting. Genetic methods for target essentiality typically begin with allelic-replacement mutagenesis (gene knockout) assay. If the gene for a target of interest is known, a common misconception is that lack of growth of a genetic knockout strain validates essentiality of the target. This observation only suggests that the target *may* be essential for bacterial growth. Follow-up testing to confirm this should include conditional knockouts containing inducible plasmids for growth recovery, as well as evaluation of levels of suppression required to prevent bacterial growth. Not only should these assays be performed in an agar plate assay, but also within a living organism–e.g a mouse or rat disease-state model. Rubin and co-workers developed a unique mutation assay and used it to identify growth-attenuating genes in a mouse infection model of *Mtb*.[67,68] Prior to their report, these techniques had been somewhat limited in scope. For example, signature tagged mutagenesis (STM) is a technique

utilizing a series of 50–100 transposons that have been tagged with known nucleotide sequences used to monitor their presence within a pool of mutants.[69] This technique requires a mutation to be known (or predicted) and also involves an intense amount of labor to identify each growth-attenuated mutant.[69,70] An alternative is to use PCR analysis, e.g. in genetic footprinting, to map conditional mutants at a fixed site on a chromosome. This allows for a larger analysis than STM, but requires multiple analyses of the same site for confirmation.[71,72] These techniques have been developed in an effort to reduce the amount of genetic sequencing and analysis required in whole-genome sequencing of resistant mutants.

Vulnerability of a target can be assessed by varying the level of gene expression through a knockout model containing an inducible plasmid activated by an inducer, e.g. isopropyl-β-D-thiogalactopyranoside, IPTG. Careful examination of bacterial growth in response to lowered expression rates can determine the level of inhibition needed to effectively stop bacterial growth. This conditional knockout model is not always practical depending on the bacteria's response to lowered gene expression. An alternate approach utilizes antisense RNA sequences that can downregulate the expression of proteins in *Mtb*. Antisense RNA sequences are especially attractive when they can be applied *in vivo*, allowing an animal's natural immune response to become part of the evaluation.[3] *In vivo* evaluation is highly desirable because most inhibitors will not inactivate their targets to 100% of their possible efficacy, and a target that only needs to be inactivated to 80% is much more vulnerable than one that needs to be inactivated to 99%.[73] Antisense techniques often only cause knockdown of mRNA of approximately 80% due to *in vivo*

complications like permeability, natural defense systems against nonnative sequences, etc. Unfortunately, the ability to construct a phenotypically well-regulated conditional knockout or downregulated mutant of *Mtb* has been severely hindered by the complexity of the organism.

The sensitivity of a pathway to small molecule manipulation is largely dependent on the step in the pathway being targeted. The ideal situation is to develop a small molecule inhibitor for the rate-limiting step in a biological process. This can often be a moot point in developing new therapies against tuberculosis, because so little may be known about the pathway of interest, let alone the kinetics of the individual steps. In a full genetic screen of *Mtb*, Sassetti and Rubin found that 55% of the genes important for *in vivo* growth had no functional prediction, and a full 25% of important genes had no obvious homologues outside of mycobacteria or closely related species.[68] Many target enzymes are also studied for their kinetic parameters, but very few full pathways are studied for global kinetic behavior.[73] A global view is a better approach for determining the most advantageous target within a pathway, preventing the choice of a less important, less sensitive target. Schnappinger and co-workers evaluated the BioA enzyme of *Mtb* biotin biosynthesis in depth, illustrating the three important parameters mentioned here: essentiality, vulnerability, and sensitivity.[73] The unfortunate challenge revealed by this work is the determination that BioA must be inhibited upwards of 99% to achieve the full therapeutic benefit of pathway inhibition. Recent work by Sassetti and co-workers has revealed exciting new possibilities for re-igniting antibiotic sensitivity in *Mtb*. Their work involves investigating the regulation of the metabolic pathways important for the

reduction in growth and metabolite activity characteristic of latent infections. Their research found the pathway for triacylglycerol (TAG) synthesis from glycerol and acyl-CoA to be induced by the DosR regulator, the earliest response to hypoxia seen in many granulomas.[74] This redirection of carbon into triglycerides was critical for bacteria becoming antibiotic tolerant. By inhibiting this pathway, Sassetti shows that antibiotic sensitivity is regained, creating a novel strategy to improve the efficacy of current antibiotic therapy.[74]

New discoveries like those by Rubin, Schnappinger, Sassetti, and others are vital to generating a list of new, vulnerable targets within *Mtb* for therapeutic development. The identification of an essential, vulnerable, and sensitive target is just the beginning, however, of the development of a novel agent.

1.4 Challenge 3: Lead compound and inhibitor design

Once an enzymatic target has been identified and validated, a lead compound is needed to develop effective candidates for clinical development. Lead compound and optimization stages of new *Mtb* drug development account for at least 50% of the time needed to develop a new therapeutic (**Figure 1.7**).[3]

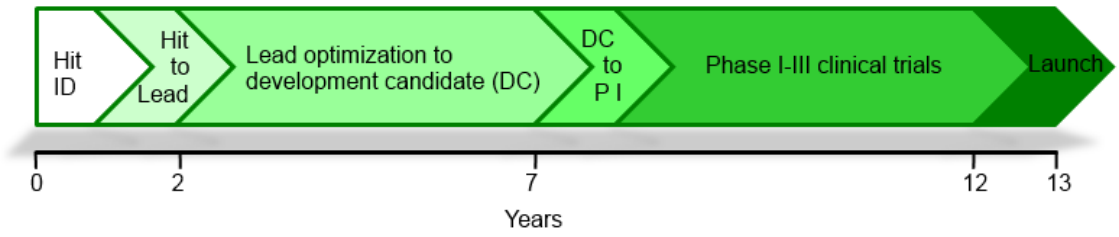

Figure 1.7. Estimated timeline for the development of a new *Mtb* therapeutic, with unlimited resources. Lead identification and optimization often accounts for at least 50% of the time to release of a new therapeutic.[3]

An important emerging factor of marrying a lead compound and target is the relatively narrow focus which the popular target-based approach brings to a drug design strategy. In an isolated compound-target system, optimized lead compounds may act very differently than they would within a disease-state model. With a library of techniques being developed for the identification of new lead compounds, researchers need to weigh the pros and cons for each approach in relation to their goals in order to successfully move forward in the drug design process. The following attempts to highlight some of the considerations important to popular design strategies.

With the advent of high-throughput screening (HTS), we have seen many research groups move towards this method for identifying lead compounds for drug discovery. Traditionally, this employs the use of a single enzymatic target that has been validated as essential in other testing. As this target-based approach matures, we are beginning to see that it is not a foolproof method for lead compound development. Inhibitors that are identified from a target-based biochemical assay may fail to show whole cell activity for a myriad of reasons: poor permeability, susceptibility to bacterial efflux mechanisms, redundancy in the pathway of interest, rapid development of resistance, and lack of

vulnerability of the target to inhibition *in vivo*. Discussions of the merits of HTS for antibacterial and mycobacterial drug discovery can be found elsewhere and will not be detailed here.[3,75] In an attempt to address some of these shortcomings, some groups are moving towards blending the traditional phenotypic or whole-cell testing with a high-throughput format that will quickly generate information about *in vivo* action against the pathogen of interest, as opposed to simple biochemical activity against a target. This newer approach to screening presents its own set of challenges, such as miniaturizing a whole-cell assay so that it can be reliably replicated thousands of times, and the need to subsequently determine the mechanism of action of identified inhibitors.[3] Several hybrid strategies have emerged and shown promise for identifying new scaffolds for *Mtb* drug development. Researchers at Southern Research Institute screened a focused library of scaffolds biased in design by mimicking current kinase inhibitor scaffolds and binding sites. They first virtually screened the library against a panel of kinases with published crystal structures before screening a smaller subset in a whole-cell assay against *Mtb*.[76] Other researchers have developed a hybrid technique called target-based whole-cell screening (TB-WCS) that makes use of conditional mutant strains wherein the target of interest is regulated using antisense interference or inducible promoter strategies.[77] This approach seems to combine some of the best of both worlds of screening techniques. With compounds biased towards a target of interest, you can determine if the compound 1) acts on the target of interest (or at least the pathway of interest), and 2) achieves enough cellular penetration to achieve reasonable whole cell activity with each compound screened. As is illustrated in the study by Abrahams, et. al., however, this

approach will not be broadly applicable to all essential targets within *Mtb* because it requires the ability to isolate viable conditional mutants in specific genetic backgrounds. Even in this study, they were only able to successfully evaluate two of the three essential targets in which they were interested.[77]

Aside from HTS, other target-based strategies for inhibitor design include the related techniques of structure-based and virtual design.[78] When a crystal structure of a known, biologically relevant target is available, it is possible to use computer programs to design compounds that could block interactions important for native activity. If the co-crystal structure with a known inhibitor is available, direct interactions can be evaluated and the compound structure adjusted to increase binding affinity (and, by extension, activity against *Mtb*) according to the available space in the crystal structure. The structural biology techniques and access to equipment needed for the generation of high resolution crystal structures is expensive and can be challenging to obtain, making this an uncommon technique for most researchers. It is more likely that a crystal structure of the enzyme of interest, or at least of homologous enzymes will be available. From this data, researchers can often rationally design compounds or modifications to lead compounds to create inhibitors with improved enzymatic activity. Some approaches apply computer modeling programs before synthesizing inhibitors. This *in silico* design/screening has recently lead to reports of lead compounds against new targets in *Mtb*.[79,80] One report focuses on a well-studied enzyme, dihydrofolate reductase (DHFR), which has been successfully targeted in cancer chemotherapeutics and some antibacterial therapeutics, but current investigational compounds show a distinct lack of activity against

*mt*DHFR.[79,81] By modeling of simple tripeptides as lead compounds, the investigators were able to identify sequences with predicted nanomolar activity against *mt*DHFR, three orders of magnitude more potent than any other reported compounds, and a predicted 120-fold selectivity over *h*DHFR.[79] While peptides are not often found to be useful drug candidates themselves, peptidomimetic strategies could be employed to modify the lead compound to a more drug-like structure. Where this report falls short is in the enzymatic validation of the virtually screened compounds. While many chemistry groups often lack the structural biology/computational capabilities to perform these virtual screens, structural biology groups may lack the chemical expertise to validate their computational models, a step that we believe is too valuable to leave for other researchers. A similar study was also performed on the *Mtb* shikimate kinase (SK). This target is highly attractive as the shikimate biosynthetic pathway is essential in bacteria but absent in mammals.[82] With 3D crystal structures available of the SK enzyme, the investigators were able to design small peptidic molecules that were predicted to bind with 10-fold higher affinity than a previously described compound.[80] This study again shows the versatility and usefulness of rational, structural design and the utility of virtual screening to rank desired compounds according to likelihood of activity. The true promise of this lead compound is as yet unknown, however, as enzymatic and whole-cell activity have not been reported.

Another approach that relies on correlating crystallographic structural information and cellular activity is fragment-based design. Briefly, this technique investigates low-molecular-weight molecules (< 250 Da) for binding within an active site by soaking them

into crystals of the enzyme of interest at high (mM) concentrations (**Figure 1.8**). Structural determination of how these fragments bind to the target of interest (either through X-ray crystallography or NMR techniques) can then be used to design linkers to tether together complimentary fragments creating a macromolecular inhibitor structure. A more thorough discussion of these techniques can be found elsewhere.[75,78,83]

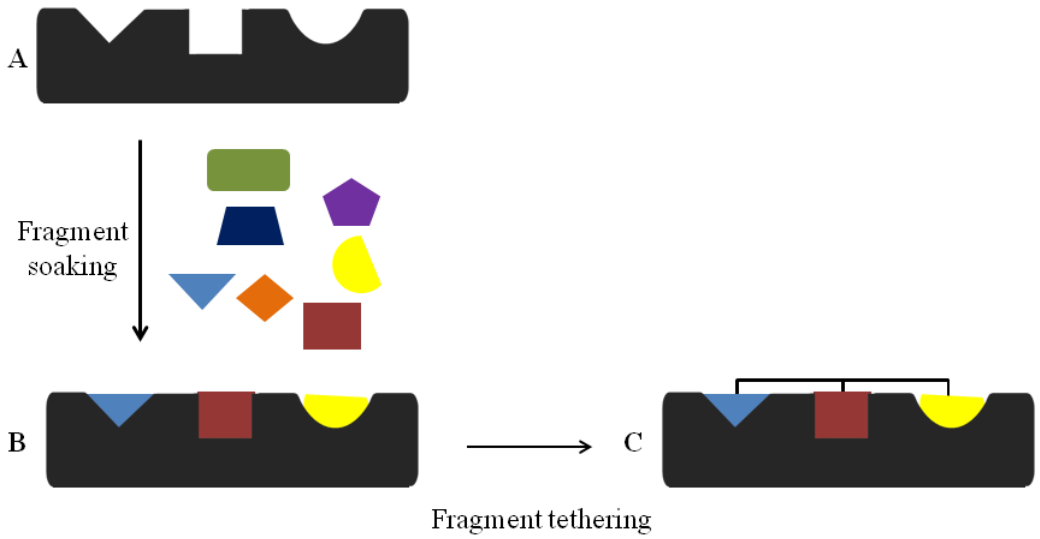

Figure 1.8. General steps to fragment-based drug design: (A) known target with crystal structure solved; (B) crystal structure determined after soaking low-molecular weight fragments at mM concentrations; (C) medicinal chemistry used to tether fragments into a macromolecular inhibitor design.

Abell and co-workers successfully employed a fragment-based strategy to design inhibitors of PanC, an adenylating enzyme in the pantothenate biosynthetic pathway in *Mtb* that catalyzes the condensation between pantoic acid and β-alanine, producing pantothenate.[84] After screening a library of 1300 compounds by WaterLOGSY NMR, they identified a lead compound with a K_D of 1 mM. This lead compound, 5-methoxyindole, was then incrementally grown by adding fragments and observing the

effect on the relative binding of the inhibitor. This iterative process enabled them to develop an inhibitor with a K_D of 1.8 μM, 1000-fold greater than their starting compound.[84] This process involved many different evaluation platforms: additional WaterLOGSY NMR, X-ray crystallography, isothermal titration calorimetry (ITC), and thermal shift assay. Fragment-based design, like structural or virtual design, also requires a wide range of resources: chemical expertise, protein expression and purification, and structural determination. These resources can be difficult and expensive to compile.

Integrated systems biology approaches known as "omics" technologies (including genomics, transcriptomics, proteomics, and metabolomics) have developed as potential tools for research into disease states and therapeutic response.[85–87] These approaches rely heavily on the observance of biomarkers from affected individuals. A biomarker is a biological character that is objectively measured and evaluated as an indicator of a physiological or pathological process, or pharmacological response(s) to a therapeutic or preventative measure.[88] In drug discovery, a biomarker could play a key role by reducing the attrition of drugs at a late-stage in the development pipeline, thereby significantly reducing the overall cost of drug development. An ideal biomarker would be able to evaluate delivery of drugs to their target of interest, predict pathophysiological mechanisms of reaction/response, and predict clinical effects (e.g. predicting drug interactions, particularly in relation to HIV/AIDS and *Mtb* therapeutics).[89] Nearly any tissue or bodily fluid can be used for biomarker evaluation, however the fluid that gives the most general information and is the most easily collected is peripheral blood. Blood samples contain genes, transcripts, proteins, lipids, and metabolites at appreciable levels

for analysis. Recently, early success has been reported with metabolomic analysis to differentiate between similar *Mtb* strains. Metabolomics is the study of global changes in the profile of small-molecule metabolites expressed by cellular processes throughout the body, such as metabolic and catabolic intermediates, hormones, signaling molecules, secondary metabolites, and small structural lipids.[90] In their study, du Preez and Loots used gas chromatography-mass spectrometry (GC–MS) analysis of bacterial cultures to identify metabolites that differ between wild-type and rifampin-resistant TB. Their analysis allowed them to identify the resistant strains, but also clearly differentiate between the different *rpoB* gene mutations in each resistant strain.[91] While this study was conducted only within bacteria and not within infected patients, it illustrates the utility of metabolomics as a way to identify biomarkers that could potentially predict if a patient will be drug resistant. Development of this method for diagnostics would require very high sensitivity as the bacterial burden is very small with respect to the rest of the body.

A complimentary strategy involving structural biology and medicinal chemistry to evaluate enzymatic activity in conjunction with whole-cell activity against *Mtb* should be employed when developing lead compounds. No one strategy has proved adequate to produce successful lead compounds on its own, but a multidisciplinary approach that evaluates a target and inhibitor from multiple angles promises to identify compounds that have the best potential to become clinical candidates.

1.5 Challenge 4: Mechanisms of action

With the advances seen in molecular biology techniques and the tightening of regulations for the safety of patients, there is increasing pressure to identify the mechanism of action for a new therapeutic. As discussed above, we still have much to learn about how *Mtb* processes are connected to, and affected by, one another. Recent investigations into the mechanism of action (MOA) for many antibacterial compounds, including antimycobacterial agents, has illustrated just how complex this interrelationship can be. The MOAs of most antibacterial agents in use today, including anti-TB drugs, predominantly fall into four classes: inhibition of DNA replication and repair, interference with protein biosynthesis, inhibition of cell wall turnover, and inhibition of a unique biochemical process (e.g. DHFR inhibitors).[92,93] These molecular interactions have long been thought to be the causative effect in the bactericidal activity seen in many approved antimycobacterial agents. While each class of antibacterial compounds has distinct drug-target interactions, it has become accepted that there may be similar downstream effects that ultimately lead to bacterial cell death.[92,94–98] While this research has been largely performed on simpler Gram-positive and Gram-negative organisms, this evidence is compelling enough to extend its implications to include mycobacterial species as well. In an attempt to further understand how bactericidal compounds exert their activity, J. J. Collins and colleagues began observing cellular changes in model organisms like *E. coli* and *S. aureus* upon treatment with various antibacterial compounds. They observed that DNA gyrase inhibitors induce a breakdown in the iron

regulatory pathway, promoting the formation of reactive oxygen species (ROS). More specifically, hydroxyl radicals were formed via internal iron and the Fenton reaction through the reduction of hydrogen peroxide by ferrous iron (**Figure 1.9**).[95]

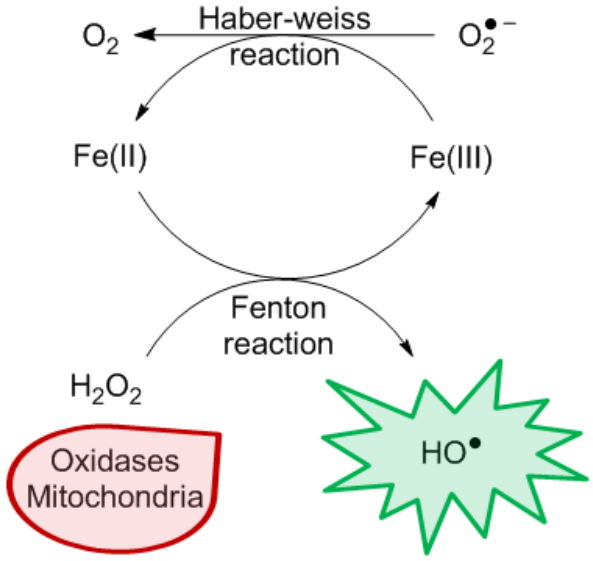

Figure 1.9. Internal hydroxyl radical formation via the Fenton reaction. Disregulation of this pathway leads to a build-up of hydroxyl radicals, a commonly observed consequence of antibacterial compounds.

Direct observation of hydroxyl radicals formed during treatment with antibiotics can be achieved using the dye hydroxyphenyl fluorescein (HPF). Iron chelators, e.g. 2,2′-dipyridyl, and hydroxyl radical scavengers, e.g. thiourea, were used as controls to confirm the dye's specificity for hydroxyl radicals in a biological matrix. The 2,2′-dipyridyl prevents hydroxyl radical formation by sequestering unbound iron, and thiourea is known to be a potent mitigator of damaging hydroxyl radicals in both eukaryotic and prokaryotic systems. Following validation of their methods, Collins and co-workers tested representative compounds from each of the three antibacterial compound classes

listed above.[92] Not only were they able to confirm that all bactericidal antibiotics show significant increases in hydroxyl radical formation, but they also confirmed that bacteriostatic protein synthesis inhibitors e.g. erythromycin and tetracycline, did not induce the formation of hydroxyl radicals. The generation of free iron for the formation of hydroxyl radicals likely comes from leaching of iron from iron-sulfur clusters, a process well-accepted to be precipitated by superoxide and the Haber-weiss reaction. Superoxide generation in *E. coli* is largely due to the respiratory electron transport chain, driven by oxygen and the conversion of NADH to NAD^+. Genes involved in the NADH-coupled electron transport chain were upregulated in bacteria treated with bactericidal drugs of any MOA (see above). In a separate study, Collins and co-workers showed that aminoglycosides and other ribosomal inhibitors also induce free radical formation through misfolding of proteins.[94] These studies were confirmed through the generation of single-gene knockout mutants of *E. coli* that sensitized the bacteria to even minor disturbances in membrane protein folding and translocation.

Most recently, Walker and co-workers have reported observations on DNA damage by bactericidal antibiotics.[98] Their study shows the oxidation of nucleosides, especially deoxyguanosine into 8-oxo-deoxyguanosine (8-oxo-dG), can cause double-strand DNA breaks (DSBs) that are lethal to the bacterial cell. Base excision repair enzymes will normally remove lesions like 8-oxo-dG before they become problematic. However, if there is an elevated level of ROS present to create these lesions and multiple strand breaks are generated, the cell may not be able to maintain proper cell cycling and metabolism. This type of mechanism is now implicated for the cell killing activity of the

aminogylcoside kanamycin.[98] As suggested in their conclusions, antibacterial adjuvants may be developed that target DNA repair enzymes. These types of compounds could increase the effectiveness of an antibiotic, prolonging its clinical relevance. The main bacterial response to DNA damage, i.e. the SOS response, induces more highly error-prone DNA polymerases that allow the bacteria to mutate its DNA in order to survive the xenobiotic stress. Inhibition of this response could potentiate all of the major classes of bactericidal antibiotics by shutting down this key mitigator of ROS damage to DNA.[97] All of the above studies highlight that while we may design antibacterial compounds to maximize a specific drug-target interaction, the direct results of that interaction may not be the truly bactericidal event we expect it to be. Downstream consequences to modulating cellular processes may be just as, if not more, important than the initial interaction.

Not only are ROS implicated in mechanisms for bacterial cell death, they are also implicated in mechanisms of bacterial drug resistance. There are a number of known mechanisms by which bacteria generate genetic resistance to antibiotics: the exchange of genetic material with another organism, the activation of latent genetic elements, and the mutagenesis of its own DNA.[99] As discussed above, bactericidal antibiotics often induce the production of ROS through a breakdown of iron regulatory dynamics causing a spike in the production of potential DNA damaging agents like hydroxyl radicals. These oxidative species can generate lesions in DNA that are not properly repaired by the relatively promiscuous DNA polymerases within bacteria and, if the cell remains viable, the mutation persists. While this process can occur *in vivo* even in the absence of

antibiotic, sublethal doses of a compound will increase the number of mutagenic events occurring. This increase in genetic variation from generation to generation dramatically increases the chance for the bacteria to develop resistance to the antibiotic treatment.[95]

Further evidence for ROS as a method of bacterial genetic mutation ultimately leading to antibiotic resistance was recently presented by Kohanski and co-workers.[96] They successfully developed a method to track ROS-mediated mutagenesis and its correlation to antibiotic resistance. In a systematic manner it was shown that antibiotics increase the overall mutation rate during bacterial growth, and that this increase is heavily dependent on the formation of ROS.[96] Treatment of bacteria with antibiotics under anaerobic conditions or in the presence of a hydroxyl radical scavenger like thiourea showed mutation rates near the basal levels of untreated cells. Following treatment with a sublethal dose of a single antibiotic under aerobic conditions, mutation rates were elevated and an increase in MIC for a wide range of antibiotics was observed.[96]

While the above discussion is the currently accepted model for the bactericidal effects of many antibiotics, recent reports have begun to question this model.[100,101] In back-to-back publications, the laboratories of James Imlay and Kim Lewis have independently shown that ROS may not be the ultimate executioners of bactericidal antibiotics.

Liu and Imlay re-tested a number of the reported conditions from the work of Collins and co-workers, and found that the antibiotics in questions were just as active under anaerobic conditions--when ROS are not being produced.[100] In the same report, they also showed that a transcription factor in *E coli* known to be upregulated under H_2O_2 stress was not induced by treatment of ampicillin or norfloxacin. They concluded from their results that

classic bactericidal antibiotics do not promote H_2O_2 formation, which was proposed to lead to DNA damage, and that oxygen appears dispensible for antibiotic toxicity.[100] They do admit that there may be other general stress mechanisms that may be important for bactericidal activity of antibiotics, as they cannot offer any additional insight into their activity from these studies.

Keren and co-workers corroborate and compliment the work of Liu and Imlay.[101] This report focuses more on the use of thiourea, hydroxyphenyl fluorescein (HPF) as indicators of ROS generation in bacterial culture. They found that the reported protective effects of thiourea could be abolished simply by increasing antibiotic concentration to therapeutically relevant levels.[101] Additional results confirm that antibiotics are just as active under anaerobic conditions, when ROS cannot be generated, similar to Liu, et. al. Finally, they suggest some reasons for the conflicting evidence produced regarding ROS and antibiotics: 1) the concentration of the antibiotic used can have a large effect on the efficacy of bacterial killing, 2) the mechanism of thiourea protection is unclear, and may not involve ROS scavenging, 3) HPF fluorescent shifts can be observed under both aerobic and anaerobic conditions suggesting it is not a specific indicator of ROS.[101]

The above exemplifies that difficulty in understanding the mechanism of action for bactericidal antibiotics, however all of the above authors agree that better understanding of the mechanism by which a compound acts would aid the design of a better analogue from a lead structure.[97,100,101] In some instances, drugs need to be bioactivated in order to exert their bactericidal or bacteriostatic action on the infectious pathogen. In the past, this was often elucidated after the drug had already been approved and widely used to treat

infections. For example, both INH and PZA are bioactivated to their bactericidal agents (as described above).[15,16,40] Ethionamide (**1-9**, ETA) has been shown to behave in a similar manner to INH (**Figure 1.10**). First discovered in 1956, ETA was developed as an analogue of nicotinamide, which had been shown to be moderately active against *Mtb*.[102] ETA is bioactivated by the monooxygenase EthA to give a sulfinic acid (**11**) that can undergo radical chemistry, producing an imidoyl radical (**1-12**) that can form adducts with NAD (**1-13**).[103] ETA-NAD adducts are potent tight-binding inhibitors of InhA, just like INH, and were shown to bind in a nearly identical orientation to INH-NAD adducts through co-crystal structures.[103]

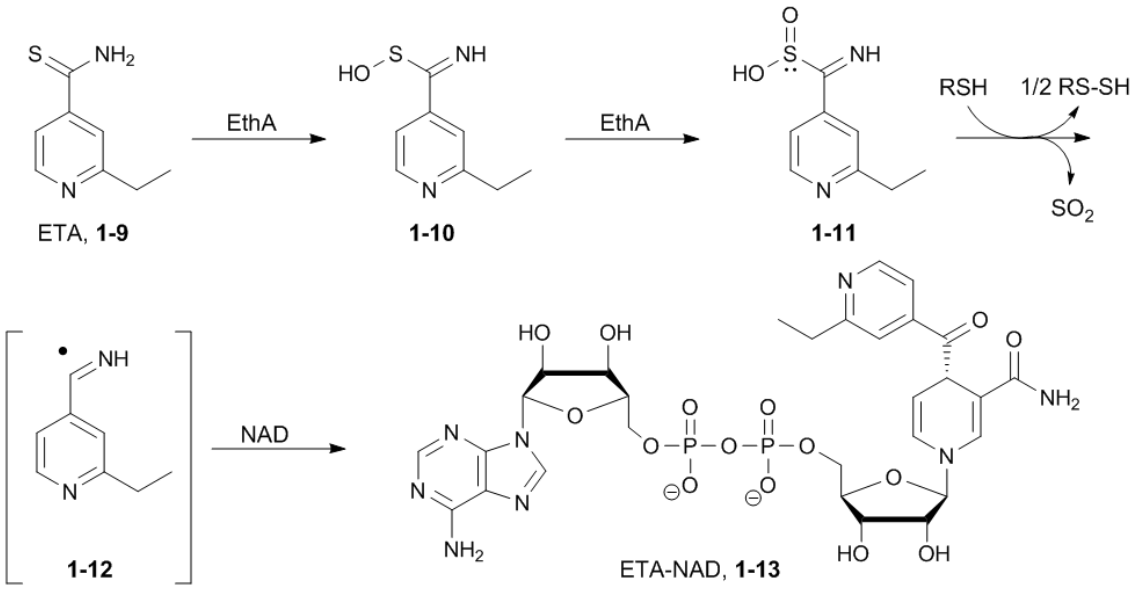

Figure 1.10. Bioactivation of ETA. ETA-NAD adducts bind to InhA almost identically to INH-NAD adducts.

Whether due to our better understanding of bacterial cell pathways or our increasingly sophisticated screening techniques, new compounds are being identified that require

bioactivation for activity. PA-824 is a new anti-TB compound in the nitroimidazole class (**1-14**, **Figure 1.11**). Traditionally a source of antiprotozoal agents, random screening efforts have identified chemicals of this class with highly potent antitubercular activity.[104] It has been shown that PA-824 is bactericidal and appears to act through the release of nitric oxide (NO), a highly reactive nitrogen species that mammals innately use against mycobacterial infections.[105] The proposed mechanism of activation is through F420 deazaflavin-dependent nitroreductase (Ddn) reduction of the C-3 of PA-824 to give a dihydroimidazole intermediate.[105] This intermediate more readily loses nitrous acid, which is disproportionated to nitric oxide (NO). Additional experiments suggested that nitrogen species (like NO) are likely responsible for PA-824's bactericidal activity under anaerobic conditions (typical of quiescent *Mtb*), whereas metabolism in aerobic conditions likely produces ROS that are responsible for bacterial killing.[106,107] As expected, mutations involving Ddn genes were the most common to produce resistance in bacteria when studied.[108] No adverse side effects have been reported in the Phase I clinical safety trials of PA-824, and limited Early Bactericidal Activity (EBA) studies have shown no adverse effects.[109] PA-824 shows synergistic cooperation with PZA, the combination therapy showing the best anti-TB activity *in vitro*.[110]

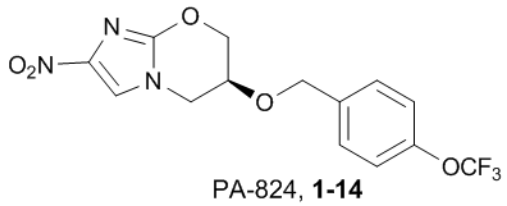

PA-824, **1-14**

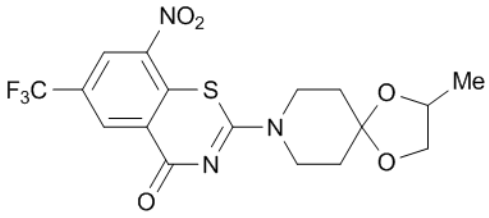

BTZ038, **1-15**

Figure 1.11. Structures of PA-824, and BTZ038. Both investigational compounds have shown required bioactivation for *Mtb* activity.

Related compounds currently under investigation are the benzothiazinones (e.g. BTZ038 **1-15**, **Figure 1.11**). BTZ compounds also contain a nitroaromatic core and appear to act through a novel mechanism of action. These compounds have shown extraordinary activity against *Mtb*, with MIC values upwards of 20-fold below that of INH.[111]

Genetic analysis has confirmed the target of BTZ compounds to be decaprenylphosphoryl-β-D-ribose oxidase (DprE1) and decaprenylphosphoryl-D-2-keto erythro pentose reductase (DprE2), which are responsible for the essential epimerization of arabinan precursors in mycobacterial cell wall components.[111,112] Without these arabinan molecules, the cell wall cannot be completed, leading to cell destabilization and ultimately lysis. Further study showed that some sort of activation of BTZ molecules must happen within the mycobacteria, as they have been shown to modify cysteine residues within the DprE1 target enzyme.[112] Still ongoing in the study of this class of

compounds is the search for an independent enzyme that first reduces the BTZ nitro group to a reactive nitroso intermediate. It is also possible for this to happen within DprE1 itself, although no evidence has yet been given to support that hypothesis. A 4-week efficacy study in mice did show a decrease in bacterial burden, however the possible side effects in mammalian cells have not yet been fully addressed.[111] While the starting point for development may arise from random screenings, rationally designing or exploiting prodrug or bioactivatable moieties into inhibitors could be a very effective strategy for bypassing some of the difficult pathological problems associated with *Mtb*, as well as increase the likelihood of oral absorption and distribution *in vivo*.

There are many research groups actively pursuing new anti-TB compounds, but there are additional challenges to be faced once a clinical candidate has been identified. New compounds will likely need to work in synergy with existing *Mtb* therapies to help slow the development of drug-resistant bacteria. Many investigational compounds have shown drastically improved efficacy in combination with first-line agents, especially PZA. As more mycobacterial strains develop resistance to these compounds, these combinations will also lose efficacy. New compounds that are able to be incorporated into multiple drug regimens, not just combinations involving the frontline agents, are highly desirable to avoid this consequence. New anti-TB compounds also need to be evaluated for their efficacy in concert with antiretroviral therapies. As discussed earlier, there is an especially alarming rate of disease and death in TB/HIV co-infection. Rifampin, a known CYP3A4 and P-glycoprotein (P-gp) efflux pump inducer, dramatically reduces the levels of antiretrovirals *in vivo*, which can cause serum levels to fall below IC_{50} levels, allowing

drug resistant viruses to be selected. Compounds currently in development should be evaluated for their ability to induce (or inhibit) these important metabolic processes so as to avoid complications in co-therapy.

1.6 Challenge 5: Modeling activity against *Mycobacterium tuberculosis*

When a compound has been identified as a potential drug candidate through rigorous SAR and enzymatic studies, further preclinical evaluation is required before being able to enter human clinical trials. A great hurdle in *Mtb* drug discovery has been the development of predictive *in vitro* and *in vivo* models that genuinely reflect the outcome for human *Mtb* infection. Herein we will attempt to highlight best practices and some of the challenges still faced in *Mtb* models. For a more exhaustive review, see other publications.[113–115]

Mtb is a highly transmittable pathogen that requires Biosafety Level 3 (BSL-3) facilities to perform bacterial culture and/or animal work. These facilities are not readily available to all researchers, nor can all of them afford such sophisticated equipment. Other, less pathogenic, bacteria have been used as surrogates for *Mtb* for *in vitro* study. Most extensively used are *Mycobacterium smegmatis*, and *Mycobacterium bovus BCG*.[116] The genome of *M. smegmatis* was first sequenced in 2001 and shown to have closer homology to *Mtb* than originally thought.[117,118] *M. smegmatis* was shown to have close homologues of 12 of the 19 genes thought to be involved in virulence in *Mtb*.[117] Adding this to a lack of pathogenicity in humans (BSL-1 pathogen) and short generation time of

3–4 hours, *M. smegmatis* is an attractive surrogate for the study of compounds against *Mtb* enzymes and growth. Caution should be exercised, as others have pointed out, that relying on *M. smegmatis* too rigorously may cause false positive results, or miss *Mtb* active compounds all together.[119] Further study of the utility of *M. smegmatis* and BCG reveal evidence for these concerns. Whole-cell screenings of a LOPAC library and the NIH Diversity Set and Spectrum Collection versus *M. smegmatis*, *M. bovus BCG*, and *M. tuberculosis* showed striking differences in the number of *Mtb* inhibitors identified. *M. smegmatis* missed 50% of the LOPAC library hits in *Mtb*, and 48% in the NIH collection. In comparison, *M. bovus BCG* missed only 34% of the LOPAC hits and 7% of the NIH hits.[116] Until better *in vitro* models are developed that show more correlative activity compared to *Mtb*, these inconsistencies must be taken into consideration when investigating new compounds.

Compounding the difficulties with *in vitro* modeling are the challenges for *in vivo* animal models. Mouse models are currently the most heavily utilized model for infectious disease for a number of reasons: ease of handling, affordability of housing and care, the availability of inbred, mutant, and genetically altered strains, and the wide range of reagents developed for their study.[120] While these models are extremely useful in early stages of preclinical development to evaluate the efficacy of an investigational compound to eradicate disease, there are drawbacks to comparing these results to human disease. As previously discussed, many people are infected with what is termed latent TB where they present an immunological response to the bacterial stimulus, but show no clinical or microbiological evidence of infection.[121] Mice do not develop the latent disease to the

same extent unless antibiotics are introduced, and this does not adequately reflect the human condition. Pathologically, mice do not form granulomas with the same spectrum of heterogeneity as those seen in human disease (e.g. caseous and necrotic lesions). These differences in manifestation of the disease can have a direct impact on how well the results of a mouse study will translate to human disease, and it is difficult to predict these effects. Both guinea pigs and rabbits have also been studied and have shown manifestation of TB disease more closely resembling the human infection. Rabbits are usually infected with *M. bovus* because *Mtb* susceptible animals, while reported in legacy literature, have been lost. Both models suffer from a lack of immunological reagents available for more detailed study, and rabbits require substantially more material for efficacy testing due to their larger size.[113] Non-human primates (NHPs) are likely the best candidate species for an animal model of TB due to their genomic, physiological, and immunological similarities to humans.[115] The major drawback to the utilization of NHPs is the large expense of the animals, and their housing and care in a BSL-3 level facility. Recently, there has been a resurgence in the use of cynomolgus macaques due to their faithful representation of human disease both in the manifestation of latently infected individuals, and the heterogeneity in the pathology of disease.[113,115] These models have contributed greatly to our understanding of the disease itself, as well as our current and developing therapies against it.

Preclinical development should also work towards a better understanding of some of the pharmacodynamic properties of investigational compounds. The two most extensively used *in vitro* models for the susceptibility of bacteria to treatment are the Wayne-Hayes

hypoxia model and the hollow fiber infection model (HFIM). The HFIM model, originally described by Hollingshead in relation to observing tumor cell lines, attempts to model the pharmacodynamics of a living system.[122] Drusano and co-workers adapted it by using a semi-permeable fiber that can be inoculated with colony-forming units (CFUs) of *Mtb* that are allowed to grow in fiber.[123] Media is then pumped through the fiber where it equilibrates throughout the chamber and allows nutrients to reach the bacteria for growth (**Figure 1.12**). An antibiotic or investigational compound can then be injected into the flowing media to be disseminated into the fiber, allowing for simulation of pharmacokinetic profiles. The cells within the fiber are removed after a predetermined amount of time and evaluated for parameters such as viability and acquired resistance. These hollow fibers can also be implanted within mice for similar evaluation from an *in vivo* system.[122] The Wayne-Hayes model, originally described in 1996, slowly introduces hypoxia to culturing *Mtb* to force them into a quiescent, or latent, state.[124] Treatment of these cultures with antibiotics will then evaluate a compound's ability to fight latent infection as compared to more actively replicating bacteria. This is one of the relatively few ways of modeling even a part of the conditions seen in latent infection. Other systems rely on nutrient starvation to force the bacteria into a lowered metabolic state, and still others use multiple stresses to help achieve multiple outcomes of latent infection.[114]

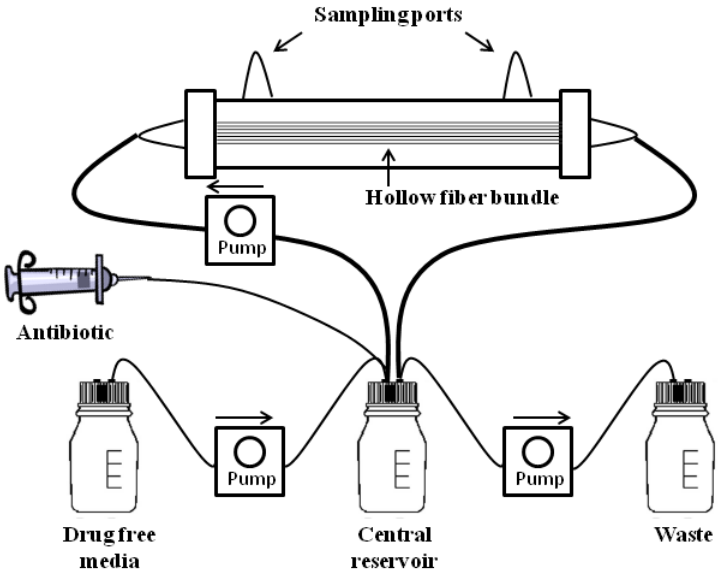

Figure 1.12. Hollow fiber infection model. Adapted from Drusano, et al.[123]

Models of *Mtb* infection have progressed tremendously in the last two decades. While there is still no single model that best evaluates all aspects of *Mtb* infection, the use of multiple models should give reasonable confidence as to the promise of a new therapeutic candidate. Unfortunately, this evaluation can come at significant financial burden, which has only become more difficult to overcome as many countries are experiencing economic turmoil.

1.7 Challenge 6: Monetary challenge

Over the past two decades, funding for new drug discovery research has become increasingly competitive. Funding agencies are becoming more stringent in their requirements for funding a proposed project, and many important projects are not

acquiring adequate funding to be conducted. Outside of academics, large pharmaceutical companies must pick disease indications to invest in, and often choose those with the greatest possibility for return. *Mtb* is largely a problem in poorer countries, where there are fewer and less advanced medical facilities available for their citizens. Many of these countries would not be able to afford an expensive new anti-TB therapy, even if it would help many ease a significant health burden. For these, and other business reasons, many companies are not investing in anti-TB research. This difficult funding situation only hurts the ability of TB research to move forward.

There are also some practical financial hurdles to *Mtb* therapy development that need to be overcome. Once a compound is approved for Phase II clinical trials, large cohorts of patients who are actively infected with *Mtb* must be found, enrolled, and monitored throughout a study. These trials must be rigorously documented and controlled in order to prove the efficacy of a new therapeutic to the FDA and other regulatory bodies. Groups of patients of this size are often only found in countries on the African and Asian continents, usually far away from where the candidate compound has been developed. It is a huge financial challenge to set-up a trial facility, transport and hire a staff to run the trial, and then monitor and document the results to the satisfaction of the regulatory committees. As the TB crisis continues to grow, governments of countries with large TB burdens have begun to partner with researchers to help fund and facilitate these studies, doing what they can to encourage new therapy development.

1.8 Conclusions

The global need for new *Mtb* therapeutics continues as the field grows its knowledge regarding the pathogen, host immune response, and techniques for new therapy development. In order to efficiently address this growing pandemic, we need to continue to utilize complementary strategies to evaluate new therapeutic agents from multiple angles. This will allow promising candidates to move through the development pipeline faster, as well as terminate programs that will have irreconcilable problems in preclinical or clinical development. There is still a great need for better predictive models of *Mtb* behavior, both *in vitro* and *in vivo*, that will correlate to human infection. This could be through better understanding of NHP models, or through the development of better tools for lower-order animal models (e.g. guinea pigs and rabbits) that may be more accessible to more researchers. To develop these models and tools, we need to continue to investigate the basic pathology and life cycle of this highly complex and well-adapted pathogen.

New compounds need to be identified through complimentary approaches that combine the specificity of a target-based approach with the physiological evaluation of a phenotypic or whole-cell approach. This will allow for the quickest evaluation of the viability of a lead for future development, reducing both the time and cost required to develop a preclinical candidate. A combined effort will create the knowledge and opportunity needed to develop the next generation of antitubercular compounds that will remove this public health threat from the global theater.

1.9 References

1. White, A. R. Effective antibacterials: At what cost? The economics of antibacterial resistance and its control. *J. Antimicrob. Chemother.* **2011**, *66*, 1948–1953.

2. Silver, L. L. Challenges of antibacterial discovery. *Clin. Microbiol. Rev.* **2011**, *24*, 71–109.

3. Payne, D. J.; Gwynn, M. N.; Holmes, D. J.; Pompliano, D. L. Drugs for bad bugs: Confronting the challenges of antibacterial discovery. *Nat. Rev. Drug Discovery* **2007**, *6*, 29–40.

4. Wright, G. D. Antibiotics: A new hope. *Chem. Biol.* **2012**, *19*, 3–10.

5. Fischbach, M. A.; Walsh, C. T. Antibiotics for emerging pathogens. *Science* **2009**, *325*, 1089–1093.

6. Klein, E.; Smith, D. L.; Laxminarayan, R. Hospitalizations and deaths caused by methicillin-resistant *Staphylococcus aureus*, United States, 1999-2005. *Emerging Infect. Dis.* **2007**, *13*, 1840–1846.

7. World Health Organization. *Global tuberculosis report 2012*; Geneva, Switzerland, **2012**.

8. Barry, C. E., 3rd; Blanchard, J. S. The chemical biology of new drugs in the development for tuberculosis. *Curr. Opin. Chem. Biol.* **2010**, *14*, 456–466.

9. Koul, A.; Arnoult, E.; Lounis, N.; Guillemont, J.; Andries, K. The challenge of new drug discovery for tuberculosis. *Nature* **2011**, *469*, 483–490.

10. Velayati, A. A.; Masjedi, M. R.; Farnia, P.; Tabarsi, P.; Ghanavi, J.; Ziazarifi, A. H.; Hoffner, S. E. Emergence of new forms of totally drug-resistant tuberculosis bacilli: Super extensively drug-resistant tuberculosis or totally drug-resistant strains in iran. *Chest* **2009**, *136*, 420–425.

11. Udwadia, Z. F.; Amale, R. A.; Ajbani, K. K.; Rodrigues, C. Totally drug-resistant tuberculosis in India. *Clin. Infect. Dis.* **2012**, *54*, 579–581.

12. CDC. Emergence of *Mycobacterium tuberculosis* with extensive resistance to second-line drugs --- worldwide, 2000--2004. *MMWR* **2006**, *55*, 301–305.

13. Aldrich, C. C.; Boshoff, H. I.; Remmel, R. P. Antitubercular Agents. In *Burger's Medicinal Chemistry, Drug Discovery and Development, 7th Edition*, Abraham, D. J.; Rotella, D. P., Eds. John Wiley and Sons, Inc.: **2010**; pp 713–813.

14. Fox, H. H. The chemical approach to the control of tuberculosis. *Science* **1952**, *116*, 129–134.

15. Nguyen, M.; Claparols, C.; Bernadou, J.; Meunier, B. A fast and efficient metal-mediated oxidation of isoniazid and identification of isoniazid-NAD(H) adducts. *ChemBioChem* **2001**, *2*, 877–883.

16. Vilchéze, C.; Jacobs, W. R., Jr. The mechanism of isoniazid killing: Clarity through the scope of genetics. *Annu. Rev. Microbiol.* **2007**, *61*, 35–50.

17. Rawat, R.; Whitty, A.; Tonge, P. J. The isoniazid-NAD adduct is a slow, tight-binding inhibitor of InhA, the *Mycobacterium tuberculosis* enoyl reductase: Adduct affinity and drug resistance. *Proc. Natl. Acad. Sci. U.S.A.* **2003**, *100*, 13881–13886.

18. Johnson, R.; Streicher, E. M.; Louw, G. E.; Warren, R. M.; Helden, P. D. v.; Victor, T. C. Drug resistance in *Mycobacterium tuberculosis*. *Curr. Issues Mol. Biol.* **2006**, *8*, 97–112.

19. Desta, Z.; Soukhova, N. V.; Flockhart, D. A. Inhibition of cytochrome P450 (CYP450) isoforms by isoniazid: Potent inhibition of CYP2C19 and CYP3A. *Antimicrob. Agents Chemother.* **2001**, *45*, 382–392.

20. Wen, X.; Wang, J.-S.; Neuvonen, P. J.; Backman, J. T. Isoniazid is a mechansim-based inhibitor of cytochrome P_{450} 1A2, 2A6, 2C19 and 3A4 isoforms in human liver microsomes. *Eur. J. Clin. Pharm.* **2002**, *57*, 799–804.

21. Binda, G.; Domenichini, E.; Gottardi, A.; Orlandi, B.; Ortelli, E.; Pacini, B.; Fowst, G. Rifampicin, a general review. *Arzneimittelforschung* **1971**, *21*, 1907–1977.

22. Rifampin. *Tuberculosis* **2008**, *88*, 151–154.

23. Maggi, N.; Arioli, V.; Sensi, P. Rifamycins. XLI. A new class of active semisynthetic rifamycins. N-substituted aminomethyl derivatives of refamycin SV. *J. Med. Chem.* **1965**, *8*, 790–793.

24. Bemer-Melchior, P.; Bryskier, A.; Drugeon, H. B. Comparison of the *in vitro* activities of rifapentine and rifampicin against *Mycobacterium tuberculosis* complex. *J. Antimicrob. Chemother.* **2000**, *46*, 571–575.

25. Wehrli, W.; Knüsel, F.; Schmid, K.; Staehelin, M. Interaction of rifamycin with bacterial RNA polymerase. *Proc. Natl. Acad. Sci. U.S.A.* **1968**, *61*, 667–673.

26. Wehrli, W.; Knüsel, F.; Staehelin, M. Action of rifamycin on RNA-polymerase from sensitive and resistant bacteria. *Biochem. Biophys. Res. Commun.* **1968**, *32*, 284–288.

27. Ramaswamy, S.; Musser, J. M. Molecular genetic basis of antimicrobial agent resistance in *Mycobacterium tuberculosis*: 1998 update. *Tubercle Lung Dis.* **1998**, *79*, 3–29.

28. la Porte, C. J. L.; Colbers, E. P. H.; Bertz, R.; Voncken, D. S.; Wikstrom, K.; Boeree, M. J.; Koopmans, P. P.; Hekster, Y. A.; Burger, D. M. Pharmacokinetics of adjusted-dose lopinavir-ritonavir combined with rifampin in healthy volunteers. *Antimicrob. Agents Chemother.* **2004**, *48*, 1553–1560.

29. Finch, C. K.; Chrisman, C. R.; Baceiwicz, A. M.; Self, T. H. Rifampin and rifabutin drug interactions: An update. *Arch. Intern. Med.* **2002**, *162*, 985–992.

30. Thomas, J. P.; Baughn, C. O.; Wilkinson, R. G.; Shepherd, R. G. A new synthetic compound with antituberculosis activity in mice: Ethambutol (dextro-2,2'-(ethylenediimino)-di-I-butanol). *Am. Rev. Respir. Dis.* **1961**, *83*, 891–893.

31. Lucchesi, M.; Mancini, P. The antimycobacterial activity of ethambutol (ETB). *Antibiot. Chemotherap.* **1970**, *16*, 230–238.

32. Yates, M. D.; Collins, C. H. Sensitivity of opportunist mycobacteria to rifampicin and ethambutol. *Tubercule* **1981**, *62*, 117–121.

33. Takayama, K.; Kilburn, J. O. Inhibition of synthesis of arabinogalactan by ethambutol in *Mycobacterium smegmatis*. *Antimicrob. Agents Chemother.* **1989**, *33*, 1493–1499.

34. Ramaswamy, S. V.; Amin, A. G.; Goksel, S.; Stager, C. E.; Dou, S. J.; El Sahly, H.; Moghazeh, S. L.; Kreiswirth, B. N.; Musser, J. M. Molecular genetic analysis of nucleotide polymorphisms associated with ethambutol resistance in human isolates of *Mycobacterium tuberculosis*. *Antimicrob. Agents Chemother.* **2000**, *44*, 326–336.

35. Shen, X.; Shen, G. M.; Wu, J.; Gui, X. H.; Li, X.; Mei, J.; DeRiemer, K.; Gao, Q. Association between embB codon 306 mutations and drug resistance in *Mycobacterium tuberculosis*. *Antimicrob. Agents Chemother.* **2007**, *51*, 2618–2620.

36. Leibold, J. E. The ocular toxicity of ethambutol and its relation to dose. *Ann. N. Y. Acad. Sci.* **1966**, *135*, 683–1120.

37. Kushner, S.; Dalalian, H.; Sanjurjo, J. L.; F. L. Bach, J.; Safir, S. R.; V. K. Smith, J.; Williams, J. H. Experimental chemotherapy of tuberculosis. II. The synthesis of pyrazinamides and related compounds. *J. Am. Chem. Soc.* **1952**, *74*, 3617–3621.

38. Solotorovsky, M.; Gregory, F. J.; Ironson, E. J.; Bugie, E. J.; Oneill, R. C.; Pfister, K. Pyrazinoic acid amide-An agent active against experimental murine tuberculosis. *Soc. Exp. Biol. Med. Proc.* **1952**, *79*, 563–565.

39. Stottmeier, K. D.; Beam, R. E.; Kubica, G. P. Determination of drug susceptibility of mycobacteria to pyrazinamide in 7H10 agar. *Am. Rev. Respir. Dis.* **1967**, *96*, 1072–1075.

40. Konno, K.; Feldmann, F. M.; McDermott, W. Pyrazinamide susceptibility and admidase activity of tubercle bacilli. *Am. Rev. Respir. Dis.* **1967**, *95*, 461–469.

41. Zhang, Y.; Scorpio, A.; Nikaido, H.; Sun, Z. Role of acid pH and deficient efflux of pyrazinoic acid in unique susceptibility of *Mycobacterium tuberculosis* to pyrazinamide. *J. Bacteriol.* **1999**, *181*, 2044–2049.

42. Scorpio, A.; Lindholm-Levy, P.; Heifets, L.; Gilman, R.; Siddiqi, S.; Cynamon, M.; Zhang, Y. Characterization of *pncA* mutations in pyrazinamide-resistant *Mycobacterium tuberculosis*. *Antimicrob. Agents Chemother.* **1997**, *41*, 540–543.

43. Shi, W.; Zhang, X.; Jian, X.; Yuan, H.; Lee, J. S.; Barry, C. E. 3rd; Wang, H.; Zhang, W.; Zhang, Y. Pyrazinamide inhibits trans-translocation in *Mycobacterium tuberculosis*. *Science* **2011**, *333*, 1630–1632.

44. Zierski, M.; Bek, E. Side-effects of drug regimens used in short-course chemotherapy for pulmonary tuberculosis. A controlled clinical study. *Tubercle* **1980**, *61*, 41–49.

45. Chang, K. C.; Leung, C. C.; Yew, W. W.; Lau, T. Y.; Tam, C. M. Hepatotoxicity of pyrazinamide: cohort and case-control analyses. *Am. J. Respir. Crit. Care Med.* **2008**, *177*, 1391–1396.

46. Andries, K.; Verhasselt, P.; Guillemont, J.; Gohlmann, H. W.; Neefs, J. M.; Winkler, H.; Van Gestel, J.; Timmerman, P.; Zhu, M.; Lee, E.; Williams, P.; de Chaffoy, D.; Huitric, E.; Hoffner, S.; Cambau, E.; Truffot-Pernot, C.; Lounis, N.; Jarlier, V. A diarylquinoline drug active on the ATP synthase of *Mycobacterium tuberculosis*. *Science* **2005**, *307*, 223–237.

47. Huitric, E.; Verhasselt, P.; Koul, A.; Andries, K.; Hoffner, S.; Andersson, D. I. Rates and mechanisms of resistance development in *Mycobacterium tuberculosis* to a novel diarylquinoline ATP synthase inhibitor. *Antimicrob. Agents Chemother.* **2010**, *54*, 1022–1028.

48. Cohen, J. Approval of novel TB drug celebrated-with restraint. *Science* **2013**, *339*, 130.

49. Koul, A.; Dendouga, N.; Vergauwen, K.; Molenberghs, B.; Vranckx, L.; Willebrords, R.; Ristic, Z.; Lill, H.; Dorange, I.; Guillemont, J.; Bald, D.; Andries, K. Diarylquinolines target subunit c of mycobacterial ATP synthase. *Nat. Chem. Biol.* **2007**, *3*, 323–324.

50. Diacon, A. H.; Pym, A.; Grobusch, M.; Patientia, R.; Rustomjee, R.; Page-Shipp, L.; Pistorius, C.; Krause, R.; Bogoshi, M.; Churchyard, G.; Venter, A.; Allen, J.; Palomino, J. C.; DeMarez, T.; Heeswijk, R. P. G. v.; Lounis, N.; Meyvisch, P.; Verbeeck, J.; Parys, W.; Beule, K. d.; Andries, K.; McNeeley, D. F. The diarylquinoline TMC207 for multidrug-resistant tuberculosis. *N. Engl. J. Med.* **2009**, *360*, 2397–2405.

51. Russell, D. G.; Barry, C. E., 3rd; Flynn, J. L. Tuberculosis: What we don't know can, and does, hurt us. *Science* **2010**, *328*, 852–856.

52. Tsai, M. C.; Chakravarty, S.; Zhu, G.; Xu, J.; Tanaka, K.; Koch, C.; Tufariello, J.; Flynn, J.; Chan, J. Characterization of the tuberculous granuloma in murine and human lungs: Cellular composition and relative tissue oxygen tension. *Cell. Microbiol.* **2006**, *8*, 218–232.

53. Lin, P. L.; Pawar, S.; Myers, A.; Pegu, A.; Fuhrman, C.; Reinhart, T. A.; Capuano, S. V.; Klein, E.; Flynn, J. L. Early events in *Mycobacterium tuberculosis* infection in cynomolgus macaques. *Infect. Immun.* **2006**, *74*, 3790–3803.

54. Barry, C. E., 3rd; Boshoff, H. I.; Dartois, V.; Dick, T.; Ehrt, S.; Flynn, J.; Schnappinger, D.; Wilkinson, R. J.; Young, D. The spectrum of latent tuberculosis: Rethinking the biology and intervention strategies. *Nat. Rev. Microbiol.* **2009**, *7*, 845–855.

55. Kaplan, G.; Post, F. A.; Moreira, A. L.; Wainwright, H.; Kreiswirth, B. N.; Tanverdi, M.; Mathema, B.; Ramaswamy, S. V.; Walther, G.; Steyn, L. M.; Barry, C. E.; Bekker, L. G. *Mycobacterium tuberculosis* growth at the cavity surface: a microenvironment with failed immunity. *Infect. Immun.* **2003**, *71*, 7099–7108.

56. Dannenberg, A. M. J. Pathogenesis of pulmonary *Mycobacterium bovus* infection: Basic principles established by the rabbit model. *Tuberculosis (Edinb)* **2001**, *81*, 87–96.

57. MacMicking, J. D.; Taylor, G. A.; McKinney, J. D. Immune control of tuberculosis by IFN-gamma-inducible LRG-47. *Science* **2003**, *302*, 654–659.

58. Voskuil, M. I.; Viconti, K. C.; Schoolnik, G. K. *Mycobacterium tuberculosis* gene expression during adaptation to stationary phase and low-oxygen dormancy. *Tuberculosis* **2004**, *84*, 218–227.

59. Gutierrez, M. G.; Master, S. S.; Singh, S. B.; Taylor, G. A.; Colombo, M. I.; Deretic, V. Autophagy is a defense mechanism inhibiting BCG and *Mycobacterium tuberculosis* survival in infected macrophages. *Cell* **2004**, *119*, 753–766.

60. Alonso, S.; Pethe, K.; Russell, D. G.; Purdy, G. E. Lysosomal killing of *Mycobacterium* mediated by ubiquitin-derived peptides is enhanced by autophagy. *Proc. Natl. Acad. Sci. U.S.A.* **2007**, *104*, 6031–6036.

61. Via, L. E.; Lin, P. L.; Ray, S. M.; Carrillo, J.; Allen, S. S.; Eum, S. Y.; Taylor, K.; Klein, E.; Manjunatha, U.; Gonzales, J.; Lee, E. G.; Park, S. K.; Raleigh, J. A.; Cho, S. N.; McMurray, D. N.; Flynn, J. L.; Barry, C. E., 3rd. Tuberculous granulomas are hypoxic in guinea pigs, rabbits, and nonhuman primates. *Infect. Immun.* **2008**, *76*, 2333–2340.

62. Keane, J.; Gershon, S.; Wise, R. P.; Mirabile-Levens, E.; Kasznica, J.; Schwieterman, W. D.; Siegel, J. N.; Braun, M. M. Tuberculosis associated with infliximab, a tumor necrosis factor α-neutralizing agent. *N. Engl. J. Med.* **2001**, *345*, 1098–1104.

63. Mohan, A. K.; Coté, T. R.; Block, J. A.; Manadan, A. M.; Siegel, J. N.; Braun, M. M. Tuberculosis following the use of etanercept, a tumor necrosis factor inhibitor. *Clin. Infect. Dis.* **2004**, *39*, 295–299.

64. Ulrichs, T.; Kosmiadi, G. A.; Jõrg, S.; Pradl, L.; Titukhina, M.; Mishenko, V.; Gushina, N.; Kaufmann, S. H. E. Differential organization of the local immune

response in patients with active cavitary tuberculosis or with nonprogressive tuberculoma. *J. Infect. Dis.* **2005**, *192*, 89–97.

65. Sams-Dodd, F. Target-based drug discovery: Is something wrong? *Drug Discovery Today* **2005**, *10*, 139–147.

66. Monaghan, R. L.; Barrett, J. F. Antibacterial drug discovery--Then, now and the genomics future. *Biochem. Pharmacol.* **2006**, *71*, 901–909.

67. Sassetti, C. M.; Boyd, D. H.; Rubin, E. J. Comprehensive identification of conditionally essential genes in mycobacteria. *Proc. Natl. Acad. Sci. U.S.A.* **2001**, *98*, 12712–12717.

68. Sassetti, C. M.; Rubin, E. J. Genetic requirements for mycobacterial survival during infection. *Proc. Natl. Acad. Sci. U.S.A.* **2003**, *100*, 12989–12994.

69. Mei, J.-M.; Nourbakhsh, F.; Ford, C. W.; Holden, D. W. Identification of *Staphylococcus aureus* virulence genes in a murine model of bacteraemia using signature-tagged mutagenesis. *Mol. Microbiol.* **1997**, *26*, 399–407.

70. Chiang, S. L.; Mekalanos, J. J.; Holden, D. W. In vivo genetic analysis of bacterial virulence. *Ann. Rev. Micrbiol.* **1999**, *53*, 129–154.

71. Smith, V.; Botstein, D.; Brown, P. O. Genetic footprinting: A genomic strategy for determining a gene's function given its sequence. *Proc. Natl. Acad. Sci. U.S.A.* **1995**, *92*, 6479–6483.

72. Akerley, B. J.; Rubin, E. J.; Camilli, A.; Lampe, D. J.; Robertson, H. M.; Mekalanos, J. J. Systematic identification of essential genes by *in vitro mariner* mutagenesis. *Proc. Natl. Acad. Sci. U.S.A.* **1998**, *95*, 8927–8932.

73. Woong Park, S.; Klotzsche, M.; Wilson, D. J.; Boshoff, H. I.; Eoh, H.; Manjunatha, U.; Blumenthal, A.; Rhee, K.; Barry, C. E., 3rd; Aldrich, C. C.; Ehrt, S.; Schnappinger, D. Evaluating the sensitivity of *Mycobacterium tuberculosis* to biotin deprivation using regulated gene expression. *PLoS Pathog.* **2011**, *7*, e1002264.

74. Baek, S.-H.; Li, A. H.; Sassetti, C. M. Metabolic regulation of mycobacterial growth and antibiotic sensitivity. *PLoS Biol.* **2011**, *9*, e1001065.

75. Duckworth, B. P.; Nelson, K. M.; Aldrich, C. C. Adenylating enzymes in *Mycobacterium tuberculosis* as drug targets. *Curr. Top. Med. Chem.* **2012**, *12*, 766–796.

76. Reynolds, R. C.; Ananthan, S.; Faaleolea, E.; Hobrath, J. V.; Kwong, C. D.; Maddox, C.; Rasmussen, L.; Sosa, M. I.; Thammasuvimol, E.; White, E. L.; Zhang, W.; John A. Secrist, I. High throughput screening of a library based on kinase inhibitor scaffolds against *Mycobacterium tuberculosis* H37Rv. *Tuberculosis* **2012**, *92*, 72–83.

77. Abrahams, G. L.; Kumar, A.; Savvi, S.; Hung, A. W.; Wen, S.; Abell, C.; Barry, C. E., 3rd; Sherman, D. R.; Boshoff, H. I.; Mizrahi, V. Pathway-selective sensitization of *Mycobacterium tuberculosis* for target-based whole-cell screening. *Chem. Biol.* **2012**, *19*, 844–854.

78. Coxon, G. D.; Cooper, C. B.; Gillespie, S. H.; McHugh, T. D. Strategies and challenges involved in the discovery of new chemical entities during early-stage tuberculosis drug discovery. *J. Infect. Dis.* **2012**, *205 Suppl. 2*, S258–S264.

79. Kumar, M.; Vijayakrishnan, R.; Subba Rao, G. In silico structure-based design of a novel class of potent and selective small peptide inhibitor of *Mycobacterium tuberculosis* dihydrofolate reductase, a potential target for anti-TB drug discovery. *Mol. Divers.* **2010**, *14*, 595–604.

80. Kumar, M.; Verma, S.; Sharma, S.; Srinivasan, A.; Singh, T. P.; Kaur, P. Structure-based in silico design of a high-affinity dipeptide inhibitor for novel protein drug target shikimate kinase of *Mycobacterium tuberculosis*. *Chem. Biol. Drug Des.* **2010**, *76*, 277–284.

81. White, E. L.; Ross, L. J.; Cunningham, A.; Escuyer, V. Cloning, expression, and characterization of *Mycobacterium tuberculosis* dihydrofolate reductase. *FEMS Microbiol. Lett.* **2004**, *232*, 101–105.

82. Parish, T.; Stoker, N. G. The common aromatic amino acid biosynthesis pathway is essential in *Mycobacterium tuberculosis*. *Microbiology (Reading, U.K.)* **2002**, *148*, 3069–3077.

83. Ciulli, A.; Abell, C. Fragment-based approaches to enzyme inhibition. *Curr. Opin. Biotechnol.* **2007**, *18*, 489–496.

84. Hung, A. W.; Silvestre, H. L.; Wen, S.; Ciulli, A.; Blundell, T. L.; Abell, C. Application of fragment growing and fragment linking to the discovery of inhibitors of *Mycobacterium tuberculosis* pantothenate synthetase. *Angew. Chem. Int. Ed. Engl.* **2009**, *48*, 8452–8456.

85. Schnackenberg, L. K.; Jones, R. C.; Thyparambil, S.; Taylor, J. T.; Han, T.; Tong, W.; Hansen, D. K.; Fuscoe, J. C.; Edmondson, R. D.; Beger, R. D.; Dragan, Y. P. An integrated study of acute effects of valproic acid in the liver using

metabonomics, proteomics, and transcriptomics platforms. *OMICS* **2006**, *10*, 1–14.

86. Chen, S. An "omics" approach to determine the mechanisms of acquired aromatase inhibitor resistance. *OMICS* **2011**, *15*, 347–352.

87. Debnath, M.; Pandey, M.; Bisen, P. S. An omics approach to understand the plant abiotic stress. *OMICS* **2011**, *15*, 739–762.

88. Biomarkers Definitions Working Group. Biomarkers and surrogate endpoints: Preferred definitions and conceptual framework. *Clin. Pharmacol. Ther.* **2001**, *69*, 89–95.

89. Parida, S. K.; Kaufmann, S. H. The quest for biomarkers in tuberculosis. *Drug Discovery Today* **2010**, *15*, 148–157.

90. Ryals, J. Metabolomics - An important emerging science. In *Drug Discovery: Business Briefing. PharmaTech 2004*, Boulton, E., Ed. Business Briefings Ltd: **2004**; pp 51–54.

91. du Preez, I.; Loots du, T. Altered fatty acid metabolism due to rifampicin-resistance conferring mutations in the rpoB Gene of *Mycobacterium tuberculosis*: mapping the potential of pharmaco-metabolomics for global health and personalized medicine. *OMICS* **2012**, *16*, 596–603.

92. Kohanski, M. A.; Dwyer, D. J.; Hayete, B.; Lawrence, C. A.; Collins, J. J. A common mechanism of cellular death induced by bactericidal antibiotics. *Cell* **2007**, *130*, 797–810.

93. Villemagne, B.; Crauste, C.; Flipo, M.; Baulard, A. R.; Deprez, B.; Willand, N. Tuberculosis: the drug development pipeline at a glance. *Eur. J. Med. Chem.* **2012**, *51*, 1–16.

94. Kohanski, M. A.; Dwyer, D. J.; Wierzbowski, J.; Cottarel, G.; Collins, J. J. Mistranslation of membrane proteins and two-component system activation trigger antibiotic-mediated cell death. *Cell* **2008**, *135*, 679–690.

95. Dwyer, D. J.; Kohanski, M. A.; Collins, J. J. Role of reactive oxygen species in antibiotic action and resistance. *Curr. Opin. Microbiol.* **2009**, *12*, 482–489.

96. Kohanski, M. A.; DePristo, M. A.; Collins, J. J. Sublethal antibiotic treatment leads to multidrug resistance via radical-induced mutagenesis. *Mol. Cell.* **2010**, *37*, 311–320.

97. Kohanski, M. A.; Dwyer, D. J.; Collins, J. J. How antibiotics kill bacteria: From targets to networks. *Nat. Rev. Microbiol.* **2010**, *8*, 423–435.

98. Foti, J. J.; Devadoss, B.; Winkler, J. A.; Collins, J. J.; Walker, G. C. Oxidation of the guanine nucleotide pool underlies cell death by bactericidal antibiotics. *Science* **2012**, *336*, 315–319.

99. Wright, G. D. The antibiotic resistome: The nexus of chemical and genetic diversity. *Nat. Rev. Microbiol.* **2007**, *5*, 175–186.

100. Liu, Y.; Imlay, J. A. Cell death from antibiotics without the involvement of reactive oxygen species. *Science* **2013**, *339*, 1210–1213.

101. Keren, I.; Wu, Y.; Inocencio, J.; Mulcahy, L. R.; Lewis, K. Killing by bactericidal antibiotics does not depend on reactive oxygen species. *Science* **2013**, *339*, 1213–1216.

102. Grumbach, F. Experimental antituberculous activity of certain isonicotinic thioamides substituted on the nucleus. *C. R. Hebd. Seances Acad. Sci.* **1956**, *242*, 2187–2189.

103. Wang, F.; Langley, R.; Gulten, G.; Dover, L. G.; Besra, G. S.; Jacobs, W. R., Jr.; Sacchettini, J. C. Mechanism of thioamide drug action against tuberculosis and leprosy. *J. Exp. Med.* **2007**, *204*, 73–78.

104. Nagarajan, K.; Shankar, R. G.; Rajappa, S.; Shenoy, S. J.; Costa-Pereira, R. Nitroimidazoles XXI 2,3-dihydro-6-nitroimidazo [2,1-*b*] oxazoles with antitubercular activity. *Eur. J. Med. Chem.* **1989**, *24*, 631–633.

105. Singh, R.; Manjunatha, U.; Boshoff, H. I. M.; Ha, Y. H.; Niyomrattanakit, P.; Ledwidge, R.; Dowd, C. S.; Lee, I. Y.; Kim, P.; Zhang, L.; Kang, S.; Keller, T. H.; Jiricek, J.; Barry, C. E. 3rd. PA-824 kills nonreplicating *Mycobacterium tuberculosis* by intracellular NO release. *Science* **2008**, *322*, 1392–1395.

106. Stover, C. K.; Warrener, P.; VanDevanter, D. R.; Sherman, D. R.; Arain, T. M.; Langhorne, M. H.; Anderson, S. W.; Towell, J. A.; Yuan, Y.; McMurray, D. N.; Krelswirth, B. N.; Barry, C. E. 3rd; Baker, W. R. A small-molecule nitroimidazopyran drug candidate for the treatment of tuberculosis. *Nature* **2000**, *405*, 962–966.

107. Anderson, R. F.; Shinde, S. S.; Maroz, A.; Boyd, M.; Palmer, B. D.; Denny, W. A. Intermediates in the reduction of the antituberculosis drug PA-824, (6S)-2-nitro-6-{[4-(trifluoromethoxy)benzyl]oxy}-6,7-dihydro-5H-imidazo[2,1-b][1, 3]oxazine, in aqueous solution. *Org. Biomol. Chem.* **2008**, *6*, 1973–1980.

108. E.; Daniels, L.; Dick, T.; Pang, S. S.; Barry, C. E., 3rd. Identification of a nitroimidazo-oxazine-specific protein involved in PA-824 resistance in *Mycobacterium tuberculosis*. *Proc. Natl. Acad. Sci. U.S.A.* **2006**, *103*, 431–436.

109. OPC-67683. *Tuberculosis (Edinb)* **2008**, *88*, 2.

110. Grosset, J. H.; Singer, T. G.; Bishai, W. R. New drugs for the treatment of tuberculosis: hope and reality. *Int. J. Tuberc. Lung Dis.* **2012**, *16*, 1005–1014.

111. Makarov, V.; Manina, G.; Mikusova, K.; Mollmann, U.; Ryabova, O.; Saint-Joanis, B.; Dhar, N.; Pasca, M. R.; Buroni, S.; Lucarelli, A. P.; Milano, A.; De Rossi, E.; Belanova, M.; Bobovska, A.; Dianiskova, P.; Kordulakova, J.; Sala, C.; Fullam, E.; Schneider, P.; McKinney, J. D.; Brodin, P.; Christophe, T.; Waddell, S.; Butcher, P.; Albrethsen, J.; Rosenkrands, I.; Brosch, R.; Nandi, V.; Bharath, S.; Gaonkar, S.; Shandil, R. K.; Balasubramanian, V.; Balganesh, T.; Tyagi, S.; Grosset, J.; Riccardi, G.; Cole, S. T. Benzothiazinones kill *Mycobacterium tuberculosis* by blocking arabinan synthesis. *Science* **2009**, *324*, 801–804.

112. Trefzer, C.; Rengifo-Gonzalez, M.; Hinner, M. J.; Schneider, P.; Makarov, V.; Cole, S. T.; Johnsson, K. Benzothiazinones: prodrugs that covalently modify the decaprenylphosphoryl-b-D-ribose 2'-epimerase DprE1 of *Mycobacterium tuberculosis*. *J. Am. Chem. Soc.* **2010**, *132*, 13663–13665.

113. Flynn, J. L. Lessons from experimental *Mycobacterium tuberculosis* infections. *Microbes Infect.* **2006**, *8*, 1179–1188.

114. Patel, K.; Jhamb, S. S.; Singh, P. P. Models of latent tuberculosis: Their salient features, limitations, and development. *J. Lab. Physicians* **2011**, *3*, 75–79

.

115. Kaushal, D.; Mehra, S.; Didier, P. J.; Lackner, A. A. The non-human primate model of tuberculosis. *J. Med. Primatol.* **2012**, *41*, 191–201.

116. Altaf, M.; Miller, C. H.; Bellows, D. S.; O'Toole, R. Evaluation of the *Mycobacterium smegmatis* and BCG models for the discovery of *Mycobacterium tuberculosis* inhibitors. *Tuberculosis (Edinb)* **2010**, *90*, 333–337.

117. Reyrat, J.-M.; Kahn, D. *Mycobacterium smegmatis*: An absurd model for tuberculosis? *Trends Microbiol.* **2001**, *9*, 472–473.

118. See also TIGR website: http://www.tigr.org

119. Barry, C. E. 3rd. *Mycobacterium smegmatis*: An absurd model for tuberculosis? A response. *Trends Microbiol.* **2001**, *9*, 473–474.

120. Beamer, G. L.; Turner, J. Murine models of susceptibility to tuberculosis. *Arch. Immunol. Ther. Exp. (Warsz)* **2005**, *53*, 469–483.

121. Lin, P. L.; Rodgers, M.; Smith, L.; Bigbee, M.; Myers, A.; Bigbee, C.; Chiosea, I.; Capuano, S. V.; Fuhrman, C.; Klein, E.; Flynn, J. L. Quantitative comparison of active and latent tuberculosis in the cynomolgus macaque model. *Infect. Immun.* **2009**, *77*, 4631–4642.

122. Hollingshead, M. G.; Alley, M. C.; Camalier, R. F.; Abbott, B. J.; Mayo, J. G.; Malspeis, L.; Grever, M. R. In vivo cultivation of tumor cells in hollow fibers. *Life Sci.* **1995**, *57*, 131–141.

123. Drusano, G. L.; Sgambati, N.; Eichas, A.; Brown, D.; Kulawy, R.; Louie, A. Effect of administration of moxifloxacin plus rifampin against *Mycobacterium tuberculosis* for 7 of 7 days versus 5 of 7 days in an in vitro pharmacodynamic system. *mBio* **2011**, *2*, e00108–e00111.

124. Wayne, L. G.; Hayes, L. G. An in vitro model for sequential study of shiftdown of *Mycobacterium tuberculosis* through two stages of nonreplicating persistance. *Infect. Immun.* **1996**, *64*, 2062–2069.

Chapter 2. Synthesis of Adenylation Inhibitors as Antitubercular Agents and Evaluation of Their Oral Bioavailability in a Rodent Model

The following chapter is original work designed by Kathryn M. Nelson and Dr. Courtney C. Aldrich. The organic synthesis and animal dosing, blood draws, and sample work-up was performed by KMN, with minimal assistance from Dr. Kishore Viswanathan. LC–MS/MS analysis was performed by Dr. Benjamin Duckworth, with data interpretation by KMN and Dr. Duckworth. The enzymatic binding constants were determined by Daniel Wilson or Dr. Viswanathan. The MIC data against *Mycobacterium tuberculosis* were determined by Dr. Helena I. Boshoff of the National Institutes of Health. All previously published figures are appropriately cited. Plasma stability assays were performed by Dr. Duckworth, with data analysis shared by Dr. Duckworth and KMN. Simulated gastric fluid assays were performed and analyzed by KMN.

2.1 Introduction

2.1.1 Siderophore inhibitors as antitubercular agents

There is a dire need for new antitubercular agents that target new mechanisms of action. Iron is an essential micronutrient for almost all known bacterial organisms, with few notable exceptions including *Borrelia burgdorferi*.[1] The concentration of free iron in

human serum is approximately 10^{-24} M, which is too low to support bacterial colonization and growth.[2] In an effort to overcome this iron limitation, pathogens such as *Mycobacterium tuberculosis* (*Mtb*) synthesize small molecule iron (Fe^{3+}) chelators, termed siderophores, for iron acquisition. Pathways of siderophore biosynthesis, secretion, and re-import are especially important for scavenging iron in limiting environments such as a human host. The inhibition of the biosynthesis of these molecules has emerged as a promising strategy for new drug development.[3–6] *Mtb* biosynthesizes a suite of siderophore structures called the mycobactins and carboxymycobactins, differentiated by the identity of the long chain attached at the central lysine residue in the core structure (**Figure 2.1**). The biosynthetic pathway for mycobactin synthesis in *Mtb* has been shown to be essential for growth and virulence in iron-limiting conditions, making it especially attractive as a drug target.[7]

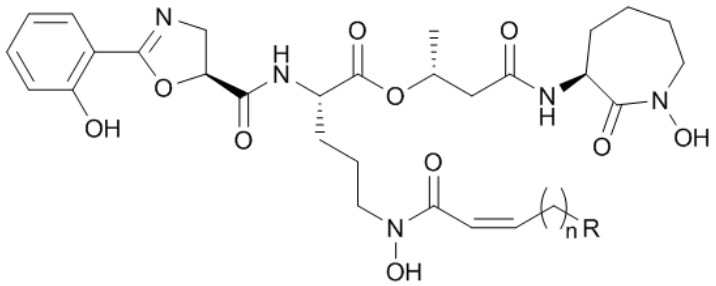

Mycobactins: n = 17, 19; R = CH_3
Carboxymycobactins: n = 2-9; R = COOH

Figure 2.1. Structure of mycobactins and carboxymycobactins in *Mtb*. The central lysine residue contains either a long alkyl or acyl chain depending on the type of siderophore produced.

Several observations have established the necessity of mycobactins for *Mtb* pathogenesis. The targeted genetic inactivation of *mbtB*, a gene involved in the biosynthesis of

mycobactins, resulted in a mutant able to replicate under iron-replete conditions but unable to grow under iron-deficient conditions.[8] A Δ*mbtB Mtb* mutant was attenuated for growth in macrophages and incapable of establishing an infection in an immunocompromised mouse model.[8] Finally, the *in vivo* gene expression profiles of *Mtb* show that the iron-responsive gene *mbtB* is highly upregulated in an infection model.[9] Mycobactins are biosynthesized by a mixed non-ribosomal peptide synthetase-polyketide synthase (NRPS-PKS) assembly line initiated by the adenylating enzyme MbtA (**Figure 2.2**).

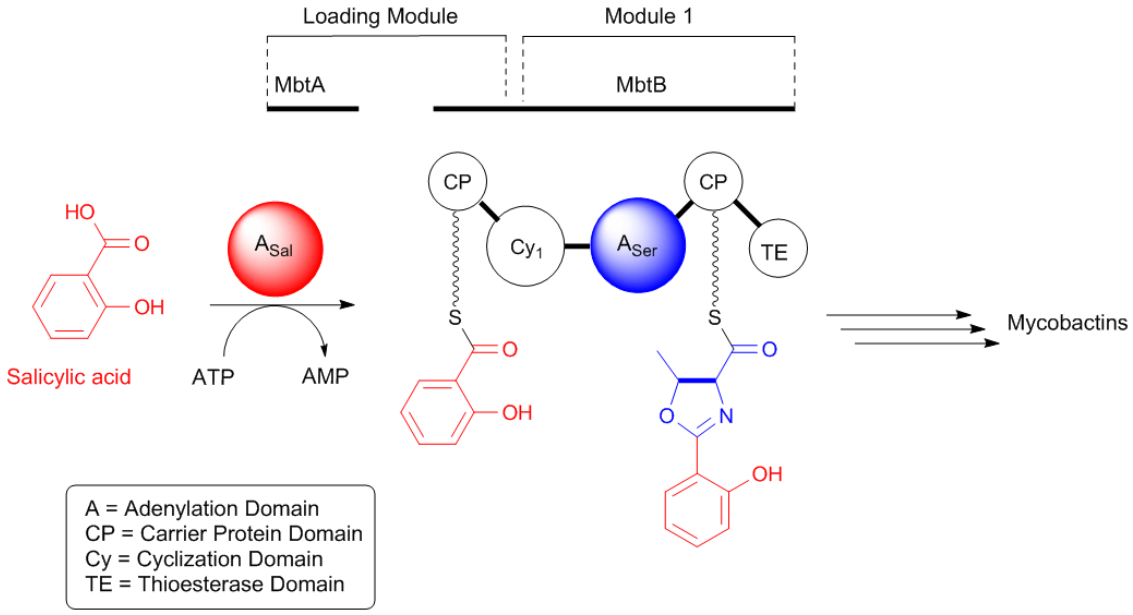

Figure 2.2. MbtA is the first step in the biosynthesis of all mycobactins in *Mtb*, loading the salicylic acid cap to begin the NRPS-PKS biosynthetic pathway.

MbtA activates salicylic acid, to form an acyl-adenylate intermediate, followed by the transfer of the acyl-adenylate onto the *N*-terminal thiolation domain of MbtB. [7,10] Our lab and others have developed a potent nanomolar bisubstrate inhibitor of MbtA, 5′-*O*-[*N*-

(salicyl)sulfamoyl]adenosine (Sal-AMS, **2-1**), as a mimic of the acyl-adenylate intermediate that has impressive antitubercular activity under iron-deficient conditions with a minimum inhibitory concentration (MIC) of 0.39 μM.[3,4,11] The design of this inhibitor takes advantage of both the salicylic acid and ATP binding domains, but replaces the labile acyl phosphate with a more stable isosteric acyl sulfamate (**Figure 2.3**).

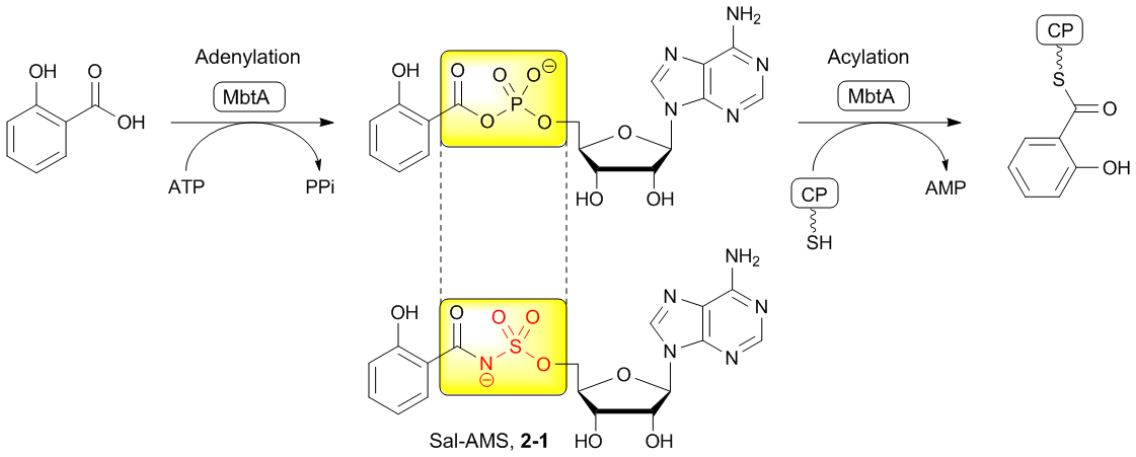

Figure 2.3. Design of 5'-*O*-[*N*-(salicyl)sulfamoyl]adenosine (Sal-AMS,**2-1**). This bisubstrate mimic incorporates a stable acyl sulfamate isotere in replacement of the labile acyl phosphate. Partially adapted from Vannada, et. al.[13]

This compound is the first to have demonstrated selectivity for aryl acid adenylating enzymes (AAAEs) as a class of enzymes, showing potency against enzymes from a number of different bacteria.[3,11,12] Because MbtA is the initiating enzyme in the NRPS-PKS biosynthetic pathway for all mycobactins and carboxymycobactins, this enzyme is a universal target for the inhibition of siderophores in *Mtb*.

2.1.2 Initial evaluation of lead compound Sal-AMS

Our first inhibitor against MbtA, Sal-AMS, has been thoroughly studied *in vitro*. As shown in Table 2.1, Sal-AMS has been shown to be a slow, tight-binding inhibitor against MbtA, with picomolar binding affinity (K_D) and nanomolar activity with respect to the natural substrates (appK_i) (**Table 2.1**).

Table 2.1. Observed and calculated values for enzymatic and whole-cell activity and physicochemical characteristics of Sal-AMS **2-1**.

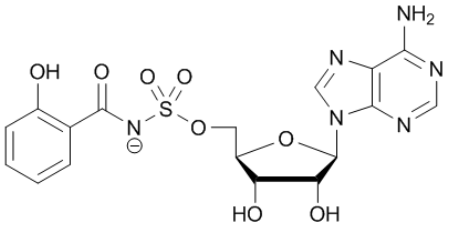

Sal-AMS, **2-1**

Parameter	Value
MbtA appK_i	6.6 nM[4]
MbtA K_D[a]	1 pM[14]
MIC (*Mtb* H37Rv)[b]	0.39 μM[4]
CC50 (Vero cells)[c]	> 100 μM[15]
ClogP[d]	0.29
pK_a[e]	3.0

[a]Confirmed by isothermal titration calorimetry. [b]MIC, the concentration required to achieve no observable growth during assay. [c]Inhibition of cellular growth using an MTT assay and African green monkey *Cercopithecus aethiops* kidney cells (Vero, ATCC). [d]Calculated using ChemBioDraw 13.0 [e]Calculated using MarvinSketch 5.12.3

As such a tight binding inhibitor of MbtA, the residence time (t_R) of Sal-AMS in the active site of the enzyme becomes a substantial factor (**Equations 1, 2**).

$$K_D = \frac{k_{off}}{k_{on}} \quad (\mathbf{1})$$

$$t_R = \frac{1}{k_{off}} \quad (\mathbf{2})$$

From our knowledge of an structurally and functionally homologous adenylating enzyme, EntE, that activates 2, 3-dihydroxybenzoic acid from *E. coli*, we estimate the residence time of Sal-AMS in MbtA to be approximately 36 days.[16] This lengthy residence within the enzyme active site effectively renders the enzyme inert until it is degraded and recycled by the cell. This means that inactivation of MbtA can be achieved at concentrations in serum well above the MIC measured against *Mtb*. Sal-AMS already shows impressive activity against whole-cell *Mtb* in iron limiting conditions at 0.39 μM, relatively close to the activity of isoniazid (INH, 0.1 μM), which is still one of the most potent compounds used against *Mtb* infection today (see Chapter 1 for more discussion of TB therapeutics).

Although this data looks very promising for drug development, we anticipate Sal-AMS to have a low oral bioavailability based on its unfavorable physicochemical properties. While it has become standard practice to evaluate lead drug compounds according to Lipinski's seminal work on drug-like compounds,[17] it has been pointed out by him and others that antibacterial compounds are often exceptions to these rules.[17–19] It is still important to consider, however, the calculated partition coefficient (ClogP, 0.29) and the pK_a of the sulfamate nitrogen (3.0) in Sal-AMS, which indicate that nearly 100% of the compound in solution is in a charged state at physiological pH. With this highly polar, highly charged character, this compound is unlikely to be able to pass easily through cell

membranes, and is likely to be quickly excreted renally. To address these issues, we have examined the structure-activity relationship (SAR) studies previously conducted in the lab. These studies thoroughly and systematically examined the impact of each domain of Sal-AMS on enzyme inhibition of MbtA from *M. tuberculosis* as well as whole-cell antitubercular activity. These SAR studies have explored the aryl,[14] linker,[13,20,21] glycosyl,[12] and nucleobase[15,22] domains (**Figure 2.4**).

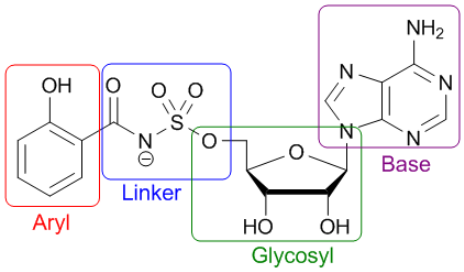

Figure 2.4. Structure-activity relationship domains previously investigated for Sal-AMS, **2-1**.

These results have provided a comprehensive understanding of the minimal structural requirements to maintain enzymatic and whole-cell activity, and have also served to define positions amenable to modification (**Figure 2.5**). We have been able to use this data in our effort to design more pharmacokinetically favorable compounds, while maintaining a high level of activity against our target of interest. The aryl and linker regions are both very intolerant to modification. As shown below, even deviation from a 2-hydroxyl to a 2-amino substitution on the aryl ring (**2-2**) results in a 116-fold loss in enzymatic activity, and a complete loss of *Mtb* growth inhibition. Limited modifications at the 4-position of the aryl ring were tolerated, with a 4-amino substitution (**2-5**)

resulting in a moderate (six-fold) loss in MbtA inhibition, and a four-fold loss in *Mtb* growth inhibition. Changing the linker from a sulfamate (**2-1**) to a sulfamide (**2-6**) modestly improved both enzymatic and whole-cell activity, but any other changes dramatically reduced activity. Modifications at the glycosyl ring were generally tolerated. At least one hydroxyl group appears necessary for activity (**2-11** vs. **2-12** and **2-13**), but the ribose ring can be substituted for a carbocyclic ring with retention of activity (**2-10**). The largest modifications were tolerated in the adenine base. The N^6 position could not be substituted for other heteroatoms (**2-15**), but small alkyl substitutions retained (**2-16**, **2-17**), and even improved (**2-18**) MbtA and *Mtb* inhibition. Molecular dynamics simulations of MbtA revealed plasticity in the nucleobase binding pocket that could allow the binding of Sal-AMS derivatives with large substituents at the C-2 of the purine (**2-20**, **2-21**, **2-22**).[23] 2-Ph-Sal-AMS, **2-20**, was the most potent inhibitor yet identified with an appK_i of 0.27 nM, and exceptionally potent antitubercular activity under iron-deficient conditions at 0.049 μM.[15,22,23]

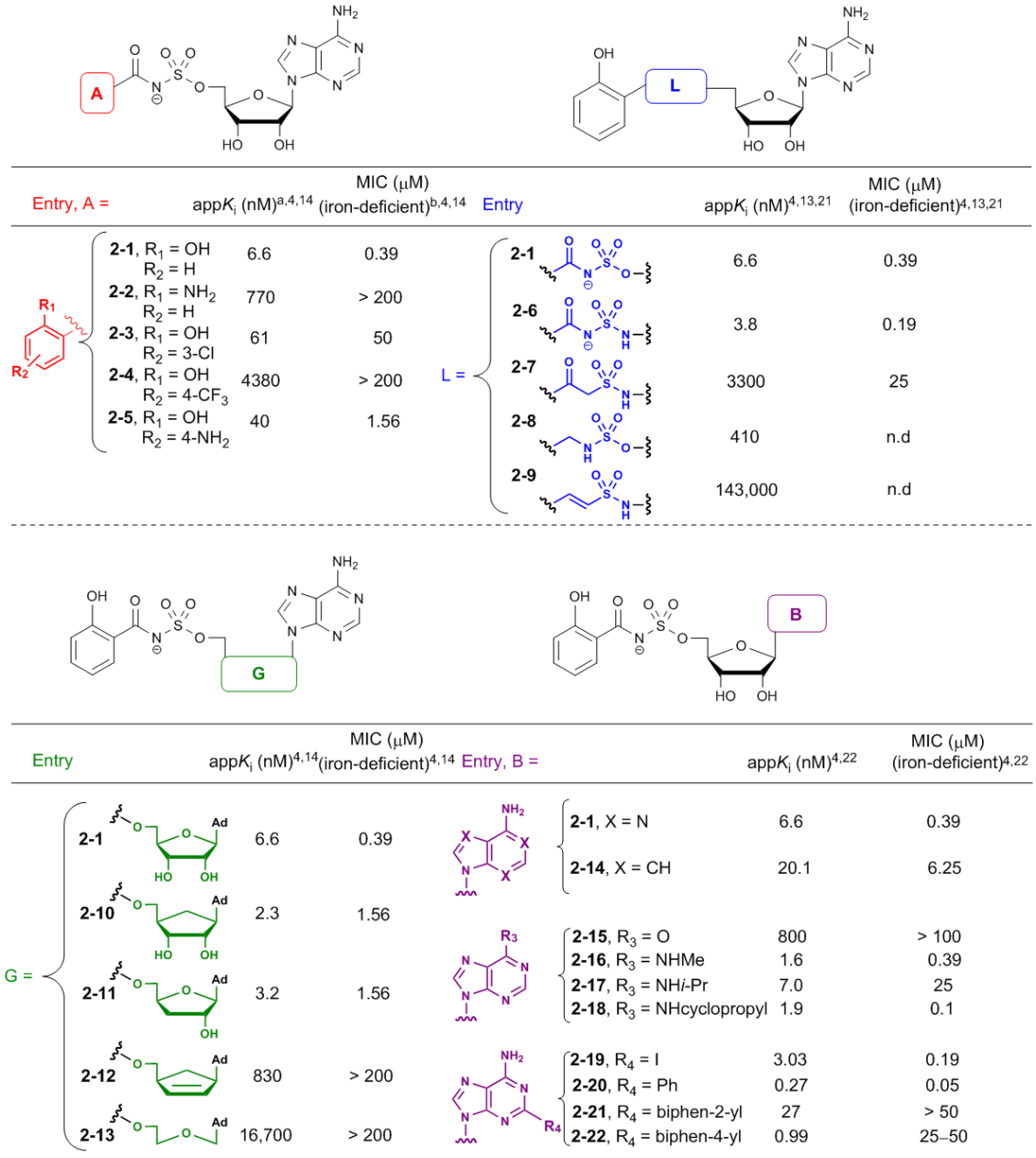

Figure 2.5. Some results of SAR studies on Sal-AMS, **1**. This table contains only representative examples from each study. For more detailed results, see the indicated references within the table. [a]Assay performed by Daniel Wilson, with 7 nM MbtA, 10 mM ATP, 250 μM salicylic acid, 1 mM PPi.[b]Assay performed by Dr. Helena I. Boshoff, grown in normal pH 6.6 glycerol-alanine-salts (GAS) medium without ferric ammonium citrate.

From the SAR studies discussed above, we propose to synthesize new analogues that possess improved pharmacokinetic properties while still maintaining potent enzymatic and antitubercular activity in two different ways (**Figure 2.6**). The first is through modifications predicted to increase the pK_a on the sulfamate nitrogen. Replacing the oxygen in the sulfamate linker with a nitrogen to make a sulfamide linker is predicted to increase the pK_a of the acidic nitrogen by 1-2 units. Addition of an electron donating 4-amino substitution on aryl ring is also calculated to slightly increase the pK_a. These two modifications could potentially increase the pK_a to around 5. In the second approach, we plan to increase the lipophilicity (based on ClogP) of the compound through the addition of aliphatic substitutions and/or small ester prodrugs. Firstly, in a prodrug approach, we could acetylate the 2′, 3′ hydroxyl and phenol groups. This modification should increase the lipophilicity of the compounds relative to Sal-AMS, allowing for permeation through the intestinal wall. Once absorbed into the enterocyte, esterases in the plasma or liver can nonspecifically cleave the acetates to produce the parent compound. Second, addition of small aliphatic groups at the N-6 position of the adenine base and larger aromatic groups at the C-2 position of the base are calculated to increase the ClogP. The most promising substitutions (i.e. N^6-cyclopropyl and C-2 phenyl) will be synthesized and evaluated first, with further analogues being synthesized based on these results.

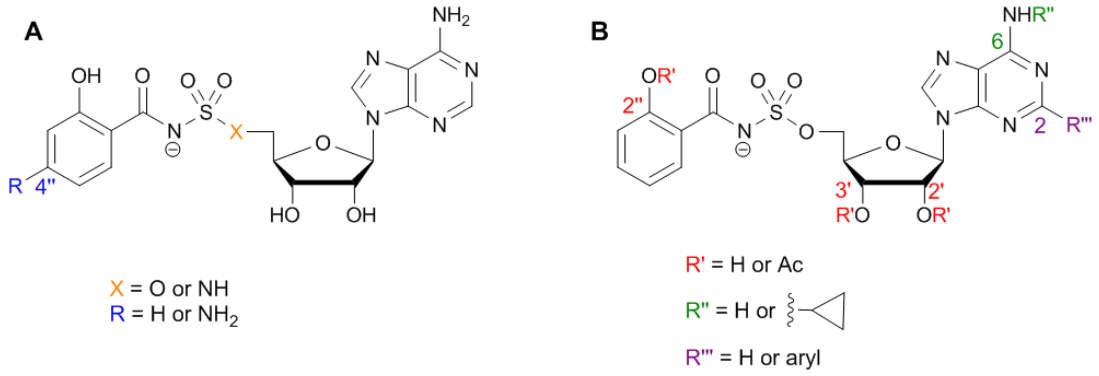

Entry	Modification	pK_a[a]	ClogP[b]	PSA (Ang^2)[a]
1	X = O, R = H	3.03	0.29	209.21
2	X = NH, R = H	4.11	-1.11	212.01
3	X = NH, R = NH_2	4.14	-2.34	238.03
4	R' = Ac	3.02	0.76	227.42
5	R" = 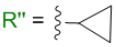	3.04	1.70	195.22
6	R"' = Phenyl	3.03	2.39	209.21

Figure 2.6. Sal-AMS inhibitor design based on results from SAR studies. (**A**) Modifications predicted to increase the pK_a of the sulfamate nitrogen. (**B**) Modifications predicted to increase the ClogP, and thereby increase the lipophilicity of the compounds. [a]Calculated using MarvinSketch 5.12.3. [b]Calculated using ChemBioDraw 13.0.

2.2 Research objectives

The principle aim of this research was to evaluate the siderophore biosynthesis inhibitors in cannulated rats for pharmacokinetic evaluation. This required the synthesis of greater than 30 mg of each final compound and validation of purity. Purity of greater than 98% was achieved by semi-prepartive or preparative reverse-phase high performance liquid chromatography (RP-HPLC) of all final compounds, and analytical purity RP-HPLC prior to administration.

For our initial evaluation of *in vivo* pharmacokinetics, we chose to administer and

observe compound bioavailability in Sprague-Dawley rats. Rats were chosen because of their larger size and ability to complete a single crossover study with one animal. This reduces the potential inter-animal variability seen when using mice (e.g. C57Bl/6), as each time point requires a separately dosed and sacrificed mouse due to the small volume of blood that can be obtained. The results obtained and reported herein will aid in the development of the next generation of compounds that will eventually lead to a preclinical candidate for efficacy studies against *Mtb*.

2.3 Results

2.3.1 Synthesis of Sal-AMS (2-1) and sulfamide linked analogue (2-6)

In order to compare the oral bioavailability of our compounds to the parent, we first had to synthesize a large quantity of Sal-AMS (**2-1**) for these studies. The synthesis of this compound has been reported in our previous publications,[4] however a slightly modified route was developed during this scale-up synthesis (**Scheme 2.1**).

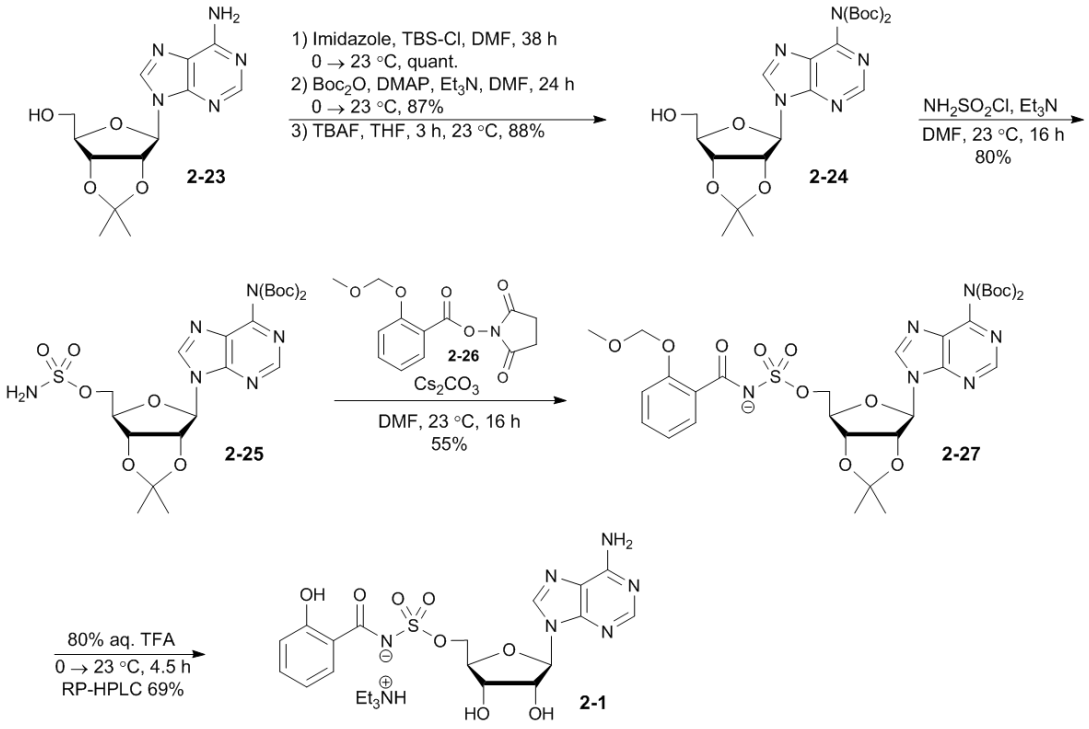

Scheme 2.1. Synthesis of Sal-AMS (**2-1**) using a slightly modified route to what has previously been reported by our lab.[4] See discussion below for improvement in sulfmoylation from **2-24** to **2-25**.

Beginning from the commercially available 2′,3′-*O*-isopropylidene adenosine **2-23**, we first protected the 5′-hydroxyl with *tert*-butyldimethylsilyl chloride (TBSCl) in quantitative yield. Reaction with excess di-*tert*-butyl dicarbonate then led to the N^6-bis-Boc protected intermediate. Deprotection of the 5′-hydroxyl with tetra-*n*-butylammonium fluoride (TBAF) resulted in protected intermediate **2-24**. This three-step process can be scaled up to more than 10 grams with excellent yields. Following production of **2-24**, sulfamoylation was accomplished in DMF with triethylamine as a base.[24] A simple aqueous work-up was often enough to obtain clean product without column chromatography when the N^6 position was protected. Sulfamate **2-25** was coupled with

N-hydroxysuccinimidyl-2-(methoxymethyloxy)benzoate **2-26** in the presence of cesium carbonate to give the penultimate, fully protected Sal-AMS precursor **2-27** in moderate yield. Global deprotection was achieved with 80% aqueous trifluoroacetic acid (TFA). The crude product was then thoroughly dried and immediately purified by RP-HPLC. The final product was a white solid after lyophilization. It was possible to purify Sal-AMS **2-1** by normal phase silica chromatography, however we required > 95% purity for administering these compounds to animals. This purity level was never successfully achieved after normal phase chromatography.

Initial synthesis of the sulfamide linked analogue (**2-6**) was hindered by many protecting group steps that made throughput of intermediates difficult. In response to this challenge, a Mitsunobu reaction was developed by Dr. Paul Sibbald in our lab that successfully installed a protected sulfamide linker in a single step (**Scheme 2.2**). This reaction required precise control of the equivalents of all reagents added in order to be successful. Compounds **2-24** (1.0 equiv) and **2-28** (1.1 equiv) were dissolved with triphenylphosphine (Ph_3P, 1.1 equiv) in THF and cooled to 0 °C. Diisopropyl azodicarboxylate (DIAD, 1.1 equiv) was then added as a solution in THF by syringe pump over 90 minutes. The reaction was stirred at 23 °C for at least 16 hours (longer if scaled up larger than 1.0 g) to give sulfamide **2-29**. Following sulfamide installation, cesium carbonate (Cs_2CO_3) mediated coupling with **2-26** gave **2-30** in moderate yield. Global deprotection with aqueous TFA followed by RP-HPLC resulted in compound **2-6** as the triethylammonium salt. This improved route cut the number of required steps in half (from 6 to 3 beginning from **2-24**) for this synthesis, greatly improving throughput

for this compound.

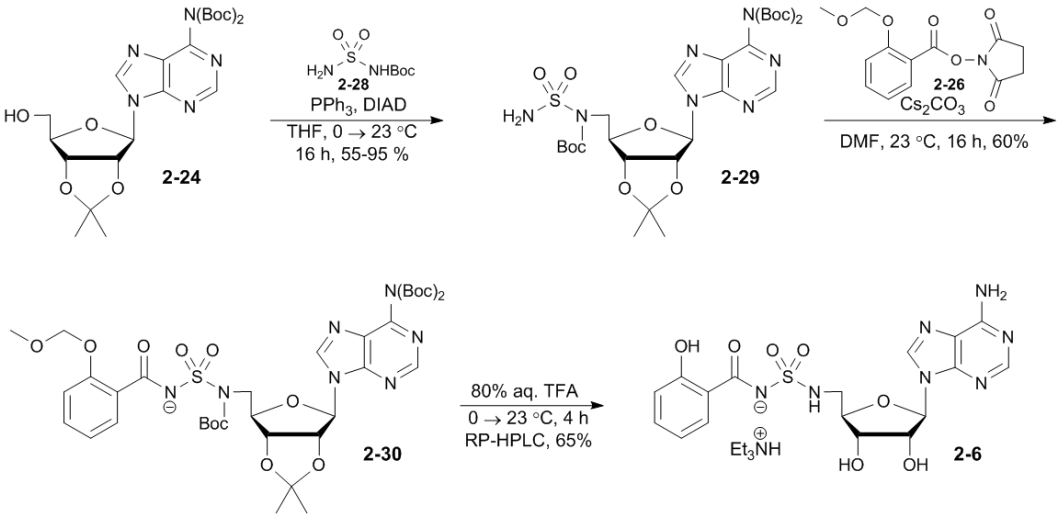

Scheme 2.2. Synthesis of a sulfamide linked analogue of Sal-AMS (**2-6**).

2.3.2 Synthesis of 5′-Amino-5′-deoxy-5′-*N*-[(4-amino-2-hydroxybenzoyl)sulfamoyl]-adenosine (2-34)

The next analogue to be synthesized in this set replaced the sulfamate linker with a sulfamide linker, and added the 4-amino substitution on the aryl ring in an effort to further increase the pK_a of the linker's acidic nitrogen. In analogous fashion to the sulfamide linker synthesis in **Scheme 2.2** above, we began from sulfamide **2-29** (**Scheme 2.3**). A CDI-mediated coupling generated the penultimate protected product **2-33** in moderate yields. Activation of **2-31** with CDI led to a highly activated cyclic anhydride (**2-32**) that was generated *in situ*, then reacted directly with sulfamide **2-29** with catalytic cesium carbonate. A two-step deprotection via catalytic hydrogenolysis followed by

treatment with 80% aqueous TFA afforded the desired nucleoside **2-34**. RP-HPLC purification gave high purity (> 95%) product in moderate yield.

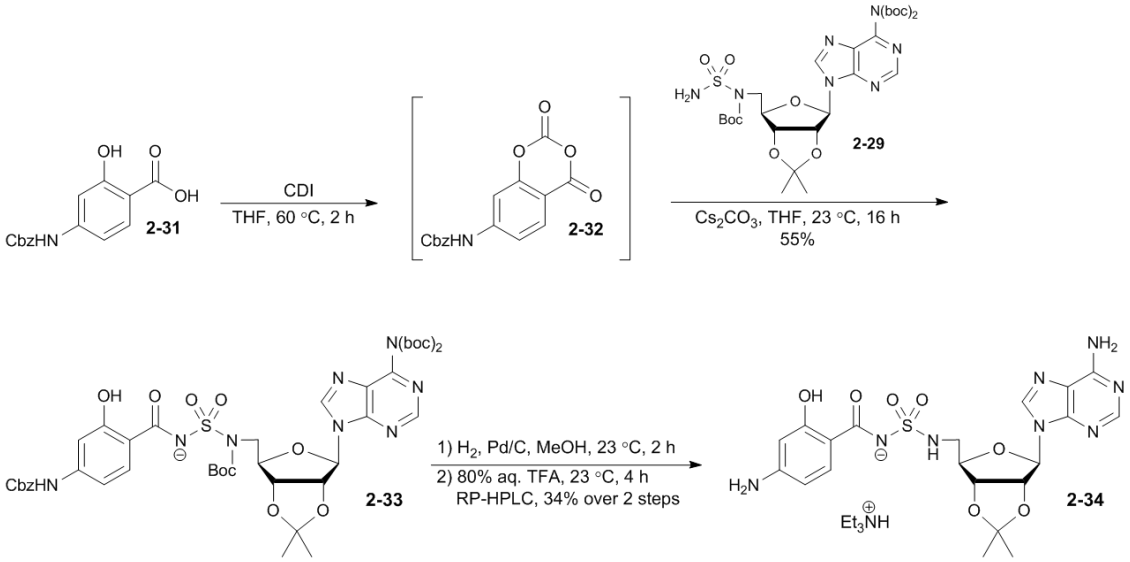

Scheme 2.3. Route for the synthesis of a sulfamide-linked and 4-amino aryl substituted analogue of Sal-AMS (**2-34**).

2.3.3 Synthesis of 5′-Amino-N^6-cyclopropyl-5′-deoxy-5′-*N*-[*N*-(2-hydroxybenzoyl)sulfamoyl]adenosine (2-41)

Our next analogue incorporated both a sulfamide linker in an attempt to raise the pK_a of the acidic nitrogen, and an N^6-cyclopropyl group in an effort to increase the lipophilicity of the compound.

The synthesis began the same as we have previously reported for N^6-substituted Sal-AMS analogues (**Scheme 2.4**).[22] This analogue was completed prior to the development of the Mitsunobu chemistry to directly install the sulfamide linker. Consequently, we first installed an azide at the 5′ position of **2-36** with DPPA as an azido source in a Mitsunobu

reaction,[25] followed by reduction to give the 5′-amino 5′-deoxy intermediate **2-37**. Addition of the sulfamide was achieved in high yield with the dimethylaminopyridinium-activated substrate **2-38** previously described.[26] Deprotection of the carboxybenzyloxy (Cbz) group gave the free sulfamide **2-39** that was then coupled with succinimide **2-26** which gave the penultimate protected intermediate **2-40**. Final deprotection with aqueous TFA led to final compound **2-41**. Initial purification by filtration over a plug of silica gel removed impurities prior to HPLC purification.

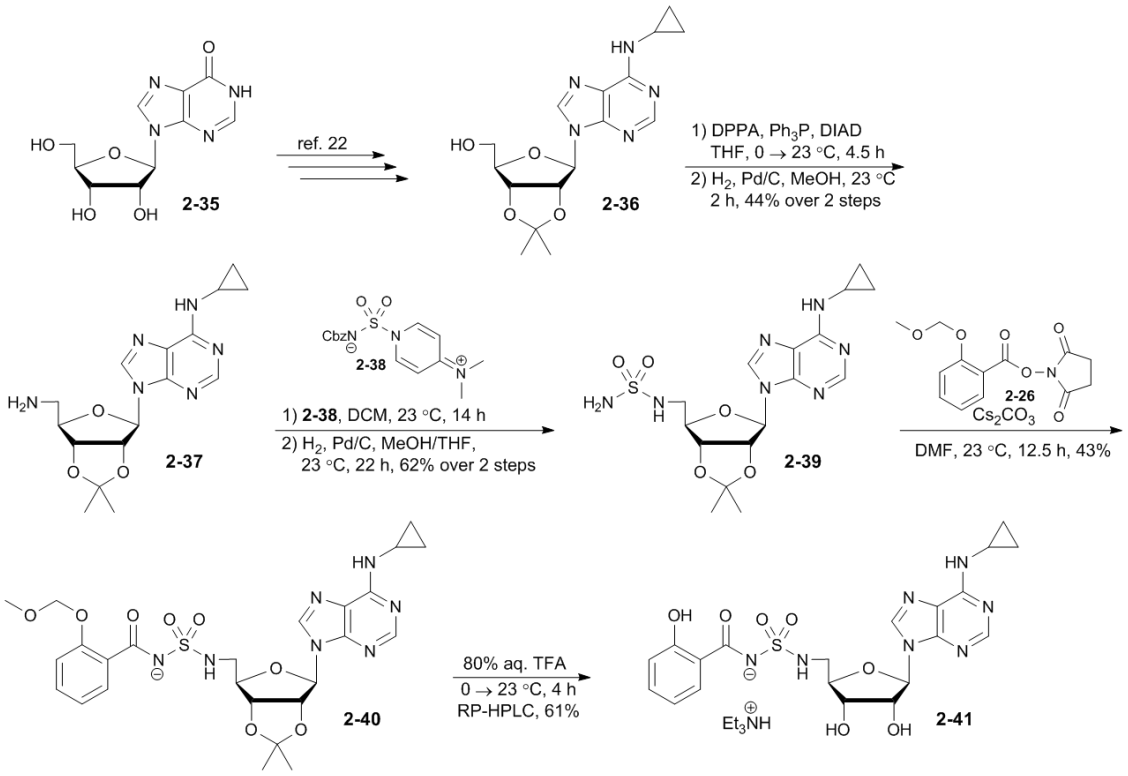

Scheme 2.4. Route for synthesis of N^6-cyclopropyl, sulfamide linked Sal-AMS analogue **2-41**.

2.3.4 Synthesis of 2-Phenyl-N^6-cyclopropyl-5′-*O*-[*N*-(2-hydroxyl)sulfamoyl]adenosine (2-50)

The most lipophilic analogue targeted contains the N^6-cyclopropyl group as well as a C-2 phenyl substitution on the adenine base. Beginning from guanosine, chemistry elegantly described by Matsuda and co-workers provided the N^6-chloro-2-iodo intermediate **2-43** (**Scheme 2.5**).[27]

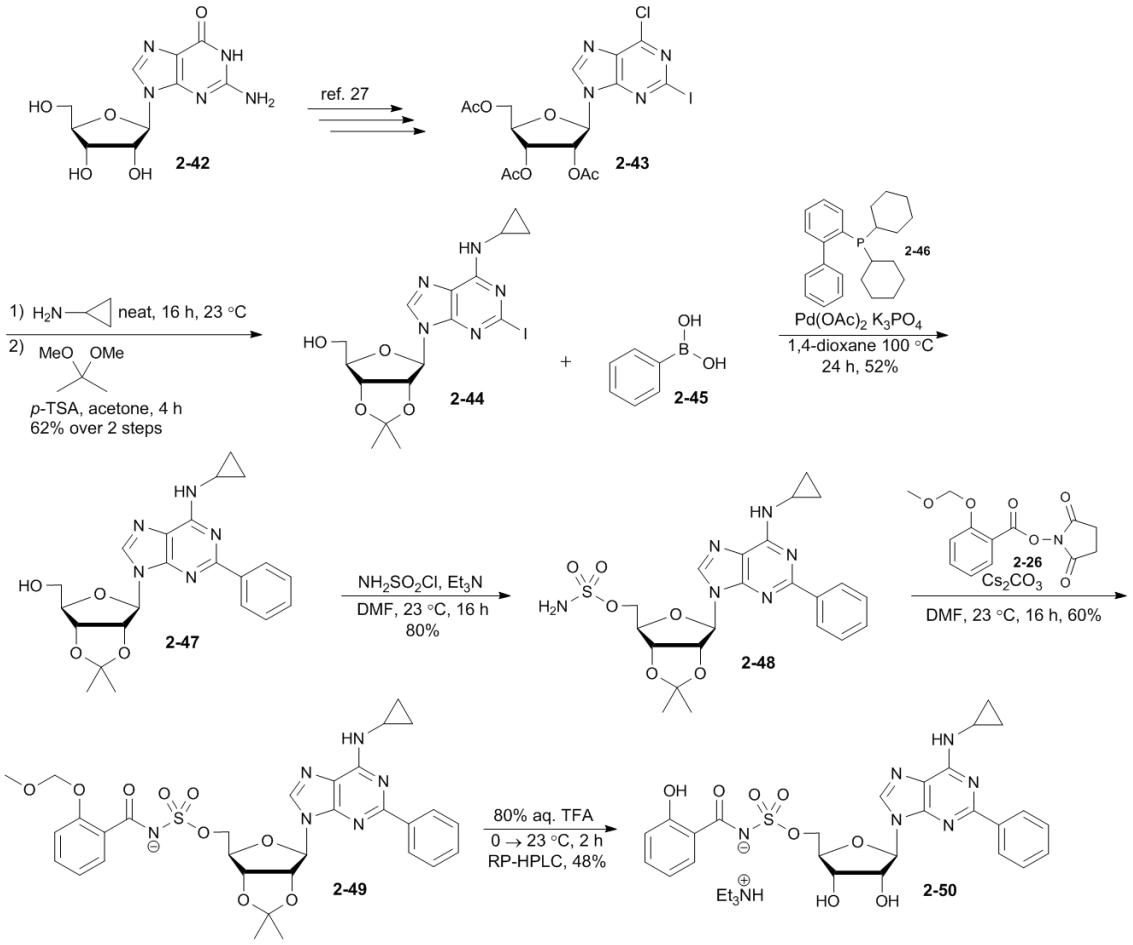

Scheme 2.5. Route to access the N^6-cyclopropyl-2-phenyl derivative of Sal-AMS (**2-50**).

The synthesis of this compound has been previously reported by our group,[23] however this synthesis employed the improved sulfamoylation conditions described above. After three steps, which can be scaled to upwards of 25 grams successfully, 6-chloro-2-iodo-2′,3′,5′-*O*-acetyladenosine (**2-43**) was converted to N^6-cyclopropyl-2-iodoadenosine by reaction with neat cyclopropylamine at room temperature. Following protection of the 2′- and 3′-hydroxyl groups as the acetonide with 2,2′-dimethoxypropane (**2-44**), a palladium-catalyzed Suzuki coupling was used to install the phenyl group at the C-2 position (**2-47**). The phosphine ligand (**2-46**) was observed to slowly oxidize to the corresponding oxide and thus was stored in a glove box under N_2 atmosphere. The 5′-hydroxyl was first sulfamoylated by the modified triethylamine-mediated reaction described above, then coupled with succinimide **2-26** to give the fully protected intermediate **2-49**. TFA-mediated deprotection afforded compound **2-50** recovered in moderate yields after RP-HPLC purification. This compound was much easier to monitor by thin-layer chromatography (TLC) during all the above reactions due to its increased lipophilicity. Similar to Sal-AMS, even though **2-50** could be purified by normal phase silica chromatography, RP-HPLC was required for the high level of purity necessary for administration to animals.

2.3.5 Synthesis of acetate prodrugs of Sal-AMS (2-51 and 2-52)

A simple acetate prodrug was the first prodrug design attempted for Sal-AMS. Acetates are quickly hydrolyzed by non-specific esterases *in vivo*.[28] The tri-acetate derivative of

Sal-AMS was prepared by direct acetylation of Sal-AMS employing acetic anhydride and pyridine in DMF (**Scheme 2.6**). These conditions were notable since competitive acetylation at the N^6 position of adenosine was not observed.

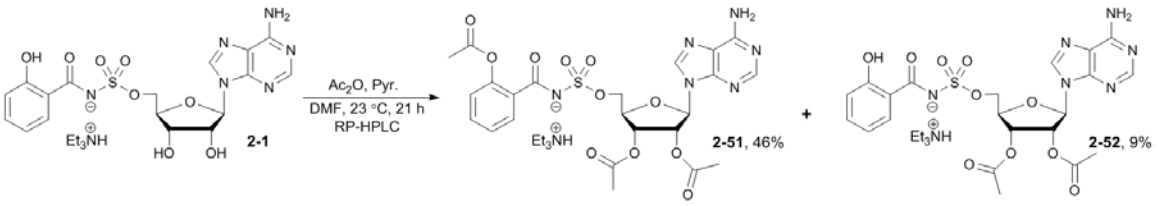

Scheme 2.6. Synthesis of a tri-acetate prodrug of Sal-AMS (**2-51**).

Compound **2-51** was first purified on normal phase silica and isolated as an approximate 5:1 mixture of tri-and di-acetates **2-51** and **2-52**. Further purification by RP-HPLC was required to obtain pure **2-51**.

We were interested in examining whether there is a difference in the bioavailabilities of the di- and tri-acetate prodrugs **2-51** and **2-52**. The amount of di-acetate **2-52** obtained by direct acetylation was inadequate, thus we developed a synthetic route to this compound beginning from sulfamate **2-25** coupled with *N*-hydroxysuccinimidyl-2-(benzyloxy)benzoate **2-53** to provide **2-54** (**Scheme 2.7**). TFA-mediated deprotection of the acetonide followed by acetylation of the resultant free 2 and 3′ alcohols afforded **2-55**. Catalytic hydrogenolysis and RP-HPLC purification led to the di-acetate product **2-52** in moderate yield.

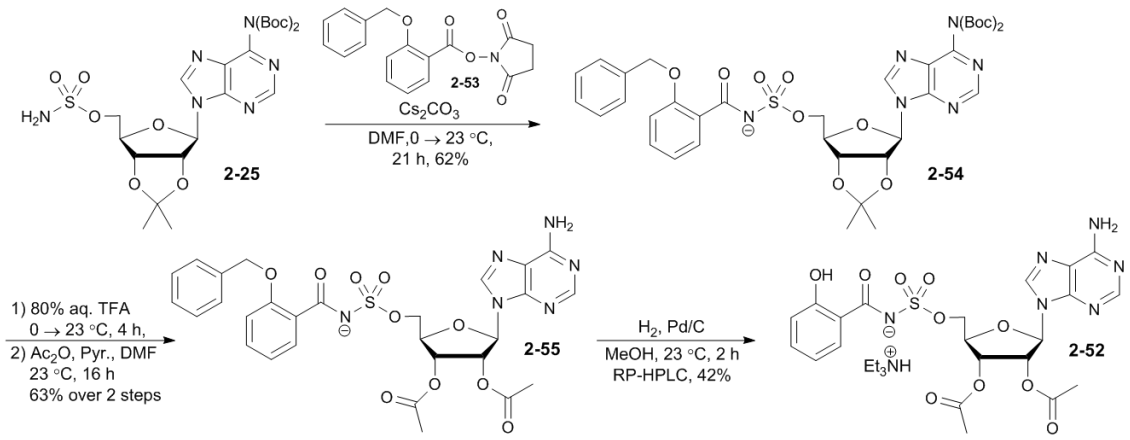

Scheme 2.7. Direct synthesis of a di-acetate prodrug of Sal-AMS (**2-52**).

2.3.6 Oral bioavailability of siderophore biosynthesis inhibitors

Our lab had previously synthesized and evaluated the enzymatic activity and antitubercular activity of compounds **2-1** and **2-6**. The other analogs had not yet been analyzed. **Table 2.2** summarizes the inhibitory activities against MbtA of the compounds synthesized to date. Enzymatic activities were measured by either Daniel Wilson or Dr. Kishore Viswanathan from our lab.

Table 2.2. Enzymatic activity of siderophore inhibitors against MbtA.

	appK_i (nM)
Sal-AMS (**2-1**)[12]	6.6 ± 1.5
Compound **2-6**[12]	3.7 ± 0.6
Compound **2-34**	8.9 ± 0.7
Compound **2-41**	1.1 ± 0.4
Compound **2-50**	0.7 ± 0.1
Compound **2-51**	n.d.[a]
Compound **2-52**	n.d.

[a]n.d. = not determined

Compounds **2-51** and **2-52** were not analyzed as they are prodrugs for Sal-AMS and not expected to bind MbtA or be active against *Mtb* alone.

We chose to evaluate these compounds in female Sprague-Dawley rats obtained with indwelling catheters in the right jugular vein and left femoral vein for infusion and blood draws, respectively. The rats allowed us to complete entire corssover bioavailability studies with a single animal instead of having to sacrifice animals at each time point. This should decrease the error possible in our studies, and improve our confidence in the data. **Table 2.3** summarizes the results detailed below. We initially chose to dose orally (PO) at 25 mg/kg and intravenously (IV) at 2.5 mg/kg, hoping to achieve a bioavailability of at least 10% with our best candidate.

Table 2.3. Summary of bioavailability measured for isoniazid (INH) and MbtA inhibitors in a rodent model.

Compound	Dosing route	Dose (mg/kg)	$t_{1/2}$ (min)	C_0 or C_{max} (µg/mL)	AUC (min * µg/mL)	F
INH	IV	6	19	124	371	65%
	PO	30	81.5 ± 7.8[a]	13.5 ± 0.4	1634 ± 186	
	IV[29]	20	23.4	n.d.[b]	1842 ± 126	n.d.[b]
Sal-AMS **2-1**	IV	2.5	11.1 ± 2.3	48.4 ± 12.8	427 ± 94	1.2 ± 0.3%
	PO	25	81	0.42 ± 0.16	49.7 ± 8.4	
Compound **2-6**	IV	2.5	10.6 ± 0.7	28.8 ± 4.7	250 ± 49	5.9 ± 1.3%
	PO	25	105 ± 17	0.61 ± 0.06	152 ± 19	
Compound **2-34**	IV	2.5	14.0 ± 3.1	7.1 ± 6.0	50.2 ± 38.6	5.2 ± 4.1%
	PO	25	273 ± 154	0.10 ± 0.02	10.6 ± 2.1	
Compound **2-41**	IV	2.5	15.1 ± 1.3	25.4 ± 6.9	209 ± 76	1.0 ± 0.4%
	PO	25	78.2 ± 10.3	0.14 ± 0.03	18.1 ± 2.1	
Compound **2-50**	IV	2.5	15.5 ± 10.6	28.4 ± 9.7	184 ± 30	0.3 ± 0.1%
	PO	25 (n = 2)	33.3	0.111 ± 0.001	4.0 ± 0.9	
		25 (n = 1)	118	14.8	1361	88%
Compound **2-51**	IV	2.5	22.4 ± 1.0	7.4 ± 0.9	173 ± 11	0.2 ± 0.2%
	PO	25	n.d[b]	0.03 ± 0.01	2.9 ± 0.8	
Compound **2-52**	IV **2-52**	2.5	19.8 ± 12.0	3.4 ± 0.6	18.9 ± 2.8	0%
	IV **2-1**	2.5	13.4 ± 2.9	1.4 ± 0.2	25.8 ± 5.6	
	PO	25	< LOD[c]	< LOD	< LOD	

[a]The true half-life of a compound is measured during IV dosing as the serum half-life. While a half-life can be determined during oral (PO) dosing, this value will vary based on other factors such as uptake and absorption and therefore does not represent the true half-life of the compound. [b]Not determined. [c]LOD = Limit of detection.

We began our studies by administering a known antitubercular agent, isoniazid (INH). This is a well studied compound, with many published results regarding its oral dosing and detection in rat plasma.[29–33] Dosing in duplicate we were able to successfully reproduce similar $t_{1/2}$ and AUC values compared to other reported rodent models dosed at similar levels (**Figure 2.7**).[29] Notably, the half-life of INH in rats is reported at 24 minutes, and our model gave a half-life of 19 minutes. The half-life of INH in humans is reported to be approximately 90 minutes for fast acetylators (a measure of INH metabolism) and 220 minutes for slow acetylators.[30]

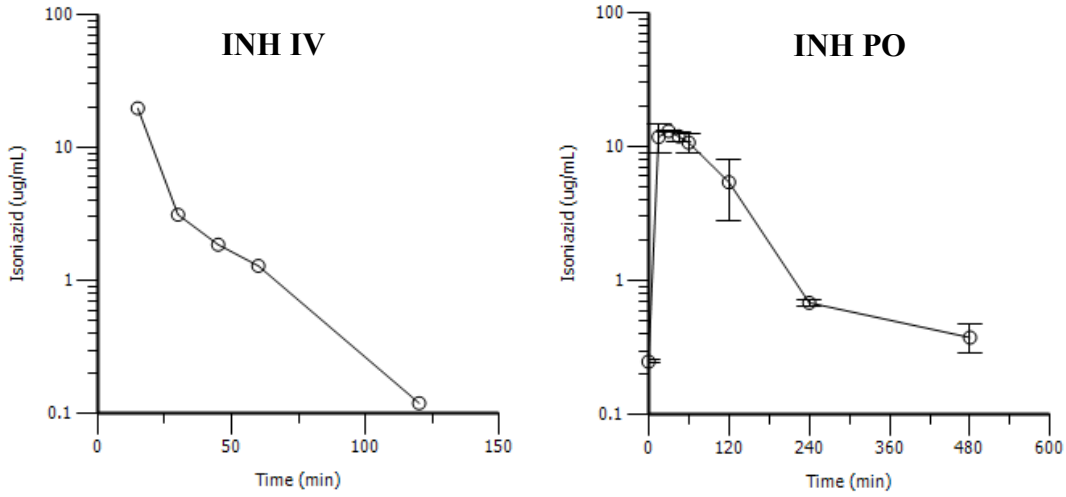

N = 2	IV	PO
Dose (mg/kg)	6	30
$t_{1/2}$ (min)	19	81.5 ± 7.8
C_0 or C_{max} (µg/mL)	124	13.5 ± 0.4
AUC_{0-inf} (min*µg/mL)	1356	153 ± 189

Figure 2.7. Concentration-time profiles and measured values for oral and intravenous dosing of isoniazid (INH) in rats.

Satisfied that the sampling technique from rats produced reliable data, we began to dose our synthetic compounds. For our purposes, we will be using the half-life ($t_{1/2}$) value in a qualitative manner, attempting to maximize the half-life in this rat model before moving our best compound forward into a second animal or efficacy study. As expected, Sal-AMS (**Figure 2.8**) shows poor oral bioavailability (1.2%) and a very fast half-life ($t_{1/2}$ = 11.1 min). While we are not satisfied with a bioavailability of 1.2%, we were encouraged to see that the C_{max} achieved here (0.42 µg/mL) is more than two times the MIC observed against *Mtb* (0.18 µg/mL).

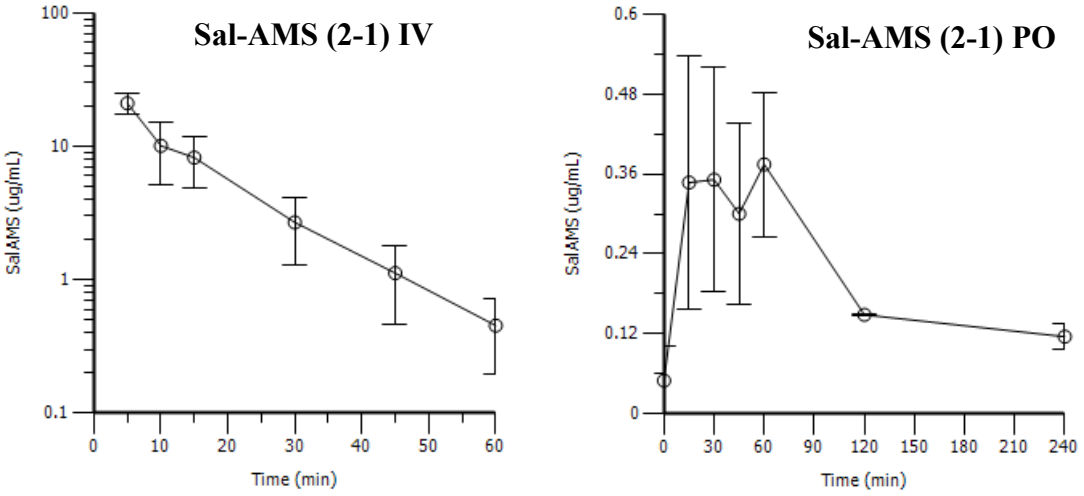

N = 3	**IV**	**PO**
Dose (mg/kg)	2.5	25
$t_{1/2}$ (min)	11.1 ± 2.3	81
C_0 or C_{max} (µg/mL)	48.4 ± 12.8	0.42 ± 0.16
$AUC_{0–240}$ (min*µg/mL)	427 ± 94	49.7 ± 8.4

Figure 2.8. Concentration-time profiles and measured values for oral and intravenous dosing of Sal-AMS (**2-1**) in rats.

The next compound we evaluated was the sulfamide linked analogue (**2-6**, **Figure 2.9**). As a reminder, this compound was designed to increase the pK_a of the nitrogen in the linker. It is calculated that compound **2-6** has a pK_a of 4.1, compared to 3.0 for Sal-AMS (**2-1**). Sulfamide **2-6** showed a similar half-life (10.6 min), and a 50% increase in C_{max} (0.61 µg/mL) with a five-fold increase in bioavailability at nearly 6%. This suggests to us that an increase in pK_a could be a viable modification for improving the oral bioavailability of our compounds.

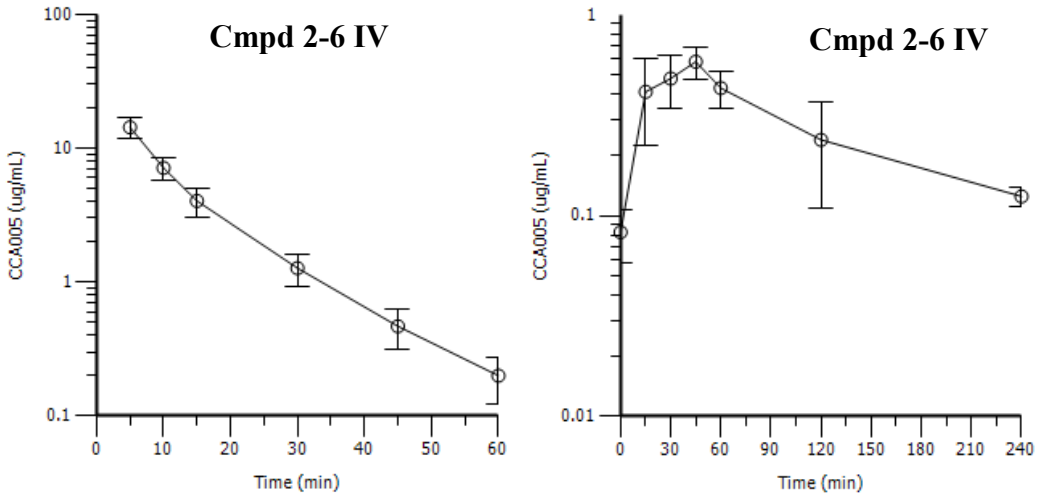

N = 3	**IV**	**PO**
Dose (mg/kg)	2.5	25
$t_{1/2}$ (min)	10.6 ± 0.7	105 ± 17
C_0 or C_{max} (µg/mL)	28.8 ± 4.7	0.61 ± 0.06
$AUC_{0–240}$ (min*µg/mL)	250 ± 49	67.9 ± 11.9

Figure 2.9. Concentration-time profiles and measured values for oral and intravenous dosing of compound **2-6** in rats.

We hypothesized that compound **2-34** could improve the oral bioavailability further, if increasing the pK_a of the linker nitrogen does impact absorption, however the calculated impact of this modification is smaller than the impact of the sulfamide modification (pK_a increases from 4.1 to 4.2). Using the data shown in **Figure 2.10**, the oral bioavailability of compound **2-34** was calculated at 5.2%, but with a high variability at 4.1%. This comes from a larger deviation among the IV doses administered to the animals. This value is virtually the same as that seen for compound **2-6**. Although we did not see an increase in oral bioavailability, we saw a 40% increase in the half-life of this compound (14 min vs. 10 min for **2-6**). The maximum concentration was also slightly lower than that achieved with compound **2-6.**

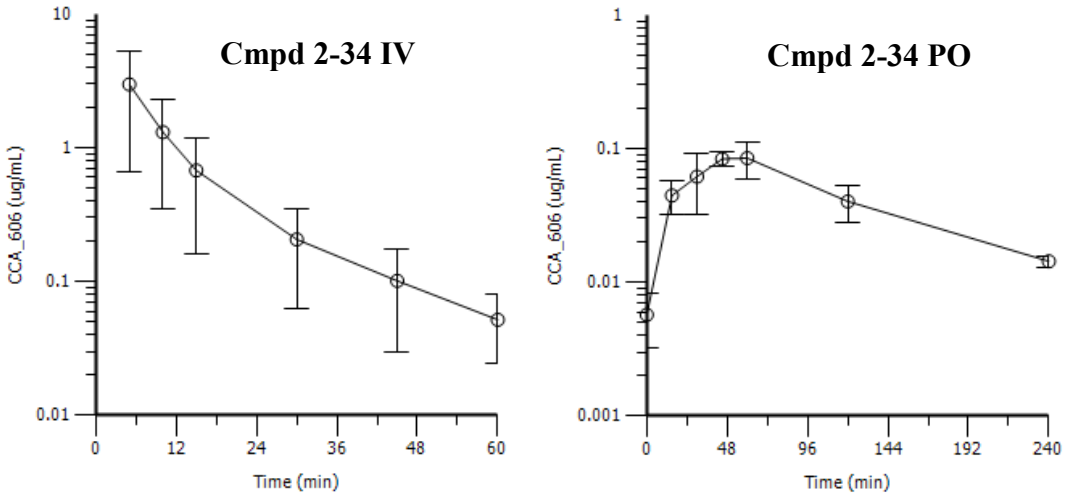

N = 3	**IV**	**PO**
Dose (mg/kg)	2.5	25
$t_{1/2}$ (min)	14.0 ± 3.1	273 ± 154
C_0 or C_{max} (μg/mL)	7.1 ± 6.0	0.10 ± 0.02
$AUC_{0–240}$ (min*μg/mL)	50.2 ± 38.6	10.6 ± 2.1

Figure 2.10. Concentration-time profiles and measured values for oral and intravenous dosing of compound **2-34** in rats.

Another modification that we hoped would continue to build on the success from compound **2-6** was compound **2-41,** incorporating both the sulfamide linker and an aliphatic group to increase the pK_a of the linker and the lipophilicity of the molecule, respectively (**Figure 2.11**). Compound **2-41** contains an N^6-cyclopropyl group that is predicted to increase the octanol-water partition coefficient of the molecule slightly (ClogP) from 0.29 to 0.31, and the sulfamide linker increasing the pK_a of the acidic nitrogen that had already displayed increased bioavailability. Unfortunately, the N^6-cyclopropyl addition did not display an additive effect in improving the oral bioavailability. The bioavailability actually dropped back to 1.0%, nearly the identical level for Sal-AMS. We were encouraged, however, to see that the half-life of compound **2-41** increased by nearly 50% to 15 minutes.

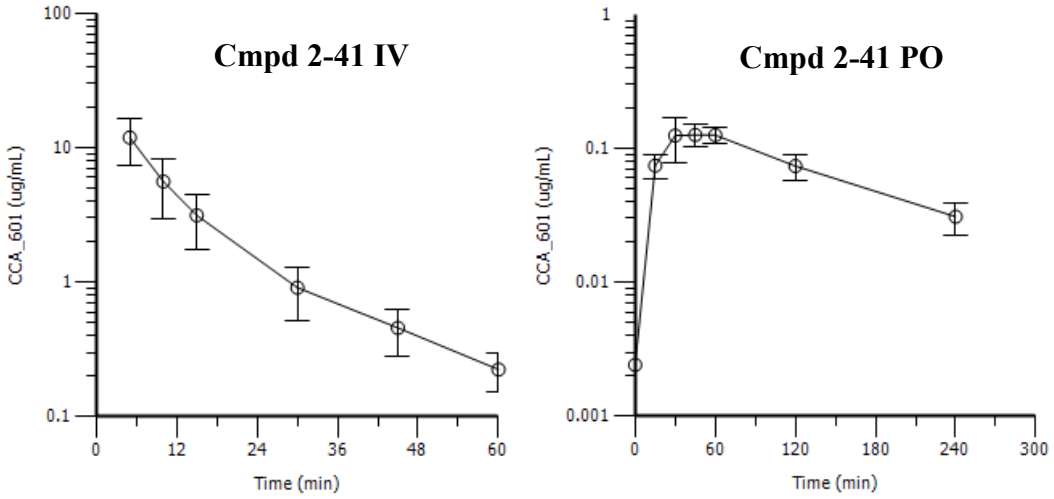

N = 3	**IV**	**PO**
Dose (mg/kg)	2.5	25
$t_{1/2}$ (min)	15.1 ± 1.3	78.2 ± 10.3
C_0 or C_{max} (μg/mL)	25.4 ± 6.9	0.14 ± 0.03
AUC_{0-240} (min*μg/mL)	209 ± 76	18.1 ± 2.1

Figure 2.11. Concentration-time profiles and measured values for oral and intravenous dosing of compound **2-41** in rats.

The next compound we tested was the N^6-cyclopropyl-2-phenyl derivative (**2-50**). This compound was designed to dramatically increase the ClogP, with a calculated value of 3.80. We first analyzed this change with the same sulfamate linkage as Sal-AMS so it was more directly comparable to the parent compound (**Figure 2.12**). As shown in **Table 2.3**, this compound was our worst yet tested, with a bioavailability of 0.3%. It is possible that this compound has now become too lipophilic to adequately solubilize in the aqueous environment of the gut. We did observe that **2-50** was not soluble in water or the 0.5% sodium carboxymethylcellulose solution used in dosing the other compounds. We found that a 25% wt/vol solution of hydroxypropyl β-cyclodextrin was required to completely solubilize this compound, indicating it had dramatically increased in lipophilicity.

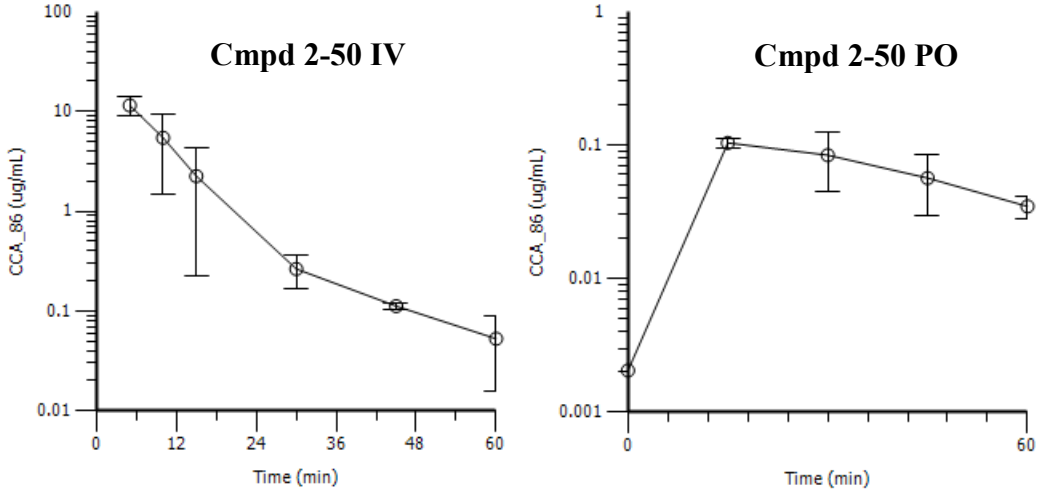

N = 2	**IV**	**PO**
Dose (mg/kg)	2.5	25
$t_{1/2}$ (min)	15.5 ± 10.6	33.3
C_0 or C_{max} (μg/mL)	28.4 ± 9.7	0.111 ± 0.001
AUC_{0-240} (min*μg/mL)	184 ± 30	4.0 ± 0.9

Figure 2.12. Concentration-time profiles and measured values for oral and intravenous dosing of compound **2-50** for 2 rats.

We also had an anomalous result with one of our animals during this study. One of three animals displayed impressive absorption of compound **2-50** with a bioavailability of 88% (**Figure 2.13**). Additional discussion regarding this phenomenon can be found in discussion section **2.4.2**.

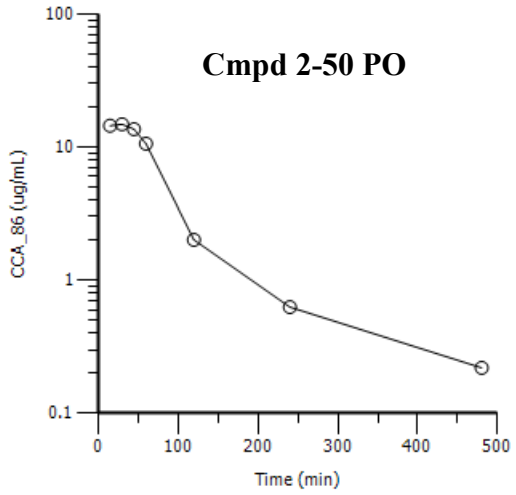

N = 1	**PO**
Dose (mg/kg)	25
$t_{1/2}$ (min)	118
C_0 or C_{max} (µg/mL)	14.8
$AUC_{0–240}$ (min*µg/mL)	1361

Figure 2.13. Single animal anomalous result from oral dosing of compound **2-50** in one rat.

Finally, we tested the bioavailability of our two acetate prodrug compounds. We analyzed our plasma samples for the concentrations of both Sal-AMS and the parent prodrug at each time point, expecting that the promoieties would help the compound pass through the intestinal wall, and then be quickly cleaved once in the bloodstream. First, the tri-acetate compound **2-51** was delivered in the same 25% wt/vol hydroxypropyl β-cyclodextrin solution as used for compound **2-50**. Negligible oral bioavailability was observed. We were unable to observe any of the parent compound in the plasma samples, but were greatly interested in the change in the oral concentration-time profile of Sal-AMS that we observed when dosing this compound (**Figure 2.14**). During oral dosing, we initially saw a standard absorption followed by elimination of Sal-AMS. After 2

hours, however, we saw the concentration of Sal-AMS in plasma again begin to increase. At the last time point of the study (8 hours) the concentration was still rising, even above that of the initial C_{max}.

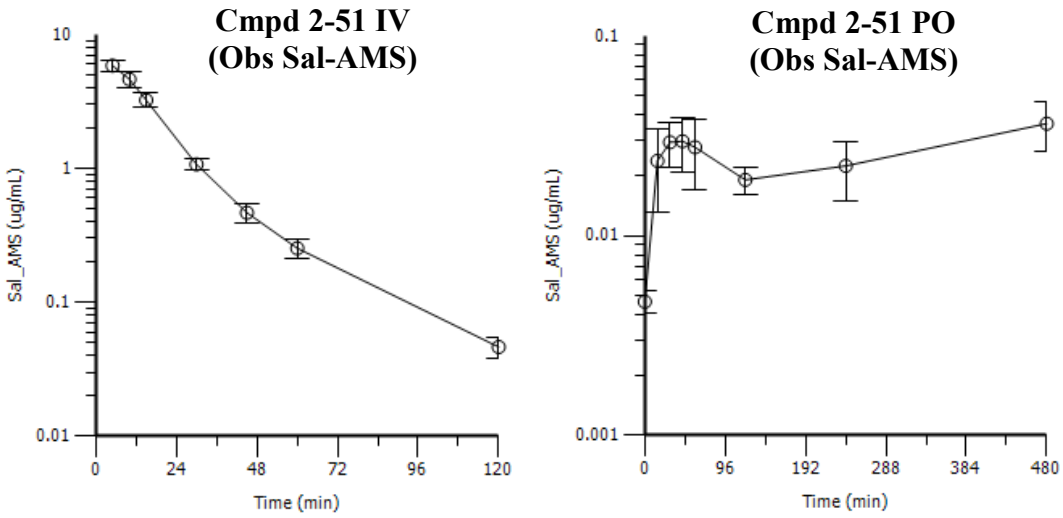

N = 3	**IV**	**PO**
Dose (mg/kg)	2.5	25
$t_{1/2}$ (min)	22.4 ± 1.0[a]	n.d.[b]
C_0 or C_{max} (µg/mL)	7.4 ± 0.9	0.032 ± 0.008
AUC_{0-240} (min*µg/mL)	173 ± 11	2.9 ± 0.8

Figure 2.14. Concentration-time profiles and measured values for oral and intravenous dosing of the tri-acetyl Sal-AMS prodrug, compound **2-51** in rats. [a]The $t_{1/2}$ for Sal-AMS is artificially inflated because it includes the time for prodrug absorption and cleavage, meaning it is not a true measure of the half-life for the compound. [b]n.d. = not determined.

A simple plasma stability time course was run on the prodrug, monitoring the loss of each acetate promoiety. As shown in **Figure 2.15**, the tri-acetate compound is very quickly degraded, however the di- and mono-acetate compounds have much longer half lives in plasma. We do see a slow increase in Sal-AMS over time, and this slower-than-expected prodrug cleavage may be a secondary explanation for the second increase in Sal-AMS concentration seen in the later plasma time points in **Figure 2.14**. See discussion section

2.4.3 below for more on this phenomenon.

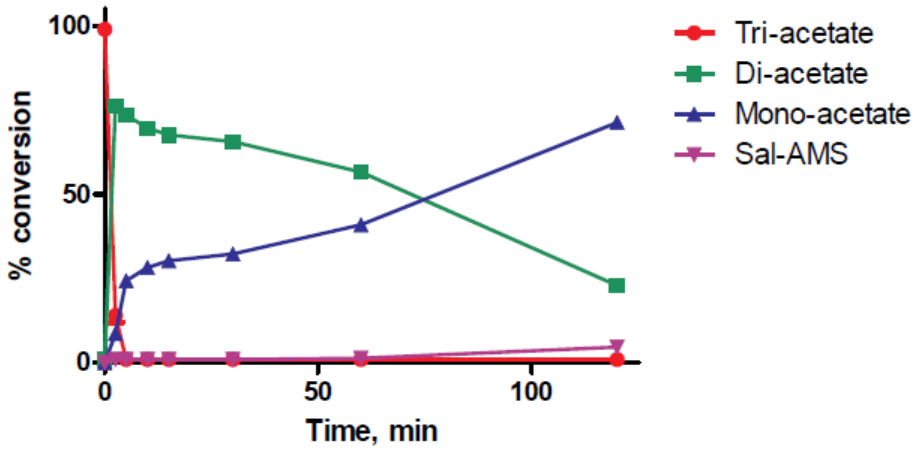

Figure 2.15. Stability of tri-acetate prodrug compound **2-51** at 10 μM in pooled female Sprague-Dawley rat plasma. The tri-acetate compound is very quickly degraded in plasma. The di-acetate (22% remaining) and mono-acetate (73% remaining) compounds are much longer lived, making the overall increase in Sal-AMS (**2-1**, 5% released) slow.

We also performed a pH stability test in simulated gastric fluid (SGF) at pH 1.2. These results, shown in **Figure 2.16**, indicate that the tri-acetate prodrug is also very stable to the acidic pH of gastric fluids (83% remaining after 2 h). While some di-acetate and mono-acetate were identified by mass spectrometry, we never observed liberation of the parent compound Sal-AMS. These results show that the tri-acetate compound is either not efficiently absorbed, or was not completely converted to Sal-AMS once absorbed. In either case, this makes the stability data in plasma important for understanding the *in vivo* behavior of this compound.

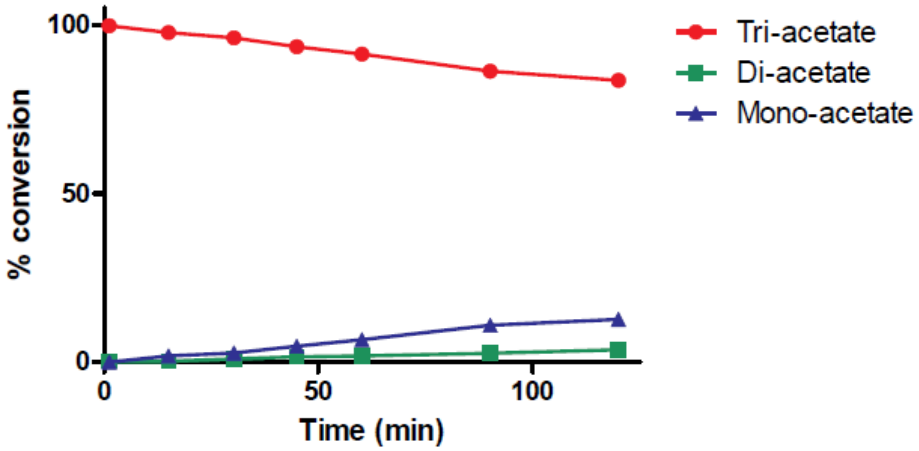

Figure 2.16. Stability of compound **2-51** at 100 μM in simulated gastric fluid (SGF) pH 1.2. The tri-acetate is very stable (83% remaining after 2 h), with only small amounts of di-acetate (3.7% after 2 h) and mono-acetate (12.3% after 2 h) identified. No Sal-AMS (**2-1**) was observed during the course of the study.

Finally, we evaluated the di-acetate prodrug, which has a free phenol hydroxyl. This compound was also dosed in the 25% wt/vol hydroxypropyl β-cyclodextrin solution and we were unable to observed any compound in the plasma samples from oral dosing. As shown in **Figure 2.17**, we were unable to detect quantifiable levels of either Sal-AMS (**2-1**) or compound **2-52** after oral dosing. When looking at the IV dosing data, we were able to see both compound **2-52** and **2-1**, which were both quickly eliminated. We did see a moderate inflation to the $t_{1/2}$ of Sal-AMS when measured during IV dosing (13 min here vs. 11 min when dosed directly), likely due to time required for prodrug cleavage.

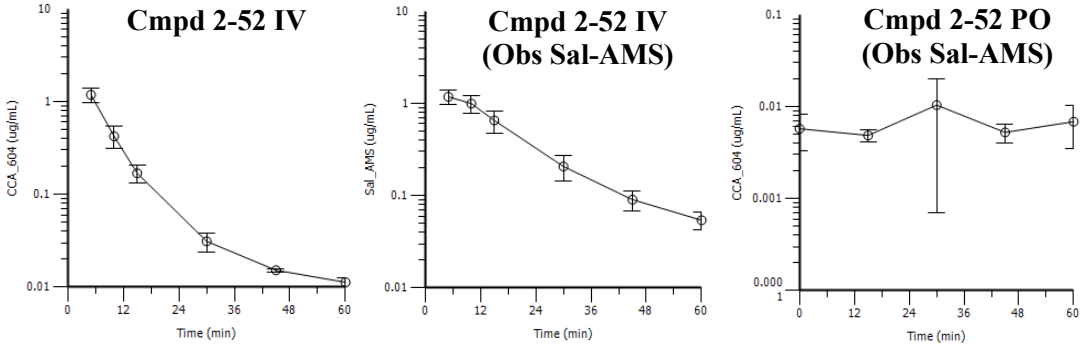

N = 3	**IV (Cmpd 2-52)**	**IV (Sal-AMS, 2-1)**	**PO**
Dose (mg/kg)	2.5		25
$t_{1/2}$ (min)	19.8 ± 12.0	13.4 ± 2.9	< LQ[a]
C_0 or C_{max} (µg/mL)	3.4 ± 0.6	1.4 ± 0.2	< LQ
AUC_{0-60} (min*µg/mL)	18.9 ± 2.8	25.8 ± 5.6	< LQ

Figure 2.17. Concentration-time profiles and measured values for oral and intravenous dosing of the di-acetate Sal-AMS prodrug, compound **2-52** in rats. The oral dosing samples did not show any quantifiable amounts of compound **2-52** or Sal-AMS (**2-1**). [a]LQ = limit of quantitation

The IV data indicates that compound **2-52** remains intact in biological fluids as we were able to measure its half-life after IV dosing. The same plasma stability assay was done on compound **2-52** and extraordinary stability of the di-acetate compound was observed (**Figure 2.18**). This is especially surprising as the di-acetate degradation product of the tri-acetate prodrug degrades into both the mono-acetate compound and eventually the parent Sal-AMS (as shown in **Figure 2.15**). More Sal-AMS was liberated from the di-acetate prodrug than the tri-acetate prodrug, however the prodrug cleavage is inefficient at best.

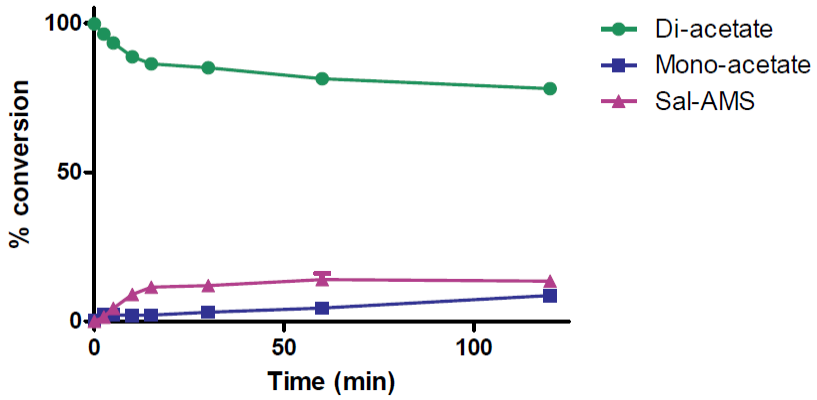

Figure 2.18. Stability of di-acetate prodrug compound **2-52** at 10 µM in pooled female Sprague-Dawley rat plasma. The di-acetate compound (78% remaining) is surprisingly stable in plasma. The mono-acetate (9% remaining) very slowly appears in plasma, and the overall increase in Sal-AMS (**2-1**, 11% released) is slow.

The degradation product observed with a mass matching a di-acetate during the plasma stability test of the tri-acetate showed the same retention time as synthetic compound **2-52**, suggesting that it is the same compound. Why the synthetic compound would be so stable compared to the degradation product from the tri-acetate compound is still under investigation. We continued with our analysis of **2-52** by also running it in the same pH stability assay in SGF, pH 1.2 (**Figure 2.19**). Compound **2-52** was stable in the low pH solution, suggesting that the parent di-acetate prodrug needs to be absorbed for this compound to reach circulation.

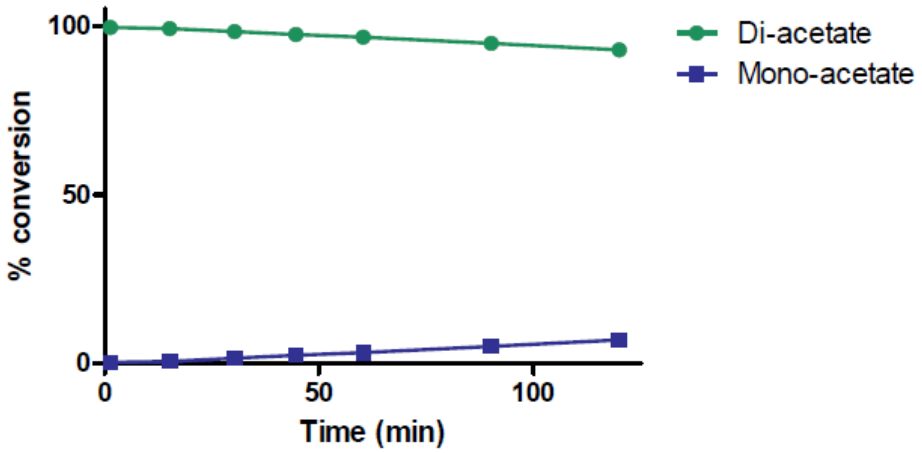

Figure 2.19. Stability of compound **2-52** at 100 μM in simulated gastric fluid (SGF) pH 1.2. The di-acetate is stable to the acidic conditions (93% remaining after 2 h), with very little mono-acetate (7% after 2 h) identified. No Sal-AMS (**2-1**) was observed during the course of the study.

2.4 Discussion

2.4.1 Strategies for increasing oral bioavailability

Orally bioavailable formulations are highly desirable for new therapeutics. As discussed in Chapter 1 above, *Mtb* is highly endemic in areas where healthcare access is limited. In such areas, orally bioavailable medications that can be stored and taken in the home are a necessity for fidelity to long-term treatment. As no previous animal work had been performed in our lab, we sought the council of Dr. Rory Remmel, a collaborator of ours and a drug metabolism expert, to advise us on our model development.

We designed our compounds keeping in mind the guidelines first promoted by Dr. Christopher Lipinski in his seminal paper discussing approaches to estimate the solubility and permeability of compounds intended for drug development.[17] Beginning with

evaluation of Sal-AMS (**2-1**), we find that we do not violate any of the four "rule of 5" guidelines. We do recognize, however that Sal-AMS is a highly polar compound with a linker that will be mostly charged at physiological pH, making membrane permeability less likely. Our design goals to lower the charge on the linker group, while bringing the ClogP into the 2–5 range would help us remain within the rule of 5 guidelines, but improve some of these permeability problems.

Other recent work regarding properties that can influence oral bioavailability was also considered. Not only is high polar surface area known to be detrimental for intestinal absorption,[34,35] but both molecular flexibility and hydrogen bond formation by amide bonds have been indicated as negative for oral absorption.[36,37] Analogues that increase lipophilicity should address the high polar surface area concerns, and there is only a single amide bond in these compounds, so we do not expect high levels of water complexation. A recent review from Veber and colleagues also found that rotatable bond count was a surprisingly useful correlate to oral bioavailability.[38] With seven rotatable bonds, we meet the criteria of 10 or fewer put forth by Veber, et. al. as desirable for oral bioavailability.[38] All of these considerations made us hopeful that we would be able to improve the oral bioavailability of Sal-AMS with our current set of analogues.

2.4.2 Anomalous high oral bioavailability of compound 2-50

The animal with abnormally high amounts of compound **2-50** after oral dosing was found have an infection associated with its femoral vein catheter. During the study, we noticed

the animal appeared to be favoring its left front leg, and to have some swelling in that area. The veterinarian staff at the University of Minnesota diagnosed the animal with an abscessed infection. Approximately 2 hours into the study, the animal was administered 1 mg/kg ketoprofen followed by 60,000 IU/kg penicillin intramuscularly. Sulfamethazine was added to the drinking water as an added antibacterial for the next 2 days. We do not believe that these additional doses of therapeutics affected the absorption or elimination of compound **2-50**, as the curve in **Figure 2.13** shows the compound to be over halfway eliminated at the time of administration (2 hours) and continues a monoexponential decline. We also continued to observe the animal throughout the remainder of the study and the following 2 days and saw normal eating and defecating, indicating normal gastrointestinal functions. After the 2 days, we saw that the animal was not improving, so it was sacrificed and necropsied by Dr. Krista Walkowiak of the University of Minnesota veterinarian staff to determine the cause of the abscess. There was foreign material associated with the catheter tubing that was identified by Harlan Laboratories as bedding material likely left behind during surgery. During necropsy, we also looked for any open sores or cuts in the esophagus or intestinal tract that may have affected absorption, but did not observe any abnormalities.

After discussions with University of Minnesota veterinarians and our collaborator Dr. Rory Remmel, we hypothesize that the inflammation, stress and possible sepsis experienced by this animal due to the infection may have been able to loosen the intestinal tight junctions, thereby allowing for greater drug absorption. There is some literature evidence suggesting that stress and inflammation can affect the tight junctions

of both the intestine and the colon.[39,40]

2.4.3 Prodrugs of nucleosides

Natural nucleosides do not efficiently pass through cell membranes by passive diffusion, but have both Na^+-dependent concentrative transporters and Na^+-independent equilibrative transporters that facilitate their penetration of the gastrointestinal tract.[41] While this may seem like an exciting pathway for exploiting delivery of therapeutic compounds, it has also been shown that nucleoside transporters have low turnover capacities. Typical drug concentrations in the intestine would quickly saturate these transporters, and their impact on drug absorption can therefore be minimal.[41]

Multiple prodrug approaches have been successfully used to deliver nucleoside-based therapeutic compounds for the treatment of diseases such as HIV, hepatitis B virus (HBV), hepatitis C virus (HCV), and some cancers. Nucleoside analogues also continue to be investigated for new therapeutic development. A prodrug is usually a pharmacologically inactive analogue of the parent drug that can either spontaneously or enzymatically be converted to the active drug once in the body.[41] Prodrugs therefore need to be sufficiently stable for administration, while labile enough for efficient release once absorbed.

While a prodrug strategy was not originally the focus for this project, it was a suggested potential route for increasing lipophilicity while keeping the highly active parent compound as the therapeutic agent. The simple acetate prodrug was easily accessible, as

described in section **2.3.5**, which allowed us to incorporate these candidates into our first group of compounds for animal evaluation.

We hypothesize that the later increase in Sal-AMS appearance observed in **Figure 2.14** is due to two factors: limited solubility of the prodrug in biological fluids, and the inefficient cleavage of the promoieties *in vivo*. Compounds **2-51** and **2-52** were solubilized in 25% wt/vol hydroxypropyl β-cyclodextrin for oral administration, and may only be slowly solubilized once in the aqueous gastrointestinal tract for passage through the intestinal wall. This could make it appear as if Sal-AMS is slowly being absorbed, which occurs when compounds become too water-insoluble, making their bioavailability dissolution-rate limited.[42] If this were the only factor affecting the absorption of these compounds, it may be possible to adjust the solubilizing excipient or mixture to improve absorption. A wide variety of excipients, cosolvents, and emulsifying agents are only some of the currently approved components used in oral formulations today.[43] Additional study of both compounds through plasma and pH stability studies, however, have shown us that these promoieties are unexpectedly stable. The di-acetate **2-52** shows very little apparent degradation after 2 hours in rat plasma at 37 °C (**Figure 2.18**), and both prodrugs are stable to SGF over 2 hours at 37 °C (**Figures 2.16** and **2.19**). The plasma stability data observed for the di-acetate **2-52** was not consisent with that of tri-acetate **2-51**. The rate of cleavage of **2-52** appears to begin with first-order kinetics, then levels off at approximately 15–30 minutes. This assay needs to be repeated in order to draw conclusions regarding the synthetic di-acetate compound's stability in rat plasma. Without efficient cleavage of these promoieties, even a dramatic increase in absorption will not

effectively increase the delivery of the active compound.

2.4.4 Trends in oral bioavailability for siderophore inhibitors

Increasing the pK_a of the sulfamate linker nitrogen proved the most beneficial modification for oral bioavailability, increasing bioavailability from 1.2% to 5.2% and 5.9% for compounds **2-1**, **2-34**, and **2-6**, respectively. Addition of lipophilic moieties did not increase bioavailability, and actually decreased overall absorption. This could be due to both the insolubility of our analogues in the aqueous environment of the gastrointestinal tract (e.g. compound **2-50**), and possibly the lack of recognition of these compounds by formerly exploited nucleoside transporters (e.g. compound **2-41**). A prodrug strategy did not substantially improve the bioavailability of Sal-AMS (**2-1**), but it appears that this may be due to multiple factors that include insolubility of the prodrugs, and their surprising stability in plasma. A modified prodrug design that is more readily cleaved in plasma and more soluble in biological fluids may help improve these results.

2.5 Conclusions

This project has successfully started the next step for preclinical development of siderophore biosynthesis inhibitors for the treatment of *Mtb*. We synthesized a small set of compounds based on enzymatic and whole-cell testing against a target enzyme (MbtA) and organism (*Mtb*). We then started the *in vivo* evaluation of our compounds in the hope

of identifying a candidate compound and determining an acceptable dose to progress into an animal efficacy study. Our first set of compounds, while not as successful as we would like, has informed us about the structural design of our analogues. It is recognized that the pK_a of our compounds have the greatest effect on bioavailability, and addition of lipophilic groups has not yet resulted in any increased absorption. It is important to observe that while we had previously discovered modifications that could be made to retain and improve the enzymatic and whole-cell activity of these compounds against MbtA and *Mtb*, these modifications do not necessarily translate into good oral bioavailability and pharmacokinetic parameters. Based on what was learned from our initial *in vitro* SAR studies, we are now embarking on *in vivo* SAR studies, which will help use develop the best compound for preclinical development.

2.6 Experimental details

2.6.1 General procedures for the synthesis of siderophore biosynthesis inhibitors

All reactions were performed under an inert atmosphere of dry argon in oven-dried (150 °C) glassware. ^{1}H and ^{13}C NMR experiments were recorded on a Varian 600 MHz spectrometer (Palo Alto, CA). Proton chemical shifts are reported in ppm from an internal standard of residual chloroform (7.26 ppm), methanol (3.31 ppm), or dimethyl sulfoxide (2.50 ppm). Carbon chemical shifts are reported in ppm from an internal standard of residual chloroform (77.0 ppm) or methanol (49.1 ppm). Proton chemical

data are reported as follows: chemical shift, multiplicity (s = singlet, d = doublet, t = triplet, q = quartet, m = multiplet, br = broad, ovlp = overlapping), coupling constant, and integration. High resolution mass spectra were acquired on an Agilent TOF II TOF/MS (Agilent Technologies, Santa clara, CA) instrument equipped with either an ESI or APCI interface. Semi-preparative reverse-phase HPLC was performed on a Varian Prostar 210 solvent system equipped with a UV/Vis detector (Varian, Inc., Palo Alto, CA) with a Phenomenex Gemini 10 µm C18 110 Å (250 × 10.0 mm) column (Phenomenex, Torrance, CA) at a flow rate of 5.0 mL/min with detection at 254 nm; preparative reverse-phase HPLC was performed on a Varian Prostar 210 solvent system equipped with a UV/Vis detector (Varian, Inc./Agilent Technologies, Santa Clara, CA) with a Phenomenex Gemini 10 µm C18 110 Å (250 × 21.2 mm) column (Phenomenex, Torrance, CA) at a flow rate of 20 mL/min with detection at 254 nm. Flash chromatography was performed on an ISCO Combiflash Companion® purification system (Teledyne Isco, Lincoln, NE) with prepacked silica gel cartridges and the indicated solvent system.

All commercial reagents (Sigma-Aldrich, Fisher, Fluka, Strem) were used as provided. 2-Iodoadenosine was obtained from Tokyo Chemical Industry Co. (Portland, OR, USA). Sulfamoyl chloride was prepared by the method of Heacock without recrystallization.[44] An anhydrous solvent dispensing system (JC Meyer Solvent Systems, Laguna Beach, CA) with two packed columns of neutral alumina was used for drying THF, DMF and DCM and the solvents were dispensed under Argon.

Compounds: **2-1**,[4] **2-6**,[4] **2-24**,[45] **2-26**,[4] **2-28**,[47] **2-31**,[14] **2-36**,[22] **2-38**,[47] **2-43**,[27] **2-44**,[23] **2-**

47,[23] **2-49–50**,[23] and **2-53**,[4] were prepared as described, and all spectroscopic data agreed with reported values.

2.6.2 N^6,N^6-bis(*tert*-Butoxycarbonyl)-2′,3′-*O*-isopropylidene-5′-*O*-(sulfamoyl)adenosine (2-25)

A stirring solution of **2-24** (1.5 g, 2.96 mmol, 1 equiv) and Et_3N (0.42 mL, 3.01 mmol, 1.02 equiv) in DMF (7 mL) was cooled to 0 °C. Sulfamoyl chloride (0.854 g, 7.39 mmol, 2.5 equiv) was added as a solid and the reaction mixture was stirred at 0 °C for 2 h, then allowed to warm to 23 °C. After 14 h at 23 °C, the reaction mixture was concentrated to a crude oil, then redissolved in EtOAc (50 mL). The organic layer was washed excessively with DI H_2O (5 × 30 mL), followed by saturated aqueous NaCl (30 mL). The organic layer was then dried over $MgSO_4$, filtered, and concentrated under reduced pressure to afford the title compound (1.40 g, 80%) as a colorless foamy oil; spectroscopic data agrees with literature values.[46]

2.6.3 N^6,N^6-bis(*tert*-Butoxycarbonyl)-2′,3′-*O*-isopropylidene-5′-*O*-{*N*-[2-(methoxymethoxy)benzoyl]sulfamoyl}adenosine triethylammonium salt (2-27)

To a stirring solution of **2-25** (1.0 g, 1.7 mmol, 1 equiv) in DMF (17 mL) cooled to 0 °C was added **2-26** (0.71 g, 2.6 mmol, 1.5 equiv) as a solid followed by Cs_2CO_3 (1.67 g, 5.1 mmol, 3.0 equiv). The reaction mixture was allowed to warm to 23 °C and stirred for 16

h. The reaction was filtered and concentrated under reduced pressure to a dark oil, and purification by flash chromatography (linear gradient 0–6% MeOH/DCM with 1% Et_3N) afforded the title compound (800 mg, 55%) as a clear oil. R_f = 0.50 (5% MeOH/DCM with 1% Et_3N); ^{1}H NMR (600 MHz, CD_3OD) δ 1.28 (t, *J* = 7.2 Hz, 9H), 1.37 (s, 3H), 1.39 (s, 18H), 1.64 (s, 3H), 3.19 (q, *J* = 7.2 Hz, 6H), 3.44 (s, 3H), 4.36 (dd, *J* = 11.4, 3.6 Hz, 1H), 4.40 (dd, *J* = 11.4, 2.4 Hz, 1H), 4.66 (s, 1H), 5.18 (s, 2H), 5.28 (d, *J* = 6.0 Hz, 1H), 5.49 (t, *J* = 3.0 Hz, 1H), 6.42 (s, 1H), 6.99 (t, *J* = 7.8 Hz, 1H), 7.14 (d, *J* = 8.4 Hz, 1H), 7.29 (t, *J* = 7.8 Hz, 1H), 7.45 (d, *J* = 7.2 Hz, 1H), 8.85 (s, 1H), 8.91 (s, 1H); ^{13}C NMR (150 MHz, CD_3OD) δ 9.4, 25.7, 27.7, 28.1, 48.0, 53.7, 56.8, 69.9, 83.6, 85.5, 85.8, 86.0, 92.5, 96.5, 115.5, 117.1, 122.7, 129.9, 130.5, 131.2, 146.9, 151.2, 151.7, 153.3, 154.7, 155.8; HRMS (ESI–): calculated for $C_{32}H_{41}N_6O_{13}S$ $[M - H]^-$ 749.2458, found 749.2482 (3.2 ppm error).

2.6.4 *N*^{6},*N*^{6}-bis(*tert*-Butoxycarbonyl)-5′-{*N*-[(*tert*-butoxycarbonyl)sulfamoyl]amino}-5′-deoxy-2′, 3′-*O*-isopropylideneadenosine (2-29)

To a stirring solution of **2-24** (0.60 g, 1.2 mmol, 1.0 equiv), **2-28** (0.255 g, 1.3 mmol, 1.1 equiv), and Ph_3P (0.341 g, 1.3 mmol, 1.1 equiv) in THF (30.75 mL) cooled to 0 °C was added DIAD (0.25 mL, 1.3 mmol, 1.1 equiv) as a solution in THF (10.25 mL) by syringe pump over 90 min. After complete addition, the reaction mixture was allowed to warm to 23 °C and continued to stir. After 16 h, the mixture was concentrated under reduced pressure to a dark yellow oil and immediately purified by flash chromatography (linear

gradient 0–100% EtOAc/hexanes) to give the title compound as a foamy oil (0.789 g, 96%). R_f = 0.25 (1:1 EtOAc/hexanes); ^{1}H NMR (600 MHz, $CDCl_3$) δ 1.43 (s, 21H), 1.49 (s, 9H), 1.60 (s, 3H), 3.98 (dd, *J* = 14.4, 6.6 Hz, 1H), 4.04 (dd, *J* = 15.6, 6.0 Hz, 1H), 4.39 (q, *J* = 6.0 Hz, 1H), 5.18 (t, *J* = 6.0 Hz, 1H), 5.38 (d, *J* = 6.6 Hz, 1H), 6.19 (d, *J* = 1.2 Hz, 1H), 8.20 (s, 1H), 8.85 (s, 1H); ^{13}C NMR (150 MHz, $CDCl_3$) δ 25.6, 27.4, 27.9, 28.2, 48.4, 82.1, 84.1, 84.5, 85.0, 85.4, 90.0, 115.3, 129.6, 144.2, 150.5, 150.8, 151.7, 152.3, 152.6; HRMS (ESI–): calculated for $C_{28}H_{42}N_7O_{11}S$ $[M - H]^-$ 684.2668, found: 684.2685 (2.5 ppm error).

2.6.5 N^6,N^6-bis(*tert*-Butoxycarbonyl)-5′-(*N*-*tert*-butoxycarbonyl-*N*-{[(2-methoxymethoxy)benzoyl]sulfamoyl})amino-5′-deoxy-2′,3′-*O*-isopropylideneadenosine triethylammonium salt (2-30)

To a stirring solution of **2-29** (0.52 g, 0.75 mmol, 1.0 equiv) in DMF (7.5 mL) cooled to 0 °C was added Cs_2CO_3 (0.74 g, 2.25 mmol, 3.0 equiv) followed by **2-26** (0.32 g, 1.13 mmol, 1.5 equiv). The reaction mixture was allowed to stir at 0 °C for 30 min, then stirred at 23 °C for 20 h. The reaction mixture was then filtered and concentrated under reduced pressure to a yellow-orange oil that was purified by flash chromatography (linear gradient 0–10% MeOH/DCM with 1% Et_3N) to give the title compound (0.38 g, 53%) as an off-white solid. R_f = 0.37 (10% MeOH/DCM with 1% Et_3N); ^{1}H NMR (600 MHz, $CDCl_3$) δ 1.14 (t, *J* = 7.2 Hz, 9H), 1.37 (s, 9H), 1.39–1.41 (m, 21H), 1.64 (s, 3H), 3.47 (s, 3H), 3.57 (q, *J* = 7.2 Hz, 6H), 4.22 (d, *J* = 6.0 Hz, 2H), 4.64 (td, *J* = 6.0, 2.4 Hz, 1H),

5.15 (s, 2H), 5.21 (dd, J = 6.0, 3.6 Hz, 1H), 5.24 (d, J = 7.8 Hz, 1H), 6.30 (s, 1H), 6.95 (t, J = 8.4 Hz, 1H), 7.03 (d, J = 8.4 Hz, 1H), 7.21 (t, J = 7.8 Hz, 1H), 7.54 (d, J = 7.8 Hz, 1H), 8.69 (s, 1H), 8.87 (s, 1H); ^{13}C NMR (150 MHz, $CDCl_3$) δ 7.9, 25.5, 27.4, 28.0, 46.1, 52.8, 56.3, 81.4, 82.3, 83.7, 84.5, 85.0, 90.3, 96.5, 114.3, 118.0, 121.9, 129.0, 129.8, 131.3, 144.0, 150.0, 150.3, 151.6, 152.2, 152.5, 153.0, 154.5; HRMS (ESI–): calculated for $C_{37}H_{50}N_7O_{14}S$ $[M - H]^-$ 848.3142, found 848.3146 (0.5 ppm error).

2.6.6 N^6,N^6-bis(*tert*-Butoxycarbonyl)-5′-(*N*-*tert*-butoxycarbonyl-*N*-{*N*-[(4-benzyloxycarboxyamino-2-hydroxy)benzoyl]sulfamoyl})amino-5′-deoxy-2′,3′-*O*-isopropylideneadenosine triethylammonium salt (2-33)

To a stirring solution of **2-31** (0.75g, 2.62 mmol, 3 equiv) in DMF (4.4 mL) was added CDI (0.51 g, 3.15 mmol, 3.6 equiv) and the mixture heated to 60 °C for 2 h. The reaction mixture was cooled to 23 °C, and **2-36** (0.60 g, 0.87 mmol, 1.0 equiv) was added as a solution in DMF (4.4 mL) followed by solid Cs_2CO_3 (0.43 g, 1.31 mmol, 1.5 equiv), and stirred for 15 h. The crude reaction mixture was concentrated under reduced pressure to a dark oil and purified by flash chromatography (linear gradient 0–5% MeOH/DCM with 1% Et_3N) to give the title compound as a waxy light yellow solid (0.46 g, 50%). R_f = 0.61 (10% MeOH/DCM with 1% Et_3N); ^{1}H NMR (600 MHz, CD_3OD) δ 1.09 (t, J = 7.2 Hz, 9H), 1.36 (s, 9H), 1.38 (s, 18H), 1.40 (s, 3H), 1.61 (s, 3H), 2.67 (q, J = 7.2 Hz, 6H), 4.05 (dd, J = 15.0, 6.6 Hz, 1H), 4.18 (dd, J = 15.0, 7.2 Hz, 1H), 4.63 (td, J = 7.2, 3.0 Hz, 1H), 5.17 (s, 2H), 5.27 (dd, J = 5.4, 3.0 Hz, 1H), 5.57 (dd, J = 6.0, 3.0 Hz, 1H), 6.33 (d, J = 2.4

Hz, 1H), 6.82 (d, *J* = 9.0 Hz, 1H), 7.06 (s, 1H), 7.30 (d, *J* = 7.2 Hz, 1H), 7.36 (t, *J* = 7.8 Hz, 1H), 7.41 (d, *J* = 7.8 Hz, 1H), 7.75 (d, *J* = 8.4 Hz, 1H), 8.74 (s, 1H), 8.89 (s, 1H); ^{13}C NMR (150 MHz, CD_3OD) δ 10.9, 25.7, 27.7, 28.2, 28.5, 47.3, 53.8, 67.7, 83.8, 84.0, 85.4, 87.3, 92.1, 106.8, 109.9, 115.5, 116.0, 129.1, 129.3, 129.7, 130.7, 131.9, 134.6, 138.1, 145.0, 147.3, 151.2, 151.6, 153.3, 154.4, 154.5, 155.4, 162.4, 173.6; HRMS (ESI–): calculated for $C_{43}H_{53}N_8O_{15}S$ $[M - H]^-$ 953.3357, found 953.3328 (3.0 ppm error).

2.6.7 5′-Deoxy-5′-({*N*-[(2-hydroxy-4-amino)benzoyl]sulfamoyl}amino)adenosine (2-34)

To a Parr flask purged with Ar was added Pd/C (0.05 g, 0.47 mmol, 10% by weight), followed by **2-33** (0.50 g, 0.52 mmol, 1 equiv) dissolved in anhydrous MeOH (5.2 mL). The flask was evacuated and back-filled with H_2 five times before filling the flask to 40 psi H_2 and shaking on a Parr shaker at 23 °C. After 1 h, reaction was filtered over a pad of celite and concentrated under reduced pressure to a clear oil that was used directly.

To a flask containing the crude reaction mixture from above chilled to 0 °C was added 80% aqueous TFA (5.2 mL) that had also been chilled to 0 °C. The reaction was stirred for 1 h at 0 °C, 12 h at 4 °C, and 5 h at 23 °C. The reaction was concentrated under reduced pressure to remove all traces of TFA. Purification by preparative reverse-phase HPLC on a Phenomenex Gemini 10 μm C18 110 Å (250 × 21.2 mm) column was done at a flow rate of 20 mL/min with a gradient of 5–25% MeCN in 10 mM aqueous triethylammonium bicarbonate over 10 min, followed by 25% MeCN for 5 min. The

retention time of the product was 9.0 minutes (k' = 2.0) and the appropriate fractions were pooled and lyophilized to afford the title compound (90 mg, 34%) as a white solid. ^{1}H NMR (600 MHz, CD_3OD) δ 1.20 (t, J = 7.2 Hz, 9H), 2.95 (q, J = 7.2 Hz, 6H), 3.29–3.31 (m, 2H), 4.23 (dd, J = 6.6, 4.2 Hz, 1H), 4.35 (dd, J = 5.4, 3.0 Hz, 1H), 4.85–4.86 (m, 1H), 5.93 (d, J = 6.6 Hz, 1H), 6.05 (s, 1H), 6.12 (d, J = 9.0 Hz, 1H), 7.62 (d, J = 9.0 Hz, 1H), 8.30 (s, 1H), 8.31 (s, 1H); ^{13}C NMR (150 MHz, CD_3OD) δ 10.1, 46.6, 47.7, 73.2, 75.0, 86.1, 90.6, 101.9, 107.4, 110.9, 120.9, 132.4, 142.0, 150.7, 154.3, 154.6, 157.5, 163.7, 175.0; HRMS (ESI−): calculated for $C_{17}H_{19}N_8O_7S$ $[M - H]^-$ 479.1103, found 479.1095 (1.7 ppm error).

2.6.8 5′-Amino-*N*^{6}-cyclopropyl-5′-deoxy-2′,3′-*O*-isopropylideneadenosine (2-37)

DIAD (3.4 mL, 17.3 mmol, 1.5 equiv) was dissolved in THF (284 mL) that had been cooled to 0 °C. Ph_3P (4.5 g, 17.3 mmol, 1.5 equiv) was added as a solution in THF (61 mL), and the solution stirred at 0 °C for 15 min. Compound **2-43** (4.0 g, 11.5 mmol, 1.0 equiv) was added as a solution in THF (61 mL), and the solution stirred at 0 °C for 15 min. DPPA (4.96 mL, 23.0 mmol, 2.0 equiv) was added directly and the solution allowed to stir at 0 °C for 15 min then at 23 °C for 4.5 h. The reaction was quenched with distilled H_2O (200 mL). The mixture was extracted with CH_2Cl_2 (3 × 200 mL), and the combined organic layers were dried over $MgSO_4$, filtered, and concentrated under reduced pressure to a clear oil that was dried under high vacuum for at least 4 h before being used directly in the next step.

To a Parr flask purged with Ar was added Pd/C (0.185 g, 1.73 mmol, 10% by weight, added in 2 portions), followed by half the crude reaction mixture from above dissolved in anhydrous MeOH (49.5 mL). The flask was evacuated and back-filled with H_2 5 times before filling the flask to 30 psi H_2 and shaking on a Parr shaker at 23 °C. After 1.75 h, the reaction was filtered over a pad of celite, concentrated under reduced pressure to a dark oil, and purified by flash chromatography (linear gradient 0–10% MeOH/DCM). The same procedure was repeated with the second half of the crude reaction mixture to give the title compound as a foamy oil (0.76 g, 44% over 2 steps). R_f = 0.05 (10% MeOH/DCM); ^{1}H NMR (600 MHz, CD_3OD) δ 0.61–0.64 (m, 2H), 0.85–0.88 (m, 2H), 1.35 (s, 3H), 1.57 (s, 3H), 2.92 (d, J = 5.4 Hz, 2H), 3.35 (s, 1H), 4.21–4.24 (m, 1H), 5.01 (dd, J = 6.6, 3.6 Hz, 1H), 5.46 (dd, J = 6.6, 3.0 Hz, 1H), 6.13 (d, J = 3.0 Hz, 1H), 8.21 (s, 1H), 8.28 (s, 1H); ^{13}C NMR (150 MHz, CD_3OD) δ 7.7, 25.7, 27.7, 44.6, 55.0, 83.3, 85.0, 88.3, 91.70, 91.71, 115.7, 121.4, 141.7, 154.0, 157.2; HRMS (ESI+): calculated for $C_{16}H_{23}N_6O_3$ $[M + H]^+$ 347.1826, found 347.1821 (1.4 ppm error).

2.6.9 N^6-Cyclopropyl-5′-deoxy-2′,3′-*O*-isopropylidene-5′-[(sulfamoyl)amino]adenosine (2-39)

To a stirring solution of **2-37** (0.5 g, 1.44 mmol, 1.0 equiv) in CH_2Cl_2 (20.6 mL) was added **2-38** (0.63 g, 1.88 mmol, 1.3 equiv) and the mixture stirred at 23 °C for 14 h. The crude reaction was concentrated under reduced pressure to a foamy oil that was used directly in the next step.

To a Parr flask purged with Ar was added Pd/C (0.075 g, 0.7 mmol, 10% by weight), followed by the crude reaction mixture from above dissolved in anhydrous MeOH/THF (10 mL/5 mL). The flask was evacuated and back-filled with H_2 five times before filling the flask to 30 psi H_2 and shaking on a Parr shaker at 23 °C for 22 h. The reaction was filtered over a pad of celite, concentrated under reduced pressure to a clear oil, and purified by flash chromatography (linear gradient 0–10% MeOH/DCM) to give the title compound as a clear foamy oil (0.35 g, 62% over 2 steps). R_f = 0.13 (10% MeOH/DCM); ^{1}H NMR (600 MHz, CD_3OD) δ 0.63 (dd, *J* = 8.4, 4.2 Hz, 2H), 0.87 (dd, *J* = 7.2, 4.8 Hz, 2H), 1.34 (s, 3H), 1.59 (s, 3H), 3.35–3.36 (m, 1H), 3.37–3.41 (m, 2H), 4.46 (d, *J* = 2.4 Hz, 1H), 5.09 (dd, *J* = 6.0, 2.4 Hz, 1H), 5.31 (dd, *J* = 6.0, 4.2 Hz, 1H), 6.02 (d, *J* = 4.2 Hz, 1H), 8.15 (s, 1H), 8.34 (s, 1H); ^{13}C NMR (150 MHz, CD_3OD) δ 7.7, 25.7, 27.8, 46.1, 50.0, 83.2, 84.5, 85.3, 93.1, 115.8, 121.5, 141.8, 154.1, 157.3; HRMS (ESI–): calculated for $C_{16}H_{22}N_7O_5S$ $[M - H]^-$ 424.1409, found 424.1415 (1.4 ppm error).

2.6.10 N^6-Cyclopropyl-5′-deoxy-2′,3′-*O*-isopropylidene-5′-({*N*-[(2-methoxymethoxy)benzoyl]sulfamoyl}amino)adenosine triethylammonium salt (2-40)

To a stirring solution of **2-39** (0.2 g, 0.47 mmol, 1.0 equiv) in DMF at 0 °C was added **2-26** (0.20 g, 0.71 mmol, 1.5 equiv) followed by Cs_2CO_3 (0.46 g, 1.41 mmol, 3 equiv). The mixture was stirred at 0 °C for 30 min, then warmed to 23 °C and stirred for 12.5 h. The crude reaction was concentrated under reduced pressure to a brown oil and purified by flash chromatography (linear gradient 0–10% MeOH/EtOAc with 1% Et_3N) to give the

title compound as a 1:1 mixture with **2-26** that was taken on directly to the next step.

2.6.11 5′-*N*-[*N*-(2-Hydroxybenzoyl)sulfamoylamino]-N^6-cyclopropyl-5′-deoxyadenosine triethylammonium salt (2-41)

To a flask containing **2-40** (0.13 g, 0.19 mmol, 1.0 equiv) cooled to 0 °C was added 80% aqueous TFA (2.0 mL) that had also been chilled to 0 °C. After 30 min at 0 °C, the reaction was concentrated under reduced pressure to remove all traces of TFA. Purification by preparative reverse-phase HPLC on a Phenomenex Gemini 10 μm C18 110 Å (250 × 21.2 mm) column at a flow rate of 20 mL/min isocractic at 22% MeCN in 10 mM aqueous triethylammonium bicarbonate for 10 min, followed by washing the column with 90% MeCN for 5 min prior to re-equilibration. The retention time of the product was 7.2 minutes (k' = 1.4) and the appropriate fractions were pooled and lyophilized to afford the title compound (70.2 mg, 61%) as a white solid. ^{1}H NMR (600 MHz, CD_3OD) δ 0.63-0.66 (m, 2H), 0.87-0.90 (m, 2H), 1.12 (t, J = 7.8 Hz, 9H), 2.65 (s, 1H), 2.77 (q, J = 7.2 Hz, 6H), 3.33 (d, J = 4.2 Hz, 2H), 4.25 (q, J = 4.2 Hz, 1H), 4.37 (q, J = 3.0 Hz, 1H), 4.87 (solvent ovlp, 1H), 5.93 (d, J = 6.6 Hz, 1H), 6.75–6.79 (m, 2H), 7.26 (t, J = 7.8 Hz, 1H), 7.88 (d, J = 7.8 Hz, 1H), 8.24 (s, 1H), 8.40 (s, 1H); ^{13}C NMR (176 MHz, CD_3OD) δ 7.7, 10.5, 40.6, 46.7, 47.4, 73.2, 74.9, 86.0, 90.8, 118.0, 119.2, 121.2, 121.5, 131.0, 134.0, 141.8, 154.2, 157.3, 162.1, 174.3; HRMS (ESI–): calculated for $C_{20}H_{22}N_7O_7S$ $[M - H]^-$ 504.1307, found 504.1313 (1.1 ppm error).

2.6.12 N^6-Cyclopropyl-2′,3′-*O*-isopropylidene-2-phenyl-5′-*O*-(sulfamoyl)adenosine (2-48)

To a stirring solution of **2-47** (0.1 g, 0.24 mmol, 1.0 equiv) in DMF (1.0 mL) cooled to 0 °C was added Et_3N (0.3 mL, 0.24 mmol, 1.02 equiv) and solid sulfamoyl chloride (0.07 g, 0.59 mmol, 2.5 equiv) and the reaction allowed to stir at 0 °C for 1 h, then stirred for an additional 15 h at 23 °C. The reaction mixture was concentrated under reduced pressure to an opaque solid before diluting into EtOAc (30 mL). The organic layer was washed with deionized H_2O (3 × 30 mL) followed by saturated aqueous NaCl (30 mL). The organic layer was dried over $MgSO_4$, filtered, and concentrated under reduced pressure to a foamy white solid (0.95 g, 80%): all spectroscopic data agrees with literature values.[23]

2.6.13 2′,3′-*O*-di-Acetyl-5′-*O*-{*N*-[(2-acetyloxy)benzoyl]sulfamoyl}adenosine triethylammonium salt (2-51)

To a stirring solution of **2-1** (0.1 g, 0.18 mmol, 1.0 equiv) in DMF was added pyridine (0.05 mL, 0.68 mmol, 3.8 equiv) followed by acetic anhydride (0.11 mL, 1.13 mmol, 6.4 equiv) and the mixture allowed to stir at 23 °C for 21 h. The crude reaction mixture was concentrated under reduced pressure to a yellow oil and purified by flash chromatography (linear gradient 0–5% MeOH/DCM with 1% Et_3N) to afford an approximately 5:1 mixture of **2-51** and **2-52**. **2-51** was purified by semi-preparative reverse-phase HPLC on

a Phenomenex Gemini 10 μm C18 110 Å (250 × 10.0 mm) column at a flow rate of 5 mL/min with a linear gradient 20-70% MeCN in 10 mM aqueous triethylammonium bicarbonate for 10 min, followed by 70% MeCN for 5 min. The retention time of the product was 6.6 minutes (k' = 1.6) and the appropriate fractions were pooled and lyophilized to afford the title compound (57.8 mg, 46%) as a white solid. R_f = 0.25 (10% MeOH/DCM with 1% Et_3N); ^{1}H NMR (600 MHz, CD_3OD) δ 1.27 (q, J = 7.2 Hz, 9H), 2.00 (s, 3H), 2.13 (s, 3H), 2.26 (s, 3H), 3.17 (t, J = 6.0 Hz, 6H), 4.40 (dd, J = 14.4, 3.6 Hz, 1H), 4.44 (dd, J = 9.6, 3.0 Hz, 1H), 4.54 (d, J = 3.0 Hz, 1H), 5.70–5.71 (m, 1H), 5.89 (t, J = 6.0 Hz, 1H), 6.29 (d, J = 6.0 Hz, 1H), 7.02 (d, J = 7.8 Hz, 1H), 7.23 (t, J = 7.8 Hz, 1H), 7.41 (t, J = 7.2 Hz, 1H), 7.86 (d, J = 7.8 Hz, 1H), 8.19 (s, 1H), 8.59 (s, 1H); ^{13}C NMR (150 MHz, CD_3OD) δ 9.4, 20.3, 20.6, 21.4, 48.0, 69.1, 73.2, 75.3, 82.9, 87.0, 120.2, 124.1, 126.7, 131.9, 132.2, 133.1, 141.3, 150.8, 150.9, 154.2, 157.2, 171.0, 171.5, 172.0, 173.8; HRMS (ESI–): calculated for $C_{23}H_{23}N_6O_{11}S$ $[M - H]^-$ 591.1151, found 591.1170 (3.2 ppm error).

2.6.14 5′-*O*-[*N*-(2-Benzyloxybenzoyl)sulfamoyl]-N^6, N^6-bis(*tert*-butoxycarbonyl)-2′, 3′-*O*-isopropylideneadenosine triethyammonium salt (2-54)

To a stirring solution of **2-25** (0.54 g, 0.92 mmol, 1.0 equiv) in DMF (9.2 mL) cooled to 0 °C was added **2-53** (0.45 g, 1.38 mmol, 1.5 equiv) followed by Cs_2CO_3 (0.60 g, 1.84 mmol, 2.0 equiv) and the mixture was stirred at 23 °C for 21 h. The crude reaction mixture was concentrated under reduced pressure to a yellow oil that was taken up in

EtOAc (200 mL) and filtered. The precipitate was washed with additional EtOAc (200 mL), and the combined filtrate was concentrated under reduced pressure and purified by flash chromatography (linear gradient 0–5% MeOH/EtOAc with 1% Et_3N) to give the title compound as a white foamy oil (0.51 g, 62%). R_f = 0.37 (10% MeOH/EtOAc with 1% Et_3N); ^{1}H NMR (600 MHz, CD_3OD) δ 1.13 (t, J = 7.2 Hz, 9H), 1.35 (s, 3H), 1.40 (s, 18H), 1.61 (s, 3H), 2.83 (q, J = 7.2 Hz, 6H), 4.19–4.20 (m, 2H), 4.41 (dd, J = 6.0, 3.6 Hz, 1H), 5.12–5.13 (m, 3H), 5.38 (dd, J = 6.0, 3.6 Hz, 1H), 6.37 (d, J = 3.0 Hz, 1H), 6.95 (t, J = 7.8 Hz, 1H), 7.05 (d, J = 8.4 Hz, 1H), 7.25 (t, J = 7.8 Hz, 1H), 7.31–7.34 (m, 3H), 7.46 (d, J = 7.8 Hz, 1H), 7.52 (d, J = 7.2 Hz, 2H), 8.84 (s, 1H), 8.89 (s, 1H); ^{13}C NMR (150 MHz, CD_3OD) δ 10.2, 25.7, 27.8, 28.2, 47.4, 69.8, 71.6, 83.1, 85.4, 86.0, 86.2, 92.5, 115.3, 121.3, 121.9, 128.9, 129.2, 129.3, 129.6, 129.9, 130.3, 131.7, 131.9, 138.7, 146.8, 151.2, 151.7, 153.3, 154.6, 157.2, 176.9; HRMS (ESI–): calculated for $C_{37}H_{43}N_6O_{12}S$ $[M - H]^-$ 795.2665, found 795.2659 (0.8 ppm error).

2.6.15 2′,3′-*O*-di-Acetyl-5′-*O*-[*N*-(2-hydroxybenzoyl)sulfamoyl]adenosine triethylammonium salt (2-52)

To a flask containing **2-54** (0.51 g, 0.56 mmol, 1.0 equiv) chilled to 0 °C was added 80% aqueous TFA (6 mL) that had also been chilled to 0 °C and the mixture stirred at 0 °C for 1 h then at 23 °C for 3 h. The reaction mixture was concentrated under reduced pressure to a yellow oil and dried under high vacuum to remove all traces of TFA, then dissolved as a stirring solution in dry DMF (6.1 mL) to which was added pyridine (0.17 mL, 2.1

mmol, 3.8 equiv) followed by acetic anhydride (0.33 mL, 3.5 mmol, 6.4 equiv) and the mixture stirred at 23 °C for 16 h. The reaction was concentrated under reduced pressure to remove all traces of DMF before being used directly in the next step.

To a round-bottomed flask containing the crude product from above (0.25 g, 0.33 mmol, 1.0 equiv) purged with argon was added anhydrous MeOH (3.4 mL) followed by Pd/C (0.03 g, 0.28 mmol, 10% by weight) and the flask evacuated by house vacuum and back-filled with an H_2 balloon 3 times before being allowed to stir vigorously under an H_2 balloon at 23 °C for 2 h. The crude reaction mixture was filtered over a pad of celite and concentrated under reduced pressure to a dark oil. Purification by semi-preparative reverse-phase HPLC on a Phenomenex Gemini 10 μm C18 110 Å (250 × 10.0 mm) column at a flow rate of 5 mL/min isocratic at 35% MeCN in 10 mM aqueous triethylammonium bicarbonate for 10 min, followed by 70% MeCN for 5 min. The retention time of the product was 5.4 minutes (k' = 1.2) and the appropriate fractions were pooled and lyophilized to afford the title compound (90.0 mg, 42%) as a white solid. R_f = 0.18 (10% MeOH/DCM with 1% Et_3N); ^{1}H NMR (600 MHz, CD_3OD) δ 1.23 (t, J = 7.2 Hz, 9H), 2.00 (s, 3H), 2.10 (s, 3H), 3.03 (q, J = 7.2 Hz, 6H), 4.44 (dd, J = 12.0, 3.0 Hz, 1H), 4.47 (dd, J = 11.4, 3.6 Hz, 1H), 4.53 (q, J = 3.6 Hz, 1H), 5.70 (dd, J = 5.4, 3.6 Hz, 1H), 5.89 (t, J = 6.0 Hz, 1H), 6.27 (d, J = 6.6 Hz, 1H), 6.75–6.79 (m, 2H), 7.28 (t, J = 7.2 Hz, 1H), 7.93 (d, J = 7.8 Hz, 1H), 8.18 (s, 1H), 8.56 (s, 1H); ^{1}H NMR (600 MHz, DMSO-d_6) δ 1.17 (t, J = 7.2 Hz, 9H), 1.99 (s, 3H), 2.10 (s, 3H), 3.09 (q, J = 7.2 Hz, 6H), 4.25 (dd, J = 11.4, 4.8 Hz, 1H), 4.33 (dd, J = 11.4, 4.2 Hz, 1H), 4.44 (q, J = 4.2 Hz, 1H), 5.56 (dd, J = 5.4, 4.2 Hz, 1H), 5.90 (t, J = 6.0 Hz, 1H), 6.20 (d, J = 6.0 Hz, 1H), 6.72–

6.75 (m, 2H), 7.26 (t, J = 7.2 Hz, 1H), 7.36 (br s, 2H), 7.81 (d, J = 7.8 Hz, 1H), 8.14 (s, 1H), 8.46 (s, 1H), 13.5 (s, 1H); ^{13}C NMR (150 MHz, CD_3OD) δ 9.9, 20.3, 20.6, 47.8, 69.1, 73.0, 75.3, 82.7, 87.1, 118.0, 119.4, 120.2, 120.7, 131.6, 134.5, 141.3, 150.8, 154.2, 157.5, 162.3, 171.0, 171.5, 175.3; HRMS (ESI–): calculated for $C_{21}H_{21}N_6O_{10}S$ $[M - H]^-$ 549.1045, found 549.1048 (0.5 ppm error).

2.6.16 Procedures for the measurement of oral bioavailability of siderophore inhibitors in Sprague-Dawley rats

Sprague-Dawley rats (female, 250–274 g, Harlan Laboratories, Inc. Indianapolis, IN), were obtained with surgically implanted in-dwelling dual jugular vein/femoral vein catheters for compound infusion and blood withdrawal, respectively. Catheters were maintained by following the Harlan Surgically Modified Animal Models: Catheter Maintenance Recommendations provided by Harlan Laboratories. All animal care, housing, and laboratory procedures were approved by the University of Minnesota Institutional Animal Care and Use Committee (IACUC) prior to these investigations (IACUC #1208A18543). The animal care and housing was maintained by University of Minnesota Research Animal Resources (RAR) and veterinarian staff. Rats were allowed to acclimate for 7 days prior to participation in a study to ensure proper patency of the catheter lines as well as to observe that there were no adverse effects on the animals due to surgery or shipping. Oral doses of investigational compounds (25 mg/kg) were suspended in either 0.5% sodium carboxymethylcelluose (Aldrich, St. Louis, MO;

compounds **2-1**, **2-6**, **2-34**, and **2-41**) or dissolved in 25% wt/vol hydroxypropyl β-cyclodextrin (Cargill, Inc. Cedar Rapids, IA; **2-50**, **2-51**, and **2-52**) in sterile water as solubility allowed. Animals were sampled in triplicate and initially dosed via oral gavage with a ball-tipped feeding needle inserted through the mouth and esophagus with a 10 mg/mL solution of compound. The rats were restrained by holding them with 2 fingers over their shoulders with the thumb wrapped around underneath their shoulders to tilt their head up, and solution dispensed over 15–20 seconds. Rats were returned to their cages after drug administration with access to food and water *ad libitum*, and blood was removed in 0.25 mL aliquots from the left femoral vein catheter via tuberculin syringe with a sterile 22 gauge blunted needle (SAI Infusions, Inc. Lake Villa, IL) at the following time points: 0, 15, 30, 45, 60, 120, 240, and 480 min. Blood was immediately injected into a 2 mL vacutainer (Becton Dickinson, Franklin Lakes, NJ) containing 3.6 mg K_2 EDTA. Subsequently, blood was centrifuged at 2,000 × *g* in a microcentrifuge (Eppendorf, Enfield, CT) to separate the plasma from the hematocrit. Plasma was separated into two 50 μL aliquots that were immediately chilled on ice and transferred to -80 °C within 2 h.

Rats were given a 3 day period to wash any remaining compound from their system. Intravenous doses of investigational compounds (2.5 mg/kg) were prepared in either 0.05% sodium carboxymethylcellulose (Aldrich, St. Louis, MO; **2-1**, **2-6**, **2-34**, and **2-41**) or 25% wt/vol hydroxypropyl β-cyclodextrin (Cargill, Inc. Cedar Rapids, IA; **2-50**, **2-51**, and **2-52**) in sterile water as solubility allowed. The same triplicate set was then dosed via infusion in the right jugular vein catheter over 5 seconds via a tuberculin syringe with a

sterile 22 gauge blunted needle (SAI Infusions, Inc). Rats were returned to their cages after drug administration with access to food and water *ad libitum*, and 0.25 mL aliquots of blood were removed from the left femoral vein catheter via tuberculin syringe with a sterile 22 gauge blunted needle (SAI Infusions, Inc. Lake Villa, IL) at the following time points: 0, 5, 10, 15, 30, 45, 60, 120, 240, and 480 min. Blood was immediately injected into a 2 mL vacutainer (Becton Dickinson, Franklin Lakes, NJ) containing 3.6 mg K_2 EDTA and then transferred to a microcentrifuge tube. Subsequently, blood was centrifuged at 2,000 × *g* in a microcentrifuge (Eppendorf, Enfield, CT) to separate the plasma from the hematocrit. Plasma was separated into two 50 µL aliquots that were immediately chilled on ice and transferred to -80 °C within 2 h.

All plasma samples were analyzed by LC–MS/MS by Dr. Benjamin Duckworth of the Center for Drug Design, University of Minnesota.

Instrumentation

LC–MS/MS analysis was performed using a Agilent (Santa Clara, CA) 1260 Infinity gradient solvent delivery system, an Agilent 1260 Infinity HiP ALS autosampler, an Agilent 1260 column oven, and an AB SCIEX QTRAP 5500 (Framingham, MA) mass spectrometer fitted with an electrospray ionization source. The instruments were run using Analyst Software (version 1.5.2, AB SCIEX).

Chromatography

Reverse-phase HPLC analysis was performed by gradient HPLC on a Kinetix C18 column (50 mm × 2.1 mm, 2.6 µm particle size; Phenomenex, Torrance, CA) for Sal-AMS derivatives and a Synergy Hydro RP (250 mm × 2.0 mm, 4 µm particle size;

Phenomenex) for isoniazid. Mobile phase A was 0.1% aqueous formic acid while mobile phase B was 0.1% formic acid in acetonitrile. Initial conditions were 5% B from 0 to 0.5 min, after which the %B was increased to 95% from 0.5 to 1 min. The column was washed in 95% B for 3 min, returned to 5% over 0.2 min, and allowed to re-equilibrate for 3.8 min in 5% B to provide a total run time of 8 min. The flow rate was 0.5 mL/min and the column oven was maintained at 40 °C. The injection volume was 10 µL.

Mass spectrometry

All analytes were analyzed in positive ionization mode by Multiple Reaction Monitoring (MRM) with the following mass spectrometry settings: entrance potential = 10 V; curtain gas = 40 psi; collision gas = medium; ionspray voltage = 5500 V; temperature = 600 °C; ion source gas 1 = 45 psi; ion source gas 2 = 40 psi. Nitrogen was used for the nebuliser and collision gas. To determine the optimum MRM settings (Table 1), each analyte was infused at a concentration of 10 µM (in 1:1 water:acetonitrile containing 0.1% formic acid) onto the MS by a syringe pump at a flow of 10 µL/min.

Compound	Parent Ion (*m/z*)	Fragment Ion (*m/z*)	Declustering Potential (V)	Collision Energy (V)	Collision Cell Exit Potential (V)
INH	138.0	177.2	40	19	24
Nicotinamide	123.0	106.1	40	21	14
2-1	467.1	347.2	130	25	16
2-6	466.1	267.1	60	23	14
2-34	506.1	369.1	79	30	14
2-41	481.0	136.1	140	51	18
2-50	583.0	252.2	90	70	30
2-51	593.0	352.1	80	26	20
2-52	551.0	352.2	140	23	19

Plasma Sample Preparation

Plasma (20 μL) was protein-precipitated with acetonitrile (ACN, 200 μL) containing internal standard. For compounds **2-1**, **2-6**, **2-34**, **2-41**, **2-51**, and **2-52**, compound **2-50** was used as the internal standard at a final concentration of 100 nM in ACN. Compound **2-1** (500 nM) was used as the internal standard for the analysis of **2-50** in plasma samples. For INH analysis, nicotinamide (50 μM) was used as the internal standard. After adding ACN containing internal standard, samples were vortexed for 5 seconds, centrifuged at 14,000 × g for 1 min at 4 °C, and the supernatant was analyzed via LC–MS/MS. Standards were prepared in pooled female Sprague-Dawley rat plasma in K_2EDTA (BioChemed, Winchester, VA) and processed in a similar fashion as animal plasma samples.

Data Analysis

Analyte and internal standard peak areas were calculated with MultiQuant Software (version 2.0.2, AB SCIEX, Framingham, MA). Analyte peak areas were normalized to internal standard peak areas, and the concentrations were calculated with the appropriate standard curve. Standard curves displayed good linearity with $R^2 = 0.99$. Pharmacokinetic parameters were calculated from concentration-time profiles by non-compartamental analysis using Phoenix WinNonLin (version 6.3, Pharsight).

2.6.17 Procedure for the measurement of stability of prodrugs 2-51 and 2-52 in simulated gastric fluid (SGF)

Prodrugs (100 μM final concentration) were incubated at 37 °C in simulated gastric fluid (SGF, pH 1.2).[48] In triplicate, SGF samples (980 μL) were pre-incubated for 5 min at 37 °C followed by the addition of 20 μL of a 5 mM DMSO stock solution of the compound. The final incubation volume was 1.0 mL and aliquots (100 μL) were removed from the incubation solution at 0, 15, 30, 45, 60, 90, and 120 min, and immediately injected (25 μL) onto the HPLC. Analysis was conducted on an HPLC system composed of an Agiletn 1,100 Liquid Chromatograph (Agilent Technologies, Santa Clara, CA) using a Phenomenex Gemini 5 μm C18 110 Å (250 × 4.6 mm) column (Phenomenex, Torrance, CA) and a Shimadzu UV/Vis detector (Shimadzu, Kyoto, Japan) at a wavelength of 254 nm operated at a flow rate of 1 mL/min isocratic at 35% MeCN in 10 mM aqueous triethylammonium bicarbonate for 6.5 min. Compound **2-51** had a retention time of 4.1 min (k' = 1.4), and compound **2-52** had a retention time of 5.4 min (k' = 2.2). The mono-acetate degradation product was identified by low resolution LC–MS on an Agilent TOF II TOF/MS (Agilent Technologies, Santa clara, CA) instrument equipped with an ESI interface with a retention time of 3.3 min (k' = 0.94). Stability was determined by calculating the percentage of the prodrug remaining after the final incubation time point.

2.7 References

1. Posey, J. E.; Gherardini, F. C. Lack of a role for iron in the lyme disease pathogen. *Science* **2000**, *288*, 1651–1653.

2. Aisen, P.; Leibman, A.; Zweier, J. Stoichiometric and site characteristics of the binding of iron to human transferring. *J. Biol. Chem.* **1978**, *253*, 1930–1937.

3. Ferreras, J. A.; Ryu, J. S.; Di Lello, F.; Tan, D. S., Quadri, L. E. Small-molecule inhibition of siderophore biosynthesis in *Mycobacterium tuberculosis* and *Yersinia pestis*. *Nat. Chem. Biol.* **2005**, *1*, 29–32.

4. Somu, R. V.; Boshoff, H.; Qiao, C.; Bennett, E. M.; Barry, C. E., 3rd; Aldrich, C. C. Rationally designed nucleoside antibiotics that inhibit siderophore biosynthesis of *Mycobacterium tuberculosis*. *J. Med. Chem.* **2006**, *49*, 31–34.

5. Quadri, L. E. Strategic paradigm shifts in the antimicrobial drug discovery process of the 21st century. *Infect. Disord. Drug Targets* **2007**, *7*, 230–237.

6. Miethke, M.; Marahiel, M. A., Siderophore-based iron acquisition and pathogen control. *Microbiol. Mol. Biol. Rev.* **2007**, *71*, 413–51.

7. Chavadi, S. S.; Stirrett, K. L.; Edupuganti, U. R.; Vergnolle, O.; Sadhanandan, G.; Marchiano, E.; Martin, C.; Qiu, W-G.; Soll, C. E.; Quadri, L. E. N. Mutational and phylogenetic analyses of the mycobacterial *mbt* gene cluster. *J. Bacteriol.* **2011***, 193*, 5905–5913.

8. De Voss, J. J.; Rutter, K.; Schroeder, B. G.; Su, H.; Zhu, Y.; Barry, C. E., 3rd. The salicylate-derived mycobactin siderophores of *Mycobacterium tuberculosis* are essential for growth in macrophages. *Proc. Natl. Acad. Sci. U.S.A*. **2000**, *97*, 1252–1257.

9. Timm, J.; Post, F. A.; Bekker, L. G.; Walther, G. B.; Wainwright, H. C.; Manganelli, R.; Chan, W. T.; Tsenova, L.; Gold, B.; Smith, L.; Kaplan, G.; McKinney, J. D. Differential expression of iron-, carbon-, and oxygen-responsive mycobacterial genes in the lungs of chronically infected mice and tuberculosis patients. *Proc. Natl. Acad. Sci. U.S.A*. **2003**, *100*, 14321–14326.

10. Quadri, L. E.; Sello, J.; Keating, T. A.; Weinreb, P. H.; Walsh, C. T. Identification of a *Mycobacterium tuberculosis* gene cluster encoding the biosynthetic enzymes for assembly of the virulence-conferring siderophore mycobactin. *Chem. Biol.* **1998**, *5*, 631–645.

11. Miethke, M.; Bisseret, P.; Beckering, C. L.; Vignard, D.; Eustache, J.; Marahiel, M. A. Inhibition of aryl acid adenylation domains involved in bacterial siderophore synthesis. *FEBS J.* **2006**, *273*, 409–419.

12. Somu, R. V.; Wilson, D. J.; Bennett, E. M.; Boshoff, H. I.; Celia, L.; Beck, B. J.; Barry, C. E. 3rd; Aldrich, C. C. Antitubercular nucleosides that inhibit siderophore biosynthesis: SAR of the glycosyl domain. *J. Med. Chem.* **2006**, *49*, 7623–7635.

13. Vannada, J.; Bennett, E. M.; Wilson, D. J.; Boshoff, H. I.; Barry, C. E. 3rd; Aldrich, C. C. Design, synthesis, and biological evaluation of beta-ketosulfonamide adenylation inhibitors as potential antitubercular agents. *Org. Lett.* **2006**, *8*, 4707–4710.

14. Qiao, C. H.; Gupte, A.; Boshoff, H. I.; Wilson, D. J.; Bennett, E. M.; Somu, R. V.; Barry, C. E., 3rd; Aldrich. C. C. 5'-*O*- [(*N*-Acyl)sulfamoyl]adenosines as antitubercular agents that inhibit MbtA: An adenylation enzyme required for siderophore biosynthesis of the mycobactins. *J. Med. Chem.* **2007**, *50*, 6080–6094.

15. Gupte, A.; Boshoff, H. I.; Wilson, D. J.; Neres, J.; Labello, N. P.; Somu, R. V.; Xing, C.; Barry, C. E. 3rd; Aldrich, C. C. Inhibition of siderophore biosynthesis by 2-triazole substituted analogues of 5'-*O*-[*N*-(salicyl)sulfamoyl]adenosine: antibacterial nucleosides effective against *Mycobacterium tuberculosis*. *J. Med. Chem.* **2008**, *51*, 7495–7507.

16. Sikora, A. l.; Wilson, D. J.; Aldrich. C. C.; Blanchard, J. S. Kinetic and inhibition studies of dihydroxybenzoate-AMP ligase from *Escherichia coli*. *Biochemistry* **2010**, *49*, 3648–3657.

17. Lipinski, C. A.; Lombardo, F.; Dominy, B. W.; Feeney, P. J. Experimental and computational approaches to estimate solubility and permeability in drug discovery and development settings. *Ad. Drug Del. Rev.* **2001**, *46*, 3–26.

18. Leeson, P.D.; Davis, A. M. Time-related differences in the physical property profiles of oral drugs. *J. Med. Chem.* **2004**, *47*, 6338–6348.

19. O'Shea, R.; Moser, H.E. Physicochemical properties of antibacterial compounds: Implications for drug discovery. *J. Med. Chem.* **2008**, *51*, 2871–2878.

20. Bisseret, P.; Thielges, S.; Stephane, B.; Miethke, M.; Marahiel, M. A.; Eustache, J. Synthesis of a 2-indolylphosphonamide derivative with inhibitory activity against yersiniabactin biosynthesis. *Tetrahedron Lett.* **2007**, *48*, 6080–6083.

21. Qiao, C. H.; Wilson, D. J.; Bennett, E. M.; Aldrich, C. C. A mechanism-based aryl carrier protein/thiolation domain affinity probe. *J. Am. Chem. Soc.* **2007**, *129*, 6350–6351.

22. Neres, J.; Labello, N. P.; Somu, R. V.; Boshoff, H. I.; Wilson D. J.; Vannada, J.; Chen, L.; Barry, C. E. 3rd; Bennett, E. M.; Aldrich, C. C. Inhibition of siderophore biosynthesis in *Mycobacterium tuberculosis* with nucleoside bisubstrate analogues: Structure activity relationships of the nucleobase domain of 5'-*O*-[*N*-(salicyl)sulfamoyl]adenosine. *J. Med. Chem.* **2008**, *51*, 5349–5370.

23. Labello, N. P; Bennett, E. M.; Ferguson, D. M.; Aldrich, C. C. Quantitative three dimensional structure linear interaction energy model of 5'-*O*-[*N*-(salicyl)sulfamoyl]adenosine and the aryl acid adenylating enzyme MbtA. *J. Med. Chem.* **2008**, *51*, 7154–7160.

24. Maryanoff, B. E.; Costanzo, M. J.; Nortey, S. O.; Greco, M. N.; Shank, R. P.; Schupsky, J. J.; Ortegon, M. P.; Vaught, J. L. Structure-activity studies on anticonvulsant sugar sulfamates related to topiramate. Enhanced potency with cyclic sulfate derivatives. *J. Med. Chem.* **1998**, *41*, 1315–1343.

25. Black. F. J.; Kocienski, P. J. Synthesis of phalluside-1 and sch II using 1,2-metallate rearrangements. *Org. Biomol. Chem.* **2010**, *8*, 1188–1193.

26. Lu, X.; Zhang, H.; Tonge, P. J.; Tan, D. S. Mechanism-based inhibitors of MenE, an acyl-CoA synthetase involved in bacterial menaquinone biosynthesis. *Bioorg. Med. Chem. Lett.* **2008**, *18*, 5963–5966.

27. Matsuda, A.; Shinozaki, M.; Yamaguchi, T.; Homma, H.; Nomoto, R.; Miyaska, T.; Watanabe, Y.; Abiru, T. Nucleosides and nucleotides. 103. 2-Alkynyladenosines: A novel class of selective adenosine A_2 receptor agonists with potent antihypertensive effects. *J. Med. Chem.* **1992**, *35*, 241–252.

28. Beaumont, K.; Webster, R.; Gardner, I.; Dack, K. Design of ester prodrugs to enhance oral absorption of poorly permeable compounds: Challenges to the discovery scientist. *Curr. Drug Metab.* **2003**, *4*, 461–485.

29. Belanger, P. M.; Lalande, M.; Dore, F. M.; Labrecque, G. Temporal variations in the pharmacokinetics of isoniazid and *N*-acetylisoniazid in rats. *Drug. Metab. Dispos.* **1989**, *17*, 91–97.

30. Isoniazid. *Tuberculosis* **2008**, *88*, 112–116.

31. Ng, K-y.; Zhou, H.; Zhang, Y. L.; Hybertson, B.; Randolph, T.; Christians, U. Quantification of isoniazid and acetylisoniazid in rat plasma and alveolar

macrophages by liquid chromatography-tandem mass spectrometry with on-line extraction. *J. Chromatogr. B* **2007**, *847*, 188–198.

32. Baldan, H. M.; De Rosa, H. J.; Brunetti, I. L.; Ximenes, V. F.; Machado, R. G. P. The effect of rifampicin and pyrazinamide on isoniazid pharmacokinetics in rats. *Biopharm. Drug Dispos.* **2007**, *28*, 409–413.

33. Zhou, H.; Zhang, Y.; Biggs, D. L.; Manning, M. C.; Randolph, T. W.; Christians, U.; Hybertson, B. M.; Ng, K-y. Microparticle-based lung delivery of INH decreases INH metabolism and targets alveolar macrophages. *J. Control. Release* **2005**, *107*, 288–299.

34. Palm, K.; Stenber, P.; Luthman, K.; Artursson, P. Polar molecular surface properties predict the intestinal absorption of drugs in humans. *Pharm. Res.* **1997**, *14*, 568–571.

35. Clark, D. E. Rapid calculation of polar molecular surface area and its application to the prediction of transport phenomena. 1. Prediction of intestinal absorption. *J. Pharm. Sci.* **1999**, *88*, 807–814.

36. Navia, M. A.; Chaturvedi, P.R. Design principles for orally bioavailable drugs. *Drug Discovery Today* **1996**, *1*, 179–189.

37. Smith, A. B. III; Hirschmann, R.; Pasternak, A.; Yao, W.; Sprengler, P. A.; Halloway, M. K.; Kuo, L. C.; Chen, Z.; Darke, P. L.; Schleif, W. A. An orally bioavailable pyrrolinone inhibitor of HIV-1 protease: Computation analysis and X-ray crystal structure of the enzyme complex. *J. Med. Chem.* **1997**, *40*, 2440–2444.

38. Veber, D. F.; Johnson, S. R.; Cheng, H-Y.; Smith, B. R.; Ward, K. W.; Kopple, K. D. Molecular properties that influence the oral bioavailability of drug candidates. *J. Med. Chem.* **2002**, *45*, 2615–2623.

39. Schulzke, J. D.; Ploeger, S.; Amasheh, M.; Fromm, A.; Zeissig, S.; Troeger, H.; Richter, J.; Bojarski, C.; Schumann, M.; Fromm, M. Epithelial tight junctions in intestinal inflammation. *Ann. N. Y. Acad. Sci.* **2009**, *1165*, 294–300.

40. Ponferrada, Á.; Caso, J. R.; Alou, L.; Colón, A.; Sevillano, D.; Moro, M. A.; Lizasoain, I.; Menchén, P.; Gómez-Lus, M.; Lorenzo, P.; Cos, E.; Leza, J. C.; Menchén, L. The role of PPARγ on restoration of colonic homeostasis after experimental stress-induced inflammation and dysfunction. *Gastroenterology* **2007**, *132*, 1791–1803.

41. Balimane, P. V.; Sinko, P. J. Involvement of multiple transporters in the oral

absorption of nucleoside analogues. *Adv. Drug Deliv. Rev.* **1999**, *39*, 183–209.

42. Li, F.; Maag, H.; Alfredson, T. Prodrugs of nucleoside analogues for improved oral absorption and tissue targeting. *J. Pharm. Sci.* **2008**, *97*, 1109–1134.

43. Strickley, R. G. Solubilizing excipients in oral and injectable formulations. *Pharm. Res.* **2004**, *21*, 201–230.

44. Heacock, D.; Forsyth, C. J.; Shiba, K.; Musier-Forsyth, K. Synthesis and aminoacyl-tRNA synthetase inhibitory activity of prolyl adenylate analogs. *Bioorg. Chem.* **1996**, *24*, 273–289.

45. Smit, C.; Blümer, J.; Eerland, M. F.; Albers, M. F.; Müller, M. P.; Goody, R. S.; Itzen, A.; Hedber, C. Efficient synthesis and applications of peptides containing adenylylated tyrosine residues. *Angew. Chem. Int. Ed.* **2011**, *50*, 9200–9204.

46. Ikeuchi, H.; Meyer, M. E.; Ding, Y.; Hiratake, J.; Richards, N. G. A critical electrostatic interaction mediates inhibitor recognition by human asparagine synthetase. *Bioorg. Med. Chem.* **2009**, *17*, 6641–6650.

47. Kurokawa, T.; Kim, M.; Du Bois, J. Synthesis of 1,3-diamines through rhodium-catalyzed C–H insertion. *Angew. Chem. Int. Ed.* **2009**, *48*, 2777–2779.

48. US Pharmacopeia Test Solution for Simulated Gastric Fluid. http://www.pharmacopeia.cn/v29240/usp29nf24s0_ris1s126.html.

Chapter 3. A Light-Activated Probe for the Study of Adenylation Domains in *Mycobacterium tuberculosis*

The following chapter involves original work designed by Dr. Benjamin Duckworth and Dr. Courtney C. Aldrich. The synthesis of the probes was first performed by Dr. Duckworth, with improvement and full characterization performed by Kathryn M. Nelson. The biological assays were performed by Dr. Duckworth and Daniel Wilson. KMN compiled the LC–MS/MS data into Table 3.1 and analyzed this data for the purposes of this thesis. This work was published in *ACS Chemical Biology*, and some figures and excerpts are reproduced with permission from that journal (see preface above).

3.1 Introduction

3.1.1 Chemical probes for investigation of target enzymes

Chemical probes are becoming an increasingly common tool in medicinal chemistry research. The design and application of these probes varies across different disciplines. Small fluorescent probes find use in bioimaging. By using small-molecule synthetic organic dyes that specifically interact with a target of interest, researchers can observe biomolecules in their native environments.[1] These probes further our understanding of the

biological roles (including production, trafficking, etc) of biomolecules in living systems. Probes have also found great application in proteomics. The field of proteomics aims to not only identify all members of the protein, but also attempts to assign protein function, protein localization, and the mapping of regulatory pathways and networks for those proteins. Chemical techniques aide this process by chemically separating or modifying the proteome to facilitate analysis of smaller fractions of proteins within the proteome, splitting the data into more manageable pieces.[2] As discussed in Chapter 1, target identification is becoming increasingly important in modern drug discovery. Chemical probes have become a critical tool for many in identifying and confirming a therapeutic target, as well as identifying secondary targets for efforts to reduce side effects.

As the popularity of chemical probes grows, so have trends in generally successful or problematic techniques emerged. Recent publications have generated some general guidelines that should be followed when designing a chemical probe for any of the above applications, the details of which are beyond the scope of this discussion.[3–6] Workman and Collins have summarized these guidelines into four general categories (**Figure 3.1**): 1) chemical properties, 2) biological potency, 3) biological selectivity, and 4) context for use.[4] While these general considerations seem obvious, the practical challenge of addressing all four in one molecule can mount quickly.

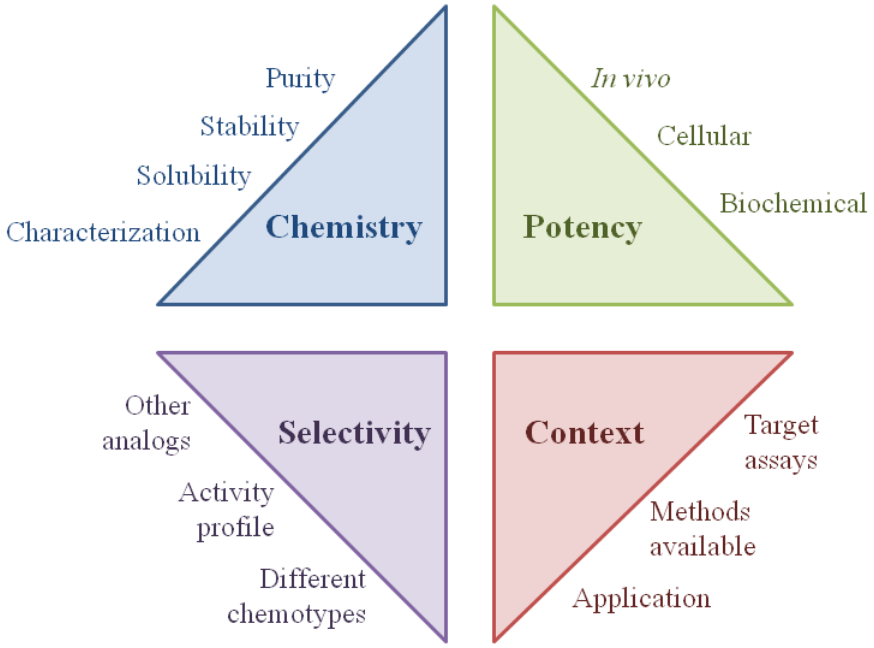

Figure 3.1. Guidelines for the design of new chemical probes broken into four general categories. Adapted from Workman and Collins.[4]

From a chemical perspective, a probe must be easy to access synthetically with good purity, solubility, and stability–particularly to any acidic or basic environments it may experience in an assay. Chemical probes should be used in cellular assays whenever possible to evaluate membrane permeability and toxicological effects. The biological potency of a probe is largely dependent on its intended use, however the selectivity of a probe can be the most limiting factor for its design. Probes need to be evaluated for their selectivity in a broad manner to ensure that the observed effects are not due to off-target activity, but solely the intended target(s). Finally, the design and use of a probe must be tailored to permeate both mammalian and bacterial cells, and cannot necessarily be extracted from another design and system (e.g. probes investigating cancer chemotherapy

targets). While it is true that chemical tools need to meet at least some basic criteria in order to be useful for their particular purpose, the above guidelines need to be evaluated in a dynamic manner with the intended application. Especially when investigating a new target, iterative probe design may be necessary as more is learned about the ligand-target system, as well as the pharmacokinetic properties of the parent structure. New designs should not be discarded because they do not fit all the "rules", but assessed for their usefulness by these guidelines.

3.1.2 Investigating a secondary target of Sal-AMS (3-1) in *Mtb*

As discussed in Chapter 2, the inhibition of siderophore biosynthesis has emerged as a novel strategy for the development of new antibacterial agents for *Mtb* and other pathogenic bacteria.[7–9] While *Mtb* requires iron for its survival; the concentration of free iron is highly restricted in biological fluids, due in large part to the insolubility of iron under aerobic conditions and the sequestration by iron-binding proteins such as transferrin and lactoferrin.[10,11] To survive these limiting conditions, *Mtb* biosynthesizes, excretes, and re-uptakes mycobactins; the family of siderophores responsible for iron acquisition in *Mtb*.[12] Several observations have established the necessity of mycobactins for *Mtb* pathogenesis, which were discussed in Chapter 2 and will not be repeated here.[13,14] Our lab and others have developed a potent nanomolar bisubstrate inhibitor of MbtA, 5′-*O*-[*N*-(salicyl)sulfamoyl]adenosine (Sal-AMS, **3-1**), as a mimic of the acyl-adenylate intermediate that has impressive antitubercular activity under iron-deficient

conditions with a minimum inhibitory concentration (MIC) of 0.39 μM.[7,15,16] The design of this inhibitor takes advantage of both the salicylic acid and ATP binding domains, but replaces the labile acyl phosphate with a more stable isosteric acyl sulfamate (**Figure 3.2**).

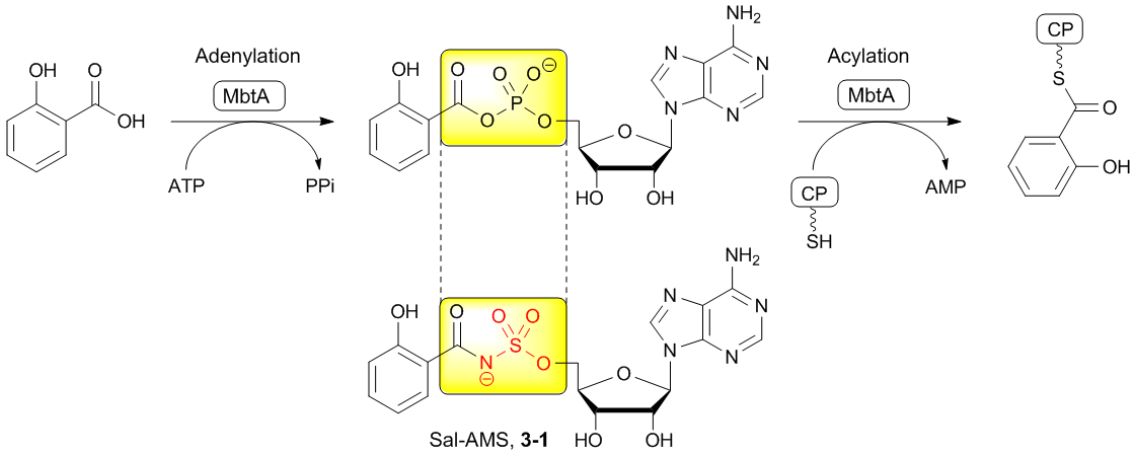

Figure 3.2. Design of 5'-*O*-[*N*-(salicyl)sulfamoyl]adenosine (Sal-AMS, **3-1**). The bisubstrate mimic incorporates a stable acyl sulfamate isotere in replacement of the labile acyl phosphate. Partially adapted from Vannada, et. al.[17]

Sal-AMS also shows activity in iron-replete conditions (MIC = 1.56 μM), suggesting a potential secondary mechanism of action due to off-target binding.[8] Adenylation (activation of a carboxylic acid as the AMP ester) in *Mtb* is a ubiquitous process in both primary and secondary metabolic pathways including protein synthesis, glycolysis, lipid metabolism, and cofactor biosynthesis. There are 67 putatively encoded adenylation enzymes in *Mtb*, any of which may represent potential off-targets of Sal-AMS.[18] Furthermore, Sal-AMS could potentially bind any one of the numerous adenosine-binding proteins in *Mtb*.

3.1.3 Design of a clickable photoaffinity probe for the study of MbtA

When we first reported Sal-AMS, we hypothesized it would only be active against *Mtb* under iron-limiting conditions, mimicking the environment seen by the bacteria when infecting a human host. It has been shown that under these iron-limiting conditions, siderophore biosynthesis is heavily upregulated.[14] Since the bacteria should be able to acquire iron through other mechanisms in iron-replete conditions, we did not expect to see whole-cell activity against *Mtb* in these conditions. What we observed, however, was activity against the bacteria under both conditions (**Table 3.1**, **Section 3.3.3** below). Adenylation (activation of a carboxylic acid as the AMP ester) is a ubiquitous process in both primary and secondary metabolic pathways in *Mtb*, including protein synthesis, glycolysis, lipid metabolism, and cofactor biosynthesis. In fact, *Mtb* putatively encodes for at least 67 enzymes that catalyze adenylation, any of which may represent potential off-targets of Sal-AMS.[18] Furthermore, Sal-AMS could also potentially bind any one of the numerous adenosine-binding proteins in *Mtb*. A comprehensive understanding of the mechanism of action of Sal-AMS will facilitate the design of improved chemical probes to unequivocally chemically validate siderophore biosynthesis as a virulence target, and improve the selectivity of our inhibitors as antitubercular agents.

Of the several strategies available for identifying and/or validating drug targets, affinity-based protein profiling (ABPP) has proven highly effective for target discovery.[19–22] A successful ABPP experiment begins with the design of a chemical probe that can both bind and cross-link to the target enzyme (**Figure 3.3**).

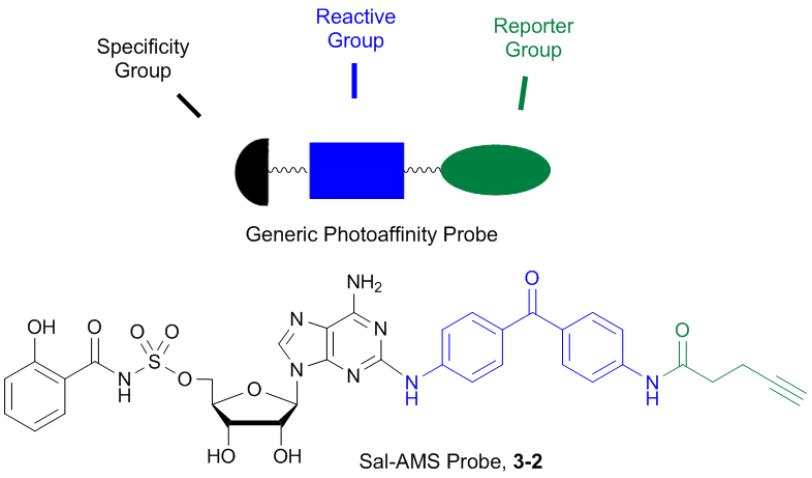

Figure 3.3. Photoaffinity probe design. A photoaffinity probe generally has three parts: (1) Specificity Group - imparts selectivity for your enzyme of interest, (2) Reactive Group - a photoreactive group that can be selectively activated to covalently cross-link to the enzymes that have bound the probe, and (3) Reporter Group - any group that can be used directly or as a handle for labeling with a fluorescent or other tagged group. Shown below is the structure of the Sal-AMS probe (**3-2**) used in this study.

The Sal-AMS probe (**3-2**, **Figure 3.3**) mimics the substrate Sal-AMS. The portion of the probe colored in black (Sal-AMS) imparts the binding selectivity for MbtA and potential off-target proteins. Previously mentioned SAR studies from our lab indicated that MbtA tolerates modification of Sal-AMS at the C-2 position of the adenine base.[24] Therefore, the reactive and reporter groups were tethered at the C-2 position. For a reactive group, we chose to use the photoreactive benzophenone moiety that has seen previous success in cross-linking photoaffinity probes to proteins.[25] Prior to UV activation, this photo-

activatable group must be stable and allow the probe to bind its protein target(s). Exposure of the benzophenone group to 365 nm (UV) light generates a reactive species that covalently cross-links to any amino acid residues in close proximity.[26, 27] While the benzophenone is a relatively bulky group, SAR studies suggest that it would be well tolerated for MbtA binding. Furthermore, it is generally accepted that the photocross-linking efficiency of benzophenone is higher than that of aryl azides.[26] Therefore, a small alkyne handle was incorporated, onto which a fluorescent- or biotin-azide could be installed via the copper-mediated [3+2] cycloaddition ("click" reaction) post-photolysis to aid in visualization and enrichment, respectively.[28]

To elucidate the protein targets of an inhibitor, the photoaffinity probe is first incubated with the proteome through incubation with whole cells or cell lysate (**Figure 3.4A**). Ultraviolet irradiation with the appropriate wavelength allows the probe to covalently cross-link to proteins bound by the probe. After UV photolysis, the labeled proteins are then separated by gel electrophoresis or by liquid chromatography coupled with mass spectrometry (LC−MS). In a separate experiment, the proteome is pre-incubated with excess inhibitor (in this case, Sal-AMS will be used) prior to probe incubation and photolysis (**Figure 3.4B**). Protein targets are identified by the disappearance of fluorescent labeling upon pre-incubation with inhibitor. In order to successfully apply ABPP to target discovery, careful attention must be given to developing and validating the chemical probe. The probe reported herein represents the first photoaffinity probe developed for an adenylating enzyme in *Mtb*. Since *Mtb* and other pathogenic bacteria contain numerous adenylating enzymes involved in a multitude of essential cellular

functions, we expect the strategy outlined here for our probe development will be broadly useful for proteomic profiling of adenylating enzymes.

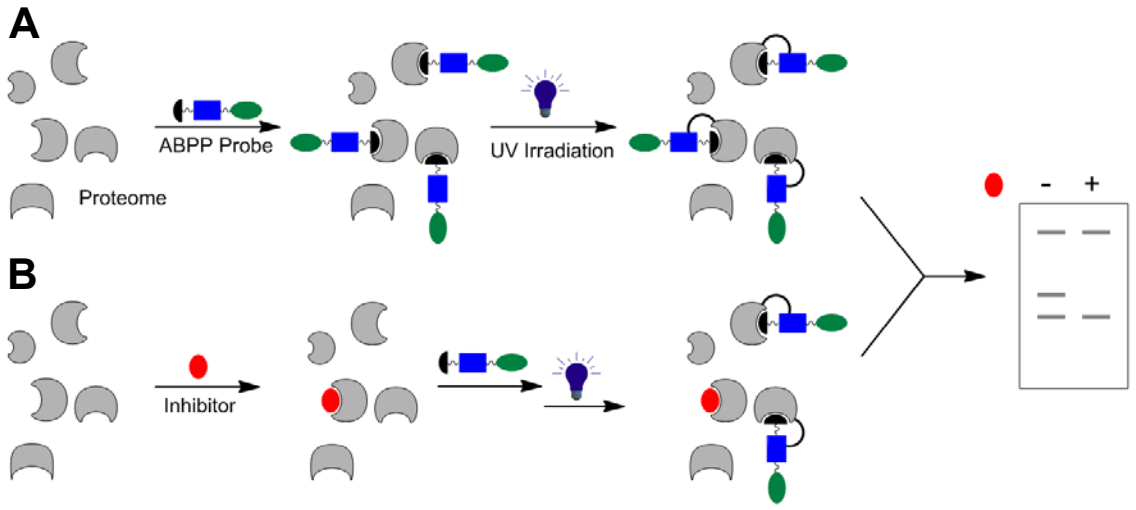

Figure 3.4. (A) General strategy for photoaffinity labeling of a class of enzymes using a photoaffinity probe and gel electrophoresis as the detection method. (B) Preincubation with excess inhibitor before labeling with a probe. Adapted from Duckworth, et al.[23]

3.2 Research Objectives

A light-activated benzophenone molecule was developed for use as a probe to determine the target specificity of our lead compound Sal-AMS (**3-1**) against the adenylating enzyme MbtA from the mycobactin biosynthetic pathway in *Mtb*. Previous structure-activity relationship studies from our lab have shown that MbtA tolerates modification at the C-2 position of the adenine base in Sal-AMS. We chose this position to link the photoactive benzophenone and a small alkyne handle through which we plan to attach a fluorescent-azide reporter group or biotin-azide enrichment group via a copper-mediated [3+2] cycloaddition ("click" reaction). This probe will used to confirm MbtA as a cellular

target of Sal-AMS, and investigate other potential targets for Sal-AMS action.

3.3 Results

3.3.1 Synthesis of a clickable photoaffinity probe for the study of MbtA

The original synthesis was performed by Dr. Benjamin Duckworth of the Aldrich lab. His synthesis was relatively inefficient (0.4% overall yield), so the synthesis was improved to generate more probe for the whole cell assays, as well as generate characterization data acceptable for publication. The synthesis of probe **3-2** began with a peptide coupling between the known acid **3-3**[29] and the symmetrical 4,4'-diaminobenzophenone **3-4**. Initially, this coupling was carried out by standard DCC coupling conditions, with poor yields (**Scheme 3.1**). A scan of coupling conditions found that reaction with 3-(diethoxyphosphoryloxy)-1,2,3-benzotriazin-4(3*H*)-one (DEPBT, **3-5**) and triethylamine (Et_3N) as a base for 72 hours gave greatly improved yield of the yneamide **3-6**. The long reaction time required for acceptable yield is hypothesize to be due to the inherent low reactivity of the aromatic amine, however the robust activity DEPBT of allowed for good overall yield. It was also possible to recover much of the unreacted starting materials for continued reaction.

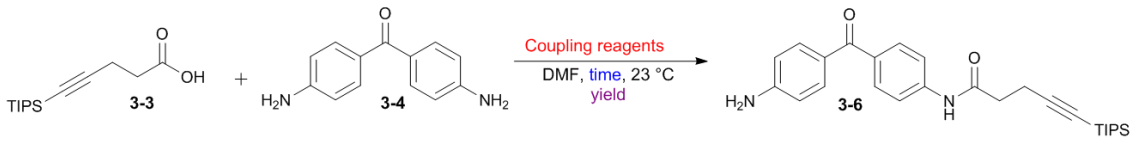

Entry	Coupling Reagents	Time	Yield
	DCC, HOBt	20 h	16%
1	DCC, HOBt	20 h	30%
2	EDC, HOBt, DIPEA	20 h	32%
3	CDI	20 h	31%
4	PyBOP, DIPEA	20 h	40%
5	HATU	20 h	44%
6	DEPBT, Et_3N	20 h	50%
7	DEPBT, Et_3N	72 h	71%

Scheme 3.1. Improved coupling conditions for step 1 of the synthesis of Sal-AMS photoaffinity probe **3-2**.

The free aromatic amine of **3-6** was then coupled to 2-iodo-2′,3′-isopropylideneadenosine (**3-7**) under Buchwald-Hartwig coupling conditions to achieve the 2-substituted adenosine **3-8** in moderate yield (**Scheme 3.2**). The palladium catalyst was added in two portions 2.5 hours apart to avoid charring. Optimization of this reaction also showed a high sensitivity to the purity of the 1,4-dioxane used as solvent. Highly pure, dry solvent was required to avoid high rates of homo-coupling of the iodo reagent. The silyl protecting group was then removed from the alkyne with standard tetrabutylammonium fluoride conditions to obtain intermediate **3-9**.

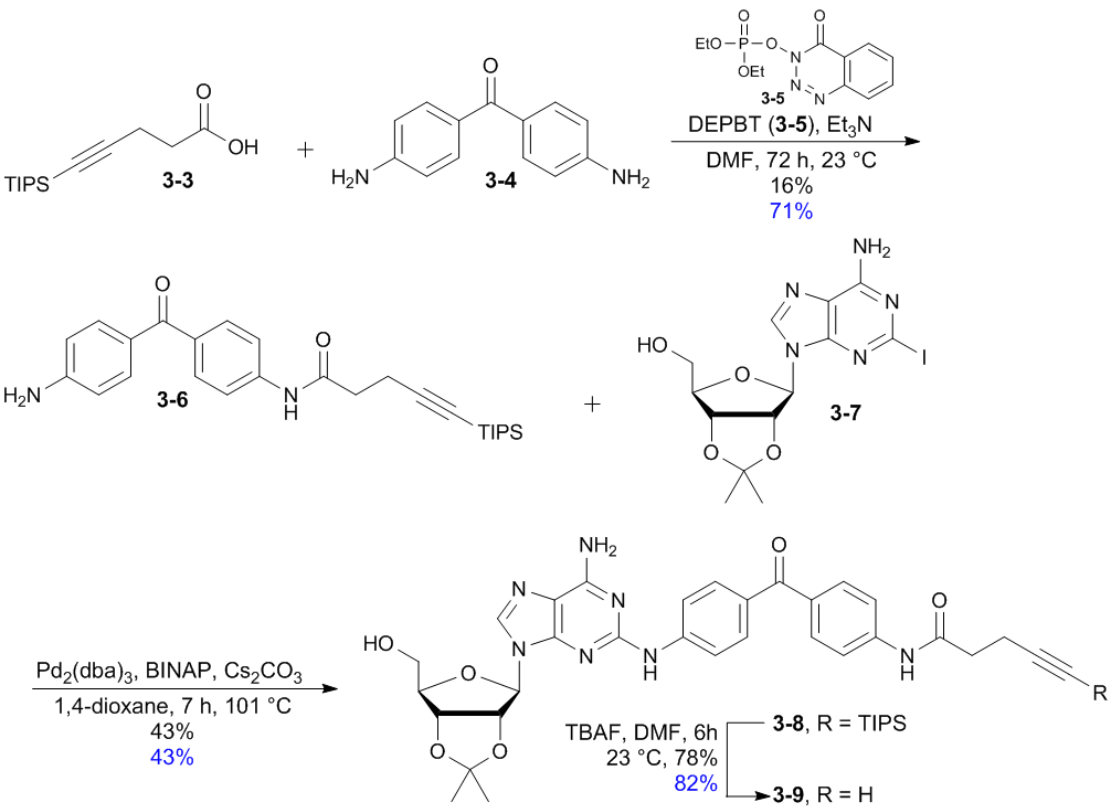

Scheme 3.2. First steps in the improved synthesis of Sal-AMS photoaffinity probe **3-2**. Initial synthetic yields are shown the top line, improved yields are shown on the bottom.

The initial sulfamoylation conditions involved DME as the solvent, and resulted in only moderate yields (47%). Changing the solvent to DMA led to sulfamoylation in high yields (80%) without a basic catalyst yielding intermediate **3-10** (**Scheme 3.3**). It is hypothesized that the starting material (**3-9**) and sulfamoyl chloride are better solubilized in DMA, leading to higher catalytic turnover of the reaction. DMA is also mildly basic (pK_a = 9.1), which may facilitate the reaction. Cesium carbonate-mediated coupling of the free amine with *N*-hydroxysuccinimidyl-2-(methoxymethyloxy)benzoate **3-11** gave the protected penultimate intermediate. Acidic deprotection with aqueous trifluoroacetic acid revealed the final probe **3-2**. The probe was isolated as the triethylammonium salt in

high purity (> 97%) by RP-HPLC. This ensured that no contamination was introduced into the assay from the synthesis of the probe. The overall yield was improved by 13.5-fold to 5.4%.

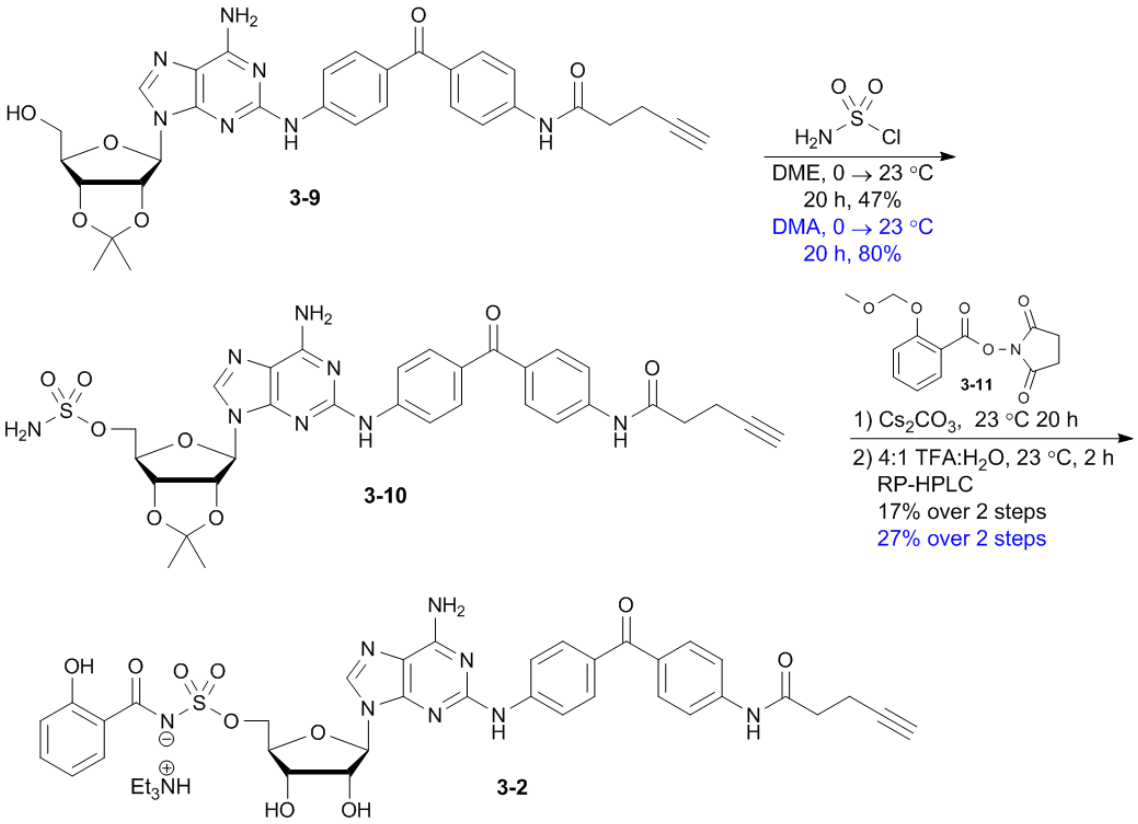

Scheme 3.3. Completed improved synthesis of Sal-AMS photoaffinity probe **3-2**. Initial synthetic yields are shown the top line, improved yields are shown on the bottom.

3.3.2 Control experiments with photoaffinity probe 3-2 and recombinant MbtA

A photoaffinity probe that is useful in studying the properties of its parent inhibitor must recapitulate both the *in vitro* and *in vivo* activities. Therefore, the ability of probe **3-2** to inhibit MbtA was measured by Daniel Wilson of our lab with a [^{32}P]PP$_i$-ATP exchange assay.[15] The apparent inhibition constant (appK_i) of probe **3-2** with MbtA was 0.94 nM

(**Table 3.1**), roughly 7-fold lower than that of Sal-AMS (**3-1**).[15] This result is not surprising, since it was found that C-2 modifications of Sal-AMS led to enhanced binding affinity.[24] To ensure that the probe displays a similar phenotype to Sal-AMS (**3-1**), the antitubercular activity of compound **3-2** was evaluated against *Mtb* H37Rv.

Table 3.1. Inhibition of MbtA and *M. tuberculosis* H37Rv by Sal-AMS **1** and photoaffinity probe **3-2**.

	MbtA appK_i (nM)[b]	**MIC (μM) (Iron-deficient)[c]**	**MIC (μM) (Iron-rich)[d]**	**Selectivity Factor (*S*)**
Sal-AMS (**3-1**)[a]	6.6	0.39	1.56	4
Probe (**3-2**)	0.94	3–6	50	8–17

[a]See reference 24. [b]Assay performed by Daniel Wilson with 7 nM MbtA, 10 mM ATP, 250 μM salicylic acid, 1 mM PP_i. [c]Grown and tested by Dr. Helena I. Boshoff in normal pH 6.6 glycerol-alanine-salts (GAS) medium without ferric ammonium citrate. [d]Grown and tested by Dr. Helena I. Boshoff in normal pH 6.6 glycerol-alanine-salts (GAS) medium supplemented with 200 μM ferric ammonium citrate.

Under iron-deficient conditions, the minimum inhibitory concentration of probe **3-2** that resulted in complete inhibition of observable cell growth (MIC) is 3−6 μM, as compared to 0.39 μM for Sal-AMS (**3-1**).[24] Under iron-rich conditions, the MIC was 50 μM for probe **3-2**, as compared to 1.56 μM for Sal- AMS (**3-1**). From these data, one can extract the selectivity factor (*S*), which is the ratio of activity under iron-rich over activity in iron-deficient conditions. Assuming that Sal-AMS is not inhibiting MbtA in iron-rich conditions, this selectivity factor should be high. However, the selectivity is relatively low (S = 1.56/0.39 = 4), indicating Sal-AMS may inhibit other targets. The selectivity factor for probe **3-2** is 8−17. These data confirm probe **3-2** displays a similar phenotype to the parent inhibitor, suggesting it is an acceptable probe for photoaffinity proteomic profiling.

To evaluate the ability of the photoaffinity probe to photolabel pure recombinant MbtA, Dr. Benjamin Duckworth in our lab first incubated the enzyme with probe **3-2** and photolyzed at 365 nm. Coupling with a rhodamine-azide conjugate (TAMRA-N3) under standard click chemistry conditions,[28] followed by denaturing gel electrophoresis allowed the proteins to be separated and visualized by in-gel fluorescence scanning (**Figure 3.5**).

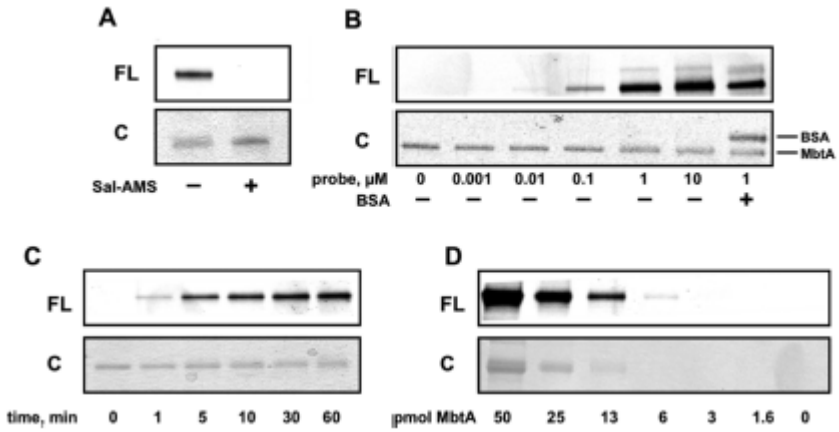

Figure 3.5. *In vitro* labeling of pure MbtA with probe **3-2** by Dr. Benjamin Duckworth of our lab. (A) Labeling of MbtA and competition with excess Sal-AMS (**3-1**). (B) Concentration dependence of probe **3-2**. (C) UV photolysis time studies. (D) Limit of detection of MbtA labeling. FL = fluorescence, C = Coomassie. Reprinted with permission.[23]

Pre-incubation of excess Sal-AMS (**1**) prior to the addition of probe **3-2** results in no observed protein labeling, indicating that probe **3-2** binds to the active site of MbtA competitively (**Figure 3.5A**). After determining the optimal concentration of probe for MbtA labeling, and demonstrating specificity by minimal labeling of BSA, maximum incubation time (30 minutes) and labeling efficiency (20%) were both determined (**Figure 3.5B** and **C**). To assess the sensitivity of probe **3-2**, in-gel fluorescence scanning was used to determine the lower limit of MbtA that could be detected. Dr. Duckworth

found that the fluorescent detection of probe **3-2** had a sensitivity of 6 pmol of MbtA (**Figure 3.5D**). Lastly, a dose−response curve was created by incubating varying concentrations of Sal-AMS (**3-1**) with a fixed concentration of MbtA and probe **3-2** prior to photolysis and TAMRA conjugation (**Figure 3.6A**). The fluorescent band intensities were plotted against Sal-AMS (**3-1**) concentration (**Figure 3.6B**) to provide an IC_{50} value of 0.26 μM for Sal-AMS (**3-1**) against probe **3-2**.

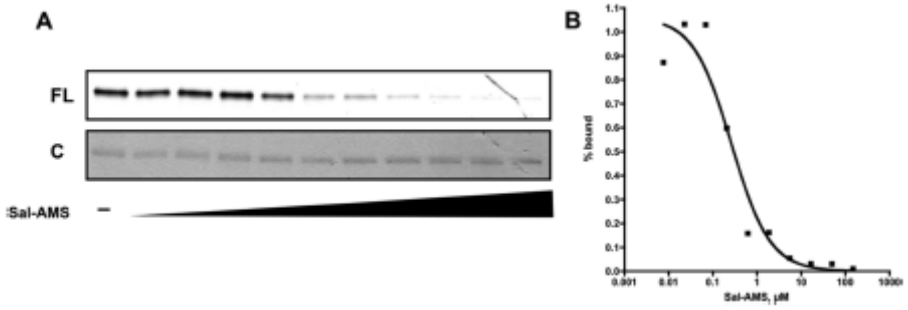

Figure 3.6. (A) Dose-response curve of Sal-AMS (**3-1**) competition with probe **3-2**. (B) Dose-response of fractional amount of probe **3-2** bound (determined from band intensities in panel A) versus Sal-AMS concentration. FL = fluorescence, C = Commassie. Reprinted with permission.[23]

3.3.3 Photoaffinity probe 3-2 labeling MbtA from cell lysates in expression and native systems

Dr. Duckworth next used probe **3-2** to label MbtA overexpressed in *E. coli* cell lysates. *E. coli* was transformed with an IPTG-inducible pET-SUMO-MbtA plasmid and the pGRO7 plasmid. *E. coli* cells were then grown either in the absence or presence of IPTG, photolabeled with probe **3-2**, and subjected to the click reaction with TAMRA-N_3. In the absence of IPTG, MbtA is not expressed (lane 1, **Figure 3.7A**). However, when IPTG is added to the growth media, a strong fluorescent band corresponding to the molecular

weight of MbtA (~73 kDa) was observed (lane 3, **Figure 3.7A**, arrow). Probe labeling was completely inhibited by pre-incubation with excess Sal-AMS (**3-1**) (lane 4, **Figure 3.7A**). Notably, probe **3-2** labeled the GroEL chaperone protein as indicated by the star in lane 3 of **Figure 3.7A**, however this labeling was nonspecific as preincubation with Sal-AMS (**3-1**) did not inhibit this labeling. These results highlight the remarkable specificity of probe **3-2** toward MbtA in crude mixtures.

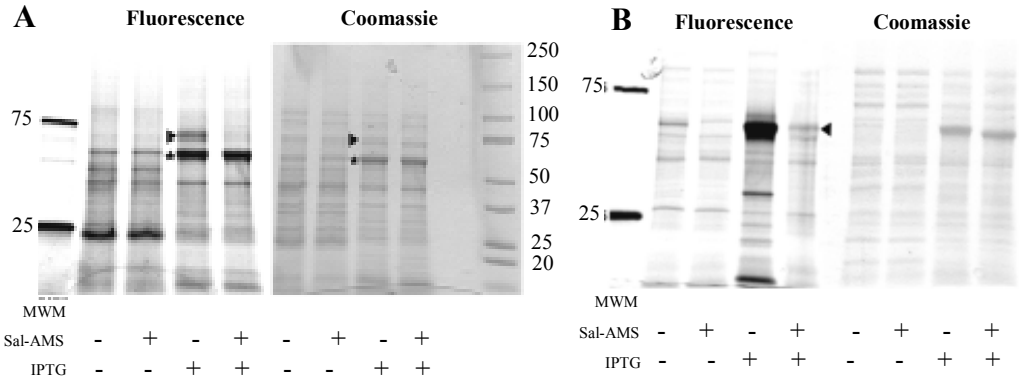

Figure 3.7. Labeling of adenylating enzymes in crude cell lysates. (A) Labeling of overexpressed MbtA in *E. coli* cell lysate. (B) Labeling of overexpressed EntE in *E. coli* cell lysate. Reprinted with permission.[23]

Encouraged by the ability of probe **3-2** to label MbtA in crude cell lysate, we were curious about the applicability of this photoaffinity probe to related adenylating enzymes. EntE from *E. coli* is the aryl acid adenylating enzyme involved in the biosynthesis of enterobactin, which activates 2,3-dihydroxybenzoic acid analogous to MbtA's activation of salicylic acid. Sal-AMS had already been shown to be a tight-binding inhibitor of EntE, with a K_i of 0.47 nM.[30] Dr. Duckworth assayed overexpressed EntE analogous to the protocol for expression and assay of MbtA thruogh the IPTG-inducible pET15b-EntE plasmid for expression in *E. coli*. Minimal labeling of EntE occurs in the absence of

IPTG, however, a strong fluorescent signal was observed (lane 3, **Figure 3.7B**, arrow) after induction by IPTG. When lysate containing overexpressed EntE was preincubated with excess Sal-AMS (**3-1**), the fluorescence signal is largely attenuated (lane 4, **Figure 3.7B**). These studies indicate the potential utility of our photoaffinity probe in studying aryl acid adenylating enzymes from different organisms.

Finally, Dr. Duckworth and Daniel Wilson tested the ability of probe **3-2** to label native (uninduced) MbtA in mycobacterial cell lysates. *Mycobacterium smegmatis* cultures were grown in iron-deficient media, lysed, and incubated with either DMSO or Sal-AMS. After UV irradiation in the presence of probe **3-2**, alkyne-labeled proteins were modified with a biotin-azide group via click chemistry. Biotin-tagged proteins were enriched with streptavidin beads, trypsin digested, and analyzed by LC−MS/MS.[31] In the absence of Sal-AMS, MbtA was identified by LC−MS/MS with an average spectral count of 4 from triplicate experiments. In the presence of excess Sal-AMS, MbtA was not enriched and identified by LC−MS/MS as evidenced by zero spectral counts in all three replicates tested (**Table 3.2**). These results indicate that MbtA, present at low concentrations in cell lysate, can be labeled in mycobacterial species. Additional targets of **3-2** were not positively identified. Other proteins reported in the hit list either have inconsistent results among the triplicate samples (as evidenced by large standard deviations), or are high abundance proteins that are likely victims of non-specific labeling. None of these additionally identified proteins are likely to be true targets of Sal-AMS (**3-1**).

Table 3.2. LC–MS/MS identification by spectral counts of proteins labeled by photoaffinity probe **3-2** from *M. smegmatis* cell lysates grown under iron-limiting conditions to simulate the upregulation of MbtA in an infected individual.

Protein	Accession #	MW	0 μM **2**		+ Sal-AMS			– Sal-AMS			+ Sal-AMS/– Sal-AMS	0 μM **2**/– Sal-AMS
			+ Sal-AMS	– Sal-AMS	10 μM **2**	1 μM **2**	0.1 μM **2**	10 μM **2**	1 μM **2**	0.1 μM **2**		
unnamed protein product	gi|118469108|ref|YP_886179.1|	63 kDa	220.6± 42.8	137.5± 31.3	168.2± 46.4	194.3± 73.1	211.7± 20.8	160.1± 22.3	164.9± 142.0	221.1± 56.4	1.1±0.4	1.0±0.1
ribosomal protein L2	gi|118173550|gb|ABK74446.1| (+2)	30 kDa	45.7 ± 14.8	41.1 ± 18.1	50.3 ± 9.3	46.5 ± 21.1	33.9 ± 10.7	38.1 ± 7.8	45.4 ± 54.7	46.4 ± 14.5	1.0±0.3	1.0±0.1
ribosomal protein S12	gi|118172589|gb|ABK73485.1| (+5)	14 kDa	8.3 ± 7.1	4.6 ± 2.9	13.3 ± 12.2	4.8 ± 2.3	4.7 ± 2.0	9.3 ± 3.4	4.9 ± 7.2	2.6 ± 1.9	1.4±2.1	1.2±1.1
groEL gene product	gi|118469510|ref|YP_885283.1|	56 kDa	13.6 ± 9.7	11.0 ± 9.9	12.2 ± 1.3	17.8 ± 18.8	3.3 ± 2.4	5.3 ± 4.4	12.3 ± 11.9	8.0 ± 5.6	1.3±2.4	1.4±0.0
unnamed protein product	gi|118468949|ref|YP_888976.1|	70 kDa	12.6 ± 3.2	4.8 ± 1.9	7.4 ± 9.8	5.0 ± 3.2	5.3 ± 0.9	2.1 ± 2.3	7.9 ± 7.9	8.8 ± 1.7	0.9±1.4	1.4±0.3
glyoxalase family protein	gi|118171233|gb|ABK72129.1| (+1)	16 kDa	0.7 ± 1.3	0.8 ± 0.7	10.6 ± 9.5	6.2 ± 2.3	0.0 ± 0.0	19.1 ± 2.6	4.5 ± 6.5	0.9 ± 1.0	0.7±1.8	0.1±0.1
acyl carrier protein	gi|118172814|gb|ABK73710.1| (+1)	11 kDa	14.1 ± 7.1	8.5 ± 6.3	13.0 ± 12.5	6.2 ± 2.1	2.2 ± 1.9	5.2 ± 2.9	1.7 ± 1.4	4.8 ± 0.8	1.8±5.7	2.9±0.5
ribosomal protein S3	gi|118174447|gb|ABK75343.1| (+2)	30 kDa	0.8 ± 0.8	0.9 ± 1.1	22.0 ± 4.8	1.4 ± 0.5	1.1 ± 1.2	1.6 ± 1.5	21.6 ± 36.0	0.6 ± 1.1	1.0±0.1	0.1±0.0
unnamed protein product	gi|118468034|ref|YP_886648.1| (+2)	81 kDa	2.8 ± 2.5	3.5 ± 2.2	2.7 ± 3.2	3.0 ± 2.4	0.7 ± 0.6	4.2 ± 2.9	7.4 ± 8.6	5.3 ± 6.3	0.4±0.5	0.6±0.1
integral membrane protein	gi|118171629|gb|ABK72525.1| (+1)	36 kDa	7.9 ± 7.0	3.3 ± 3.2	4.1 ± 3.7	4.0 ± 5.7	0.7 ± 0.6	4.5 ± 2.4	1.8 ± 0.7	4.3 ± 2.7	0.8±2.4	1.6±2.5
ribosomal protein L3	gi|118174477|gb|ABK75373.1| (+2)	23 kDa	3.5 ± 5.4	1.7 ± 1.1	1.3 ± 1.4	4.0 ± 3.0	1.1 ± 1.2	0.8 ± 0.9	2.2 ± 1.3	2.5 ± 1.3	1.2±3.9	1.4±12.0
pyruvate carboxylase	gi|118174374|gb|ABK75270.1| (+1)	121 kDa	2.3 ± 3.2	0.6 ± 1.0	1.7 ± 2.9	0.3 ± 0.5	2.1 ± 3.6	0.0 ± 0.0	1.3 ± 2.3	0.0 ± 0.0	3.1±1.2	3.2±1.2
translation elongation factor Tu	gi|118172375|gb|ABK73271.1| (+1)	44 kDa	1.8 ± 1.9	1.8 ± 1.8	3.2 ± 2.8	3.3 ± 3.0	0.4 ± 0.7	1.4 ± 2.4	1.1 ± 0.3	2.6 ± 4.4	1.4±0.6	1.0±0.0
ribosomal protein S5	gi|118170928|gb|ABK71824.1| (+2)	22 kDa	1.9 ± 2.6	2.4 ± 1.6	6.6 ± 6.2	2.8 ± 1.1	1.1 ± 1.2	1.0 ± 0.3	2.9 ± 3.1	0.6 ± 1.1	2.3±2.0	1.4±0.5
chaperonin GroS	gi|118171718|gb|ABK72614.1| (+1)	11 kDa	2.3 ± 2.7	2.9 ± 2.9	1.8 ± 1.9	1.9 ± 1.7	1.4 ± 1.3	0.0 ± 0.0	0.4 ± 0.7	1.3 ± 0.3	3.0±0.8	4.5±0.4
fatty acid synthase	gi|118169207|gb|ABK70103.1| (+1)	330 kDa	0.0 ± 0.0	0.2 ± 0.4	4.9 ± 7.7	0.5 ± 0.8	0.0 ± 0.0	0.5 ± 0.8	12.7 ± 21.2	2.0 ± 2.5	0.4±0.4	0.0±0.0

unnamed protein product	gi|118472788|ref|YP_ 890017.1| (+5)	31 kDa	0.8 0.7±	0.5 ± 0.4	0.6 ± 1.1	1.3 ± 2.2	0.3 ± 0.6	0.3 ± 0.4	4.5 ± 7.9	1.1 ± 1.0	0.4±0.2	0.3±0.1
isocitrate dehydrogenase, NADP-dependent	gi|118168719|gb|ABK 69615.1| (+1)	83 kDa	0.0 ± 0.0	0.0 ± 0.0	5.3 ± 4.7	0.3 ± 0.6	0.0 ± 0.0	2.9 ± 2.3	2.9 ± 4.0	0.6 ± 1.1	0.9±1.8	0.0±0.0
ribosomal protein S10	gi|118174744|gb|ABK 75640.1| (+1)	11 kDa	0.0 ± 0.0	0.2 ± 0.4	2.8 ± 2.4	2.2 ± 0.6	0.8 ± 1.3	3.2 ± 2.1	1.8 ± 2.0	2.6 ± 2.3	0.7±6.6	0.0±2.1
3-deoxy-7-phosphoheptulonate synthase	gi|118170211|gb|ABK 71107.1| (+2)	51 kDa	0.0 ± 0.0	0.0 ± 0.0	6.1 ± 5.6	2.3 ± 1.8	0.0 ± 0.0	4.2 ± 1.1	0.4 ± 0.7	0.0 ± 0.0	1.8±5.2	0.0±0.0
2,3-dihydroxybenzoate-AMP ligase (MbtA)	**gi|118169731|gb|ABK 70627.1| (+1)**	**59 kDa**	**0.0 ± 0.0**	**0.0 ± 0.0**	**0.0 ± 0.0**	**0.0 ± 0.0**	**0.0 ± 0.0**	**2.3 ± 1.3**	**1.9 ± 1.7**	**4.5 ± 2.4**	**0.0±0.0**	**0.0±0.0**
peptidyl-prolyl cis-trans isomerase B	gi|118169709|gb|ABK 70605.1| (+1)	19 kDa	2.4 ± 0.8	1.0 ± 0.4	2.5 ± 3.4	1.8 ± 1.0	1.1 ± 1.2	0.0 ± 0.0	1.3 ± 1.3	0.6 ± 1.1	2.8±1.9	2.6±0.4
glutathione peroxidase family protein	gi|118172613|gb|ABK 73509.1| (+1)	17 kDa	1.1 ± 1.9	1.4 ± 1.9	1.5 ± 1.9	1.8 ± 1.0	0.8 ± 1.3	1.0 ± 0.3	1.7 ± 1.5	1.3 ± 2.2	1.0±0.5	0.9±0.0
glutamine synthetase, type I	gi|118169243|gb|ABK 70139.1| (+2)	54 kDa	0.5 ± 0.5	0.7 ± 0.1	1.0 ± 0.9	2.5 ± 1.5	0.4 ± 0.7	1.2 ± 1.4	3.2 ± 2.8	1.4 ± 1.4	0.7±0.6	0.3±0.4
ribosomal protein S13p/S18e	gi|118175274|gb|ABK 76170.1| (+1)	14 kDa	3.1 ± 3.2	1.7 ± 1.1	0.8 ± 1.4	0.3 ± 0.5	0.0 ± 0.0	0.0 ± 0.0	0.4 ± 0.8	1.1 ± 1.0	0.7±1.4	4.8±2.9
Chain A, Msreca Q196n Atpgs Form Iv	gi|217035320|pdb|2ZR E|A (+2)	37 kDa	0.0 ± 0.0	0.0 ± 0.0	12.8 ± 12.8	0.6 ± 1.0	0.0 ± 0.0	3.0 ± 1.2	1.2 ± 2.1	0.0 ± 0.0	3.2±6.6	0.0±0.0
glycerol kinase	gi|118171208|gb|ABK 72104.1| (+1)	55 kDa	1.0 ± 0.9	1.9 ± 3.3	0.4 ± 0.7	0.6 ± 1.1	0.0 ± 0.0	0.8 ± 1.3	1.2 ± 2.1	1.7 ± 1.9	0.3±1.3	1.2±4.1
2-oxoglutarate dehydrogenase, E1 component	gi|118173342|gb|ABK 74238.1| (+2)	136 kDa	0.0 ± 0.0	0.0 ± 0.0	9.1 ± 15.8	0.0 ± 0.0	0.0 ± 0.0	0.0 ± 0.0	7.0 ± 12.2	0.0 ± 0.0	1.3±1.3	0.0±0.0
3-oxoacyl-[acyl-carrier-protein] synthase 1	gi|118172459|gb|ABK 73355.1| (+1)	44 kDa	0.0 ± 0.0	0.0 ± 0.0	3.6 ± 3.2	0.5 ± 0.8	0.0 ± 0.0	1.2 ± 1.4	0.4 ± 0.7	0.3 ± 0.6	2.1±3.6	0.0±0.0
chaperonin GroL	gi|118170503|gb|ABK 71399.1| (+2)	56 kDa	0.0 ± 0.0	1.2 ± 0.3	0.8 ± 1.4	0.6 ± 0.5	0.0 ± 0.0	0.0 ± 0.0	2.5 ± 4.3	1.0 ± 1.7	0.4±0.3	0.5±0.1
NAD-dependent malic enzyme	gi|118168853|gb|ABK 69749.1| (+1)	39 kDa	1.0 ± 1.7	0.0 ± 0.0	0.8 ± 1.4	0.0 ± 0.0	0.0 ± 0.0	0.9 ± 1.6	2.1 ± 3.6	0.3 ± 0.6	0.2±0.5	0.5±0.8

ribosomal protein L18	gi|118173154|gb|ABK 74050.1| (+1)	14 kDa	0.0 ± 0.0	1.2 ± 1.5	0.0 ± 0.0	1.1 ± 0.3	0.0 ± 0.0	0.0 ± 0.0	0.9 ± 0.7	1.0 ± 1.7	0.6±0.2	1.0±1.3
ribosomal protein L7/L12	gi|118169903|gb|ABK 70799.1| (+1)	13 kDa	0.3 ± 0.4	1.0 ± 1.1	0.7 ± 0.6	2.5 ± 3.7	0.0 ± 0.0	0.0 ± 0.0	0.0 ± 0.0	0.3 ± 0.6	10.2±6.1	5.8±1.5
universal stress protein family protein, putative	gi|118174190|gb|ABK 75086.1| (+1)	15 kDa	0.0 ± 0.0	0.7 ± 1.2	0.6 ± 1.1	0.9 ± 1.0	0.0 ± 0.0	0.0 ± 0.0	3.3 ± 5.7	0.0 ± 0.0	0.5±0.2	0.3±0.3
DNA-directed RNA polymerase, beta' subunit	gi|118171055|gb|ABK 71951.1| (+1)	147 kDa	0.0 ± 0.0	0.0 ± 0.0	0.0 ± 0.0	0.0 ± 0.0	0.0 ± 0.0	0.0 ± 0.0	2.9 ± 5.0	1.0 ± 1.7	0.0±0.0	0.0±0.0
methyltransferase	gi|118168887|gb|ABK 69783.1| (+2)	35 kDa	0.0 ± 0.0	0.0 ± 0.0	2.7 ± 3.2	0.6 ± 1.0	0.0 ± 0.0	0.8 ± 0.8	0.4 ± 0.8	0.0 ± 0.0	2.6±3.7	0.0±0.0
conserved hypothetical protein	gi|118174182|gb|ABK 75078.1| (+1)	24 kDa	0.0 ± 0.0	0.2 ± 0.4	0.0 ± 0.0	1.4 ± 0.5	0.4 ± 0.7	0.0 ± 0.0	0.8 ± 1.4	0.6 ± 1.1	1.2±0.5	0.2±0.4
MaoC like domain protein	gi|118172341|gb|ABK 73237.1| (+1)	31 kDa	0.0 ± 0.0	0.0 ± 0.0	4.0 ± 3.7	0.0 ± 0.0	0.0 ± 0.0	0.8 ± 0.8	0.0 ± 0.0	0.0 ± 0.0	5.0±4.8	0.0±0.0
DNA-directed RNA polymerase, beta subunit	gi|118169416|gb|ABK 70312.1| (+2)	129 kDa	0.0 ± 0.0	0.0 ± 0.0	0.0 ± 0.0	0.0 ± 0.0	0.0 ± 0.0	0.0 ± 0.0	5.0 ± 8.6	0.0 ± 0.0	0.0 ± 0.0	0.0 ± 0.0
ribosomal protein S11	gi|118168714|gb|ABK 69610.1| (+4)	15 kDa	1.1 ± 1.9	0.5 ± 0.4	1.2 ± 2.1	0.0 ± 0.0	0.0 ± 0.0	0.5 ± 0.9	0.4 ± 0.8	0.0 ± 0.0	1.3±2.6	2.5±2.1
chaperone protein DnaK	gi|118173710|gb|ABK 74606.1| (+1)	67 kDa	0.8 ± 0.8	0.5 ± 0.8	0.3 ± 0.5	0.6 ± 1.1	0.4 ± 0.7	0.0 ± 0.0	1.2 ± 2.1	0.0 ± 0.0	1.1±0.2	1.6±0.0
ribonucleoside-diphosphate reductase, beta subunit	gi|118170519|gb|ABK 71415.1| (+3)	37 kDa	0.0 ± 0.0	0.3 ± 0.5	0.0 ± 0.0	0.6 ± 1.1	0.0 ± 0.0	0.0 ± 0.0	0.8 ± 1.4	0.3 ± 0.6	0.6±0.9	0.4±0.5
putative non-ribosomal peptide synthetase	gi|118171058|gb|ABK 71954.1| (+1)	125 kDa	0.0 ± 0.0	0.0 ± 0.0	0.0 ± 0.0	0.0 ± 0.0	0.0 ± 0.0	0.0 ± 0.0	1.7 ± 2.9	0.3 ± 0.6	0.0±0.0	0.0±0.0
polyketide synthase	gi|118170878|gb|ABK 71774.1| (+1)	194 kDa	0.0 ± 0.0	0.0 ± 0.0	0.0 ± 0.0	0.0 ± 0.0	0.0 ± 0.0	0.0 ± 0.0	2.5 ± 4.6	0.3 ± 0.6	0.0±0.0	0.0±0.0
glycine oxidase ThiO	gi|118171481|gb|ABK 72377.1| (+1)	36 kDa	0.3 ± 0.4	0.0 ± 0.0	0.8 ± 1.4	0.0 ± 0.0	0.0 ± 0.0	0.0 ± 0.0	0.8 ± 1.4	0.3 ± 0.6	0.7±1.1	0.3±0.4
ABC transporter, ATP-binding protein SugC	gi|118174334|gb|ABK 75230.1| (+1)	44 kDa	0.0 ± 0.0	0.0 ± 0.0	1.8 ± 1.9	0.0 ± 0.0	0.0 ± 0.0	0.3 ± 0.5	0.0 ± 0.0	0.0 ± 0.0	6.3±3.7	0.0±0.0

replicative DNA helicase	gi|118174455|gb|ABK75351.1| (+1)	112 kDa	0.0 ± 0.0	0.0 ± 0.0	1.7 ± 2.9	0.0 ± 0.0	0.0 ± 0.0	0.0 ± 0.0	0.0 ± 0.0	0.3 ± 0.6	5.2±5.2	0.0±0.0
putative adenosylhomocysteinase	gi|116266924|gb|ABJ96308.1| (+1)	53 kDa	0.0 ± 0.0	0.0 ± 0.0	0.0 ± 0.0	0.0 ± 0.0	0.0 ± 0.0	0.0 ± 0.0	0.8 ± 1.4	0.6 ± 1.1	0.0±0.0	0.0±0.0
[NADP+] succinate-semialdehyde dehydrogenase	gi|118174982|gb|ABK75878.1| (+1)	48 kDa	0.0 ± 0.0	0.0 ± 0.0	0.0 ± 0.0	0.0 ± 0.0	0.0 ± 0.0	0.3 ± 0.4	0.0 ± 0.0	0.6 ± 1.1	0.0±0.0	0.0±0.0
transcription termination factor Rho	gi|118172484|gb|ABK73380.1| (+1)	72 kDa	0.0 ± 0.0	0.0 ± 0.0	0.0 ± 0.0	0.0 ± 0.0	0.0 ± 0.0	0.0 ± 0.0	1.2 ± 2.1	0.0 ± 0.0	0.0±0.0	0.0±0.0
conserved hypothetical protein	gi|118169265|gb|ABK70161.1| (+1)	95 kDa	0.0 ± 0.0	0.0 ± 0.0	0.0 ± 0.0	0.0 ± 0.0	0.0 ± 0.0	0.0 ± 0.0	0.8 ± 1.4	0.0 ± 0.0	0.0±0.0	0.0±0.0
phosphoribosylformyl glycinamidine synthase II	gi|118174875|gb|ABK75771.1| (+1)	81 kDa	0.0 ± 0.0	0.0 ± 0.0	0.0 ± 0.0	0.0 ± 0.0	0.0 ± 0.0	0.0 ± 0.0	0.8 ± 1.4	0.0 ± 0.0	0.0±0.0	0.0±0.0

Values are number of counts recorded by the MS from an N of 3 (mean ± standard deviation).

3.4 Discussion

The above results indicate that there are no major targets for Sal-AMS under iron-rich conditions that would explain the cytotoxic effects we see in growth assays. After consulting literature and experts in this field, we believe we may have an explanation for the activity seen under both growth conditions.

Recently, great strides have been made in the understanding of the cell biology of iron acquisition by pathogenic bacteria. In 2011, both Celica Goulding and Michael Niederweis independently showed that mycobacteria are capable of uptaking and utilizing heme from a human host as an iron source, even when the biosynthesis of mycobactins is knocked out.[32,33] Both groups constructed completely siderophore deficient strains of *Mtb* through the knockout of *mbtB* or *mbtD*, respectively. Dr. Niederweis showed that the growth of a Δ*mbtD* mutant could be rescued by adding carboxymycobactins to the growth media.[32] This mutant was unable to grow in iron-deficient media, even with the addition of ferric citrate (a ferrous iron source). Dr. Goulding's group showed that a Δ*mbtB* mutant can uptake human Fe-heme complexes for use as an iron source, and identified a gene cluster important for this active transport.[33] This does require the bacteria to encounter a heme complex outside of a red blood cell where it is normally sequestered. There is no evidence at this time to suggest that this heme uptake system would be enough to sustain growth and virulence. Dr. Goulding's group has also been a pioneer in showing that siderophores are important not only for the chelation of iron, but also for its transport across the mycobacterial cell membrane

(**Figure 3.8**).

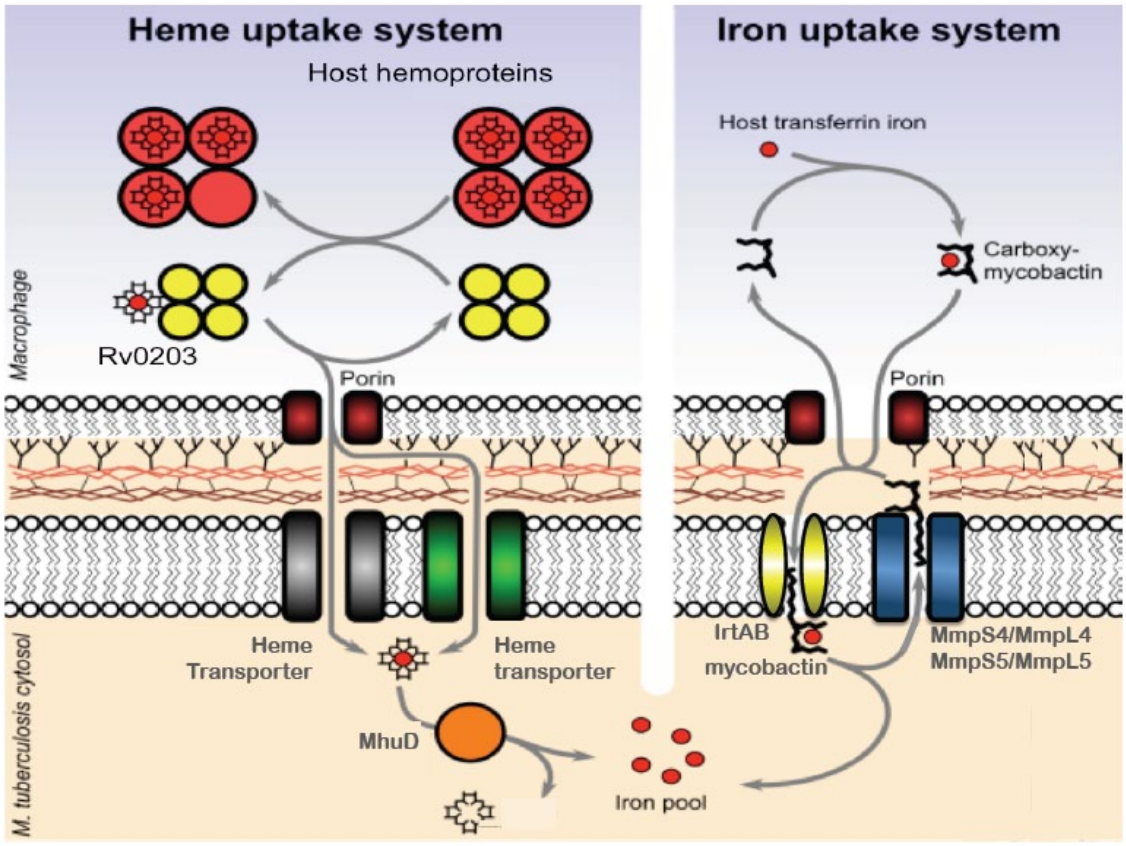

Figure 3.8. Proposed pathways for the uptake of transferrin iron and heme iron in *Mtb*. Reproduced and used with permission from the Goulding lab.[33]

The heme complex is too large and too toxic to simply diffuse through the cellular membrane, so a transport system of some kind must be involved. Other research is continuing to study siderophore export and iron import pathways, and some evidence for the essentiality of siderophore transport out of the cell for virulence has been reported.[34] Together, this data suggests that our ability to knockdown siderophore production with Sal-AMS, even in iron replete conditions, may strongly affect the bacteria's ability to grow. This could help explain our *Mtb* MIC results (**Table 3.2**). While more work still

needs to be done to completely understand this pathway, evidence continues to grow showing the iron acquisition pathway as attractive for drug development. Our prototypical inhibitor Sal-AMS (**3-1**) is therefore a promising lead compound for the development of novel antitubercular agents.

3.5 Conclusions

This work highlights the design and development of a photoaffinity probe for the study of the adenylating enzyme MbtA and how its inhibition affects the pathogenic bacteria *Mtb*. We were able to successfully synthesize a light-activated benzophenone probe that was used to determine the target specificity of Sal-AMS (**3-1**) against MbtA from the mycobactin biosynthetic pathway in *Mtb* with *M. smegmatis* as a model mycobacterial organism. The overall synthetic yield was improved by 13.5-fold through two key modifications in the synthesis. A small alkyne handle was used to attach a fluorescent-azide group and separately a biotin-azide group via a copper-mediated [3+2] cycloaddition ("click" reaction) for visualization and enrichment, respectively. This probe confirmed MbtA as a cellular target of Sal-AMS, but no other significant target enzymes were identified. Further literature analysis suggests to us that our compound may be highly selective for MbtA, and this could account for all the cellular activity we have observed, both in iron-deficient and iron-replete conditions. This data points to Sal-AMS as an ideal probe for the validation of siderophore biosynthesis as essential for virulence and growth, as well as a lead compound for the development of new antitubercular

therapeutics.

3.6 Experimental Data

3.6.1 General procedures for the synthesis of a photoaffinity probe against MbtA

All commercial reagents (Sigma-Aldrich, Fisher, Fluka, Quanta Biochem, Strem) were used as provided. Sulfamoyl chloride was prepared by the method of Heacock without recrystallization.[35] An anhydrous solvent dispensing system (JC Meyer Solvent Systems, Laguna Beach, CA) with two packed columns of neutral alumina was used for drying THF, DMF and DCM and the solvents were dispensed under argon. Anhydrous DMA (Sigma-Aldrich) was used as provided. All reactions were performed under an inert atmosphere of dry Argon in oven-dried (150 °C) glassware. Flash chromatography was performed on an ISCO Combiflash Companion® purification system (Teledyne Isco, Lincoln, NE) with prepacked silica gel cartridges and the indicated solvent system. Reverse-phase HPLC was performed on a Varian Prostar 210 solvent system equipped with a UV/Vis detector (Varian, Inc./Agilent Technologies, Santa Clara, CA) with the indicated column and solvent system. ^{1}H NMR and ^{13}C NMR experiments were recorded on a Varian 600 MHz spectrometer or a Bruker 850MHz spectrometer with a 5 mm TCI Z-gradient cryoprobe. Proton chemical shifts are reported in ppm from an internal standard of residual chloroform (7.26 ppm), or methanol (3.31 ppm). Carbon chemical shifts are reported from an internal standard of residual chloroform (77.0 ppm), or

methanol (49.1 ppm). Proton chemical data are reported as follows: chemical shift, multiplicity (s = singlet, d = doublet, t = triplet, q = quartet, m = multiplet, br = broad, ovlp = overlapping), coupling constant, and integration. High-resolution mass spectra were acquired on an Agilent TOF II TOF/MS instrument (Agilent Technologies, Santa Clara, CA) equipped with either an APCI or ESI interface.

3.6.2 Synthesis of 5-(Triisopropylsilyl)pent-4-ynoic acid (3-3).

The title compound was prepared as described. ^{1}H NMR, ^{13}C NMR, and HRMS data agree with reported values.[29]

3.6.3 *N*-[4-(4-Aminobenzoyl)phenyl]-5-(triisopropylsilyl)pent-4-ynamide (3-6)

To a stirring solution of **3-3** (470 mg, 1.8 mmol, 1.0 equiv) in DMF (18.5 mL) at 23 °C was added 3-(diethoxyphosphoryloxy)-1,2,3-benzotriazin-4(3*H*)-one (DEPBT, **3-5**) (1.1 g, 3.7 mmol, 2.0 equiv) and triethylamine (520 μL, 3.7 mmol, 2.0 equiv). After 10 min, **3-4** (590 mg, 2.8 mmol, 1.5 equiv) was added as a solid and the mixture stirred at 23 °C for 72 h. The reaction was diluted with H_2O (400 mL) and extracted with $CHCl_3$ (3 × 400 mL). The combined organic extracts were washed with saturated aqueous NaCl (400 mL), dried ($MgSO_4$), and concentrated under reduced pressure to an orange oil. Purification by flash chromatography (step gradient $CHCl_3$ to 30% EtOAc/$CHCl_3$ to 50% EtOAc/$CHCl_3$) yielded the title compound (570 mg, 71%) as an orange solid. R_f = 0.38

(30% EtOAc/$CHCl_3$); ^{1}H NMR ($CDCl_3$, 600 MHz) δ 1.02 (s, 18H), 1.03 (s, 3H), 2.63 (t, *J* = 6.6 Hz, 2H), 2.69 (t, *J* = 6.6 Hz, 2H), 6.68 (d, *J* = 6.6 Hz, 2H), 7.61 (d, *J* = 8.4 Hz, 2H), 7.67 (d, *J* = 7.2 Hz, 2H), 7.72 (d, *J* = 7.8 Hz, 2H), 8.02 (br s, 1H); ^{13}C NMR ($CDCl_3$, 150 MHz) δ 11.3, 16.5, 18.8, 37.3, 82.5, 106.9, 114.0, 119.1, 127.9, 131.2, 133.0, 134.5, 141.1, 150.8, 170.1, 194.6; HRMS (ESI+): calculated for $C_{27}H_{37}N_2O_2Si$ [M + H]+ 449.2619, found 449.2646 (error 6.0 ppm).

3.6.4 2′,3′-*O*-Isopropylidene-2-{*N*-[4-(4-{*N*-[5-(triisopropylsilyl)pent-4-ynoyl]amino}benzoyl)phenyl]amino}adenosine (3-8).

A solution of $Pd_2(dba)_3$ (0.012 g, 0.011 mmol, 0.10 equiv) and BINAP (0.022 g, 0.035 mmol, 0.15 equiv) in 1,4-dioxane (1.6 mL) that had been pre-mixed for 10 min was added to a Schlenk flask containing **7** (0.100 g, 0.23 mmol, 1.0 equiv). The mixture changed from opaque, dark red to transparent yellow over 10 min. Next, **3-6** (0.155 g, 0.35 mmol, 1.5 equiv) and Cs_2CO_3 (0.113 g, 0.35 mmol, 1.5 equiv) were added and the resulting mixture was heated at reflux. After 2.5 h, a second portion of $Pd_2(dba)_3$ (0.012 g, 0.011 mmol, 0.10 equiv) and BINAP (0.022 g, 0.035 mmol, 0.15 equiv) in 1,4-dioxane (1.6 mL) was added to the refluxing reaction. After an additional 4 h at reflux, the reaction was cooled to room temperature, filtered, and the filtrate concentrated under reduced pressure to a dark brown oil. The oil was redissolved in EtOAc (100 mL), washed with H_2O (3 × 50 mL), dried ($MgSO_4$), filtered, and concentrated under reduced pressure to a yellow oil. Purification by three successive flash columns (linear gradient 0–

10% MeOH/EtOAc) yielded the title compound (0.074 g, 43%) as a yellow amorphous solid. R_f = 0.47 (10% MeOH/EtOAc); ^{1}H NMR ($CDCl_3$, 600 MHz) δ 1.03–1.04 (m, 21H), 1.38 (s, 3H), 1.63 (s, 3H), 2.66 (t, *J* = 6.6 Hz, 2H), 2.71 (t, *J* = 6.6 Hz, 2H), 3.81 (d, *J* = 11.4 Hz, 1H), 3.95 (d, *J* = 11.4 Hz, 1H), 4.48 (s, 1H), 5.07 (d, *J* = 6.0 Hz, 1H), 5.34 (t, *J* = 4.8 Hz, 1H), 5.88 (d, *J* = 4.2 Hz, 1H), 5.93 (br s, 1H), 7.29 (br s, 1H), 7.61 (d, *J* = 8.4 Hz, 2H), 7.67 (d, *J* = 7.8 Hz, 2H), 7.71 (d, *J* = 7.8 Hz, 2H), 7.74 (d, *J* = 8.4 Hz, 2H), 8.05 (s, 1H); ^{13}C NMR ($CDCl_3$, 150 MHz) δ 11.4, 16.5, 18.8, 25.5, 27.7, 37.3, 63.2, 81.6, 82.6, 83.3, 86.4, 93.0, 106.9, 114.4, 116.1, 118.0, 119.2, 130.9, 131.4, 131.7, 134.0, 138.6, 141.4, 144.2, 150.1, 155.4, 155.9, 170.1, 194.7; HRMS (ESI+): calculated for $C_{40}H_{52}N_7O_6Si$ [M + H]+ 754.3743, found 754.3748 (error 0.7 ppm).

3.6.5 2′,3′-*O*-Isopropylidene-2-[*N*-(4-{4-[*N*-(pent-4-ynoyl)amino]benzoyl}phenyl)amino]adenosine (3-9).

To a solution of **3-8** (0.044 g, 0.06 mmol, 1.0 equiv) in THF (1 mL) was added a 1.0 M solution of tetrabutylammonium fluoride in THF (0.116 mL, 0.12 mmol, 2.0 equiv) and the mixture stirred at 23 °C for 6 h. The reaction mixture was concentrated under reduced pressure to a dark yellow oil and purified directly by flash chromatography (linear gradient 0–10% MeOH/EtOAc) to yield the title compound (0.029 g, 82%) as a yellow amorphous solid. R_f = 0.20 (10% MeOH/EtOAc); ^{1}H NMR (CD_3OD, 600 MHz) δ 1.39 (s, 3H), 1.61 (s, 3H), 2.30 (t, *J* = 3.0 Hz, 1H), 2.57 (td, *J* = 6.6, 2.4 Hz, 2H), 2.64 (t, *J* = 7.2 Hz, 2H), 3.68 (dd, *J* = 12.0, 5.4 Hz, 1H), 3.72 (dd, *J* = 12.0, 4.2 Hz, 1H), 4.33 (dd, *J* =

7.8, 4.8 Hz, 1H), 5.03 (dd, *J* = 6.0, 3.0 Hz, 1H), 5.43 (dd, *J* = 6.0, 3.0 Hz, 1H), 6.12 (d, *J* = 3.0 Hz, 1H), 7.72–7.74 (m, 6H), 7.90 (d, *J* = 9.0 Hz, 2H), 8.07 (s, 1H); ^{13}C NMR (CD_3OD, 150 MHz) δ 15.5, 25.8, 27.7, 37.1, 63.5, 70.5, 83.1, 83.6, 85.8, 88.6, 92.6, 115.3, 116.1, 118.8, 120.2, 130.9, 132.2, 132.7, 134.9, 139.5, 143.9, 147.3, 151.7, 157.6, 172.7, 196.8 (missing 1 carbon, likely due to overlap); HRMS (ESI+): calculated for $C_{31}H_{32}N_7O_6$ [M + H]+ 598.2409, found 598.2415 (error 1.0 ppm).

3.6.6 2′,3′-*O*-Isopropylidene-2-[*N*-(4-{4-[*N*-(pent-4-ynoyl)amino]benzoyl}phenyl)amino]-5′-*O*-(sulfamoyl)adenosine (3-10).

To a stirring solution of **3-9** (0.016 g, 0.025 mmol, 1.0 equiv) in dimethylacetamide (1.0 mL) at 0 °C was added solid sulfamoyl chloride (0.012 g, 0.10 mmol, 4.0 equiv). The mixture was warmed to 23 °C over approximately 3 h and then stirred for 17 h at 23 °C. The reaction was diluted with EtOAc (15 mL) and washed successively with DI H_2O (4 × 15 mL). The organic layer was dried ($MgSO_4$), filtered, and concentrated under reduced pressure to a yellow oil. Purification by flash chromatography (linear gradient 0–5% MeOH/EtOAc) afforded the title compound (0.0145 g, 80%) as an amorphous off-white solid. R_f = 0.41 (10% MeOH/EtOAc); ^{1}H NMR (CD_3OD, 600 MHz) δ 1.40 (s, 3H), 1.62 (s, 3H), 2.29 (s, 1H), 2.57 (t, *J* = 7.2 Hz, 2H), 2.64 (t, *J* = 7.2 Hz, 2H), 4.21 (dd, *J* = 10.8, 5.4 Hz, 1H), 4.35 (dd, *J* = 10.2, 4.8 Hz, 1H), 4.53 (d, *J* = 2.4 Hz, 1H), 5.16 (d, *J* = 6.0 Hz, 1H), 5.49 (d, *J* = 6.0 Hz, 1H), 6.17 (s, 1H), 7.75–7.76 (m, 6H), 7.91 (d, *J* = 8.4 Hz, 2H), 8.01 (s, 1H); ^{13}C NMR (CD_3OD, 150 MHz) δ 15.5, 25.7, 27.6, 37.1, 70.0, 70.5, 83.2,

83.6, 85.7, 85.9, 92.5, 115.5, 116.1, 119.0, 120.2, 131.0, 132.3, 132.8, 134.9, 139.5, 143.9, 147.3, 151.7, 157.67, 157.72, 172.8, 196.9; HRMS (ESI+): calculated for $C_{31}H_{33}N_8O_8S$ [M + H]+ 677.2137, found 677.2127 (error 1.5 ppm).

3.6.7 5′-*O*-[*N*-(2-Hydroxybenzoyl)sulfamoyl]-2-[*N*-(4-{4-[*N*-(pent-4-ynoyl)amino]benzoyl}phenyl)amino]adenosine triethylammonium salt (3-2).

To a solution of **3-10** (14.5 mg, 0.02 mmol, 1.0 equiv) in DMF (1.0 mL) was added **3-11**[8] (9.0 mg, 0.03 mmol, 1.5 equiv) and Cs_2CO_3 (21 mg, 0.06 mmol, 3.0 equiv) and the reaction stirred for 20 h at 23 °C. The reaction mixture was filtered and the filtrate was concentrated under reduced pressure to a colorless residue. A solution of 80% aqueous TFA (1.0 mL) was added the crude residue and the mixture was stirred at 23 °C for 2 h, then concentrated under reduced pressure to remove all traces of TFA. Purification by preparative reverse-phase HPLC on a Phenomenex Gemini 10 μm C18 110 Å (250 × 21.2 mm) column (Phenomenex, Torrance, CA) at a flow rate of 30 mL/min with a gradient of 5–80% MeCN in 20 mM aqueous triethylammonium bicarbonate over 30 min, and then held at 80% MeCN for 5 min. The retention time of the product was 16.7 minutes (k' = 4.9) and the appropriate fractions were pooled and lyophilized to afford the title compound (5.0 mg, 27%) as a light yellow solid: ^{1}H NMR (CD_3OD, 600 MHz) δ 1.20 (t, J = 7.2 Hz, 9H), 2.30 (s, 1H), 2.57 (t, J = 7.2 Hz, 2H), 2.64 (t, J = 7.2 Hz, 2H), 2.94 (d, J = 3.0 Hz, 6H), 4.31 (d, J = 2.4 Hz, 1H), 4.37 (d, J = 11.4 Hz, 1H), 4.42–4.45 (br m, 1H), 4.47 (dd, J = 11.4, 1.8 Hz, 1H), 4.82–4.83 (m, 1H), 6.06 (d, J = 6.0 Hz, 1H),

6.75–6.79 (m, 2H), 7.27 (t, J = 8.4 Hz, 1H), 7.75–7.77 (m, 6H), 7.93–7.96 (m, 3H), 8.26 (s, 1H); ^{13}C NMR (CD_3OD, 213 MHz) δ 8.7, 15.7, 37.2, 47.8, 69.9, 70.6, 72.9, 75.9, 83.7, 84.7, 89.4, 115.9, 118.1, 118.6, 119.5, 120.3, 120.9, 130.8, 131.7, 132.3, 133.0, 134.6, 135.1, 139.5, 143.9, 147.7, 152.8, 157.6, 157.8, 162.3, 172.9, 175.3, 197.1; HRMS (ESI−): calculated for $C_{35}H_{31}N_8O_{10}S$ [M− H]− 755.1889, found 755.1916 (error 3.6 ppm).

3.7 References

1. Yuan, L.; Lin, W.; Zheng, K.; Zhu, S. FRET-based small-molecule fluorescent probes: Rational design and bioimaging applications. *Acc. Chem. Res.* **2013**, *ASAP*.

2. Haedke, U.; Küttler, E. V.; Vosyka, O.; Yang, Y.; Verhelst, S. H. L. Tuning probe selectivity for chemical proteomics applications. *Curr. Opin. Chem. Biol.* **2013**, *17*, 102–109.

3. Bunnage, M. E.; Piatnitski Chekler, E. L.; Jones, L. H. Target validation using chemical probes. *Nat. Chem. Biol.* **2013**, *9*, 195–199.

4. Workman, P.; Collins, I. Probing the probes: Fitness factors for small molecule tools. *Chem. Biol.* **2010**, *17*, 561–577.

5. Cohen, P. Guidelines for the effective use of chemical inhibitors of protein function to understand their roles in cell regulation. *Biochem J.* **2010**, *425*, 53–54.

6. Frye, S. V. The art of the chemical probe. *Nat. Chem. Bio.* **2010**, *6*, 159–161.

7. Ferreras, J. A.; Ryu, J. S.; Di Lello, F.; Tan, D. S., Quadri, L. E. Small-molecule inhibition of siderophore biosynthesis in *Mycobacterium tuberculosis* and *Yersinia pestis*. *Nat. Chem. Biol.* **2005**, *1*, 29–32.

8. Somu, R. V.; Boshoff, H.; Qiao, C.; Bennett, E. M.; Barry, C. E., 3rd; Aldrich, C. C. Rationally designed nucleoside antibiotics that inhibit siderophore biosynthesis of *Mycobacterium tuberculosis*. *J. Med. Chem.* **2006**, *49*, 31–34.

9. Quadri, L. E. Strategic paradigm shifts in the antimicrobial drug discovery process of the 21st century. *Infect. Disord. Drug Targets* **2007**, *7*, 230–237.

10. Crosa, J. H.; Walsh, C. T. Genetics and assembly line enzymology of siderophore biosynthesis in bacteria. *Microbiol. Mol. Biol. Rev.* **2002**, *66*, 223–249.

11. Miethke, M.; Marahiel, M. A. Siderophore-based iron acquisition and pathogen control. *Microbiol. Mol. Biol. Rev.* **2007**, *71*, 413–451.

12. Siegrist, M. S.; Unnikrishnan, M.; McConnell, M. J.; Borowsky, M.; Cheng, T. Y.; Siddiqi, N.; Fortune, S. M.; Moody D. B.; Rubin, E. J. Mycobacterial Esx-3 is required for mycobactin-mediated iron acquisition. *Proc. Natl. Acad. Sci. U.S.A.* **2009**, *106*, 18792–18797.

13. De Voss, J. J.; Rutter, K.; Schroeder, B. G.; Su, H.; Zhu, Y.; Barry, C. E., 3rd. The salicylate-derived mycobactin siderophores of *Mycobacterium tuberculosis* are essential for growth in macrophages. *Proc. Natl. Acad. Sci. U.S.A*. **2000**, *97*, 1252–1257.

14. Timm, J.; Post, F. A.; Bekker, L. G.; Walther, G. B.; Wainwright, H. C.; Manganelli, R.; Chan, W. T.; Tsenova, L.; Gold, B.; Smith, L.; Kaplan, G.; McKinney, J. D. Differential expression of iron-, carbon-, and oxygen-responsive mycobacterial genes in the lungs of chronically infected mice and tuberculosis patients. *Proc. Natl. Acad. Sci. U.S.A*. **2003**, *100*, 14321–14326.

15. Somu, R. V.; Wilson, D. J.; Bennett, E. M.; Boshoff, H. I.; Celia, L.; Beck, B. J.; Barry, C. E., 3rd, Aldrich, C. C. Antitubercular nucleosides that inhibit siderophore biosynthesis: SAR of the glycosyl domain. *J. Med. Chem.* **2006**, *49*, 7623–7635.

16. Miethke, M.; Bisseret, P.; Beckering, C. L.; Vignard, D.; Eustache, J.; Marahiel, M. A. Inhibition of aryl acid adenylation domains involved in bacterial siderophore synthesis. *FEBS J.* **2006**, *273*, 409–419.

17. Vannada, J.; Bennett, E. M.; Wilson, D. J.; Boshoff, H. I.; Barry, C. E. 3rd; Aldrich, C. C. Design, synthesis, and biological evaluation of beta-ketosulfonamide adenylation inhibitors as potential antitubercular agents. *Org. Lett.* **2006**, *8*, 4707–4710.

18. Duckworth, B. P.; Nelson, K. M.; Aldrich, C. C. Adneylating enzymes in *Mycobacterium tuberculosis* as drug targets. *Curr. Top. Med. Chem.* **2012**, *12*, 766–796.

19. Liu, Y.; Shreder, K. R.; Gai, W.; Corral, S.; Ferris, D. K.; Rosenblum, J. S. Wortmannin, a widely used phosphoinositide 3-kinase inhibitor, also potently

inhibits mammalian polo-like kinase. *Chem. Biol.* **2005**, *12*, 99–107.

20. MacKinnon, A. L.; Garrison, J. L.; Hegde, R. S.; Tauton, J. Photo-leucine incorporation reveals the target of a cyclodepsipeptide inhibitor of cotranslational translocation. *J. Am. Chem. Soc.* **2007**, *129*, 14560–14561.

21. Puri, A. W., Bogyo, M. Using small molecules to dissect mechanisms of microbial pathogenesis. *ACS Chem. Biol.* **2009**, *4*, 603–616.

22. Eirich, J.; Orth, R.; Sieber, S. A. Unraveling the protein targets of vancomycin in living *S. aureus* and *E. faecalis* cells. *J. Am. Chem. Soc.* **2011**, *133*, 12144–12153.

23. Duckworth, B. P.; Wilson, D. J.; Nelson, K. M.; Boshoff, H. I.; Barry, C. E. 3rd; Aldrich, C. C. Development of a selective activity-based probe for adenylating enzymes: Profiling MbtA involved in siderophore biosynthesis from *Mycobacterium tuberculosis*. *ACS Chem. Biol.* **2012**, *7*, 1653–1658.

24. Neres, J.; Labello, N. P.; Somu, R. V.; Boshoff, H. I.; Wilson, D. J.; Vannada, J.; Chen, L.; Barry, C. E. 3rd; Bennett, E. M.; Aldrich, C. C. Inhibition of siderophore biosynthesis in *Mycobacterium tuberculosis* with nucleoside bisubstrate analogues: Structure activity relationships of the nucleobase domain of 5′-*O*-[*N*-(salicyl)sulfamoyl]-adenosine. *J. Med. Chem.* **2008**, *51*, 5349–5370.

25. Saghatelian, A.; Jessani, N.; Joseph, A.; Humphrey, M.; Cravatt, B. F. Activity-based probes for the proteomic profiling of metalloproteases. *Proc. Natl. Acad. Sci. U.S.A.* **2004**, *101*, 10000–10005.

26. Leslie, B. J.; Hergenrother, P. J. Identification of the cellular targets of bioactive small organic molecules using affinity reagents. *Chem. Soc. Rev.* **2008**, *37*, 1347–1360.

27. Geurink, P. P.; Prely, L. M.; van der Marel, G. A.; Bischoff, R.; Overkleeft, H. S. Photoaffinity labeling in activity-based protein profiling. *Top. Curr. Chem.* **2012**, *324*, 85–113.

28. Speers, A. E.; Cravatt, B. F. Profiling enzyme activities in vivo using click chemistry methods. *Chem. Biol.* **2004**, *11*, 535–546.

29. Dunetz, J. R.; Danheiser, R. L. Synthesis of highly substituted indolines and indoles via intramolecular [4 + 2] cycloaddition of ynamides and conjugated enynes. *J. Am. Chem. Soc.* **2005**, *127*, 5776–5777.

30. Sikora, A. L.; Wilson, D. J.; Aldrich, C. C.; Blanchard, J. S. Kinetic and inhibition studies of dihydroxybenoate-AMP ligase from *Escherichia coli*. *Biochemistry* **2010**,

49, 3648–3657.

31. Weerapana, E.; Speers, A. E.; Cravatt, B. F. Tandem orthogonal proteolysis-activity-based protein profiling (TOP-ABPP)–A general method for mapping sites of probe modification in proteomes. *Nat. Protoc.* **2007**, *2*, 1414–1425.

32. Jones, C. M.; Niederweis, M. *Mycobacterium tuberculosis* can utilize heme as an iron source. *J. Bacteriol.* **2011**, *193*, 1767–1770.

33. Tullius, M. V.; Harmston, C. A.; Owens, C. P.; Chim, N.; Morse, R. P.; McMath, L. M.; Iniguez, A.; Kimmey, J. M.; Sawaya, M. R.; Whitelegge, J. P.; Horwitz, M. A.; Goulding, C. W. Discovery and characterization of a unique mycobacterial heme acquisition system. *Proc. Natl. Acad. Sci. U.S.A.* **2011**, *108*, 5051–5056.

34. Wells, R. M.; Jones, C. M.; Xi, Z.; Speer, A.; Danilchanka, O.; Doornbos, K. S.; Sun, P.; Wu, F.; Tian, C.; Niederweis, M. Discovery of a siderophore export system essential for virulence of *Mycobacterium tuberculosis*. *PLoS Pathog.* **2013**, *9*, e1003120.

35. Heacock, D.; Forsyth, C. J.; Shiba, K.; Musier-Forsyth, K. Synthesis and aminoacyl-tRNA synthetase inhibitory activity of prolyl adenylate analogs. *Bioorg. Chem.* **1996**, *24*, 273–289.

Chapter 4. Total Synthesis and Biological Evaluation of Four Diastereomers of the Natural Product Transvalencin Z

The following chapter is original work designed by Kathryn M. Nelson and Dr. Courtney C. Aldrich. All of the included work was completed by KMN with the exception of the MIC activity data against *Mycobacterium tuberculosis* which was completed by Dr. Helena I. Boshoff at the NIH. This work was published in the *Journal of Natural Products*, and some figures and excerpts are reproduced with permission from that journal (see preface above).

4.1 Introduction

As discussed in previous chapters, there is a dire need for new antitubercular agents that act via new mechanisms of action. Natural products have been a great source of both new compounds and lead compounds for antibacterial development. Most of the major classes of antibiotics are either natural products, or derived from natural products. Beginning with penicillin in the early 1900s, β-lactams, macrolides, aminoglycosides, glycopeptides, tetracyclines, and vancomycin are all natural products or natural product-derived antibiotics that have been successfully brought to clinical use. The success of natural products for the development of antibiotics has not been limited to broad spectrum agents. Many of the clinically used antitubercular agents are also natural

products or derivatives of natural products. Streptomycin is an aminoglycoside antibiotic isolated as a fermentation product from *Streptomyces griseus*.[1] This was the first successful chemotherapeutic against *Mycobacterium tuberculosis* (*Mtb*) infection. Streptomycin is still a second-line treatment option for tuberculosis (TB) patients as it is only injectable due to its high polarity and lack of oral bioavailability (**4-1**, **Figure 4.1**).[2] Other aminoglycoside natural products that also find use as antibiotics include the natural product kanamycin (**4-2**) and its synthetic derivative amikacin (**4-3**), which have broad spectrum activity against drug-sensitive strains of *Mtb*.[3,4] Naturally occurring antitubercular agents, including the well-known products cycloserine and aminoglycoside capreomycin, are also still included on the list of second-line agents available for treatment. In addition to these natural products, the first line anti-TB agent rifampin (RIF) is a semisynthetic derivative of the ansamycin antibiotic rifamycin B.[5] Additional discussion of RIF as an antitubercular agent can be found in Chapter 1. Other natural product-derived antitubercular agents include pyrazinamide (PZA), which is a derivative of nicotinamide (vitamin B3), and para-aminosalicylic acid, which is an analogue of salicylic acid. Natural product screening has lost some of its popularity in favor of target-based rational drug design strategies (see Chapter 1 above), but natural products continue to show activity against a variety of indications, including TB.

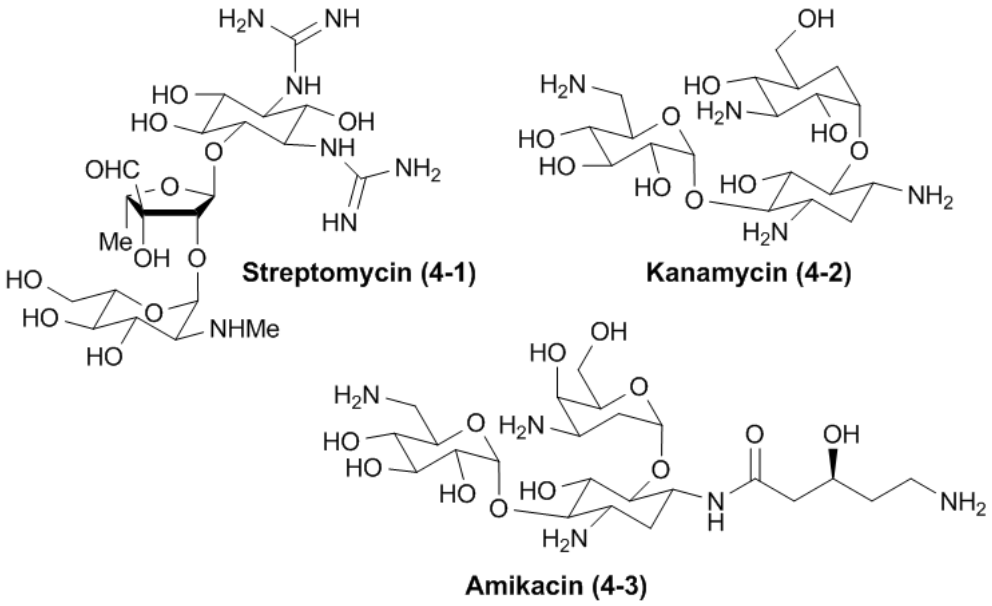

Figure 4.1. Natural products and derivative antibiotics active against *Mtb*. **4-1**, streptomycin; **4-2**, kanamycin; and **4-3**, amikacin (derivative of kanamycin)

Mukai and co-workers isolated the natural product transvalencin Z (**4-4**, **Figure 4.2**) from a clinical strain of *Nocardia transvalensis*.[6] The isolated compound exhibited potent and specific inhibition of *Mycobacterium smegmatis* with an MIC (minimum inhibitory concentration that results in > 99% reduction in observable growth) of 0.34 μM (0.125 μg/mL). There was also some activity against other acid-fast *Nocardia* spp., but no activity was seen against Gram-negative bacilli, fungi, or mammalian cell lines.[6] Our group became interested in this report as compound **4-4** also shows striking structural similarity to the mycobactin siderophores produced by *Mtb* (**Figure 4.2**). Mycobactins are a mycobacterial-specific class of siderophores, which are small molecule iron (Fe^{3+}) chelators produced by nearly all bacteria.[7]

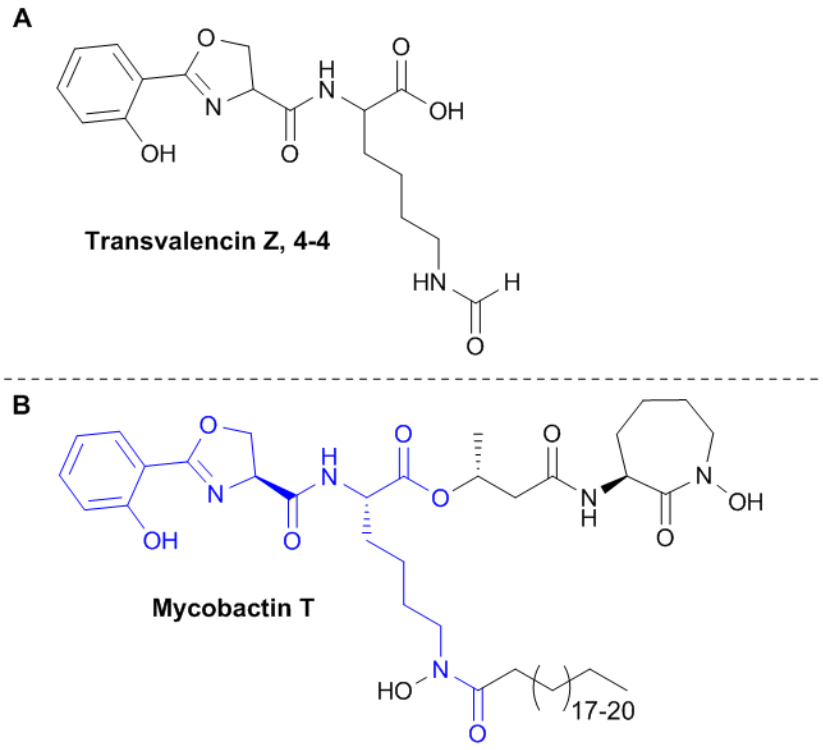

Figure 4.2. (A) Reported structure of transvalencin Z (**4-4**)[6]. (B) Structure of mycobactin-T.

Iron is necessary for bacterial cell processes in virtually every pathogen, with a few notable exceptions, including *B. burgdorferi*.[9] Bacteria have evolved pathways to synthesize, secrete, and re-import siderophores that scavenge iron in limiting environments such as a human host. The inhibition of the biosynthesis of these molecules has emerged as a promising strategy for the development of new antibacterial agents.[7,10] The mycobactins in *Mtb* are essential for growth and virulence in iron-limiting conditions, making their biosynthetic pathway especially attractive as a drug target.[11] The structural similarity of **4-4** to the core structure of the mycobactins suggests that it may exert its activity against mycobacteria by interfering with mycobactin-mediated iron scavenging. Snow originally proposed that mycobactin analogs may antagonize

mycobacterial growth in 1970.[8,12] Miller and co-workers reinforced that hypothesis with two different studies. In the first, they found that mycobactin S, produced by *M. smegmatis* and differing from mycobactin T by only one stereocenter (**Figure 4.3**), inhibits the grown of *Mtb*.[13,14]

Mycobactin	R^1	R^2	R^3	R^4	R^5	a	b	c	d	e	f
S	$C_{13\text{-}19}$	H	H	CH_3	H	-	L	L	*S*	-	L
T	$C_{17\text{-}20}$	H	H	CH_3	H	-	L	L	*R*	-	L

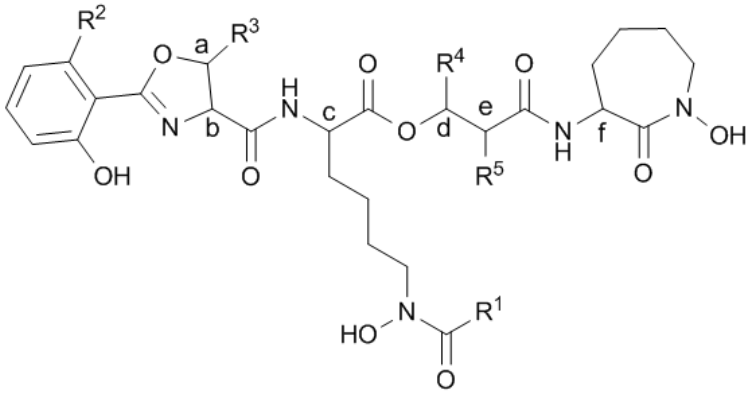

Figure 4.3. Structural differences between mycobactin S and T. Mycobactin T is a native siderophore to *Mtb*, while Mycobactin S is native to *M. smegmatis*. Mycobactin S has an MIC of 12.5 µg/mL against *Mtb* H37Rv.

Additionally, an analog of mycobactin T that replaces the β-hydroxybutyrate substitution with a 2,3-diaminoproprionate exhibited antimycobacterial activity.[15] In addition to these very similar molecules, Miller's group has demonstrated that organic molecules derived from a phenyloxazoline, which mimic the head group of the mycobactins, possess antimycobacterial activity, although they suggest this is unrelated to the antagonism of iron acquisition.[14] Quadri and co-workers recently reported a series of small molecules that incorporate a 2-hydroxyphenyl moiety that show iron-dependent antimycobacterial

activity, suggesting some interference with mycobactin-mediated iron acquisition.[16]

4.2 Research Objectives

The principle aim of this research was to identify and fully characterize the stereochemical assignments and antimycobacterial activity of the natural product transvalencin Z. To accomplish this, the four possible diastereomers will be synthesized from optically pure starting materials and carefully designed synthetic schemes to ensure enantiopurity of the final products. Comparative analysis of the characterization data and the reported data for transvalencin Z will be used to unequivocally assign the stereochemistry of the natural product, if possible. The four diastereomers will then be tested against *M. smegmatis* in an effort to determine if the activity of the natural product is dependent upon the stereochemistry. If only one of the four diastereomers is active to the same extent as reported in literature, assignment could be made based on microbiological activity. Finally, these compounds will be tested against *M. tuberculosis* H37Rv to see if the *M. smegmatis* activity reported will translate to *Mtb* activity.

4.3 Results

4.3.1 Synthesis of transvalencin Z diastereomers

Retrosynthetically, transvalencin Z can be disconnected into two major building blocks: a 2-hydroxyphenyl oxazoline acid **4-5** and an ε-formyl lysine **4-6**, as shown in **Scheme 4.1**. Building block **4-5** is a common intermediate in the synthesis of known mycobactins and their analogues previously reported by Miller and co-workers. [12–14] A dehydrative ring closure and peptide bond coupling between salicylic acid and an appropriately protected serine derivative can lead back to commercially available starting materials **4-7** and **4-8**. Building block **4-6** is derived from lysine **4-9**. Each building block can be readily synthesized in both *R* and *S* enantiomers.

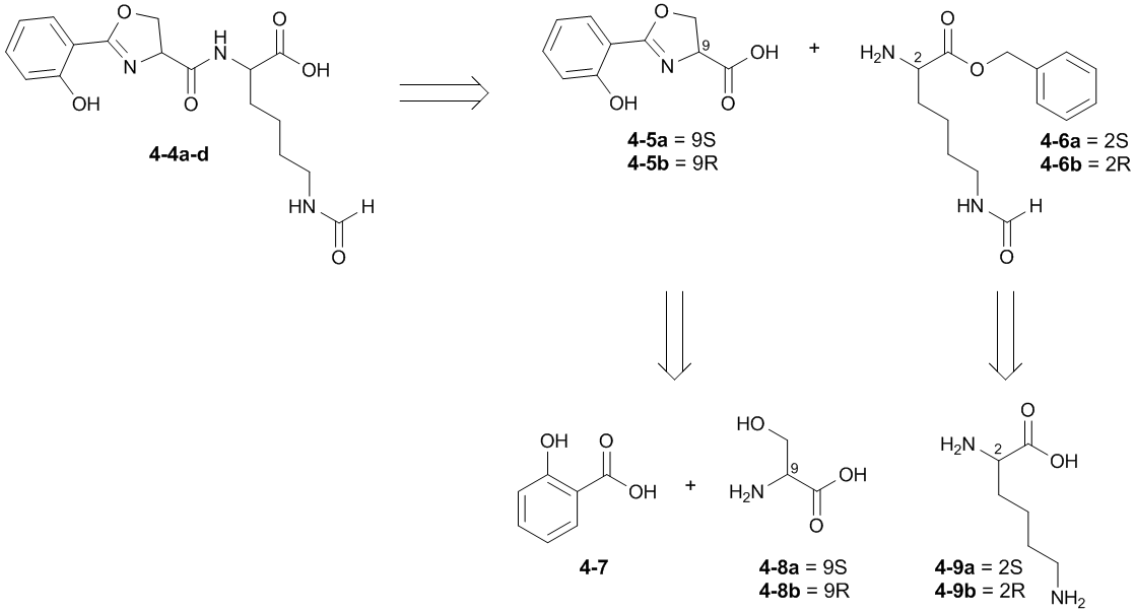

Scheme 4.1 Retrosynthetic analysis of transvalencin Z. The commercially available enantiopure serine and lysine starting materials help set the stereocenters in the final compounds.

The synthesis of building blocks **4-5a** and **4-5b** began with the benzylation of salicylic acid **4-7**,[17] followed by peptide coupling with *L*- or *D*-serine benzyl esters as previously described by Miller and co-workers to yield the serine adducts **4-12** in 90% average yield (**Scheme 4.2**).[13]

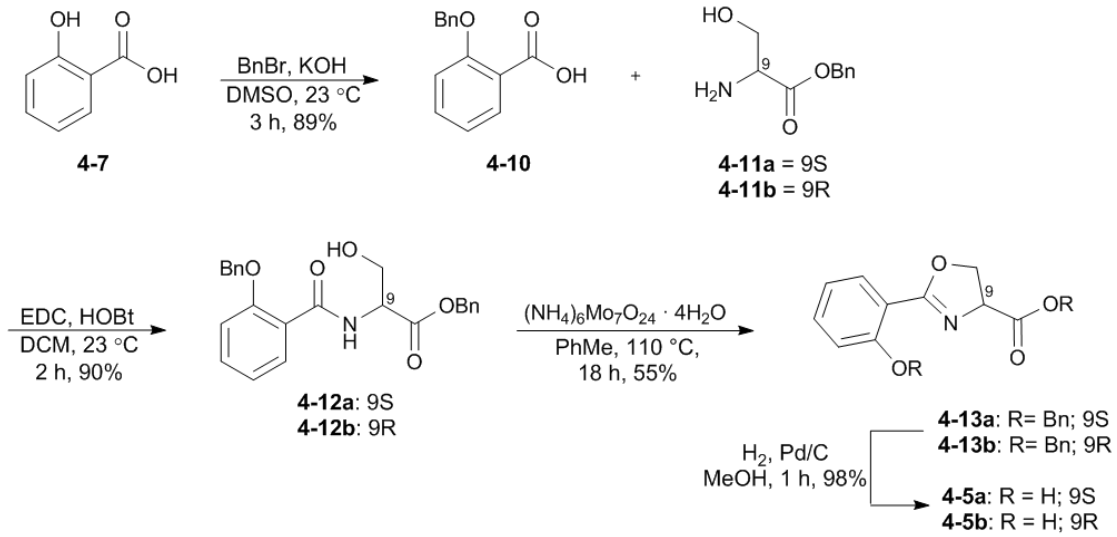

Scheme 4.2. Synthesis of the oxazoline building blocks **4-5a** and **4-5b** for transvalencin Z diastereomer synthesis.

Miller and co-workers employed Burgess' reagent (**4-14**) under refluxing conditions to give the dehydrated product **4-13**. However, we elected to use the a reported molybdenum catalyst, ammonium molybdenum tetrahydrate ($(NH_4)_6Mo_7O_{24}$•$4H_2O$).[18] Molybdenum activation was reported to retain the stereochemistry at the β-position of serine/threonine analogues, which would be useful if analogues are synthesized for structure-activity relationships in the future. This biomimetic dehydrative cyclization procedure contrasts with the Burgess' reagent method that electrophilically activates the serine hydroxyl group, followed by nucleophilic displacement by the amide carbonyl (**Scheme 4.3**).[19,20]

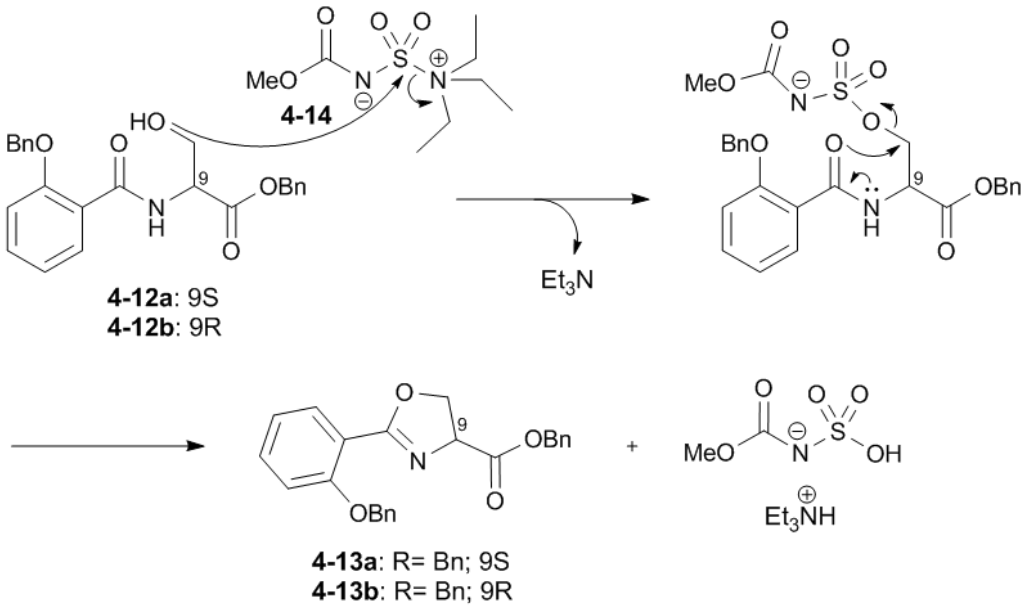

Scheme 4.3. Mechanism for dehydrative cyclization using Burgess' reagent **4-14**.

The molybdenum catalyst acts by first coordinating to the amide carbonyl thereby electrophilically activating the carbon center for intramolecular attack by the serine hydroxyl nucleophile. Dehydration of the system then affords the heterocycle **4-13** (**Scheme 4.4**).[18] Enantiopurity was confirmed by measurement of optical rotation and matching to literature values.[13] Global deprotection of **4-13** by hydrogenolysis provided acids **4-5** in nearly quantitative yields (**Scheme 4.2**). Deprotection of the phenol ether was required for the penultimate peptide coupling reaction, a phenomenon that has been documented in multiple siderophore syntheses.[14,21]

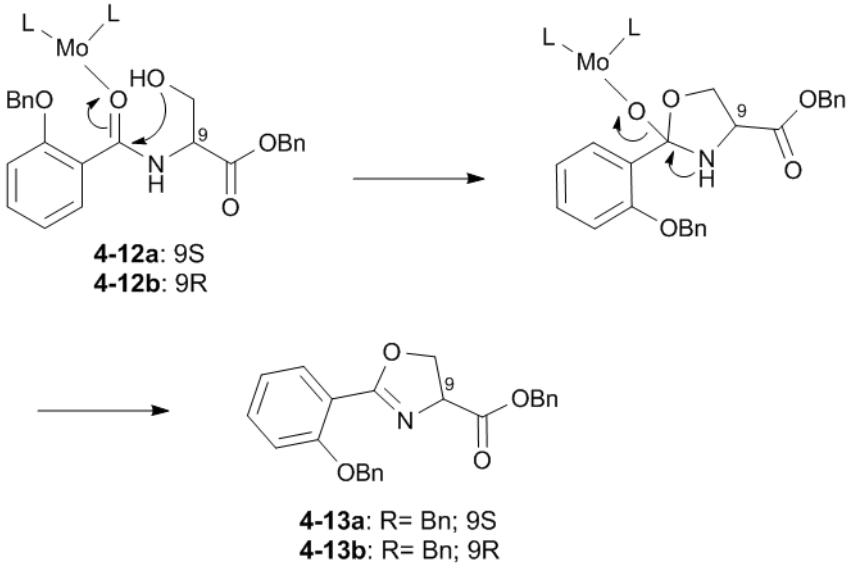

Scheme 4.4. Proposed mechanism for molybdenum catalyzed dehydrative cyclization.

Commercially available N^{α}-Fmoc- *L*- or *D*-lysine **4-15** was formylated by the mixed anhydride method reported by Hughes and Waters to give acid **4-16** (**Scheme 4.5**).[22,23] Elaboration of **4-16** to the fully protected lysine conjugate **4-17** was possible under a number of common conditions for benzyl ester formation; however, conditions involving direct alkylation (DIPEA, BnBr) were ultimately chosen to prevent possible racemization at the α-stereocenter.[24] Fmoc deprotection of **4-17** with excess piperidine afforded the free amine **4-6**.

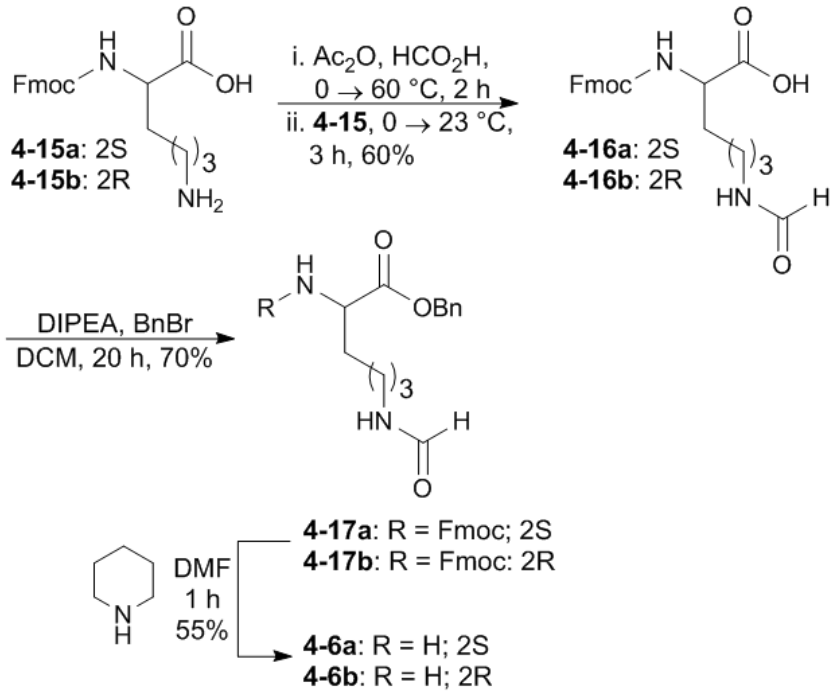

Scheme 4.5. Synthesis of the lysine building blocks **4-6a** and **4-6b** for transvalencin Z diastereomer synthesis.

Peptide coupling of acid **4-5a** and lysine **4-6a** with 1-ethyl-3-(3-dimethylaminopropyl)carbodiimide (EDC) resulted in epimerization at position C-9 to afford **4-18a** and **4-18c** in a 4.2:1 ratio as determined by HPLC (**Figure 4.4**).

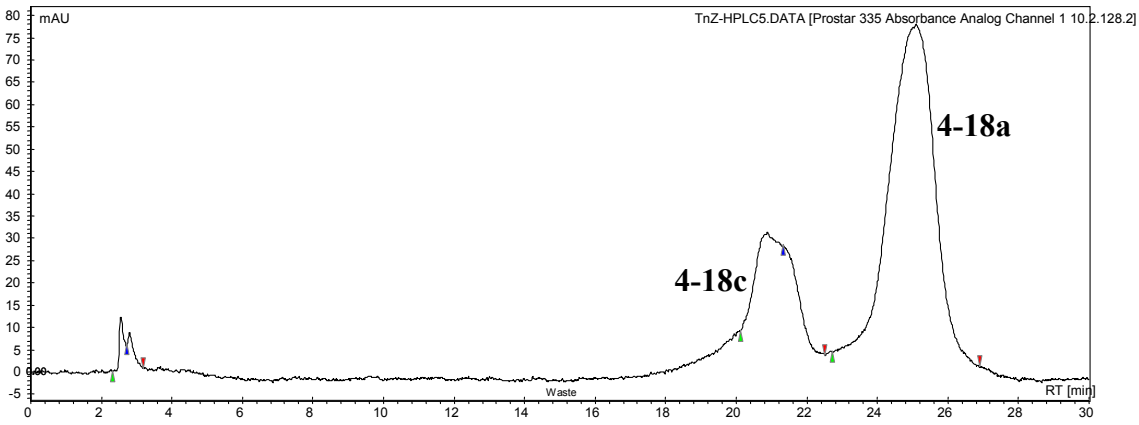

Figure 4.4. HPLC trace of epimerized product in initial peptide coupling of **4-5a** and **4-6a** using EDC coupling conditions.

Therefore, the penultimate step was performed with 3-(diethoxyphosphoryloxy)-1,2,3-benzotriazin-4(3*H*)-one (DEPBT) **4-19**, a reagent known for minimizing racemization at sensitive stereocenters (**Scheme 4.6**).[25] Hydrogenolysis of **4-18a** provided free acid **4-4a**. The remaining diastereomeric products **4-4b–d** were prepared in an analogous fashion as described for **4-4a**.

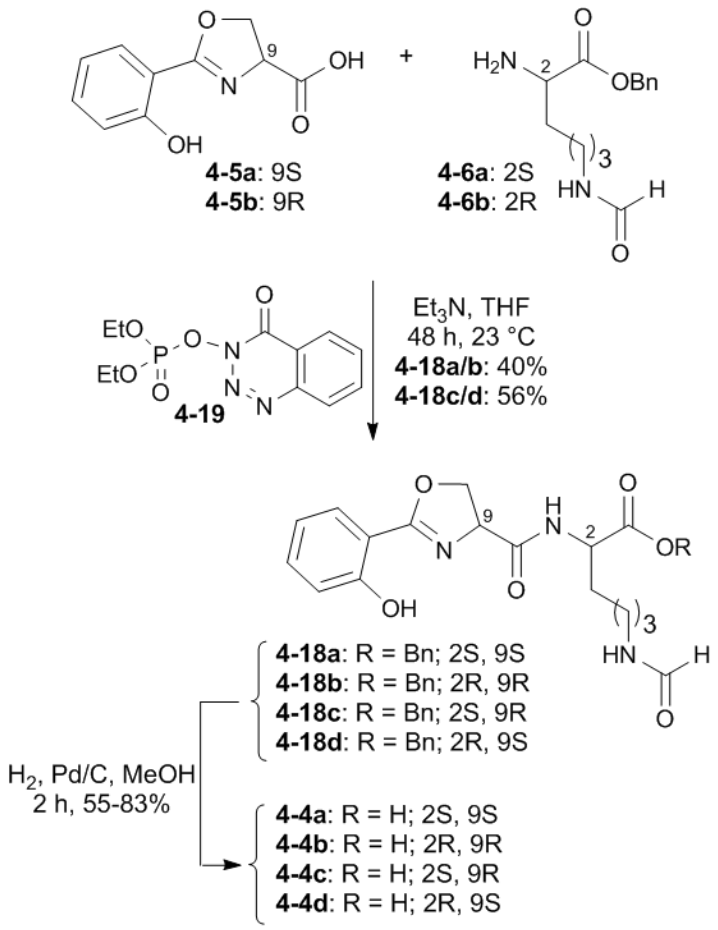

Scheme 4.6. Penultimate DEPBT coupling and final hydrogenolysis completed the total synthesis the four transvalencin Z diastereomers.

4.3.2 Biological evaluation of transvalencin Z diastereomers

In attempting to assign the stereochemistry for transvalencin Z, we also sought to confirm the biological activity reported by Mukai and co-workers.[6] We were especially interested in its potential use against mycobacteria, so we began with biological evaluation of **4-4a–d** against *Mycobacterium smegmatis* MC24517 readily available in the Aldrich laboratory. The minimum inhibitory concentration (MIC) was greater than 100 μM for all four diastereomers (**Table 4.1**). Because there can be variations in protein expression levels in different strains of bacteria, we then tested the diastereomers against the identical *M. smegmatis* strain (ATCC 607) reported, but again observed no activity. The four compounds were also tested against a panel of ten additional pathogens (*Enterococcus faecalis, Staphylococcus aureus*, *Acinetobacter baumannii, Escherichia coli, Klebsiella pneumoniae, Bacillus subtilis, Pseudomonas aeruginosa*, *Candida albicans*, *Mycobacterium bovis BCG,* and *Mycobacterium tuberculosis*) and **4-4a–d** were inactive (MIC ≥ 100 μM) against all strains evaluated. Five of these pathogens from our screen (*M. smegmatis, S. aureus, B. subtilis, E. coli,* and *C. albicans*) were also screened by Mukai and co-workers,[6] who reported MIC values of 0.34, 3.0, 44, >175, and >175 μM, respectively, which are inconsistent with our data (**Table 4.1**).

Table 4.1. MIC activity data for isolated transvalencin Z (**4-4**)[6] and synthetic **4-4a-d**.

Strain	Classification	Reported MIC 4-4 (μM)[6]	MIC 4-4a–d (μM)
M. smegmatis (ATCC 607)	Acid-fast	0.344	> 100
E. coli (ATCC 25922)	Gram-negative	> 175	> 100
B. subtilis (ATCC 6633)	Gram-positive	44	> 100
S. aureus (*MRSA*, ATCC 43300)	Gram-positive	3	> 100
C. albicans (ATCC 10231)	Fungal	> 175	> 100
A. baumannii (ATCC 19606)	Gram-negative	n.d.[a]	> 100
K. pneumoniae (ATCC 13883)	Gram-negative	n.d.	> 100
P. aeruginosa (ATCC 27853)	Gram-negative	n.d.	> 100
E. faecalis (ATCC 51299)	Gram-positive	n.d.	> 100
M. smegmatis (MC24517)	Acid-fast	n.d.	> 100
M. tuberculosis (H37Rv)[b]	Acid-fast	n.d.	> 100
M. bovis BCG strain TMC 1011 Pasteur (ATCC 35734)	Acid-fast	n.d.	> 100
S. aureus (*MRSA*, clinical IDRL 6169)	Gram-positive	n.d.	> 100
S. aureus (*MSSA*, clinical IDRL 8545)	Gram-positive	n.d.	> 100
Vero	Mammalian	n.d.	> 100

[a]n.d.: not determined, [b]Testing performed by Dr. Helena I. Boshoff

4.3.3 Characterization of transvalencin Z diastereomers

Synthetic transvalencins **4-4a–d** were isolated as amorphous white solids. The spectral data collected including ^{1}H and ^{13}C NMR, high resolution mass spectrometry, and IR

absorbance were similar to those reported by Mukai and co-workers.[6] We are certain of the absolute configuration of our compounds based on the use of chiral starting materials and knowledge of the chemical transformations for the synthesis of **4-4a–d**. The methods were chosen to reduce racemization of stereocenters in all steps, as noted above. Diastereomers of compounds **4-18a–d** could be identified by distinct retention times on reverse-phase HPLC. A similar HPLC method was able to differentiate between the diastereomers of compounds **4-4a-d** as well (**Figure 4.5**). We observed nearly equal and opposite optical rotations for each set of enantiomers, giving further support to their enantiopurity.

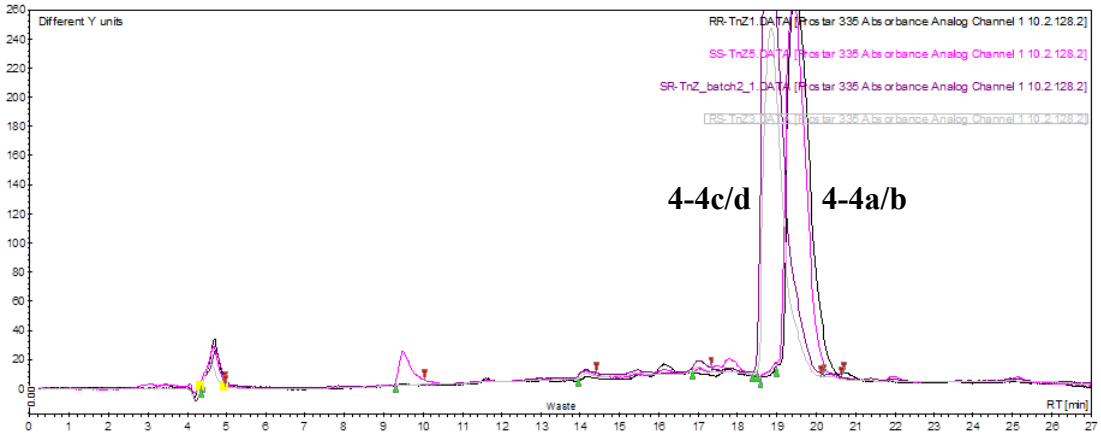

Figure 4.5. Stack plot of synthetic transvalencins **4-4a-d**. While the enantiomers overlap and are indistinguishable by retention time, the sets of diastereomers are distinct.

Most of the ^{1}H NMR chemical shifts for **4-4a–d** match those reported for transvalencin Z (**Table 4.2**). The C-2, 2-NH, and 6-NH protons show significant differences in chemical shift for **4-4a–d** compared to the reported natural product.[6] The C-2 shift at the chiral center is significant and concerning, however amide protons can be highly variable due to pH, sample concentration, and temperature of the solution, so these shifts may not be

diagnostic.[26] The optical rotation values for **4-4a–d** also do not match the reported value (+15.3°) for transvalencin Z;[6] the sets of enantiomers **4-4a–b** (+29.2°/−31.6°) and **4-4c–d** (−2.0°/+6.0°) are nearly equi-distant from this value.

Table 4.2. ^{1}H and ^{13}C data for transvalencin Z[6] and compounds **4-4a-d** in d_6-DMSO at 600 MHz.

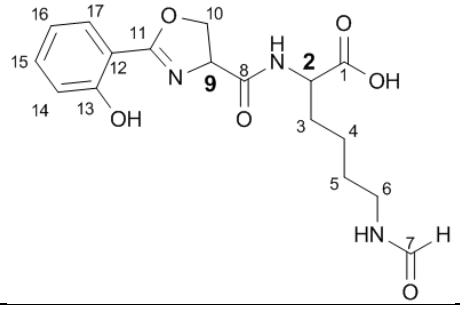

Position	transvalencin Z[6]		4-4a/b		4-4c/d	
	δ_H	δ_C	δ_H	δ_C	δ_H	δ_C
	δ_H and δ_C (ppm), mult. (*J* in Hz)					
1	11.76, br s	173.1	11.80, br s	173.3	11.81, br s	173.8
2	**3.85, q-like (6.0)**	**53.8**	**4.18, m**	**52.1**	**4.17, m**	**51.9**
2-NH	7.75, d (6.0)		7.87, ovlp m		7.85,ovlp m	
3	1.54, m	31.7	1.61, m	30.4	1.65, m	30.8
3'	1.68, m		1.71, m		1.74, m	
4	1.2, m	22.5	1.26, m	22.8	1.31, m	22.7
5	1.32, m	28.8	1.34, m	28.5	1.40, m	28.4
6	2.98, q-like (6.0)	37.1	3.05 m	36.8	3.05, t (6.0)	36.7
6-NH	7.94, br t (6.0)		8.50, d (6.6)		8.51, d (7.2)	
7	7.92, s	160.7	7.91, s	160.9	7.98, s	160.8
8		168.6		169.7		169.5
9	4.99, dd (8.0, 10.0)	67.4	4.98, t (7.8)	67.1	5.01, t (8.4)	67.0
10	4.48, t (8.0)	69.7	4.48, t (7.8)	69.2	4.50, t (7.8)	69.2
10'	4.63, dd (8.0, 10.0)		4.60, t (7.8)		4.63, t (8.4)	
11		165.9		165.8		165.7
12		159.1		159.1		158.9
13		109.8		109.8		109.8
14	7.0, br d (8.0)	116.5	6.95, d (8.4)	116.6	7.0, d (8.4)	116.4
15	6.94, br t (7.5)	119.1	6.89, t (7.8)	119.1	6.95, t (7.8)	118.9
16	7.46, ddd (1.5, 7.5, 8.0)	134.0	7.41, t (7.8)	134.0	7.46, t (7.2)	133.9
17	7.63, dd (1.5, 7.5)	128.0	7.59, d (7.8)	128.0	7.64, d (7.8)	127.9

In attempting to further confirm the properties of transvalencin Z, **4-4a–d** were screened against a panel of representative organisms (**Table 4.1**, above). We were particularly interested in expanding the number of mycobacteria strains tested to give a more complete picture of the compound's selectivity displayed in the original screen.[6] In contrast to the potent antimycobacterial activity reported for transvalencin Z, none of the four synthetic diastereomers inhibited the growth of several species of mycobacteria, including *M. smegmatis* MC24517 and ATCC607, *M. bovis BCG* and additional testing against *M. tuberculosis* H37Rv by Dr. Helena I. Boshoff at the NIH.

4.4 Discussion

Analysis of the literature describing natural products produced by *Nocardia* sp. and other structurally related natural products (e.g. siderophores such as mycobactins from *M. tuberculosis*, acinetobactin from *A. baumannii*, and nocardichelins from *Nocardia* sp.) does not reveal a trend or preference for stereochemistry. Several studies of salicyl and oxazoline/thiazoline motifs show this stereocenter (C-9 in transvalencin Z) to be *S*, resulting from naturally occurring L-serine.[19,20,27,28] However, other natural products, including brasilibactin from *Nocardia brasiliensis*, show an *R* stereocenter, which would suggest the incorporation of an epimerase in the biosynthetic machinery or the use of the less common D-serine.[29] Other natural products including amamistatins, formobactin, and nocobactin NA contain a completely saturated oxazole ring system, negating the stereocenter at this position.[30] Less work has been done on similar lysine motifs.

Biosynthetic feeding studies of natural products containing lysine motifs (C-2 in transvalencin Z) have demonstrated the *S* configuration is achieved by incorporation of predominantly L-lysine.[27] Further complicating matters, the absolute configuration has not been assigned to the only other transvalencin isolated to date (transvalencin A).[31] These conflicting literature data, combined with the lack of correlation between our activity and spectral data with the original report, make the assignment of stereochemistry in transvalencin Z impossible without the authentic isolated sample for comparison study.

4.5 Conclusions

This work highlights the development of an efficient synthesis to access the four possible diastereomers of the natural product transvalencin Z, and the attempt to assign the native stereochemistry based on spectroscopic and biological activity data. The synthetic route developed here introduces a new dehydrative ring closure to form the oxazoline that would allow for stereocontrol in future analogue syntheses.[18] Spectroscopic characterization of the synthetic diastereomers did not match the reported data for the natural product.[6] Attempted confirmation by biological activity also proved inconclusive. These results suggest that the original natural product may have been contaminated with a small amount of a highly active compound. Alternatively, the slight discrepancies in the spectroscopic data between the four synthetic diastereomers compared to the natural product suggest that the reported structure of transvalencin Z may be incorrect. It is

especially concerning that the C-2 stereocenter did not match the reported data. The synthetic methods for **4-4a–d** unequivocally produced the pure enantiomers, as confirmed by extensive NMR and HPLC analysis. It is possible that small differences in bond connections may have caused a mistake in the assignment of the natural product structure. Chemical derivatization of the freshly isolated natural product may aide in elucidating the true structure. Attempts to obtain the isolated compound or the producing strain from the Mukai research group have thus far been unsuccessful.

4.6 Experimental Data

4.6.1 General procedures for the synthesis of transvalencin Z diastereomers

All commercial reagents were used as provided unless otherwise indicated. An anhydrous solvent dispensing system (JC Meyer Solvent Systems, Laguna Beach, CA) with two packed columns of neutral alumina was used for drying THF and CH_2Cl_2 while two packed columns of molecular sieves were used to dry DMF and the solvents were dispensed under argon. Anhydrous grade MeOH and toluene were purchased from Aldrich. Flash chromatography was performed on a Combiflash Companion® system (Teledyne Isco, Lincoln, NE) equipped with flash column silica cartridges with the indicated solvent system. All reactions were performed under an inert atmosphere of dry Ar or N_2 in oven-dried (150 °C) glassware. ^{1}H and ^{13}C NMR spectra were recorded on a Varian 600 MHz spectrometer. Proton chemical shifts are reported in ppm from an

internal standard of residual chloroform (7.26), methanol (3.31), dichloromethane (5.32), or dimethylsulfoxide (2.50), and carbon chemical shifts are reported in ppm from an internal standard of residual chloroform (77.23), methanol (49.15), dichloromethane (54.00), or dimethyl sulfoxide (39.51). Proton chemical data are reported as follows: chemical shift, multiplicity (s = singlet, d = doublet, t = triplet, q = quartet, m = multiplet, br = broad, ovlp = overlapping), coupling constant, integration. High-resolution mass spectra were obtained on an Agilent TOF II TOF/MS instrument (Agilent Technologies, Santa Clara, CA) equipped with either an ESI or APCI interface. Optical rotations were measured on a Rudolph Autopol III polarimeter (Rudolph Research Analytical, Hackettstown, NJ). Melting points were measured on an electrothermal Mel-Temp manual melting apparatus (Electrothermal, Bibby Scientific, Staffordshire, UK) and are uncorrected. IR spectra were obtained on a Jasco FT/IR-4100 (Jasco Analytical Instruments, Easton, MD).

4.6.2 General procedures for microbiological evaluation of transvalencin Z diastereomers

M. smegmatis (MC24715) was a generous gift of Dr. William R. Jacobs, Jr. of the Howard Hughes Medical Institute and Department of Microbiology and Immunology, Albert Einstein College of Medicine, Bronx, NY. *S. aureus* (*MRSA*) clinical IDRL 6169 and *S. aureus* (*MSSA*) IDRL 8545 were the kind gifts of Dr. Robin Patel, Department of Laboratory Medicine and Pathology, Mayo Clinic College of Medicine, Rochester, MN;

other pathogens were obtained from the ATCC *(A. baumannii* ATCC 19606, *C. albicans* ATCC 10231, *E. faecalis* (*VRE*) ATCC 51299, *E. coli* ATCC 25922, *K. pneumoniae* ATCC 13883, *P. aeruginosa* ATCC 27853, *S. aureus* (*MRSA*) ATCC 43300, *M. smegmatis* ATCC 607, *M. bovis* BCG strain TMC1011 Pasteur ATCC 35734) and cultured as follows. Bacterial strains were streaked from frozen glycerol stocks onto solid agar plates before being subcultured in liquid medium for assay. Agar plates consisted of the following media plus agar (Difco) to a 1.5% concentration: *E. coli*, *P. aeruginosa*, and all *S. aureus*, trypticase soy; *A. baumannii*, *K. pneumoniae*, *M. bovis* BCG, and all *M. smegmatis*, nutrient broth; *E. faecalis*, brain heart infusion; and *C. albicans*, YM broth. Bacteria were cultured on agar plates overnight at 37 °C, while *C. albicans* was cultured overnight at 30 °C. After 24 h incubation, single colonies were picked and grown in broth (listed above) to an OD_{600} of 1.0, diluted to an OD_{600} of 0.003 and plated in 96-well sterile plates with 1% DMSO and varying concentrations of **4-4a–d**. Plates were read at 24 and 48 h at 600 nm on a plate reader (Molecular Devices Spectramax M5e); plate background (690 nm) was subtracted out and values were standardized to the DMSO controls. In initial microbiological testing against *M. smegmatis*, it was observed that the bacteria would often clump together during growth, causing large variations in optical density readings. Addition of the supplemental detergent Tyloxapol (Sigma, St. Louis, MO) at 0.05% by volume prevented clumping of the mycobacteria without the potentially toxic side effects observed when using Tween detergents with mycobacteria.[32] Mukai and co-workers did not report the use of any detergents for *M. smegmatis* growth.

4.6.3 General procedures for mammalian cell toxicity measurements

Cytotoxicity of each compound was determined with a standard tetrazolium assay against Vero green monkey kidney cells (ATCC CCL-81).[33,34] All tissue culture reagents were purchased from Gibco, Invitrogen (Carlsbad, California). Cells were grown in MEM media supplemented with 10% fetal bovine serum (FBS), 1% penicillin/streptomycin and 1% Glutamax. Cells were seeded at 3.0×10^4 cells per well in a 96-well microtiter plate (Corning Life Sciences, Lowell, MA) and allowed to adhere overnight. Medium was carefully aspirated and replaced with 195 μL fresh medium, and compound solutions in DMSO (5 μL) were added to give a final concentration ranging from 100–0.16 μM. All concentrations were tested in triplicate. Plates were incubated for 72 h at 37 °C and 4.5% CO_2 in a humidified chamber. The solutions were carefully removed and RPMI without phenol red containing 1.0 mg/mL 3-(4,5-dimethyl-thiazolyl-2)-2,5-diphenyltetrazolium bromide (MTT) was added (200 μL) and incubated for 3 h, after which the MTT medium was carefully removed. Isopropyl alcohol (200 μL) was added to dissolve the precipitated purple formazan crystals and the plates were read at 570 nm with a plate reader (Molecular Devices Spectramax M5e); plate background (690 nm) was subtracted out and cell viability was estimated as the percentage absorbance relative to the DMSO control. Dose response curves were generated using GraphPad Prism 5 software (GraphPad Software, San Diego, CA) and used to determine the MIC_{50} concentrations (minimal concentration that inhibits 50% of growth).

4.6.4 2-(Benzyloxy)benzoic acid (4-10) and *N*-[2-(Benzyloxy)benzoyl]-L/D-serine benzyl esters (4-12a and 4-12b)

Compounds **4-10**, **4-12a**, and **4-12b** were prepared according to literature procedures.[7,13]

4.6.5 (4*S*) and (4*R*)-Benzyl-2-[2-(benzyloxy)phenyl]-Δ^2-1,3-oxazoline-4-carboxylate (4-13a and 4-13b)

To a stirring solution of *N*-[2-(benzyloxy)benzoyl]-L-serine benzyl ester (**4-12a**), (2.0 g, 4.9 mmol, 1.0 equiv) or *N*-[2-(benzyloxy)benzoyl]-D-serine benzyl ester (**4-12b**) in toluene (50 mL) was added ammonium molybdate (VI) tetrahydrate ($(NH_4)_6MoO_{24}•4H_2O$) (2.4 g, 1.9 mmol, 0.39 equiv), and the solution was refluxed for 18 h on a Dean-Stark trap to remove the generated water. The reaction was concentrated under reduced pressure to a dark, green oil and partitioned between EtOAc and 5% aqueous $NaHCO_3$. The organic layer was washed with saturated aqueous NaCl (100 mL), dried ($MgSO_4$), and concentrated under reduced pressure to an off-white amorphous solid. Purification by flash chromatography (linear gradient 0–50% EtOAc/hexanes) on silica gel afforded the title compound (1.00 g, 55%) as an off-white solid. mp = 68–71 °C; **4-13a** $[\alpha]_D^{23}$ = + 79.1 (*c* 1.0, $CHCl_3$); **4-13b** $[\alpha]_D^{23}$ = − 81.7 (*c* 1.0, $CHCl_3$); R_f = 0.33 (30% EtOAc/hexanes); ^{1}H NMR, ^{13}C NMR, and HRMS identical to reported values.[13]

4.6.6 (4*S*) and (4*R*)-2-[2-Hydroxyphenyl]-Δ^2-1,3-oxazoline-4-carboxylic acid (4-5a and 4-5b)

(4*S*)-Benzyl-2-[2-(benzyloxy)phenyl]-Δ^2-1,3-oxazoline-4-carboxylate (**4-13a**) or (4*R*)-Benzyl-2-[2-(benzyloxy)phenyl]-Δ^2-1,3-oxazoline-4-carboxylate (**4-13b**) (0.385 g, 1.00 mmol) was dissolved in anhydrous methanol (10 mL) and added to a Parr flask containing 10% by weight Pd/C (0.039 g) under Ar. The reaction vessel was evacuated, then backfilled with hydrogen gas to 3 atm, and the mixture was shaken at 25 °C for 1 h. The reaction vessel was opened, and the reaction mixture was filtered through Celite. The filtrate was concentrated under reduced pressure to a dark red-orange oil (190 mg, 91%) and used directly in the next step without further purification. However, for analytical characterization, purification by flash chromatography (isocratic 50% EtOAc/hexanes with 1% formic acid) afforded the title compound as a clear, colorless oil. **4-5a** $[\alpha]_D^{23}$ +39.2 (*c* 1.0, MeOH); **4-5b** $[\alpha]_D^{23}$ −27.5 (c 1.0, MeOH); R_f = 0.22 (1:1 EtOAc/hexanes with 1% formic acid); ^{1}H NMR (CD_3OD, 600 MHz) δ 4.54−4.59 (m, 2H), 4.92 (apparent br t, *J* value not discernible due to broadening, 1H), 6.81 (t, *J* = 7.8 Hz, 1H), 6.89 (d, *J* = 8.4 Hz, 1H), 7.33 (t, *J* = 7.2 Hz, 1H), 7.57 (d, *J* = 7.8 Hz, 1H); ^{13}C NMR (CD_3OD, 150 MHz) δ 68.4, 70.7, 111.3, 117.7, 120.1, 129.5, 135.2, 161.1, 168.5, 174.1; HRMS (ESI−) calculated for $C_{10}H_8NO_4$ $[M - H]^-$ 206.0459, found 206.0435 (error 11.6 ppm), $C_9H_8NO_2$ $[M - CO_2]^-$ 162.0561, found 162.0552 (error 5.6 ppm).

4.6.7 (2*S*) and (2*R*)-({[(9H-Fluoren-9-yl)methyloxy]carbonyl}amino)-6-formamidohexanoic acid (4-16a and 4-16b)

Formic acid (1.5 mL, 39 mmol, 5.7 equiv) was added dropwise to acetic anhydride (4.5 mL, 48 mmol, 7.1 equiv) at 0 °C followed by heating to 60 °C for 2 h. The mixture was cooled back to 0 °C and a slurry of 2-*N*-fluorenylmethyloxycarbonyl-L-lysine (**4-15a**) or 2-*N*-fluorenylmethyloxycarbonyl-D-lysine (**4-15b**) (2.5 g, 6.79 mmol, 1.0 equiv) in CH_2Cl_2 (26.6 mL) was added. The reaction was allowed then warmed to 25 °C and stirred for 3 h. The reaction mixture was partitioned between EtOAc (75 mL) and H_2O (75 mL), and the organic layer was washed successively with H_2O (75 mL) and saturated aqueous NaCl (75 mL), dried ($MgSO_4$), filtered, and concentrated under reduced pressure. Purification by flash chromatography (linear gradient 0–7% MeOH/CH_2Cl_2 with 1% formic acid) afforded the title compound (1.61 g, 60%) as a foamy, yellow oil. ^{1}H NMR, ^{13}C NMR, and HRMS identical to reported values.[22]

4.6.8 (2*S*) and (2*R*)-Benzyl-2-({[(9H-fluoren-9-yl)methyloxy]carbonyl}amino)-6-formamidohexanoate (4-17a and 4-17b)

To a stirring slurry of 2-(*N*-fluroenylmethyloxycarbonyl)-6-*N*-formyl-L-lysine (**4-16a**) or 2-(*N*-fluroenylmethyloxycarbonyl)-6-*N*-formyl-D-lysine (**4-16b**) (1.00 g, 2.52 mmol, 1.0 equiv) in CH_2Cl_2 (25 mL) was added diisopropylethylamine (0.66 mL, 3.78 mmol, 1.5 equiv) followed by benzyl bromide (0.45 mL, 3.78 mmol, 1.5 equiv) to afford a

homogenous clear solution. The reaction was stirred for 20 h at 25 °C, then partitioned between EtOAc (100 mL) and H_2O (100 mL) and the organic layer was washed successively with saturated aqueous $NaHCO_3$ (100 mL), saturated aqueous NaCl (100 mL), dried ($MgSO_4$), and concentrated under reduced pressure. Purification by flash chromatography (linear gradient 10–100% EtOAc/hexanes) on silica gel provided the title compound (740 mg, 60%) as a yellow oil. **4-17a** $[\alpha]_D^{23} = -6.2$ (*c* 1.0, $CHCl_3$) and **4-17b** $[\alpha]_D^{23} = +7.9$ (*c* 1.0, $CHCl_3$); $R_f = 0.38$ (1:1 CH_2Cl_2/EtOAc with 1% formic acid); ^{1}H NMR (CD_2Cl_2, 600 MHz) δ 1.17–1.30 (m, 2H), 1.32–1.42 (m, 2H), 1.57–1.63 (m, 1H), 1.71–1.78 (m, 1H), 3.05–3.12 (m, 2H), 4.12 (t, *J* = 6.6 Hz, 1H), 4.22–4.32 (m, 3H), 5.03 (d, *J* = 12.6 Hz, 1H), 5.08 (d, *J* = 12.6 Hz, 1H), 7.19–7.27 (m, 7H), 7.30 (t, *J* = 7.8 Hz, 2H), 7.52 (t, *J* = 6.6 Hz, 2H), 7.67 (d, *J* = 7.2 Hz, 2H), 7.95 (s, 1H); ^{13}C NMR (CD_2Cl_2, 150 MHz) δ 22.9, 29.4, 32.4, 37.8, 47.8, 54.4, 67.3, 67.5, 120.5, 125.6, 127.6, 128.2, 128.6, 128.8, 129.1, 136.2, 141.8, 144.4, 156.5, 161.6, 172.8; HRMS (APCI+): calculated for **17a** $C_{29}H_{31}N_2O_5^+$ $[M + H]^+$ 487.2227, found 487.2228 (error 0.2 ppm).

4.6.9 (2*S*) and (2*R*)-Benzyl-2-amino-6-formamidohexanoate (4-6a and 4-6b)

To a stirring solution of (2*S*)-benzyl-2-[([(9*H*-fluoren-9-yl)methyloxy]carbonyl)amino]-6-formamidohexanoate (**4-17a**) or (2*R*)-benzyl-2-[([(9*H*-fluoren-9-yl)methyloxy]carbonyl)amino]-6-formamidohexanoate (**4-17b**) (0.600 g, 1.23 mmol, 1.0 equiv) in DMF (12 mL) was added piperidine (0.61 mL, 6.17 mmol, 5.0 equiv) and the mixture stirred for 1 h at 25 °C. The reaction was concentrated by rotary evaporation

under high vacuum to remove DMF and the crude residue was partitioned between H_2O (40 mL) and hexanes (40 mL). The hexanes layer was discarded and the aqueous layer was adjusted to pH = 10 with saturated aqueous $NaHCO_3$, extracted with 6:1 EtOAc/MeOH (3 × 40 mL), and the combined organic extracts were dried ($MgSO_4$) and concentrated under reduced pressure. Purification by flash chromatography (linear gradient 0–10% MeOH/EtOAc) over basic alumina yielded the title compound (140 mg, 50%) as a yellow oil. **4-6a** $[\alpha]_D^{23}$ = + 3.9 (*c* 1.0, CH_3OH) and **4-6b** $[\alpha]_D^{23}$ = − 1.2 (*c* 1.0, CH_3OH); R_f = 0.13 (10% MeOH/EtOAc with 1% Et_3N); ^1H NMR (CD_3OD, 600 MHz) δ 1.31–1.40 (m 2H), 1.46–1.51 (m, 2H), 1.65–1.67 (m, 1H), 1.72–1.77 (m, 1H), 3.17 (t, *J* = 7.2 Hz, 2H), 3.52 (t, *J* = 6.6 Hz, 1H), 5.15 (d, *J* = 12.6 Hz, 1H), 5.21 (d, *J* = 12.6 Hz, 1H), 7.32–7.39 (m, 5H), 8.00 (s, 1H); ^{13}C NMR (CD_3OD, 150 MHz) δ 23.8, 30.2, 35.0, 38.8, 55.1, 67.9, 129.5, 129.6, 129.7, 137.5, 163.9, 176.1; HRMS (ESI+): calculated for $C_{14}H_{21}N_2O_3$ $[M + H]^+$ 265.1547, found 265.1546 (error 0.4 ppm).

4.6.10 (2*S*, 9*S*) and (2*R*, 9*R*)-Benzyl-6-formamido-2-[(2-hydroxyphenyl)-Δ^2-1,3-oxazoline-4-carboxamido]hexanoate (4-18a and 4-18b)

To a stirring solution of (4*S*)-2-[2-hydroxyphenyl]-Δ^2-1,3-oxazoline-4-carboxylic acid (**4-5a**) (31 mg, 0.15 mmol, 1.0 equiv), and (2*S*)-benzyl-2-amino-6-formamidohexanoate (**4-6a**) or (4*R*)-2-[2-hydroxyphenyl]-Δ^2-1,3-oxazoline-4-carboxylic acid (**4-5b**) and (2*R*)-benzyl-2-amino-6-formamidohexanoate (**4-6b**) (40 mg, 0.15 mmol, 1.0 equiv) and DEPBT (49 mg, 0.16 mmol, 1.06 equiv) in THF (2.5 mL) was added Et_3N (40 μL, 0.30

mmol, 2.0 equiv) at 25 °C. After 48 h, the reaction mixture was concentrated and the residue was partitioned between EtOAc (50 mL) and H_2O (50 mL). The organic layer was washed with saturated aqueous NaCl (50 mL), dried ($MgSO_4$), filtered, and concentrated under reduced pressure to a yellow oil. Purification by flash chromatography (linear gradient 0–10% MeOH/CH_2Cl_2) afforded the title compound (16.6 mg, 24%) as an amorphous colorless solid. **4-18a** $[\alpha]_D^{23}$ = + 6.0 (*c* 1.0, CH_3OH) and **4-18b** $[\alpha]_D^{23}$ = − 6.0 (*c* 1.0, CH_3OH).; R_f = 0.65 (10% MeOH/DCM); ^{1}H NMR (CD_3OD, 600 MHz) δ 1.37–1.42 (m, 2H), 1.47–1.54 (m, 2H), 1.75–1.82 (m, 1H), 1.87–1.93 (m, 1H), 3.16 (t, *J* = 7.2 Hz, 2H), 4.48 (dd, *J* = 9.0, 4.8 Hz, 1H), 4.58 (d, *J* = 9.0 Hz, 2H), 5.00 (t, *J* = 9.0 Hz, 1H), 5.15 (d, *J* = 12.6 Hz, 2H), 5.21 (d, *J* = 12.6 Hz, 1H), 6.90 (t, *J* = 7.8 Hz, 1H), 6.95 (d, *J* = 8.4 Hz, 1H), 7.30–7.33 (m, 1H), 7.34–7.38 (m, 4H), 7.41 (td, *J* = 7.2, 1.2 Hz, 1H), 7.67 (d, *J* = 7.8, 1.2 Hz, 1H), 7.97 (s, 1H); ^{13}C NMR (CD_3OD, 150 MHz) δ 24.2, 29.9, 32.0, 38.7, 54.1, 68.2, 69.3, 70.5, 111.6, 117.8, 120.1, 129.46, 129.52, 129.6, 129.7, 135.2, 137.3, 161.1, 163.9, 168.6, 173.1, 173.3; HRMS (ESI+) calculated for $C_{24}H_{28}N_3O_6$ $[M + H]^+$ 454.1973, found 454.1994 (4.6 ppm error).

4.6.11 (2*S*, 9*R*) and (2*R*, 9*S*)-Benzyl-6-formamido-2-[(2-hydroxyphenyl)-Δ^2-1,3-oxazoline-4-carboxamido]hexanoate (4-18c and 4-18d)

Reaction conditions identical to those for **4-18a** and **4-18b**, except for the use of (4*S*)-2-[2-hydroxyphenyl]-Δ^2-1,3-oxazoline-4-carboxylic acid (**4-5a**) and (2*R*)-benzyl-2-amino-6-formamidohexanoate (**4-6b**) or (4*R*)-2-[2-hydroxyphenyl]-Δ^2-1,3-oxazoline-4-

carboxylic acid (**4-5b**) and (2*S*)-benzyl-2-amino-6-formamidohexanoate (**4-6a**). Purification by flash chromatography (linear gradient 0–10% MeOH/DCM) afforded the title compound (49.9 mg, 58%) as an amorphous colorless solid. **4-18c** $[\alpha]_D^{23}$ = – 6.7 (*c* 1.0, CH_3OH) and **4-18d** $[\alpha]_D^{23}$ = + 10.8 (*c* 1.0, MeOH); R_f = 0.61 (10% MeOH/DCM); ^{1}H NMR (CD_3OD, 600 MHz) δ 1.38–1.42 (m, 2H), 1.50–1.55 (m, 2H), 1.78–1.82 (m, 1H), 1.89–1.92 (m, 1H), 3.20 (t, *J* = 7.2 Hz, 2H), 4.85 (dd, *J* = 9.0, 5.4 Hz, 1H), 4.56–4.64 (m, 2H), 5.01 (dd, *J* = 10.6, 7.8 Hz, 1H), 5.09 (d, *J* = 12 Hz, H), 5.17 (d, *J* = 12 Hz, H), 6.91 (t, *J* = 7.2 Hz, 1H), 6.98 (d, *J* = 9.0 Hz, 1H), 7.27–7.32 (m, 5H), 7.42 (t, *J* = 7.2 Hz, 1H), 7.69 (d, *J* = 7.8 Hz, 1H), 8.01 (s, 1H); ^{13}C NMR (CD_3OD, 150 MHz) δ 24.2, 29.9, 32.0, 38.7, 54.1, 68.1, 69.3, 70.5, 111.7, 117.8, 120.1, 129.3, 129.4, 129.6, 129.7, 133.6, 135.1, 137.2, 161.0, 163.9, 168.6, 173.1, 173.2; HRMS (ESI+) calculated for $C_{24}H_{28}N_3O_6$ $[M + H]^+$ 454.1973, found 454.2004 (error 6.8 ppm).

4.6.12 (2*S*, 9*S*) and (2*R*, 9*R*)-6-Formamido-2-[(2-hydroxyphenyl)-Δ^2-1,3-oxazoline-4-carboxamido]hexanoic acid (4-4a and 4-4b)

Solid Pd/C (10% by weight, 1.7 mg) was added to a solution of (2*S*, 9*S*)-benzyl-6-formamido-2-([2-hydroxyphenyl]-Δ^2-1,3-oxazoline-4-carboxamido)hexanoate **4-18a** or (2*R*, 9*R*)-benzyl-6-formamido-2-([2-hydroxyphenyl]-Δ^2-1,3-oxazoline-4-carboxamido)hexanoate **4-18b** (16.6 mg, 0.037 mmol) in MeOH (10 mL) under Ar. The reaction vessel was evacuated then back-filled with hydrogen gas to 3 atm and the mixture was shaken at 25 °C for 2 h. The reaction vessel was opened and the reaction

mixture was filtered through Celite and the filtrate concentrated under reduced pressure. Purification by flash chromatography (linear gradient 0–10% EtOH/DCM plus 1% formic acid) afforded the title compound (13 mg, 100%) as an amorphous colorless solid. **4-4a** $[\alpha]_D^{23}$ = + 29.2 (*c* 0.1, MeOH), and **4-4b** $[\alpha]_D^{23}$ = − 31.6 (*c* 0.1, MeOH); R_f = 0.59 (10% MeOH/CH_2Cl_2 with 1% formic acid); ^{1}H NMR (DMSO-d_6, 600 MHz) δ 1.26–1.35 (m, 2H), 1.35–1.44 (m, 2H), 1.64–1.67 (m, 1H), 1.75–1.79 (m, 1H), 3.00–3.10 (m, 2H), 4.16–4.20 (m, 1H), 4.48 (t, *J* = 7.8 Hz, 1H), 4.60 (t, *J* = 7.8, 1H), 4.98 (t, *J* = 7.8 Hz, 1H), 6.89 (t, *J* = 7.8 Hz, 1H), 6.95 (d, *J* = 8.4 Hz, 1H), 7.41 (t, *J* = 8.4 Hz, 1H), 7.59 (d, *J* = 7.8 Hz, 1H), 7.83–7.90 (ovlp m, 1H), 7.91 (ovlp s, 1H), 8.50 (d, *J* = 6.6 Hz, 1H), 11.80 (br s, 1H); ^{13}C NMR (DMSO-d_6, 150 MHz) δ 22.8, 28.5, 30.4, 36.8, 52.1, 67.1, 69.2, 109.8, 116.6, 119.1, 128.0, 134.0, 159.1, 160.9, 165.8, 169.7, 173.3; HRMS (ESI−) calculated for $C_{17}H_{20}N_3O_6$ $[M - H]^-$ 362.1358, found 362.1331 (7.5 ppm error).

4.6.13 (2*S*, 9*R*) and (2*R*, 9*S*)-6-Formamido-2-[(2-hydroxyphenyl)-Δ^2-1,3-oxazoline-4-carboxamido]hexanoic acid (4-4c and 4-4d)

Reaction conditions identical as those for **4-4a** and **4-4b**, except for the use of (2*S*, 9*R*)-benzyl-6-formamido-2-([2-hydroxyphenyl]-Δ^2-1,3-oxazoline-4-carboxamido)hexanoate **4-18c** or (2*R*, 9*S*)-benzyl-6-formamido-2-([2-hydroxyphenyl]-Δ^2-1,3-oxazoline-4-carboxamido)hexanoate **4-18d** (15.5 mg, 0.03 mmol). Purification by flash chromatography (linear gradient 0–10% EtOH/CH_2Cl_2 with 1% formic acid) afforded the title compound (5.8 mg, 53%) as an amorphous solid. **4-4c** $[\alpha]_D^{23}$ = − 2.0 (*c* 0.1, MeOH)

and **4-4d** $[\alpha]_D^{23}$ = + 6.0 (*c* = 0.1, MeOH); R_f = 0.59 (10% MeOH/CH_2Cl_2 with 1% formic acid); ^{1}H NMR (DMSO-d_6, 600 MHz) δ 1.31–1.34 (m, 2H), 1.37–1.41 (m, 2H), 1.64–1.68 (m, 1H), 1.74–1.78 (m, 1H), 3.05 (t, *J* = 6.0 Hz, 2H), 4.15–4.21 (m, 1H), 4.50 (t, *J* = 7.8, 1H), 4.63 (t, *J* = 8.4 Hz, 1H), 5.01 (t, *J* = 8.4 Hz, 1H), 6.95 (t, *J* = 7.8 Hz, 1H), 7.00 (d, *J* = 8.4 Hz, 1H), 7.46 (t, *J* = 7.2 Hz, 1H), 7.64 (d, *J* = 7.8 Hz, 1H), 7.85 (olvp m, 1H), 7.98 (olvp s, 1H), 8.51 (d, *J* = 7.2 Hz, 1H), 11.81 (br s, 1H); ^{13}C NMR (DMSO-d_6, 150 MHz) δ 23.0, 28.9, 31.0, 37.2, 53.0, 67.5, 69.6, 110.2, 116.8, 119.2, 128.3, 134.2, 159.4, 161.3, 166.3, 169.9, 173.8; HRMS (ESI–) calculated for $C_{17}H_{20}N_3O_6$ $[M - H]^-$ 362.1358, found 362.1360 (0.55 ppm error).

4.7 References

1. Schatz, A.; Bugie, E.; Waksman, S. Streptomycin, a substance exhibiting antibiotic activity against Gram-positive and Gram-negative bacteria. *Proc. Soc. Exp. Biol. Med.* **1944**, *55*, 66–69.

2. Aldrich, C. C.; Boshoff, H. I.; Remmel, R. P. Antitubercular Agents. In *Burger's Medicinal Chemistry, Drug Discovery and Development, 7th Edition*, Abraham, D. J.; Rotella, D. P., Eds. John Wiley and Sons, Inc.: **2010**; pp 713–813.

3. Umezawa, H.; Ueda, M.; Maeda, K.; Yagishita, K.; Kondo, S.; Okami, Y.; Utahara, R.; Osato, Y.; Nitta, K.; Takeuchi, T. Production and isolation of a new antibiotic: Kanamycin. *J. Antibiot.* **1957**, *10*, 181–188.

4. Kawaguchi, H. Discovery, chemistry, and activity of amikacin. *J. Infect. Dis.* **1976**, *134(Suppl)*, S242–S248.

5. Rifampin. *Tuberculosis (Edinb)* **2008**, *88*, 151–154.

6. Mukai, A.; Fukai, T.; Matsumoto, Y.; Ishikawa, J.; Hoshino, Y.; Yazawa, K.; Harada, K.-i.; Mikami, Y., Transvalencin Z, a new antimicrobial compound with salicylic acid residue from *Nocardia transvalensis* IFM 10065. *J. Antibiot.* **2006**,

59, 366–369.

7. Miethke, M.; Marahiel, M. A. Siderophore-based iron acquisition and pathogen control. *Microbiol. Mol. Biol. Rev.* **2007**, *71*, 413–51.

8. Snow, G. A. Mycobactins: Iron-chelating growth factors from mycobacteria. *Bacteriol. Rev.* **1970**, *34*, 99–125.

9. Posey, J. E.; Gherardini, F. C. Lack of a role in the lyme disease pathogen. *Science* **2000**, *288*, 1651–1653.

10. Ratledge, C.; Dover, L. G. Iron metabolism in pathogenic bacteria. *Annu. Rev. Microbiol.* **2000**, *54*, 881–941.

11. Chavadi, S. S.; Stirrett, K. L.; Edupuganti, U. R.; Vergnolle, O.; Sadhanandan, G.; Marchiano, E.; Martin, C.; Qiu, W-G.; Soll, C. E.; Quadri, L. E. N. Mutational and phylogenetic analyses of the mycobacterial *mbt* gene cluster. *J. Bacteriol.* **2011***, 193*, 5905–5913.

12. Vergne, A. F.; Walz, A. J.; Miller, M. J. Iron chelators from mycobacteria (1954–1999) and potential therapeutic applications. *Nat. Prod. Rep.* **2000**, *17*, 99–116.

13. Hu, J.; Miller, M. J. Total Synthesis of a mycobactin S, a siderophore and growth promoter of *Mycobacterium smegmatis*, and determination of its growth inhibitory activity against *Mycobacterium tuberculosis*. *J. Am. Chem. Soc.* **1997**, *119*, 3462–3468.

14. Xu, Y.; Miller, M. J. Total syntheses of mycobactin analogues as potent antimycobacterial agents using a minimal protecting group strategy. *J. Org. Chem.* **1998**, *63*, 4314–4322.

15. Ferreras J. A.; Ryu J. S.; Di Lello F.; Tan D. S.; Quadri L. E. Small-molecule inhibition of siderophore biosynthesis in *Mycobacterium tuberculosis* and *Yersinia pestis*. *Nat. Chem. Biol.* **2005**, *1*, 26–32.

16. Stirrett, K. L.; Ferreras, J. A.; Jayaprakash, V.; Sinha, B. N.; Ren, T.; Quadri, L. E. N. Small molecules with structural similarities to siderophores as novel antimicrobials against *Mycobacterium tuberculosis* and *Yersinia pestis*. *Bioorg. Med. Chem. Lett.* **2008**, *18*, 2662–2668.

17. Tse, B.; Kishi, Y. Conformationally rigid tricyclic tripods: Synthesis and application to preparation of enterobactin analogs. *J. Org. Chem.* **1994**, *59*, 7807–7814.

18. Sakakura, A.; Kondo, R.; Umemura, S.; Ishihara, K. Dehydrative cyclization of serine, threonine, and cysteine residues catalyzed by molybdenum(VI) oxo compounds. *Tetrahedron* **2009**, *65*, 2102–2109.

19. Sattely, E. S.; Walsh, C. T. A latent oxazoline electrophile for N-O-C bond formation in pseudomonine biosynthesis. *J. Am. Chem. Soc.* **2008**, *130*, 12282–12284.

20. Wuest, W. M.; Sattely, E. S.; Walsh, C. T. Three siderophores from one bacterial enzymatic assembly line. *J. Am. Chem. Soc.* **2009**, *131*, 5056–5057.

21. Yamamoto, S.; Okujo, N.; Sakakibara, Y. Isolation and structure elucidation of acinetobactin, a novel siderophore from *Acinetobacter baumannii*. *Arch. Microbiol.* **1994**, *162*, 249–254.

22. Hughes, R. M.; Waters, M. L. Effects of lysine acetylation in a β-hairpin peptide: Comparison of an amide-π and a cation-π interaction. *J. Am. Chem. Soc.* **2006**, *128*, 13586–13591.

23. The reported conditions require overnight heating and a large excess (14 equivalents) of formic acid, however transformation was achieved in 3 hours at room temperature using only 7 equivalents of formic acid.

24. Wuts, P. G. M.; Greene, T. W. *Greene's Protecting Groups in Organic Synthesis*. 4th ed.; John Wiley & Sons, Inc.: Hoboken, NJ, 2007.

25. Li, H.; Jiang, X.; Ye, Y.-h.; Fan, C.; Romoff, T.; Goodman, M. 3-(Diethoxyphosphoryloxy)-1,2,3-benzotriazin-4(3*H*)-one (DEPBT): A new coupling reagent with remarkable resistance to racemization. *Org. Lett.* **1999**, *1*, 91–93

.

26. Field, L. D.; Sternhell, S.; Kalman, J. R. *Organic Structures From Spectra*. 4th Edition ed.; John Wiley & Sons Ltd: West Sussex, England, 2008.

27. Schneider, K.; Rose, I.; Vikineswary, S.; Jones, A. L.; Goodfellow, M.; Nicholson, G.; Beil, W.; Süssmuch, R. D.; Fiedler, H.-P. Nocardichelins A and B, siderophores from *Nocardia* strain acta 3026. *J. Nat. Prod.* **2007**, *70*, 932–935.

28. Young, D. C.; Kasmar, A.; Moraski, G.; Cheng, T. Y.; Walz, A. J.; Hu, J.; Xu, Y.; Endres, G. W.; Uzieblo, A.; Zajonc, D.; Costello, C. E.; Miller, M. J.; Moody, D. B. Synthesis of dideoxymycobactin antigens presented by CD1a reveals T cell fine specificity for natural lipopeptide structures. *J. Biol. Chem.* **2009**, *284*, 25087–25096.

29. Mitchell, J. M.; Shaw, J. T. Synthesis and stereochemical assignment of

brasilibactin A. *Org. Lett.* **2007**, *9*, 1679–1681.

30. Fennell, K. A.; Möllmann, U.; Miller, M. J. Syntheses and biological activity of amamistatin B and analogs. *J. Org. Chem.* **2008**, *73*, 1018–1024.

31. Hoshino, Y.; Mukai, A.; Yazawa, K.; Uno, J.; Ando, A.; Mikami, Y.; Fukai, T.; Ishikawa, J.; Yamaguchi, K. Transvalencin A, a thiazolidine zinc complex antibiotic produced by a clinical isolate of *Nocardia transvalensis* II. Structure elucidation. *J. Antibiot.* **2004**, *57*, 803–807.

32. Williams, K. J.; Boshoff, H. I.; Krishnan, N.; Gonzales, J.; Schnappinger, D.; Robertson, B. D. The *Mycobacterium tuberculosis* β-oxidation genes echA5 and fadB3 are dispensable for growth in vitro and in vivo. *Tuberculosis (Edinb)* **2011**, *91*, 549–555.

33. Mosmann, T. Rapid colorimetric assay for cellular growth and survival: Application to proliferation and cytotoxicity assays. *J. Immunol. Methods* **1983**, *65*, 55–63.

34. Denizot, F.; Lang, R. Rapid colorimetric assay for cell growth and survival: Modifications to the tetrazolium dye procedure giving improved sensitivity and reliability. *J. Immunol. Methods* **1986**, *89*, 271–277.

Chapter 5. Biotinylated Probes for the Study of Adenylation Domains in *Bacillus subtilis*

The following chapter details an assay that was originally designed by Dr. Jun Yin of the University of Chicago. The probe molecules (**5-1**, **5-2**, and **5-3**) were designed by Dr. Yin with help from Dr. Courtney C. Aldrich. Probe **5-1** was synthesized by Dr. Kimberly D. Grimes and Kathryn M. Nelson, with the material from Dr. Grimes being used for Dr. Yin's assay. Probes **5-2** and **5-3** were both synthesized by KMN. The yeast cell display assay was performed in Dr. Yin's assay. This work was published in *Chemistry and Biology*, and some figures and excerpts are reproduced with permission from that journal (see preface above).

5.1 Introduction

As discussed previously, chemical probes are becoming more common in the study of proteins and their function. In Chapter 3, we used a chemical probe to study the specificity of an inhibitor for an enzyme. In this chapter, the synthesis of a biotinylated probe to study the specificity of an enzyme for different substrates was developed.

5.1.1 Nonribosomal peptide synthetases (NRPS)

Nonribosomal peptide synthetases (NRPSs) are large multifunctional enzymes in bacteria that synthesize peptide natural products known as nonribosomal peptides (NRPs), which are diverse in structure and often possess important medicinal activities.[1,2] NRPSs do not use the mRNA-templated ribosomal machinery, and so are not restricted to the 20 proteinogenic amino acids. Their products often contain D-amino acids and unnatural α-amino acids, as well as *N*-methylation and cyclization of the peptide backbone, which enhances proteolytic stability. NRPSs utilize a modular architecture where each module is responsible for the incorporation of one amino acid substrate into the final molecule.[3,4] Each module contains three core domains: a condensation (C) domain, an adenylation (A) domain, and a peptidyl carrier protein (PCP) domain (**Figure 5.1**). The adenylation domain is responsible for the selection, activation, and loading of its substrate onto the downstream PCP domain where it is covalently attached via a thioester linkage. The thiol of the PCP domain is not from cysteine, but rather from the terminal thiol of an approximately 20 Å-long phosphopantetheine (Ppant) cofactor moiety that modifies a conserved serine residue of the PCP domain. The Ppant arm then delivers the amino acid substrate to the C domain that catalyzes peptide bond coupling between substrate molecules loaded on neighboring modules. This leads to the elongation of the peptide chain in the N to C direction. Once it reaches the final module, the full-length peptide chain is released by a thioesterase domain, followed by macrocyclization or hydrolysis to afford the final product.

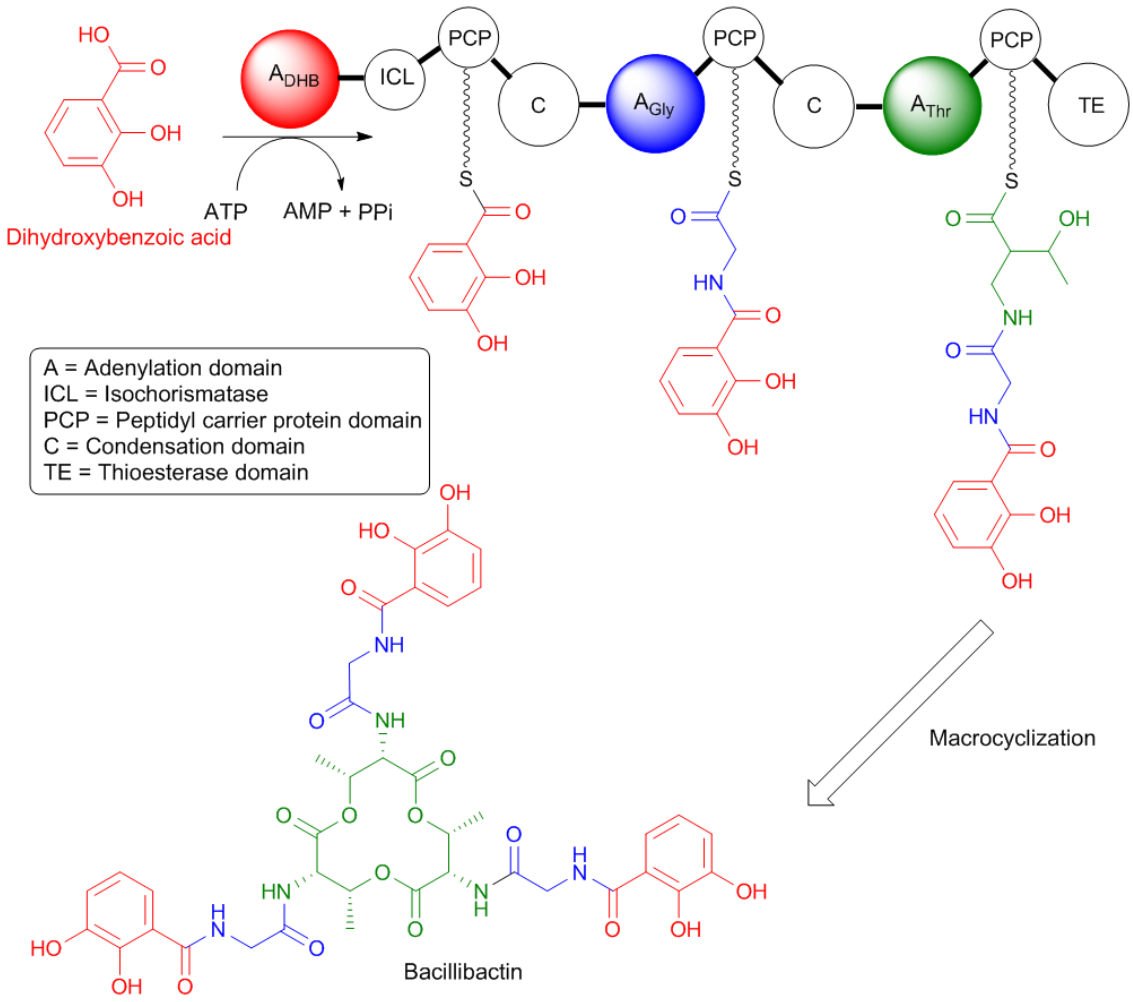

Figure 5.1. The NRPS pathway for the synthesis of bacillibactin in *Bacillus subtilis*. The adenylation (A) domains load the cognate substrates onto the peptidyl carrier protein domains (PCP). The condensation (C) domains catalyze peptide bond formation, elongating the growing peptide chain. Final release of the product is achieved through macrocyclization of a thioesterase (TE) domain. Figure adapted from May, et al.[5]

5.1.2 Adenylation domains

Adenylation domains, as the selectivity unit for chain elongation, usually activate an appropriate amino acid, but are also known to activate aryl acids as found in siderophorea, fatty acids for lipopeptides, or hydroxy acids for peptide ester containing

non-ribosomal peptides.[4,6] These domains are 55–60 kDa and contain a large N-terminal subdomain and a small C-terminal subdomain with the active site located at the domain interface. These proteins are conformationally dynamic and exist in an open apo conformation as well as two different closed holo conformations. The specificity of an adenylation domain is imparted by a substrate binding pocket lined by approximately 10 important residues (a "nonribosomal code") that comprise interactions that can enable *in silico* prediction of substrate specificity.[7–9] The adenylation-thioesterification reaction catalyzed by adenylation domains is a two-step process; in the first step, the substrate acid and ATP bind to afford a ternary complex, then their condensation affords an acyl-adenylate intermediate.[10] Following release of pyrophosphate, the C terminus of the adenylation domain undergoes a 140° rigid body rotation to allow insertion of the Ppant cofactor arm from the downstream PCP domain into the active site.[6] Acylation of the Ppant moiety, followed by release of the thioacylated PCP and AMP, completes the catalytic cycle.

5.1.3 Analogues of natural products through native synthetases

A number of strategies have been employed to attempt to modify the specificity of adenylation domains in order to incorporate nonnative building blocks into natural products. Utilizing biological machinery to produce such analogues would relieve the heavy burden felt by organic chemists when attempting SAR studies on natural product scaffolds. Some of the first attempts at utilizing NRPS scaffolds for analogue

development involved domain swapping from various assembly lines to stitch together the desired segments. This approach suffers from suboptimal interactions between these different domains, resulting in low catalytic turnover and even premature truncation of the peptide chain in some cases.[11, 12] Walsh and co-workers developed a method of directed evolution to improve these chimeric assembly lines, achieving a 10-fold improvement in catalytic activity.[11] Additional methods include the reengineering of adenylation domain specificity while preserving the native domain sequence. The nonribosomal code mentioned above has also been studied through computational mutation and modeling to predict mutants with altered substrate specificity.[13,14]

5.1.4 DhbE as a model system

This study aims to be another step in the development of methods to reengineer the specificity of adenylation domains in an effort to more easily access analogues of natural products. The model system chosen for this study was DhbE from the NRPS for bacillibactin biosynthesis in *Bacillus subtilis* (see **Figure 5.1** above). This system is ideal for an initial study due to the readily available 2.15 Å X-ray co-crystal structure with the acyl-adenylate,[5] the availability of known inhibitors,[15] and the detailed report of the kinetic mechanism for this enzyme.[10] DhbE is also active when expressed alone, and does not require the expression of a large multidomain NRPS to study its catalytic activity. Therefore, this study was designed to reengineer the binding affinity of the enzyme, but also study the catalytic turnover of loading of the nonnative substrate onto the carrier

protein through addition of stoichiometric amounts of DhbE's carrier protein DhbB.

5.2 Research Objectives

We developed a biotinylated probe that was then used by our colleague Dr. Jun Yin at the University of Chicago to re-engineer the specificity of the adenylating enzyme DhbE from the bacillibactin biosynthetic pathway in *Bacillus subtilis*, for which crystal structures and kinetic data were already reported.[5, 10] The probe was designed to mimic the acyl-adenylate intermediate in DhbE, with a long, flexible linker attached to biotin for enrichment with streptavidin. The long linker was necessary to keep the biotin far enough away from the enzyme binding domain so as not to interfere with activity. Dr. Yin and co-workers developed a yeast cell surface display assay to express fluorescently-labeled DhbE so that fluorescent-activated cell sorting (FACS) could be used to identify the correctly displayed enzyme. Mutant libraries of DhbE enzyme were incubated with our chemical probes, and biotin-streptavidin enrichment selected for binders of the non-natural probe substrates. By iteratively enriching, they were able to select for mutant DhbE enzymes that could be expressed, purified, and were shown to have dramatically shifted selectivity for non-natural substrates.

5.3 Results

5.3.1 Synthesis of chemical probes for the study of DhbE

The design of the chemical probes for the re-engineering of DhbE specificity grew from mimicking the acyl adenylate intermediate that would interact with both the acid and ATP substrate binding pockets to improve the affinity of the probe for the enzyme. The labile acyl phosphate was replaced with the isosteric sulfamate, and previous structure-activity relationship studies indicated that we could modify the C-2 position of the adenine base without severely compromising binding affinity.[16] Based on these principles, we targeted the salicyl-AMS probe **1** with a biotin attached at the C-2 position of the base with a long, flexible linker for reporting DhbE binding (**Figure 5.2**). Although the native substrate for DhbE is dihydroxybenzoic acid (DHB), we developed the probe with salicylic acid (**5-1**) due to the oxidative instability of the catechol of DHB. Two additional probes were developed that included a 3-hydroxybenzoic acid (3-HBA, **5-2**) and a 2-aminobenzoic acid (2-ABA, **5-3**) at the salicyl position to select for enzymes that preferentially recognize those substrates.

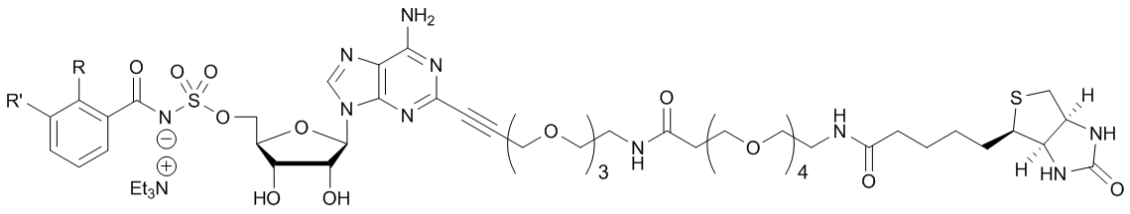

5-1, R = OH, R' = H
5-2, R = H, R' = OH
5-3, R = NH_2, R' = H

Figure 5.2. Chemical probes **5-1–3** targeted for the re-engineering of DhbE selectivity.

The synthesis of probe **5-1** began from commercially available 2-iodoadenosine (**5-4**, **Scheme 5.1**). Sonogashira coupling with alkyne linker **5-5** gave **5-6** in excellent yield. Protection of the 2'- and 3'-hydroxyls with 2,2'-dimethoxypropane, followed by sulfamoylation of the 5'-hydroxyl provided sulfamate **5-7** in moderate yield. Coupling of the sulfamate with *N*-hydroxysuccinimidyl-2-(methoxymethyloxy)benzoate **5-8** generated the fully protected intermediate **5-9**. Global deprotection with 80% aqueous trifluoroacetic acid (TFA), followed directly by cesium carbonate mediated coupling with the commercially available succinimide **5-10** yielded the crude final probe. The final material was purified by reverse-phase HPLC to afford the final probe **5-1**.

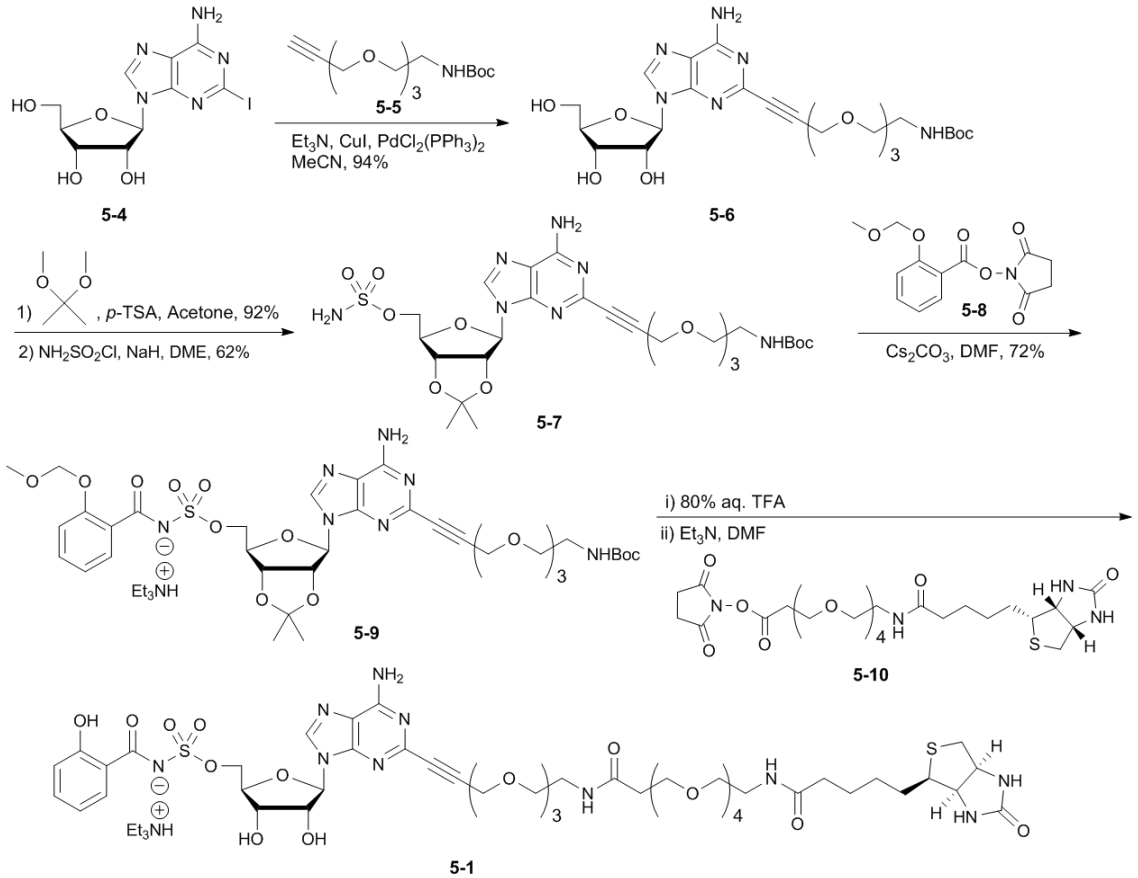

Scheme 5.1. Synthesis of DhbE probe **5-1**.

Probes **5-2** and **5-3** were synthesized in a similar way. We first prepared *N*-hydroxysuccinimidyl-3-(methoxymethyloxy)benzoate **5-12** in good yield from methyl-3-(methoxymethyloxy)benzoate **5-11** in two steps (**Scheme 5.2**). Hydrolysis of the methyl ester was achieved using sodium hydroxide and water. The crude intermediate was directly coupled to *N*-hydroxysuccinimide using standard DCC coupling conditions.

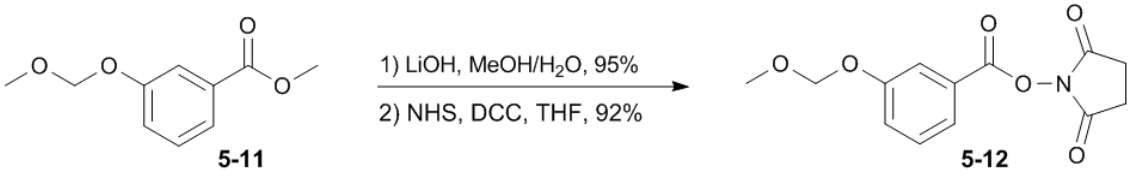

Scheme 5.2. Synthesis of *N*-hydroxysuccinimidyl-3-(methoxymethyloxy)benzoate for the synthesis of probe **5-2**

Cesium carbonate-mediated coupling of succinimide **5-12** to the sulfamate **5-7** yielded the penultimate intermediate **5-13**. Deprotection followed by coupling with **5-10** gave the final probe compound that was purified by reverse-phase HPLC to give 3-HBA probe **5-2** as the triethylammonium salt (**Scheme 5.3**).

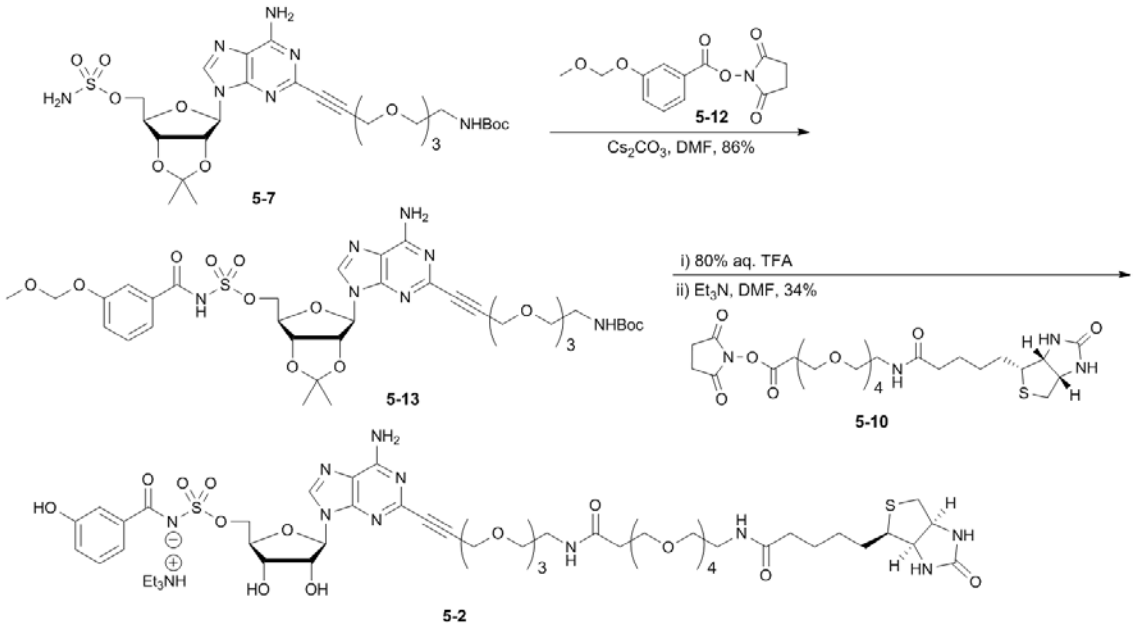

Scheme 5.3. Synthesis of 3-hydroxybenzoic acid (3-HBA) probe **5-2**.

The final probe molecule, 2-ABA **5-3**, is also accessible from intermediate **5-7** (**Scheme 5.4**). Isatoic anhydride **5-14** was coupled to the sulfamate with catalytic cesium carbonate to give amino intermediate **5-15**. Acid-mediated deprotection followed again with coupling to **5-10** generated the final probe molecule which was purified by reverse-phase HPLC, resulting in 2-ABA probe **5-3** as the triethylammonium salt.

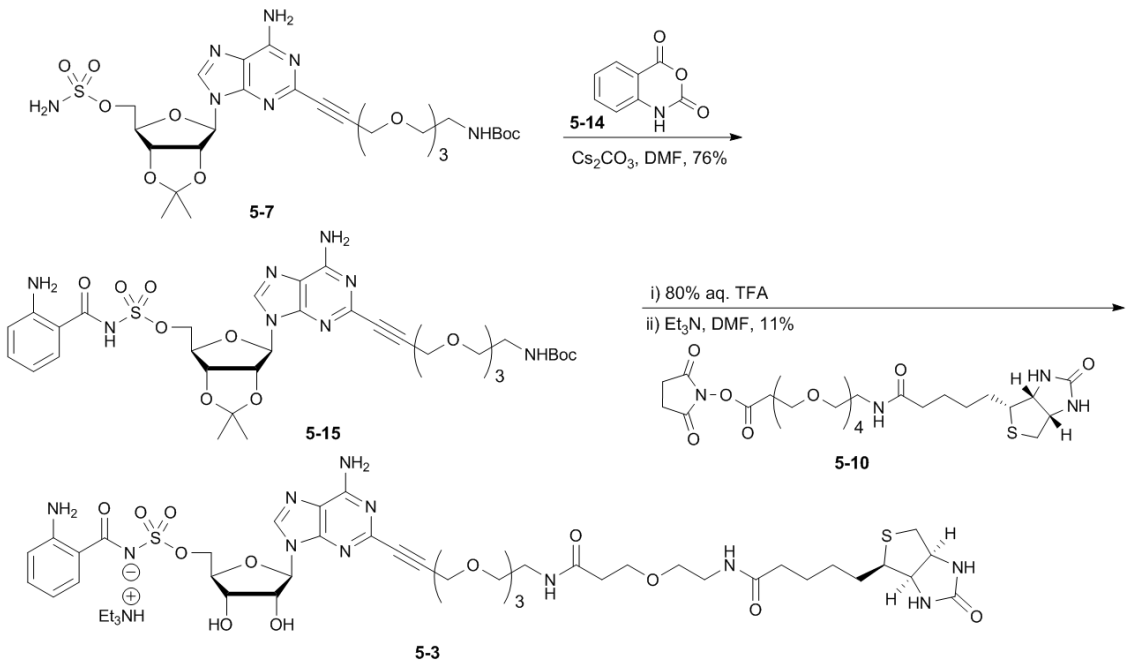

Scheme 5.4. Synthesis of 2-aminobenzoic acid (2-ABA) probe **5-3**.

5.3.2 Construction of an adenylation domain library of DhbE displayed on yeast cells

While our group was synthesizing probes **5-1**–**3**, Dr. Jun Yin of the University of Chicago was developing a unique yeast cell surface display assay that could be used to express bacterial proteins (**Figure 5.3**). While yeast cell surface display has been extensively exploited in the engineering of antibody specificity, its application to bacterial proteins is recent.[17,18] Briefly, the yeast vector pCTCON2 expresses a library of mutants of the protein of interest as a fusion to the yeast agglutinin protein Aga2p attached through disulfide bonds to Aga1p protein as part of the yeast cell wall. The yeast cell library is incubated with a fluorescently labeled antigen to allow the binding of antigen molecules to the protein displayed on the yeast surface. FACS is then used to

isolate yeast cells displaying protein mutants with high affinities with the antigen. For this application, Dr. Yin's lab cloned DhbE into the pCTCON2 vector to display the dual-tagged DhbE enzyme on the yeast cell surface. This fusion was engineered with a hemagglutinin (HA) tag and a Myc tag at the N and C termini, respectively, of DhbE to enable the detection of properly displayed protein on the cell surface. Upon binding of a biotinylated probe, the mutant enzyme will be bound to streptavidin-linked phycoerithrin (PE) beads.

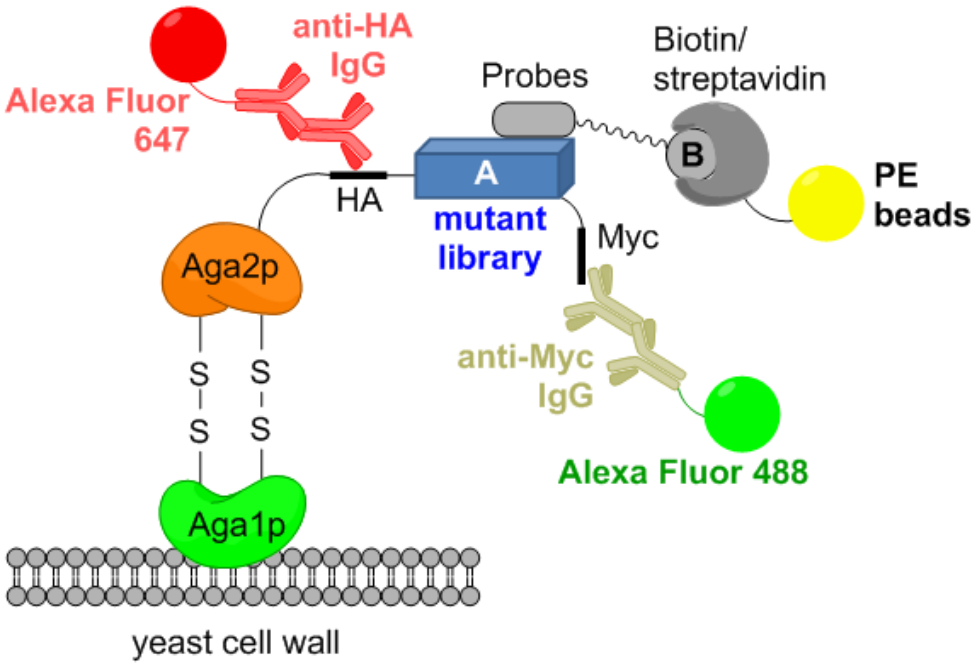

Figure 5.4. Yeast cell display. The mutant DhbE enzymes are expressed on the yeast surface as fusions through Aga2p connected through disulfide bonds to Aga1p on the cell surface. The mutants have a hemagglutinin (HA) tag on the N terminus and a Myc tag on the C terminus. These tags are detected by incubation first with mouse anti-HA and chicken anti-Myc antibodies, followed by incubation with goat anti-mouse antibody conjugated with Alexa Fluor 647 and goat anti-chicken antibody conjugated with Alexa Fluor 488. These fluorophores allow the confirmation of full length adenylation domain expression. The mutant libraries are then incubated with probe compounds **5-1**, **5-2**, or **5-3**. After binding, the biotin moiety is captured by streptavidin that is tethered to phycoeyrithrin (PE) beads for detection by flow cytometry. Reproduced with permission from Zhang, et. al.[19]

Studying the published co-crystal structure of DhbE complexed with DHB, Dr. Yin and co-workers were able to select residues for mutation that they hypothesized would be important for substrate recognition (His234, Asn235, Ala333, and Val337).[5] **Figure 5.5** shows the residues in the DhbE active site, highlighting those chosen for randomization. This randomization allowed Dr. Yin to construct an adenylation domain library with a size of 5×10^6, large enough to cover all the possible mutants in a library with four randomized residues (1.6×10^5).

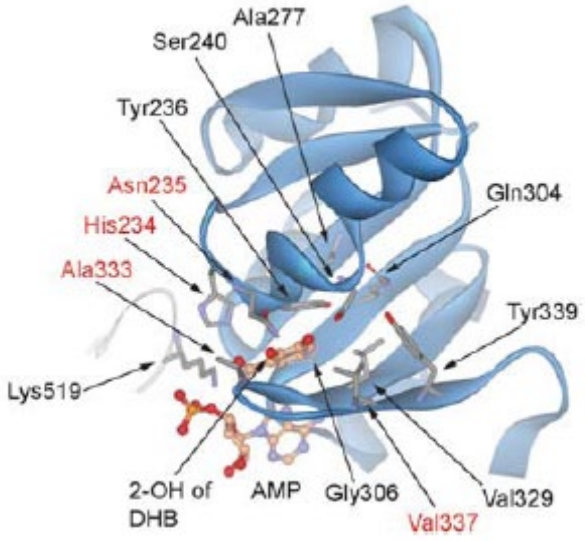

Figure 5.5. Co-crystal structure of wtDhbE and DHB-AMP. Residues important for binding are highlighted (nonribosomal code for DhbE). Randomized residues: Asn235, His234, Ala333, and Val337. (PDB 1MD8)[5] Reprinted with permission from Zhang, et. al.[19]

5.3.3 Identification of DhbE mutants with altered specificity for 3-HBA and 2-ABA

Dr. Yin and co-workers performed the yeast cell selection assay according to the protocol of Wittrup and Miller, with some modifications (for details see ref. 19).[17,18] After 5

rounds of selection, 30 mutants with specificity for 3-HBA and 2 mutants with specificity for 2-ABA were cloned and expressed (**Table 5.1**). All of the mutants had a His234Trp mutation. Specificity for 3-HBA favored an Asn235Ala mutation (also Asn235Ser > Asn235 or Asn235Gln), and an Ala333 mutation to Ser or Thr. Specificity for 2-ABA converged on a Val337 mutation to Lys or Arg, but also showed a preference for Ala333 to be replaced by Thr.

Table 5.1. Alignment of DhbE mutants selected with probes **5-2** and **5-3** by yeast cell surface display.

	Number of times selected	**Residue number**			
		234	**235**	**333**	**337**
wtDhbE		H	N	A	V
Clones selected by **5-2**					
KZ1	6	W	S	A	V
KZ2	14	W	A	A	V
KZ3	4	W	N	S	V
KZ4	2	W	Q	T	V
KZ5	2	W	Q	S	V
KZ6	1	W	T	A	V
KZ7	1	W	C	A	V
KZ8	1	W	V	A	V
Clones selected by **5-3**					
KZ11	10	W	D	T	R
KZ12	9	W	D	T	K

The Yin lab then expressed the most abundant mutants selected and tested their catalytic activities. Detailed kinetic analysis of these mutants was performed in the Yin lab, and are reported in our publication, but will not be discussed here.[19] A summary of the results are shown below in **Table 5.2**.

Table 5.2. Pyrophosphate (PPi) release rate of the aryl acid adenylation reaction catalyzed by wtDhbE and mutants.

Enzyme and substrate	K_m (μM)	k_{cat} (min^{-1})	k_{cat}/K_m ($min^{-1}mM^{-1}$)	Ratio of k_{cat}/K_m with same substrate (Mutant/wtDhbE)
wtDhbE				
DHB	4.3 ± 0.4	4.61± 0.09	1,100	
Salicylic acid	14 ± 2.2	1.90 ± 0.07	140	
3-HBA	25 ± 7.7	0.56 ± 0.02	22	
2-ABA	62 ± 17	0.34 ± 0.03	5.5	
KZ4(Trp234His)				
DHB	3.5 ± 0.8	1.45 ± 0.08	410	0.37
Salicylic acid	46 ± 4.8	0.84 ± 0.01	18	0.13
3-HBA	4.8 ± 0.7	1.14 ± 0.02	240	11
KZ12(Trp234His)				
DHB	38 ± 12	1.25 ± 0.14	33	0.03
Salicylic acid	56 ± 14	0.37 ± 0.03	6.6	0.047
2-ABA	3.5 ± 0.3	0.12 ± 0.01	34	6.2

5.4 Discussion

The increases seen in the specificity of the mutant enzymes for 3-HBA and 2-ABA are likely based on increased affinity for these substrates, as the measure k_{cat} of KZ12(Trp234His) for 2-ABA was 0.12 min^{-1}, which is similar to the k_{cat} measured for 2-ABA with wtDhbE (0.34 min^{-1}). Similarly, the k_{cat} for KZ4(Trp234His) for 3-HBA was 1.14 min^{-1}, which is only 2-fold higher than the wtDhbE with 3-HBA (0.56 min^{-1}). This illustrates a limitation to this technique for re-engineering the substrate specificity of the adenylation domain: while mutants are selected based on improved binding interactions with substrate probes, this type of selection may not improve the k_{cat} of the engineered enzyme with the nonnative substrate. These results agree with previous work on

engineering catalytic antibodies that showed tighter binding with the transition state analogue by the antibody does not lead to a higher turnover rate (k_{cat}) of the catalytic reactions.[20]

The most specific mutant for 3-HBA, KZ4, appeared to have a key Asn235Gln mutation. The Gln side chain is one CH_2 group longer than the Asn side chain in wtDhbE. This may extend the sidechain further into the substrate binding pocket to fill the space that used to be occupied by the 2-OH substituent of DHB. The amide NH_2 of the Gln residue may also form hydrogen bonds with the 3-hydroxyl group in 3-HBA.

Only 2 mutants were converged upon for 2-ABA specificity: KZ11 and KZ12. The only difference between these mutants was a Lys or Arg replacing Val337. The Lys and Arg residues at this position may interact with the 2-NH_2 group of 2-ABA. Ala333 was not assigned as a nonribosomal code residue for A-domain binding with the aryl acid substrates,[21] however a preference was shown after yeast selection for an Ala333 to Ser or Thr residues. Both mutations position hydroxyl side chains favorably for hydrogen bond interactions with the 2-ABA substrate.

Some of these mutations may have been predicted from the crystal structure. Some groups are currently using computer-aided docking programs to design mutant proteins with altered substrate specificity.[13,22] While this *in silico* technique can potentially save time on protein expression, purification, and testing, it cannot take into account differences in protein folding or active site arrangement that may occur upon residue replacement. This random mutation approach devised by Dr. Yin and co-workers allows for large groups of mutants to be screened in their native folded state. The enrichment

steps allow for the "purification" of proteins that bind the nonnative substrates with specificity, eliminating time that could be wasted on expression and purification of mutants that may prove to be ineffective binders. Care should be taken to carefully examine mutant proteins identified by the techniques detailed here,[19] however, as this study illustrates the possibility that altering the binding of the enzyme may also impact its catalytic efficiency. Scrutiny of the binding, catalytic efficiency, and overall incorporation of the nonnative substrate into the final natural product pathway must be verified for this approach to be a complete success.

5.5 Conclusions

In this study, we were able to synthesize three biotinylated probes that were used by our colleague Dr. Jun Yin at the University of Chicago to re-engineer the specificity of the adenylating enzyme DhbE from the bacillibactin biosynthetic pathway in *Bacillus subtilis*. These probes were designed with a long, flexible linker attached to biotin for enrichment with streptavidin. The long linker was necessary to keep the biotin far enough away from the enzyme binding domain so as not to interfere with activity. Dr. Yin's group was able to successfully develop a yeast cell surface display assay to display mutant libraries of DhbE that were then incubated with our chemical probes. Biotin-streptavidin enrichment selected for mutant enzymes that bound the non-natural probe molecules. By iteratively enriching, they were able to select for mutant DhbE enzymes that could be expressed, purified, and were shown to have dramatically shifted selectivity

towards non-natural substrates.

5.6 Experimental Data

5.6.1 General procedures for the synthesis of biotinylated probes against DhbE

All reactions were performed under an inert atmosphere of dry argon in oven-dried (150 °C) glassware. ^{1}H and ^{13}C NMR experiments were recorded on a Varian 600 MHz spectrometer. Proton chemical shifts are reported in ppm from an internal standard of residual chloroform (7.26 ppm) or methanol (3.31 ppm). Carbon chemical shifts are reported using an internal standard of residual chloroform (77.0 ppm) or methanol (49.1 ppm). Proton chemical data are reported as follows: chemical shift, multiplicity (s = singlet, d = doublet, t = triplet, q = quartet, m = multiplet, br = broad, ovlp = overlapping), coupling constant, and integration. High resolution mass spectra were acquired on an Agilent TOF II TOF/MS instrument (Agilent Technologies, Santa Clara, CA) equipped with either an ESI or APCI interface. Semi-preparative reverse-phase HPLC was performed on a Phenomenex Gemini 10 μm C18 110 Å (250 × 10.0 mm) column (Phenomenex, Torrance, CA) operating at 5.0 mL/min with detection at 254 nm. Flash chromatography was performed on an ISCO Combiflash Companion® purification system (Teledyne Isco, Lincoln, NE) with prepacked silica gel cartridges and the indicated solvent system.

All commercial reagents (Sigma-Aldrich, Fisher, Fluka, Strem) were used as provided.

NHSdPEG®$_4$-biotin was purchased from Quanta BioDesign, Ltd. (Powell, OH, USA) and 2-iodoadenosine from Tokyo Chemical Industry Co. (Portland, OR, USA). Sulfamoyl chloride was prepared by the method of Heacock without recrystallization.[23] Compound **5-7** was prepared according to literature procedure and all spectral data agree with reported values.[24] An anhydrous solvent dispensing system (JC Meyer Solvent Systems, Laguna Beach, CA) with two packed columns of neutral alumina was used for drying THF, DMF and DCM and the solvents were dispensed under argon. Anhydrous DME (Sigma-Aldrich) was used as provided. Compound **5-1** was completed by Dr. Kimberly Grimes of the Aldrich lab, with experimental data reported elsewhere.[19]

5.6.2 *N*-Hydroxysuccinimidyl 3-(methoxymethyloxy)benzoate (5-12)

A solution of LiOH (328 mg, 7.65 mmol, 3.0 equiv) in MeOH (27 mL) and water (3 mL) was added to methyl 3-(methoxymethyloxy)-benzoate **5-11**[25] (500 mg, 2.55 mmol, 1.0 equiv), and the reaction mixture was refluxed for 2 h. The reaction mixture was concentrated, the residue was dissolved in H_2O (25 mL), the pH was adjusted to 2, and then extracted with EtOAc (3 × 50 mL). The combined organic extracts were washed with saturated aqueous NaCl (50 mL), then concentrated under reduced pressure to afford 3-(methoxymethyloxy)-benzoic acid (440 mg, 95%), which was directly carried onto the next step.

To a solution of the crude product (440 mg, 2.41 mmol, 1.0 equiv) from above in dry THF (25 mL) at 0 °C was added *N*-hydroxysuccinimide (306 mg, 2.66 mmol, 1.1 equiv)

and DCC (498 mg, 2.41 mmol, 1.0 equiv). The resulting mixture was stirred for 30 min at 0 °C and then 16 h at 23 °C. The reaction mixture was filtered to remove the DCU precipitate, and the filtrate was concentrated under reduced pressure. Purification by flash chromatography (4:1 EtOAc/hexanes) afforded the title compound (620 mg, 92%) as a viscous, colorless oil.

5.6.3 2-[3-(2-{2-[2-(*tert*-Butoxycarbonylamino)ethoxy]ethoxy}ethoxy)prop-1-ynyl]-2′,3′-*O*-isopropylidene-5′-*O*-{*N*-[3-(methoxymethoxy)benzoyl]sulfamoyl}adenosine (5-13)

To a solution of **5-7**[24] (16 mg, 0.024 mmol, 1.0 equiv) in DMF (2.5 mL) was added **5-12** (10 mg, 0.036 mmol, 1.5 equiv) and Cs_2CO_3 (23 mg, 0.071 mmol, 3.0 equiv) and the reaction was stirred at 23 °C for 22 h. The reaction mixture was filtered and concentrated under reduced pressure to a pale yellow film. Purification by flash chromatography (linear gradient 0–15% MeOH/EtOAc) gave the title compound (17.2 mg, 86%) as a colorless oil. R_f = 0.36 (10% MeOH/EtOAc); ^{1}H NMR (600 MHz, CD_3OD) δ 1.35, (s, 3H), 1.41 (s, 9H), 1.60 (s, 3H), 3.22 (t, J = 5.4 Hz, 2H), 3.43 (s, 3H), 3.51 (t, J = 5.4 Hz, 2H), 3.61–3.62 (m, 2H), 3.64–3.65 (m, 2H), 3.70–3.71 (m, 2H), 3.78–3.79 (m, 2H), 4.34 (t, J = 4.8 Hz, 2H), 4.45 (s, 2H), 4.57 (s, 1H), 5.14 (d, J = 5.4 Hz, 1H), 5.19 (s, 2H), 5.34 (q, J = 3.6 Hz, 1H), 6.22 (d, J = 2.4 Hz, 1H), 7.10 (d, J = 8.4 Hz, 1H), 7.25 (t, J = 7.2 Hz, 1H), 7.64 (d, J = 7.8 Hz, 1H), 7.69 (s, 1H), 8.53 (s, 1H); ^{13}C NMR (150 MHz, CD_3OD) δ 25.7, 27.7, 28.9, 41.4, 56.4, 59.5, 70.0, 70.6, 71.2, 71.4, 71.5, 71.7, 80.1, 82.8, 83.5, 86.0,

86.5, 91.8, 95.7, 115.5, 117.7, 119.8, 120.4, 123.6, 130.0, 140.6, 142.3, 147.3, 150.8, 157.2, 158.5, 174.7 (missing 2 carbons, likely due to overlap); HRMS (ESI−) calculated for $C_{36}H_{48}N_7O_{14}S$ [M − H]− 834.2985, found 834.2965 (error 2.4 ppm).

5.6.4 2-[3-(2-{2-[2-({dPEG®$_4$-biotinyl}amino)ethoxy]ethoxy}ethoxy)prop-1-ynyl]-5′-*O*-{*N*-[3-(hydroxy)benzoyl]sulfamoyl}adenosine triethylammonium salt (5-2)

To **5-13** (17.2 mg, 0.021 mmol, 1.0 equiv) was added 80% aqueous TFA (2 mL). The mixture was stirred at 23 °C for 4 h, then concentrated under reduced pressure to remove all traces of TFA. To the resulting crude residue in DMF (1 mL) was added triethylamine (0.100 mL, 0.717 mmol, 34 equiv) and **5-10** (18.2 mg, 0.031 mmol, 1.5 equiv). The mixture was stirred at 23 °C for 13 h, then concentrated under reduced pressure. Purification by semi-preparative reverse-phase HPLC using a Phenomenex Gemini 10 µm C18 110 Å (250 × 10.0 mm) column (Phenomenex, Torrance, CA) and a gradient of 5–35% MeCN–10 mM aqueous triethylammonium bicarbonate over 20 minutes, followed by 35% for 8 minutes. The retention time of the product was 18.5 minutes (k' = 3.6) and the appropriate fractions were pooled and lyophilized to afford the title compound (8 mg, 34%) as an off-white solid. ^{1}H NMR (600 MHz, CD_3OD) δ 1.36–1.38 (m, 2H), 1.53–1.61 (m, 2H), 1.67–1.69 (m, 2H), 2.16 (t, J = 7.2 Hz, 2H), 2.42 (t, J = 6.0 Hz, 2H), 2.65 (d, J = 12.6 Hz, 1H), 2.87 (dd, J = 12.6, 4.8 Hz, 1H), 3.09–3.14 (m, 4H), 3.19 (s, 1H), 3.48–3.52 (m, 4H), 3.55–3.57 (m, 6H), 3.58–3.60 (m, 6H), 3.62–3.64 (m, 2H), 3.66–3.68 (m, 4H), 3.74–3.76 (m, 2H), 4.25 (q, J = 4.2 Hz, 1H), 4.29 (d, J = 3.0 Hz,

1H), 4.34 (d, J = 2.4 Hz, 1H), 4.36 (d, J = 3.0 Hz, 1H) 4.38–4.39 (m, 1H), 4.41 (s, 2H), 4.44 (q, J = 4.2 Hz, 1H), 4.65 (t, J = 5.4 Hz, 1H), 6.05 (d, J = 5.4 Hz, 1H), 6.82 (dd, J = 7.8, 2.4 Hz, 1H), 7.13 (t, J = 7.8 Hz, 1H), 7.43 (s, 1H), 7.47 (d, J = 7.8 Hz, 1H), 8.57 (s, 1H); ^{13}C NMR (150 MHz, CD_3OD) δ 10.4, 27.0, 29.6, 29.9, 36.9, 37.7, 40.5, 40.6, 41.2, 47.5, 57.1, 59.6, 61.8, 63.5, 68.4, 69.3, 70.5, 70.6, 70.7, 70.78, 70.80, 71.37, 71.45, 71.56, 71.60, 71.65, 71.69, 71.73, 72.5, 76.4, 83.4, 84.9, 89.3, 92.6, 116.8, 118.3, 119.2, 121.4, 130.0, 142.1, 147.2, 151.1, 157.1, 157.2, 158.3, 166.2, 174.2, 175.3, 176.3; HRMS (ESI−) calculated for $C_{47}H_{67}N_{10}O_{18}S_2$ [M − H]– 1123.4082, found 1123.4126 (error 3.9 ppm).

5.6.5 2-[3-(2-{2-[2-(*tert*-Butoxycarbonylamino)ethoxy]ethoxy}ethoxy)prop-1-ynyl]-2′,3′-*O*-isopropylidene-5′-*O*-{*N*-[2-(amino)benzoyl]sulfamoyl}adenosine triethylammonium salt (5-15)

To a solution of **5-7**[24] (16 mg, 0.02 mmol, 1.0 equiv) in DMF (3 mL) at 23 ºC was added **5-14** (8 mg, 0.05 mmol, 2.5 equiv) and Cs_2CO_3 (23 mg, 0.07 mmol, 3.5 equiv) and the reaction stirred for 16 h. The reaction mixture was filtered and the filtrate concentrated under reduced pressure. Purification by flash chromatography (linear gradient 0–20% MeOH/EtOAc with 1% Et_3N) afforded the title compound (12.1 mg, 76%) as a yellow oil: R_f = 0.20 (10% MeOH/EtOAc); ^{1}H NMR (600 MHz, CD_3OD) δ 1.27 (t, J = 7.2 Hz, 9H), 1.35 (s, 3H), 1.41 (s, 9H), 1.60 (s, 3H), 3.17 (q, J = 7.8 Hz, 6H), 3.22 (q, J = 6.0 Hz, 2H), 3.51 (t, J = 6.0 Hz, 2H), 3.60–3.61 (m, 2H), 3.64–3.65 (m, 2H), 3.69–3.70 (m, 2H),

3.78 (q, J = 4.2 Hz, 2H), 4.30 (dd, J = 10.8, 3.6 Hz, 1H), 4.34 (dd, J = 10.8, 3.6 Hz, 1H), 4.44 (s, 2H), 4.57 (d, J = 2.4 Hz, 1H), 5.13 (dd, J = 6.0, 1.8 Hz, 1H), 5.35 (dd, J = 6.0. 3.0 Hz, 1H), 6.23 (d, J = 3.6 Hz, 1H), 6.54 (t, J = 7.8 Hz, 1H), 6.66 (d, J = 8.4 Hz, 1H), 7.11 (t, J = 7.2 Hz, 1H), 7.89 (d, J = 7.8 Hz, 1H), 8.55 (s, 1H); ^{13}C NMR (150 MHz, CD_3OD) δ 9.4, 25.7, 27.7, 28.9, 41.4, 48.0, 55.3, 59.5, 69.9, 70.6, 71.2, 71.4, 71.5, 71.6, 80.2, 82.8, 83.5, 85.9, 86.0, 86.4, 91.8, 115.5, 116.9, 118.1, 119.8, 120.2, 132.7, 133.2, 142.4, 147.3, 150.8, 151.4, 157.2, 176.9.

5.6.6 2-[3-(2-{2-[2-({dPEG®$_4$-biotinyl}amino)ethoxy]ethoxy}ethoxy)prop-1-ynyl]-5′-*O*-{*N*-[2-(amino)benzoyl]sulfamoyl}adenosine triethylammonium salt (5-3)

To **5-15** (12.1 mg, 0.015 mmol, 1.0 equiv) was added 80% aqueous TFA (2 mL) and the mixture stirred at 23 ºC for 2.5 h, then concentrated under reduced pressure to remove all traces of TFA. The crude residue was dissolved in DMF (2 mL) and triethylamine (0.006 mL, 0.046 mmol, 3.0 equiv) and **5-10** (13 mg, 0.023 mmol, 1.5 equiv) were added. The mixture was stirred at 23 ºC for 16 h, then concentrated under reduced pressure to a yellow oil. Purification by semipreparative reverse-phase HPLC using a Phenomenex Gemini 10 μm C18 110 Å (250 × 10.0 mm) column (Phenomenex, Torrance, CA) and a gradient of 5–35% MeCN/10 mM aqueous triethylammonium bicarbonate over 20 min followed by 35% MeCN for 3 min. The retention time of the product was 19.8 minutes (k' = 4.0) and the appropriate fractions were pooled and lyophilized to afford the title compound (2.1 mg, 11%) as an off-white solid. ^{1}H NMR (600 MHz, CD_3OD) δ 1.27–

1.32 (m, 9H), 1.40–1.46 (m, 2H), 1.60–1.66 (m, 2H), 1.68–1.73 (m, 2H), 2.20 (t, *J* = 7.8 Hz, 2H), 2.46 (t, *J* = 6.0 Hz, 2H), 2.68 (q, *J* = 12.6 Hz, 1H), 2.91 (dd, *J* = 13.2, 4.8 Hz, 1H), 3.15–3.24 (m, 4H), 3.35–3.38 (m, 6H), 3.42 (br s, 1H), 3.52–3.56 (dt, *J* = 15.0, 6.0 Hz, 4H), 3.60–3.64 (m, 14H), 3.66–3.68 (m, 2H), 3.70–3.72 (m, 4H), 3.79–3.80 (m, 2H), 4.29 (dd, *J* = 7.8, 4.8 Hz, 1H), 4.32 (d, *J* = 2.4 Hz, 1H), 4.37 (dd, *J* = 10.8, 3.0 Hz, 2H), 4.43 (dd, *J* = 8.0, 3.6 Hz, 1H), 4.45 (s, 2H), 4.48 (dd, *J* = 7.8, 4.8 Hz, 1H), 4.70 (t, *J* = 6.0 Hz, 1H), 6.09 (d, *J* = 5.4 Hz, 1H), 6.55 (t, *J* = 7.2 Hz, 1H), 6.67 (d, *J* = 8.4 Hz, 1H), 7.10 (t, *J* = 8.4 Hz, 1H), 7.93 (d, *J* = 7.8 Hz, 1H), 8.63 (s, 1H); ^{13}C NMR (150 MHz, CD_3OD, assigned by HMBC and HSQC) δ 9.8, 25.4, 28.0, 28.3, 35.2, 36.3, 39.1, 39.6, 41.4, 46.5, 55.5, 57.1, 58.6, 60.0, 60.1, 61.9, 66.7, 67.0, 68.8, 69.0, 69.1, 69.3, 69.75, 69.84, 70.0, 70.06, 70.07, 70.2, 76.3, 81.1, 84.8, 99.9, 104.6, 116.6, 117.8, 119.2, 131.2, 137.3, 140.6, 149.59, 149.63, 153.4, 154.1, 158.2, 172.6, 174.7, 178.8 (missing 2 carbons; 1 ethoxy linker C and 1 aromatic C, likely due to overlap); HRMS (ESI) calculated for $C_{47}H_{68}N_{11}O_{17}S_2$ [M – H]– 1122.4242, found 1122.4344 (9.1 ppm error).

5.7 References

1. Cane, D. E.; Walsh, C. T.; Khosla, C. Harnessing the biosynthetic code: Combinations, permutations, and mutations. *Science* **1998**, *282*, 63–68.

2. Clardy, J.; Walsh, C. T. Lessons from natural molecules. *Nature* **2004**, *432*, 829–837.

3. Fischbach, M. A.; Walsh, C. T. Assembly-line enzymology for polyketide and nonribosomal peptide antibiotics: Logic, machinery, and mechanisms. *Chem. Rev.* **2006**, *106*, 3468–3496.

4. Sieber, S. A.; Marahiel, M. A. Molecular mechanisms underlying nonribosomal peptide synthesis: Approaches to new antibiotics. *Chem. Rev.* **2005**, *105*, 715–738.

5. May, J. J.; Kessler, N.; Marahiel, M. A.; Stubbs, M. T. Crystal structure of DhbE, an archetype for aryl acid activating domains of modular nonribosomal peptide synthetases. *Proc. Natl. Acad. Sci. U.S.A.* **2002**, *99*, 12120–12125.

6. Gulick, A. M. Conformational dynamics in the acyl-CoA synthetases, adenylation domains of non-ribosomal peptide synthetases, and firefly luciferase. *ACS Chem. Biol.* **2009**, *4*, 811–827.

7. Challis, G. L.; Ravel, J.; Townsend, C. A. Predictive, structure-based model of amino acid recognition by nonribosomal peptide synthetase adenylation domains. *Chem. Biol.* **2000**, *7*, 211–224.

8. Stachelhous, T.; Mootz, H. D.; Marahiel, M. A. The specificity-conferring code of adenylation domains in nonribosomal peptide synthetases. *Chem. Biol.* **1999**, *6*, 493–505.

9. von Döhren, H.; Dieckmann, R.; Pavela-Vrancic, M. The nonribosomal code. *Chem. Biol.* **1999**, *6*, R273–R279.

10. Sikora, A. L.; Wilson, D. J.; Aldrich, C. C.; Blanchard, J. S. Kinetic inhibition studies of dihydroxybenzoate-AMP ligase from *Escherichia coli*. *Biochemistry* **2010**, *49*, 3648–3657.

11. Fischbach, M. A.; Lai, J. R.; Roche, E. D.; Walsh, C. T.; Liu, D. R. Directed evolution can rapidly improve the activity of chimeric assembly-line enzymes. *Proc. Natl. Acad. Sci. U.S.A.* **2007**, *104*, 11951–11956.

12. Robbel, L.; Marahiel, M. A. Daptomycin, a bacterial lipopeptide synthesized by a nonribosomal machinery. *J. Biol. Chem.* **2010**, *285*, 27501–27508.

13. Chen, C. Y.; Georgiev, I.; Anderson, A. C.; Donald, B. R. Computational structure-based redesign of enzyme activity. *Proc. Natl. Acad. Sci. U.S.A.* **2009**, *106*, 3764–3769.

14. Thirlway, J.; Lewis, R.; Nunns, L.; Al Nakeeb, M.; Styles, M.; Struck, A. W.; Smith, C. P.; Micklefield, J. Introduction of a non-natural amino acid into a nonribosomal peptide antibiotic by modification of adenylation domain specificity. *Angew. Chem. Int. Ed.* **2012**, *51*, 7181–7184.

15. Miethke, M.; Bisseret, P.; Beckering, C. L.; Vignard, D.; Eustache, J.; Marahiel, M. A. Inhibition of aryl acid adenylation domains involved in bacterial siderophore

synthesis. *FEBS J.* **2006**, *273*, 409–419.

16. Neres, J.; Labello, N. P.; Somu, R. V.; Boshoff, H. I.; Wilson, D. J.; Vannada, J.; Chen, L.; Barry, C. E. 3rd; Bennett, E. M.; Aldrich, C. C. Inhibition of siderophore biosynthesis in *Mycobacterium tuberculosis* with nucleoside bisubstrate analogues: Structure activity relationships of the nucleobase domain of 5′-*O*-[*N*-(salicyl)sulfamoyl]-adenosine. *J. Med. Chem.* **2008**, *51*, 5349–5370.

17. Chao, G.; Lau, W. L.; Hackel, B. J.; Sazinsky, S. L.; Lippow, S. M.; Wittrup, K. D. Isolating and engineering human antibodies using yeast surface display. *Nat. Protoc.* **2006**, *1*, 755–768.

18. Miller, K. D.; Pefaur, N. B.; Baird, C. L. Construction and screening of antigen targeted immune yeast surface display antibody libraries. *Curr. Protoc. Cytom.* **2008**, *4*, Unit 4.7.

19. Zhang, K.; Nelson, K. M.; Bhuripanyo, K.; Grimes, K. D.; Zhao, B.; Aldrich, C. C.; Yin, J. Engineering the substrate specificity of the DhbE adenylation domain by yeast cell surface display. *Chem. Biol.* **2013**, *20*, 92–101.

20. Baca, M.; Scanlan, T. S.; Stephenson, R. C.; Wells J. A. Phage display of a catalytic antibody to optimize affinity for transition-state analog binding. *Proc. Natl. Acad. Sci. U.S.A* **1997**, *94*, 10063–10068.

21. Ames, B. D.; Walsh, C. T. Anthranilate-activating modules from fungal nonribosomal peptide assembly lines. *Biochemistry* **2010**, *49*, 3351–3365.

22. Eppelmann, K.; Stachelhous, T.; Marahiel, M. A. Exploitation of the selectivity-conferring code of nonribosomal peptide synthetases for the rational design of novel peptide antibiotics. *Biochemistry* **2002**, *41*, 9718–9726.

23. Heacock, D.; Forsyth, C. J.; Shiba, K.; Musier-Forsyth, K. Synthesis and aminoacyl-tRNA synthetase inhibitory activity of prolyl adenylate analogs. *Bioorg. Chem.* **1996**, *24*, 273–289.

24. Grimes, K. D.; Aldrich, C. C. A high-throughput screening fluorescence polarization assay for fatty acid adenylating enzymes in *Mycobacterium tuberculosis*. *Anal. Biochem.* **2011**, *417*, 264–273.

25. Winkle, M. R.; Ronald, R. C. Regioselective metalation reactions of some substituted (methoxymethoxy)arenes. *J. Org. Chem.* **1982**, *47*, 2101–2108.

Chapter 6. Conclusions and Future Directions

New antitubercular agents are desperately needed for the treatment of increasingly drug resistant strains of *Mycobacterium tuberculosis* (*Mtb*) that continue to develop. The development of new therapeutics can be through the discovery of new compounds for validated cellular targets, or through discovery and development of compounds against new targets yet to be exploited. A known target can make structure-activity relationships easier to study, however overcoming drug resistance at a previously targeted site can prevent successful development of new therapeutics. New targets do not have existing drug resistance problems, but need extensive validation before a new compound can be brought to preclinical development.

Our work has focused on discovering new ways to target *Mtb* through the bacteria's need for iron. In an effort to probe the biosynthetic pathway of siderophores more fully, our group had previously developed small molecule inhibitors of MbtA, the initiating enzyme in the biosynthesis of mycobactins. We used this information to synthesize and evaluate the parent compound, Sal-AMS, and its analogues *in vivo*. In Chapter 2 we described the synthesis and evaluation of a small set of compounds that we predicted would incorporate strong antimycobacterial activity and improved pharmacokinetic parameters. We hypothesized that by decreasing the acidity of the linker group and increasing the lipophilicity of the compound we could improve the bioavailability through passive diffusion. Unfortunately, we did not see very impressive oral bioavailability of our

compounds. We were encouraged to see that analogues with decreased acidity in the linker did show improvement in bioavailability, albeit moderately so. An acetate prodrug of Sal-AMS was also ineffective for improving the bioavailability of the parent compound. The tri-acetate prodrug was quickly hydrolyzed in pooled rat plasma, however the di-acetate and mono-acetate intermediates were relatively long-lived. We would need to re-test these compounds while observing all the intermediates over a longer period of time (> 8 hours) in order to accurately determine the true bioavailability of these analogues. This work sets the groundwork in the group for an *in vivo* SAR study to build bioavailability into the constraints we have for antimycobacterial potency. Some analogues that we are pursuing include some derivatives that incorporate lipophilic or fluoro groups at the 2′-position of the glycosyl moiety, as well as prodrugs of the acidic nitrogen in the linker group. It may also be useful to make mono-esters of acyloxyalkyl esters at the phenol hydroxyl. It appears this position is the most readily cleaved in rat plasma, with a half-life approximated at 1 minute. If a sufficiently permeable prodrug at this position can be developed, release of the prodrug should be efficient. We would also like to evaluate the permeability of these compounds in an additional *in vitro* assay, e.g. Caco-2 or MDCK assay to help us better understand the behavior we have observed *in vivo*.

In Chapter 3, we described a study to confirm MbtA as the target of our parent compound, Sal-AMS, as well as an attempt to identify possible additional targets of Sal-AMS action. It had previously been suggested that Sal-AMS should only be active against the bacteria in an environment where siderophore action was essential to the

bacteria's survival, i.e. iron-limiting conditions. We saw activity, however, under both iron-deficient and iron-replete conditions. From knowledge we had already gained from SAR studies performed previously in our lab, we were able to design and synthesize a light-activated probe that still shows good binding to MbtA. This compound incorporated a benzophenone as an activatable cross-linking reagent, and a terminal alkyne for use as a handle to incorporate either imaging or enrichment tags. Dr. Benjamin Duckworth, a post-doc in our lab, successfully used this compound to confirm the binding of the parent compound to MbtA, but was unable to positively identify additional proteins to which Sal-AMS may be binding. After completion of this study, we learned from our collaborator, Dr. Michael Niederweis, and others that the siderophore pathway may be necessary at all times for the bacteria's acquisition of iron. There is now some evidence that mycobacterial siderophores are in use even in iron-replete conditions in order to facilitate the diffusion of iron across the highly complex mycobacterial cell envelope. We have an ongoing collaboration with Dr. Niederweis to confirm that our compounds show activity under both conditions due to the disruption of iron acquisition by the bacteria. Rescuing growth of the mycobacteria in an iron-rich media in the presence of Sal-AMS by the addition of mycobactins would help confirm the targeted pathway and its importance to bacterial growth. Growth of resistant *Mtb* mutants would also help confirm the relevant target. Finally, efficacy studies in an *Mtb* animal infection model would be the ultimate test as to whether or not these analogues are able to inhibit mycobactin biosynthesis to a therapeutically relevant level.

In Chapter 4, the natural product transvalencin Z reported to be active against

mycobacteria was synthesized for study against *Mtb*. The two previously unassigned stereocenters allowed for 4 diastereomeric possibilities, each of which was separately synthesized for comparison to the reported spectroscopic data. Transvalencin Z resembles the structures of mycobactins in *Mtb*, siderophores produced by the bacteria for iron acquisition. Pioneering work by Dr. Marvin Miller and others has shown that structural mimics of siderophore structures can be potent inhibitors of *Mtb* growth. While we hypothesized that the reported activity against mycobacteria was related to disrupting the iron acquisition pathway, we were unable to reproduce the activity profile originally reported for transvalencin Z. Further, none of the completed diastereomers fully matched the limited spectroscopic data reported for the compound. Without an authentic standard with which to compare these synthetic transvalencin diastereomers, we were unable to draw any conclusions regarding the natural product's stereochemistry or mechanism of action. When we reached out to the authors who reported transvalencin Z, we were unable to obtain any of the originally isolated sample or the producing strain. We need to obtain the producing strain of *Nocardia* so that we can isolate the natural product and compare it to our synthetic diastereomers for absolute stereochemical assignment. This may also afford us a better understanding of the antimycobacterial properties of the compound. If the Transvalencin Z fraction again proves active against *M. smegmatis*, it would be prudent to attempt to identify the active component of this fraction, as it may be a very exciting lead compound for antimycobacterial development.

Finally, in Chapter 5 we aided our collaborator Dr. Jun Yin in the synthesis of 3 biotinylated probes for the reengineering of substrate specificity for DhbE, the aryl acid

adenylating enzyme in the bacillibactin biosynthetic pathway in *B. subtilis*. These probes were successful in allowing for the identification of mutant DhbE enzymes with increased specificity for 3-hydroxybenzoic acid and 2-aminobenzoic acid over the wild-type substrate 2, 3-dihydroxybenzoic acid. Dr. Yin and co-workers were also able to demonstrate that these mutant enzymes were capable of loading the nonnative substrates onto the carrier protein DhbB. It would be useful to attempt to express the entire bacillibactin pathway, including the mutant enzymes, to evaluate whether the nonnative substrates can successfully be incorporated into the natural product. Additional mutants that can accept more highly differentiated substrates should also be attempted, in order to understand some of the limitations of this technique.

The development of new antitubercular agents is a continual battle to remain ahead of bacterial resistance development. The studies described in this thesis have demonstrated the importance of combining synthetic methods with biochemistry, molecular biology, and analytical chemistry for the discovery of new therapeutics. This interdisciplinary approach is vital to the success of any drug development program in identifying promising (and failing) lead compounds before investing heavily in preclinical and clinical development.

Chapter 7. Bibliography

7.1 Chapter 1 References

1. White, A. R. Effective antibacterials: At what cost? The economics of antibacterial resistance and its control. *J. Antimicrob. Chemother.* **2011**, *66*, 1948–1953.

2. Silver, L. L. Challenges of antibacterial discovery. *Clin. Microbiol. Rev.* **2011**, *24*, 71–109.

3. Payne, D. J.; Gwynn, M. N.; Holmes, D. J.; Pompliano, D. L. Drugs for bad bugs: Confronting the challenges of antibacterial discovery. *Nat. Rev. Drug Discovery* **2007**, *6*, 29–40.

4. Wright, G. D. Antibiotics: A new hope. *Chem. Biol.* **2012**, *19*, 3–10.

5. Fischbach, M. A.; Walsh, C. T. Antibiotics for emerging pathogens. *Science* **2009**, *325*, 1089–1093.

6. Klein, E.; Smith, D. L.; Laxminarayan, R. Hospitalizations and deaths caused by methicillin-resistant *Staphylococcus aureus*, United States, 1999-2005. *Emerging Infect. Dis.* **2007**, *13*, 1840–1846.

7. World Health Organization. *Global tuberculosis report 2012*; Geneva, Switzerland, **2012**.

8. Barry, C. E., 3rd; Blanchard, J. S. The chemical biology of new drugs in the development for tuberculosis. *Curr. Opin. Chem. Biol.* **2010**, *14*, 456–466.

9. Koul, A.; Arnoult, E.; Lounis, N.; Guillemont, J.; Andries, K. The challenge of new drug discovery for tuberculosis. *Nature* **2011**, *469*, 483–490.

10. Velayati, A. A.; Masjedi, M. R.; Farnia, P.; Tabarsi, P.; Ghanavi, J.; Ziazarifi, A. H.; Hoffner, S. E. Emergence of new forms of totally drug-resistant tuberculosis bacilli: Super extensively drug-resistant tuberculosis or totally drug-resistant strains in iran. *Chest* **2009**, *136*, 420–425.

11. Udwadia, Z. F.; Amale, R. A.; Ajbani, K. K.; Rodrigues, C. Totally drug-resistant tuberculosis in India. *Clin. Infect. Dis.* **2012**, *54*, 579–581.

12. CDC. Emergence of *Mycobacterium tuberculosis* with extensive resistance to second-line drugs --- worldwide, 2000--2004. *MMWR* **2006**, *55*, 301–305.

13. Aldrich, C. C.; Boshoff, H. I.; Remmel, R. P. Antitubercular Agents. In *Burger's Medicinal Chemistry, Drug Discovery and Development, 7th Edition*, Abraham, D. J.; Rotella, D. P., Eds. John Wiley and Sons, Inc.: **2010**; pp 713–813.

14. Fox, H. H. The chemical approach to the control of tuberculosis. *Science* **1952**, *116*, 129–134.

15. Nguyen, M.; Claparols, C.; Bernadou, J.; Meunier, B. A fast and efficient metal-mediated oxidation of isoniazid and identification of isoniazid-NAD(H) adducts. *ChemBioChem* **2001**, *2*, 877–883.

16. Vilchéze, C.; Jacobs, W. R., Jr. The mechanism of isoniazid killing: Clarity through the scope of genetics. *Annu. Rev. Microbiol.* **2007**, *61*, 35–50.

17. Rawat, R.; Whitty, A.; Tonge, P. J. The isoniazid-NAD adduct is a slow, tight-binding inhibitor of InhA, the *Mycobacterium tuberculosis* enoyl reductase: Adduct affinity and drug resistance. *Proc. Natl. Acad. Sci. U.S.A.* **2003**, *100*, 13881–13886.

18. Johnson, R.; Streicher, E. M.; Louw, G. E.; Warren, R. M.; Helden, P. D. v.; Victor, T. C. Drug resistance in *Mycobacterium tuberculosis*. *Curr. Issues Mol. Biol.* **2006**, *8*, 97–112.

19. Desta, Z.; Soukhova, N. V.; Flockhart, D. A. Inhibition of cytochrome P450 (CYP450) isoforms by isoniazid: Potent inhibition of CYP2C19 and CYP3A. *Antimicrob. Agents Chemother.* **2001**, *45*, 382–392.

20. Wen, X.; Wang, J.-S.; Neuvonen, P. J.; Backman, J. T. Isoniazid is a mechansim-based inhibitor of cytochrome P_{450} 1A2, 2A6, 2C19 and 3A4 isoforms in human liver microsomes. *Eur. J. Clin. Pharm.* **2002**, *57*, 799–804.

21. Binda, G.; Domenichini, E.; Gottardi, A.; Orlandi, B.; Ortelli, E.; Pacini, B.; Fowst, G. Rifampicin, a general review. *Arzneimittelforschung* **1971**, *21*, 1907–1977.

22. Rifampin. *Tuberculosis* **2008**, *88*, 151–154.

23. Maggi, N.; Arioli, V.; Sensi, P. Rifamycins. XLI. A new class of active semisynthetic rifamycins. N-substituted aminomethyl derivatives of refamycin SV. *J. Med. Chem.* **1965**, *8*, 790–793.

24. Bemer-Melchior, P.; Bryskier, A.; Drugeon, H. B. Comparison of the *in vitro* activities of rifapentine and rifampicin against *Mycobacterium tuberculosis* complex. *J. Antimicrob. Chemother.* **2000**, *46*, 571–575.

25. Wehrli, W.; Knüsel, F.; Schmid, K.; Staehelin, M. Interaction of rifamycin with bacterial RNA polymerase. *Proc. Natl. Acad. Sci. U.S.A.* **1968**, *61*, 667–673.

26. Wehrli, W.; Knüsel, F.; Staehelin, M. Action of rifamycin on RNA-polymerase from sensitive and resistant bacteria. *Biochem. Biophys. Res. Commun.* **1968**, *32*, 284–288.

27. Ramaswamy, S.; Musser, J. M. Molecular genetic basis of antimicrobial agent resistance in *Mycobacterium tuberculosis*: 1998 update. *Tubercle Lung Dis.* **1998**, *79*, 3–29.

28. la Porte, C. J. L.; Colbers, E. P. H.; Bertz, R.; Voncken, D. S.; Wikstrom, K.; Boeree, M. J.; Koopmans, P. P.; Hekster, Y. A.; Burger, D. M. Pharmacokinetics of adjusted-dose lopinavir-ritonavir combined with rifampin in healthy volunteers. *Antimicrob. Agents Chemother.* **2004**, *48*, 1553–1560.

29. Finch, C. K.; Chrisman, C. R.; Baceiwicz, A. M.; Self, T. H. Rifampin and rifabutin drug interactions: An update. *Arch. Intern. Med.* **2002**, *162*, 985–992.

30. Thomas, J. P.; Baughn, C. O.; Wilkinson, R. G.; Shepherd, R. G. A new synthetic compound with antituberculosis activity in mice: Ethambutol (dextro-2,2'-(ethylenediimino)-di-I-butanol). *Am. Rev. Respir. Dis.* **1961**, *83*, 891–893.

31. Lucchesi, M.; Mancini, P. The antimycobacterial activity of ethambutol (ETB). *Antibiot. Chemotherap.* **1970**, *16*, 230–238.

32. Yates, M. D.; Collins, C. H. Sensitivity of opportunist mycobacteria to rifampicin and ethambutol. *Tubercule* **1981**, *62*, 117–121.

33. Takayama, K.; Kilburn, J. O. Inhibition of synthesis of arabinogalactan by ethambutol in *Mycobacterium smegmatis*. *Antimicrob. Agents Chemother.* **1989**, *33*, 1493–1499.

34. Ramaswamy, S. V.; Amin, A. G.; Goksel, S.; Stager, C. E.; Dou, S. J.; El Sahly, H.; Moghazeh, S. L.; Kreiswirth, B. N.; Musser, J. M. Molecular genetic analysis of nucleotide polymorphisms associated with ethambutol resistance in human isolates of *Mycobacterium tuberculosis*. *Antimicrob. Agents Chemother.* **2000**, *44*, 326–336.

35. Shen, X.; Shen, G. M.; Wu, J.; Gui, X. H.; Li, X.; Mei, J.; DeRiemer, K.; Gao, Q. Association between embB codon 306 mutations and drug resistance in *Mycobacterium tuberculosis*. *Antimicrob. Agents Chemother.* **2007**, *51*, 2618–2620.

36. Leibold, J. E. The ocular toxicity of ethambutol and its relation to dose. *Ann. N. Y. Acad. Sci.* **1966**, *135*, 683–1120.

37. Kushner, S.; Dalalian, H.; Sanjurjo, J. L.; F. L. Bach, J.; Safir, S. R.; V. K. Smith, J.; Williams, J. H. Experimental chemotherapy of tuberculosis. II. The synthesis of pyrazinamides and related compounds. *J. Am. Chem. Soc.* **1952**, *74*, 3617–3621.

38. Solotorovsky, M.; Gregory, F. J.; Ironson, E. J.; Bugie, E. J.; Oneill, R. C.; Pfister, K. Pyrazinoic acid amide-An agent active against experimental murine tuberculosis. *Soc. Exp. Biol. Med. Proc.* **1952**, *79*, 563–565.

39. Stottmeier, K. D.; Beam, R. E.; Kubica, G. P. Determination of drug susceptibility of mycobacteria to pyrazinamide in 7H10 agar. *Am. Rev. Respir. Dis.* **1967**, *96*, 1072–1075.

40. Konno, K.; Feldmann, F. M.; McDermott, W. Pyrazinamide susceptibility and admidase activity of tubercle bacilli. *Am. Rev. Respir. Dis.* **1967**, *95*, 461–469.

41. Zhang, Y.; Scorpio, A.; Nikaido, H.; Sun, Z. Role of acid pH and deficient efflux of pyrazinoic acid in unique susceptibility of *Mycobacterium tuberculosis* to pyrazinamide. *J. Bacteriol.* **1999**, *181*, 2044–2049.

42. Scorpio, A.; Lindholm-Levy, P.; Heifets, L.; Gilman, R.; Siddiqi, S.; Cynamon, M.; Zhang, Y. Characterization of *pncA* mutations in pyrazinamide-resistant *Mycobacterium tuberculosis*. *Antimicrob. Agents Chemother.* **1997**, *41*, 540–543.

43. Shi, W.; Zhang, X.; Jian, X.; Yuan, H.; Lee, J. S.; Barry, C. E. 3rd; Wang, H.; Zhang, W.; Zhang, Y. Pyrazinamide inhibits trans-translocation in *Mycobacterium tuberculosis*. *Science* **2011**, *333*, 1630–1632.

44. Zierski, M.; Bek, E. Side-effects of drug regimens used in short-course chemotherapy for pulmonary tuberculosis. A controlled clinical study. *Tubercle* **1980**, *61*, 41–49.

45. Chang, K. C.; Leung, C. C.; Yew, W. W.; Lau, T. Y.; Tam, C. M. Hepatotoxicity of pyrazinamide: cohort and case-control analyses. *Am. J. Respir. Crit. Care Med.* **2008**, *177*, 1391–1396.

46. Andries, K.; Verhasselt, P.; Guillemont, J.; Gohlmann, H. W.; Neefs, J. M.; Winkler, H.; Van Gestel, J.; Timmerman, P.; Zhu, M.; Lee, E.; Williams, P.; de Chaffoy, D.; Huitric, E.; Hoffner, S.; Cambau, E.; Truffot-Pernot, C.; Lounis, N.; Jarlier, V. A diarylquinoline drug active on the ATP synthase of *Mycobacterium tuberculosis*. *Science* **2005**, *307*, 223–237.

47. Huitric, E.; Verhasselt, P.; Koul, A.; Andries, K.; Hoffner, S.; Andersson, D. I. Rates and mechanisms of resistance development in *Mycobacterium tuberculosis* to a novel diarylquinoline ATP synthase inhibitor. *Antimicrob. Agents Chemother.* **2010**, *54*, 1022–1028.

48. Cohen, J. Approval of novel TB drug celebrated-with restraint. *Science* **2013**, *339*, 130.

49. Koul, A.; Dendouga, N.; Vergauwen, K.; Molenberghs, B.; Vranckx, L.; Willebrords, R.; Ristic, Z.; Lill, H.; Dorange, I.; Guillemont, J.; Bald, D.; Andries, K. Diarylquinolines target subunit c of mycobacterial ATP synthase. *Nat. Chem. Biol.* **2007**, *3*, 323–324.

50. Diacon, A. H.; Pym, A.; Grobusch, M.; Patientia, R.; Rustomjee, R.; Page-Shipp, L.; Pistorius, C.; Krause, R.; Bogoshi, M.; Churchyard, G.; Venter, A.; Allen, J.; Palomino, J. C.; DeMarez, T.; Heeswijk, R. P. G. v.; Lounis, N.; Meyvisch, P.; Verbeeck, J.; Parys, W.; Beule, K. d.; Andries, K.; McNeeley, D. F. The diarylquinoline TMC207 for multidrug-resistant tuberculosis. *N. Engl. J. Med.* **2009**, *360*, 2397–2405.

51. Russell, D. G.; Barry, C. E., 3rd; Flynn, J. L. Tuberculosis: What we don't know can, and does, hurt us. *Science* **2010**, *328*, 852–856.

52. Tsai, M. C.; Chakravarty, S.; Zhu, G.; Xu, J.; Tanaka, K.; Koch, C.; Tufariello, J.; Flynn, J.; Chan, J. Characterization of the tuberculous granuloma in murine and human lungs: Cellular composition and relative tissue oxygen tension. *Cell. Microbiol.* **2006**, *8*, 218–232.

53. Lin, P. L.; Pawar, S.; Myers, A.; Pegu, A.; Fuhrman, C.; Reinhart, T. A.; Capuano, S. V.; Klein, E.; Flynn, J. L. Early events in *Mycobacterium tuberculosis* infection in cynomolgus macaques. *Infect. Immun.* **2006**, *74*, 3790–3803.

54. Barry, C. E., 3rd; Boshoff, H. I.; Dartois, V.; Dick, T.; Ehrt, S.; Flynn, J.; Schnappinger, D.; Wilkinson, R. J.; Young, D. The spectrum of latent tuberculosis: Rethinking the biology and intervention strategies. *Nat. Rev. Microbiol.* **2009**, *7*, 845–855.

55. Kaplan, G.; Post, F. A.; Moreira, A. L.; Wainwright, H.; Kreiswirth, B. N.; Tanverdi, M.; Mathema, B.; Ramaswamy, S. V.; Walther, G.; Steyn, L. M.; Barry, C. E.; Bekker, L. G. *Mycobacterium tuberculosis* growth at the cavity surface: a microenvironment with failed immunity. *Infect. Immun.* **2003**, *71*, 7099–7108.

56. Dannenberg, A. M. J. Pathogenesis of pulmonary *Mycobacterium bovus* infection: Basic principles established by the rabbit model. *Tuberculosis (Edinb)* **2001**, *81*, 87–96.

57. MacMicking, J. D.; Taylor, G. A.; McKinney, J. D. Immune control of tuberculosis by IFN-gamma-inducible LRG-47. *Science* **2003**, *302*, 654–659.

58. Voskuil, M. I.; Viconti, K. C.; Schoolnik, G. K. *Mycobacterium tuberculosis* gene expression during adaptation to stationary phase and low-oxygen dormancy. *Tuberculosis* **2004**, *84*, 218–227.

59. Gutierrez, M. G.; Master, S. S.; Singh, S. B.; Taylor, G. A.; Colombo, M. I.; Deretic, V. Autophagy is a defense mechanism inhibiting BCG and *Mycobacterium tuberculosis* survival in infected macrophages. *Cell* **2004**, *119*, 753–766.

60. Alonso, S.; Pethe, K.; Russell, D. G.; Purdy, G. E. Lysosomal killing of *Mycobacterium* mediated by ubiquitin-derived peptides is enhanced by autophagy. *Proc. Natl. Acad. Sci. U.S.A.* **2007**, *104*, 6031–6036.

61. Via, L. E.; Lin, P. L.; Ray, S. M.; Carrillo, J.; Allen, S. S.; Eum, S. Y.; Taylor, K.; Klein, E.; Manjunatha, U.; Gonzales, J.; Lee, E. G.; Park, S. K.; Raleigh, J. A.; Cho, S. N.; McMurray, D. N.; Flynn, J. L.; Barry, C. E., 3rd. Tuberculous granulomas are hypoxic in guinea pigs, rabbits, and nonhuman primates. *Infect. Immun.* **2008**, *76*, 2333–2340.

62. Keane, J.; Gershon, S.; Wise, R. P.; Mirabile-Levens, E.; Kasznica, J.; Schwieterman, W. D.; Siegel, J. N.; Braun, M. M. Tuberculosis associated with infliximab, a tumor necrosis factor α-neutralizing agent. *N. Engl. J. Med.* **2001**, *345*, 1098–1104.

63. Mohan, A. K.; Coté, T. R.; Block, J. A.; Manadan, A. M.; Siegel, J. N.; Braun, M. M. Tuberculosis following the use of etanercept, a tumor necrosis factor inhibitor. *Clin. Infect. Dis.* **2004**, *39*, 295–299.

64. Ulrichs, T.; Kosmiadi, G. A.; Jõrg, S.; Pradl, L.; Titukhina, M.; Mishenko, V.; Gushina, N.; Kaufmann, S. H. E. Differential organization of the local immune

response in patients with active cavitary tuberculosis or with nonprogressive tuberculoma. *J. Infect. Dis.* **2005**, *192*, 89–97.

65. Sams-Dodd, F. Target-based drug discovery: Is something wrong? *Drug Discovery Today* **2005**, *10*, 139–147.

66. Monaghan, R. L.; Barrett, J. F. Antibacterial drug discovery--Then, now and the genomics future. *Biochem. Pharmacol.* **2006**, *71*, 901–909.

67. Sassetti, C. M.; Boyd, D. H.; Rubin, E. J. Comprehensive identification of conditionally essential genes in mycobacteria. *Proc. Natl. Acad. Sci. U.S.A.* **2001**, *98*, 12712–12717.

68. Sassetti, C. M.; Rubin, E. J. Genetic requirements for mycobacterial survival during infection. *Proc. Natl. Acad. Sci. U.S.A.* **2003**, *100*, 12989–12994.

69. Mei, J.-M.; Nourbakhsh, F.; Ford, C. W.; Holden, D. W. Identification of *Staphylococcus aureus* virulence genes in a murine model of bacteraemia using signature-tagged mutagenesis. *Mol. Microbiol.* **1997**, *26*, 399–407.

70. Chiang, S. L.; Mekalanos, J. J.; Holden, D. W. In vivo genetic analysis of bacterial virulence. *Ann. Rev. Micrbiol.* **1999**, *53*, 129–154.

71. Smith, V.; Botstein, D.; Brown, P. O. Genetic footprinting: A genomic strategy for determining a gene's function given its sequence. *Proc. Natl. Acad. Sci. U.S.A.* **1995**, *92*, 6479–6483.

72. Akerley, B. J.; Rubin, E. J.; Camilli, A.; Lampe, D. J.; Robertson, H. M.; Mekalanos, J. J. Systematic identification of essential genes by *in vitro mariner* mutagenesis. *Proc. Natl. Acad. Sci. U.S.A.* **1998**, *95*, 8927–8932.

73. Woong Park, S.; Klotzsche, M.; Wilson, D. J.; Boshoff, H. I.; Eoh, H.; Manjunatha, U.; Blumenthal, A.; Rhee, K.; Barry, C. E., 3rd; Aldrich, C. C.; Ehrt, S.; Schnappinger, D. Evaluating the sensitivity of *Mycobacterium tuberculosis* to biotin deprivation using regulated gene expression. *PLoS Pathog.* **2011**, *7*, e1002264.

74. Baek, S.-H.; Li, A. H.; Sassetti, C. M. Metabolic regulation of mycobacterial growth and antibiotic sensitivity. *PLoS Biol.* **2011**, *9*, e1001065.

75. Duckworth, B. P.; Nelson, K. M.; Aldrich, C. C. Adenylating enzymes in *Mycobacterium tuberculosis* as drug targets. *Curr. Top. Med. Chem.* **2012**, *12*, 766–796.

76. Reynolds, R. C.; Ananthan, S.; Faaleolea, E.; Hobrath, J. V.; Kwong, C. D.; Maddox, C.; Rasmussen, L.; Sosa, M. I.; Thammasuvimol, E.; White, E. L.; Zhang, W.; John A. Secrist, I. High throughput screening of a library based on kinase inhibitor scaffolds against *Mycobacterium tuberculosis* H37Rv. *Tuberculosis* **2012**, *92*, 72–83.

77. Abrahams, G. L.; Kumar, A.; Savvi, S.; Hung, A. W.; Wen, S.; Abell, C.; Barry, C. E., 3rd; Sherman, D. R.; Boshoff, H. I.; Mizrahi, V. Pathway-selective sensitization of *Mycobacterium tuberculosis* for target-based whole-cell screening. *Chem. Biol.* **2012**, *19*, 844–854.

78. Coxon, G. D.; Cooper, C. B.; Gillespie, S. H.; McHugh, T. D. Strategies and challenges involved in the discovery of new chemical entities during early-stage tuberculosis drug discovery. *J. Infect. Dis.* **2012**, *205 Suppl. 2*, S258–S264.

79. Kumar, M.; Vijayakrishnan, R.; Subba Rao, G. In silico structure-based design of a novel class of potent and selective small peptide inhibitor of *Mycobacterium tuberculosis* dihydrofolate reductase, a potential target for anti-TB drug discovery. *Mol. Divers.* **2010**, *14*, 595–604.

80. Kumar, M.; Verma, S.; Sharma, S.; Srinivasan, A.; Singh, T. P.; Kaur, P. Structure-based in silico design of a high-affinity dipeptide inhibitor for novel protein drug target shikimate kinase of *Mycobacterium tuberculosis*. *Chem. Biol. Drug Des.* **2010**, *76*, 277–284.

81. White, E. L.; Ross, L. J.; Cunningham, A.; Escuyer, V. Cloning, expression, and characterization of *Mycobacterium tuberculosis* dihydrofolate reductase. *FEMS Microbiol. Lett.* **2004**, *232*, 101–105.

82. Parish, T.; Stoker, N. G. The common aromatic amino acid biosynthesis pathway is essential in *Mycobacterium tuberculosis*. *Microbiology (Reading, U.K.)* **2002**, *148*, 3069–3077.

83. Ciulli, A.; Abell, C. Fragment-based approaches to enzyme inhibition. *Curr. Opin. Biotechnol.* **2007**, *18*, 489–496.

84. Hung, A. W.; Silvestre, H. L.; Wen, S.; Ciulli, A.; Blundell, T. L.; Abell, C. Application of fragment growing and fragment linking to the discovery of inhibitors of *Mycobacterium tuberculosis* pantothenate synthetase. *Angew. Chem. Int. Ed. Engl.* **2009**, *48*, 8452–8456.

85. Schnackenberg, L. K.; Jones, R. C.; Thyparambil, S.; Taylor, J. T.; Han, T.; Tong, W.; Hansen, D. K.; Fuscoe, J. C.; Edmondson, R. D.; Beger, R. D.; Dragan, Y. P. An integrated study of acute effects of valproic acid in the liver using

metabonomics, proteomics, and transcriptomics platforms. *OMICS* **2006**, *10*, 1–14.

86. Chen, S. An "omics" approach to determine the mechanisms of acquired aromatase inhibitor resistance. *OMICS* **2011**, *15*, 347–352.

87. Debnath, M.; Pandey, M.; Bisen, P. S. An omics approach to understand the plant abiotic stress. *OMICS* **2011**, *15*, 739–762.

88. Biomarkers Definitions Working Group. Biomarkers and surrogate endpoints: Preferred definitions and conceptual framework. *Clin. Pharmacol. Ther.* **2001**, *69*, 89–95.

89. Parida, S. K.; Kaufmann, S. H. The quest for biomarkers in tuberculosis. *Drug Discovery Today* **2010**, *15*, 148–157.

90. Ryals, J. Metabolomics - An important emerging science. In *Drug Discovery: Business Briefing. PharmaTech 2004*, Boulton, E., Ed. Business Briefings Ltd: **2004**; pp 51–54.

91. du Preez, I.; Loots du, T. Altered fatty acid metabolism due to rifampicin-resistance conferring mutations in the rpoB Gene of *Mycobacterium tuberculosis*: mapping the potential of pharmaco-metabolomics for global health and personalized medicine. *OMICS* **2012**, *16*, 596–603.

92. Kohanski, M. A.; Dwyer, D. J.; Hayete, B.; Lawrence, C. A.; Collins, J. J. A common mechanism of cellular death induced by bactericidal antibiotics. *Cell* **2007**, *130*, 797–810.

93. Villemagne, B.; Crauste, C.; Flipo, M.; Baulard, A. R.; Deprez, B.; Willand, N. Tuberculosis: the drug development pipeline at a glance. *Eur. J. Med. Chem.* **2012**, *51*, 1–16.

94. Kohanski, M. A.; Dwyer, D. J.; Wierzbowski, J.; Cottarel, G.; Collins, J. J. Mistranslation of membrane proteins and two-component system activation trigger antibiotic-mediated cell death. *Cell* **2008**, *135*, 679–690.

95. Dwyer, D. J.; Kohanski, M. A.; Collins, J. J. Role of reactive oxygen species in antibiotic action and resistance. *Curr. Opin. Microbiol.* **2009**, *12*, 482–489.

96. Kohanski, M. A.; DePristo, M. A.; Collins, J. J. Sublethal antibiotic treatment leads to multidrug resistance via radical-induced mutagenesis. *Mol. Cell.* **2010**, *37*, 311–320.

97. Kohanski, M. A.; Dwyer, D. J.; Collins, J. J. How antibiotics kill bacteria: From targets to networks. *Nat. Rev. Microbiol.* **2010**, *8*, 423–435.

98. Foti, J. J.; Devadoss, B.; Winkler, J. A.; Collins, J. J.; Walker, G. C. Oxidation of the guanine nucleotide pool underlies cell death by bactericidal antibiotics. *Science* **2012**, *336*, 315–319.

99. Wright, G. D. The antibiotic resistome: The nexus of chemical and genetic diversity. *Nat. Rev. Microbiol.* **2007**, *5*, 175–186.

100. Liu, Y.; Imlay, J. A. Cell death from antibiotics without the involvement of reactive oxygen species. *Science* **2013**, *339*, 1210–1213.

101. Keren, I.; Wu, Y.; Inocencio, J.; Mulcahy, L. R.; Lewis, K. Killing by bactericidal antibiotics does not depend on reactive oxygen species. *Science* **2013**, *339*, 1213–1216.

102. Grumbach, F. Experimental antituberculous activity of certain isonicotinic thioamides substituted on the nucleus. *C. R. Hebd. Seances Acad. Sci.* **1956**, *242*, 2187–2189.

103. Wang, F.; Langley, R.; Gulten, G.; Dover, L. G.; Besra, G. S.; Jacobs, W. R., Jr.; Sacchettini, J. C. Mechanism of thioamide drug action against tuberculosis and leprosy. *J. Exp. Med.* **2007**, *204*, 73–78.

104. Nagarajan, K.; Shankar, R. G.; Rajappa, S.; Shenoy, S. J.; Costa-Pereira, R. Nitroimidazoles XXI 2,3-dihydro-6-nitroimidazo [2,1-*b*] oxazoles with antitubercular activity. *Eur. J. Med. Chem.* **1989**, *24*, 631–633.

105. Singh, R.; Manjunatha, U.; Boshoff, H. I. M.; Ha, Y. H.; Niyomrattanakit, P.; Ledwidge, R.; Dowd, C. S.; Lee, I. Y.; Kim, P.; Zhang, L.; Kang, S.; Keller, T. H.; Jiricek, J.; Barry, C. E. 3rd. PA-824 kills nonreplicating *Mycobacterium tuberculosis* by intracellular NO release. *Science* **2008**, *322*, 1392–1395.

106. Stover, C. K.; Warrener, P.; VanDevanter, D. R.; Sherman, D. R.; Arain, T. M.; Langhorne, M. H.; Anderson, S. W.; Towell, J. A.; Yuan, Y.; McMurray, D. N.; Krelswirth, B. N.; Barry, C. E. 3rd; Baker, W. R. A small-molecule nitroimidazopyran drug candidate for the treatment of tuberculosis. *Nature* **2000**, *405*, 962–966.

107. Anderson, R. F.; Shinde, S. S.; Maroz, A.; Boyd, M.; Palmer, B. D.; Denny, W. A. Intermediates in the reduction of the antituberculosis drug PA-824, (6S)-2-nitro-6-{[4-(trifluoromethoxy)benzyl]oxy}-6,7-dihydro-5H-imidazo[2,1-b][1, 3]oxazine, in aqueous solution. *Org. Biomol. Chem.* **2008**, *6*, 1973–1980.

108. E.; Daniels, L.; Dick, T.; Pang, S. S.; Barry, C. E., 3rd. Identification of a nitroimidazo-oxazine-specific protein involved in PA-824 resistance in *Mycobacterium tuberculosis*. *Proc. Natl. Acad. Sci. U.S.A.* **2006**, *103*, 431–436.

109. OPC-67683. *Tuberculosis (Edinb)* **2008**, *88*, 2.

110. Grosset, J. H.; Singer, T. G.; Bishai, W. R. New drugs for the treatment of tuberculosis: hope and reality. *Int. J. Tuberc. Lung Dis.* **2012**, *16*, 1005–1014.

111. Makarov, V.; Manina, G.; Mikusova, K.; Mollmann, U.; Ryabova, O.; Saint-Joanis, B.; Dhar, N.; Pasca, M. R.; Buroni, S.; Lucarelli, A. P.; Milano, A.; De Rossi, E.; Belanova, M.; Bobovska, A.; Dianiskova, P.; Kordulakova, J.; Sala, C.; Fullam, E.; Schneider, P.; McKinney, J. D.; Brodin, P.; Christophe, T.; Waddell, S.; Butcher, P.; Albrethsen, J.; Rosenkrands, I.; Brosch, R.; Nandi, V.; Bharath, S.; Gaonkar, S.; Shandil, R. K.; Balasubramanian, V.; Balganesh, T.; Tyagi, S.; Grosset, J.; Riccardi, G.; Cole, S. T. Benzothiazinones kill *Mycobacterium tuberculosis* by blocking arabinan synthesis. *Science* **2009**, *324*, 801–804.

112. Trefzer, C.; Rengifo-Gonzalez, M.; Hinner, M. J.; Schneider, P.; Makarov, V.; Cole, S. T.; Johnsson, K. Benzothiazinones: prodrugs that covalently modify the decaprenylphosphoryl-b-D-ribose 2'-epimerase DprE1 of *Mycobacterium tuberculosis*. *J. Am. Chem. Soc.* **2010**, *132*, 13663–13665.

113. Flynn, J. L. Lessons from experimental *Mycobacterium tuberculosis* infections. *Microbes Infect.* **2006**, *8*, 1179–1188.

114. Patel, K.; Jhamb, S. S.; Singh, P. P. Models of latent tuberculosis: Their salient features, limitations, and development. *J. Lab. Physicians* **2011**, *3*, 75–79

.

115. Kaushal, D.; Mehra, S.; Didier, P. J.; Lackner, A. A. The non-human primate model of tuberculosis. *J. Med. Primatol.* **2012**, *41*, 191–201.

116. Altaf, M.; Miller, C. H.; Bellows, D. S.; O'Toole, R. Evaluation of the *Mycobacterium smegmatis* and BCG models for the discovery of *Mycobacterium tuberculosis* inhibitors. *Tuberculosis (Edinb)* **2010**, *90*, 333–337.

117. Reyrat, J.-M.; Kahn, D. *Mycobacterium smegmatis*: An absurd model for tuberculosis? *Trends Microbiol.* **2001**, *9*, 472–473.

118. See also TIGR website: http://www.tigr.org

119. Barry, C. E. 3rd. *Mycobacterium smegmatis*: An absurd model for tuberculosis? A response. *Trends Microbiol.* **2001**, *9*, 473–474.

120. Beamer, G. L.; Turner, J. Murine models of susceptibility to tuberculosis. *Arch. Immunol. Ther. Exp. (Warsz)* **2005**, *53*, 469–483.

121. Lin, P. L.; Rodgers, M.; Smith, L.; Bigbee, M.; Myers, A.; Bigbee, C.; Chiosea, I.; Capuano, S. V.; Fuhrman, C.; Klein, E.; Flynn, J. L. Quantitative comparison of active and latent tuberculosis in the cynomolgus macaque model. *Infect. Immun.* **2009**, *77*, 4631–4642.

122. Hollingshead, M. G.; Alley, M. C.; Camalier, R. F.; Abbott, B. J.; Mayo, J. G.; Malspeis, L.; Grever, M. R. In vivo cultivation of tumor cells in hollow fibers. *Life Sci.* **1995**, *57*, 131–141.

123. Drusano, G. L.; Sgambati, N.; Eichas, A.; Brown, D.; Kulawy, R.; Louie, A. Effect of administration of moxifloxacin plus rifampin against *Mycobacterium tuberculosis* for 7 of 7 days versus 5 of 7 days in an in vitro pharmacodynamic system. *mBio* **2011**, *2*, e00108–e00111.

124. Wayne, L. G.; Hayes, L. G. An in vitro model for sequential study of shiftdown of *Mycobacterium tuberculosis* through two stages of nonreplicating persistance. *Infect. Immun.* **1996**, *64*, 2062–2069.

7.2 Chapter 2 References

1. Posey, J. E.; Gherardini, F. C. Lack of a role for iron in the lyme disease pathogen. *Science* **2000**, *288*, 1651–1653.

2. Aisen, P.; Leibman, A.; Zweier, J. Stoichiometric and site characteristics of the binding of iron to human transferring. *J. Biol. Chem.* **1978**, *253*, 1930–1937.

3. Ferreras, J. A.; Ryu, J. S.; Di Lello, F.; Tan, D. S., Quadri, L. E. Small-molecule inhibition of siderophore biosynthesis in *Mycobacterium tuberculosis* and *Yersinia pestis*. *Nat. Chem. Biol.* **2005**, *1*, 29–32.

4. Somu, R. V.; Boshoff, H.; Qiao, C.; Bennett, E. M.; Barry, C. E., 3rd; Aldrich, C. C. Rationally designed nucleoside antibiotics that inhibit siderophore biosynthesis of *Mycobacterium tuberculosis*. *J. Med. Chem.* **2006**, *49*, 31–34.

5. Quadri, L. E. Strategic paradigm shifts in the antimicrobial drug discovery process of the 21st century. *Infect. Disord. Drug Targets* **2007**, *7*, 230–237.

6. Miethke, M.; Marahiel, M. A., Siderophore-based iron acquisition and pathogen control. *Microbiol. Mol. Biol. Rev.* **2007**, *71*, 413–51.

7. Chavadi, S. S.; Stirrett, K. L.; Edupuganti, U. R.; Vergnolle, O.; Sadhanandan, G.; Marchiano, E.; Martin, C.; Qiu, W-G.; Soll, C. E.; Quadri, L. E. N. Mutational and phylogenetic analyses of the mycobacterial *mbt* gene cluster. *J. Bacteriol.* **2011***, 193*, 5905–5913.

8. De Voss, J. J.; Rutter, K.; Schroeder, B. G.; Su, H.; Zhu, Y.; Barry, C. E., 3rd. The salicylate-derived mycobactin siderophores of *Mycobacterium tuberculosis* are essential for growth in macrophages. *Proc. Natl. Acad. Sci. U.S.A*. **2000**, *97*, 1252–1257.

9. Timm, J.; Post, F. A.; Bekker, L. G.; Walther, G. B.; Wainwright, H. C.; Manganelli, R.; Chan, W. T.; Tsenova, L.; Gold, B.; Smith, L.; Kaplan, G.; McKinney, J. D. Differential expression of iron-, carbon-, and oxygen-responsive mycobacterial genes in the lungs of chronically infected mice and tuberculosis patients. *Proc. Natl. Acad. Sci. U.S.A*. **2003**, *100*, 14321–14326.

10. Quadri, L. E.; Sello, J.; Keating, T. A.; Weinreb, P. H.; Walsh, C. T. Identification of a *Mycobacterium tuberculosis* gene cluster encoding the biosynthetic enzymes for assembly of the virulence-conferring siderophore mycobactin. *Chem. Biol.* **1998**, *5*, 631–645.

11. Miethke, M.; Bisseret, P.; Beckering, C. L.; Vignard, D.; Eustache, J.; Marahiel, M. A. Inhibition of aryl acid adenylation domains involved in bacterial siderophore synthesis. *FEBS J.* **2006**, *273*, 409–419.

12. Somu, R. V.; Wilson, D. J.; Bennett, E. M.; Boshoff, H. I.; Celia, L.; Beck, B. J.; Barry, C. E. 3rd; Aldrich, C. C. Antitubercular nucleosides that inhibit siderophore biosynthesis: SAR of the glycosyl domain. *J. Med. Chem.* **2006**, *49*, 7623–7635.

13. Vannada, J.; Bennett, E. M.; Wilson, D. J.; Boshoff, H. I.; Barry, C. E. 3rd; Aldrich, C. C. Design, synthesis, and biological evaluation of beta-ketosulfonamide adenylation inhibitors as potential antitubercular agents. *Org. Lett.* **2006**, *8*, 4707–4710.

14. Qiao, C. H.; Gupte, A.; Boshoff, H. I.; Wilson, D. J.; Bennett, E. M.; Somu, R. V.; Barry, C. E., 3rd; Aldrich. C. C. 5'-*O*- [(*N*-Acyl)sulfamoyl]adenosines as antitubercular agents that inhibit MbtA: An adenylation enzyme required for siderophore biosynthesis of the mycobactins. *J. Med. Chem.* **2007**, *50*, 6080–6094.

15. Gupte, A.; Boshoff, H. I.; Wilson, D. J.; Neres, J.; Labello, N. P.; Somu, R. V.;

Xing, C.; Barry, C. E. 3rd; Aldrich, C. C. Inhibition of siderophore biosynthesis by 2-triazole substituted analogues of 5'-*O*-[*N*-(salicyl)sulfamoyl]adenosine: antibacterial nucleosides effective against *Mycobacterium tuberculosis*. *J. Med. Chem.* **2008**, *51*, 7495–7507.

16. Sikora, A. l.; Wilson, D. J.; Aldrich. C. C.; Blanchard, J. S. Kinetic and inhibition studies of dihydroxybenzoate-AMP ligase from *Escherichia coli*. *Biochemistry* **2010**, *49*, 3648–3657.

17. Lipinski, C. A.; Lombardo, F.; Dominy, B. W.; Feeney, P. J. Experimental and computational approaches to estimate solubility and permeability in drug discovery and development settings. *Ad. Drug Del. Rev.* **2001**, *46*, 3–26.

18. Leeson, P.D.; Davis, A. M. Time-related differences in the physical property profiles of oral drugs. *J. Med. Chem.* **2004**, *47*, 6338–6348.

19. O'Shea, R.; Moser, H.E. Physicochemical properties of antibacterial compounds: Implications for drug discovery. *J. Med. Chem.* **2008**, *51*, 2871–2878.

20. Bisseret, P.; Thielges, S.; Stephane, B.; Miethke, M.; Marahiel, M. A.; Eustache, J. Synthesis of a 2-indolylphosphonamide derivative with inhibitory activity against yersiniabactin biosynthesis. *Tetrahedron Lett.* **2007**, *48*, 6080–6083.

21. Qiao, C. H.; Wilson, D. J.; Bennett, E. M.; Aldrich, C. C. A mechanism-based aryl carrier protein/thiolation domain affinity probe. *J. Am. Chem. Soc.* **2007**, *129*, 6350–6351.

22. Neres, J.; Labello, N. P.; Somu, R. V.; Boshoff, H. I.; Wilson D. J.; Vannada, J.; Chen, L.; Barry, C. E. 3rd; Bennett, E. M.; Aldrich, C. C. Inhibition of siderophore biosynthesis in *Mycobacterium tuberculosis* with nucleoside bisubstrate analogues: Structure activity relationships of the nucleobase domain of 5'-*O*-[*N*-(salicyl)sulfamoyl]adenosine. *J. Med. Chem.* **2008**, *51*, 5349–5370.

23. Labello, N. P; Bennett, E. M.; Ferguson, D. M.; Aldrich, C. C. Quantitative three dimensional structure linear interaction energy model of 5'-*O*-[*N*-(salicyl)sulfamoyl]adenosine and the aryl acid adenylating enzyme MbtA. *J. Med. Chem.* **2008**, *51*, 7154–7160.

24. Maryanoff, B. E.; Costanzo, M. J.; Nortey, S. O.; Greco, M. N.; Shank, R. P.; Schupsky, J. J.; Ortegon, M. P.; Vaught, J. L. Structure-activity studies on anticonvulsant sugar sulfamates related to topiramate. Enhanced potency with cyclic sulfate derivatives. *J. Med. Chem.* **1998**, *41*, 1315–1343.

25. Black. F. J.; Kocienski, P. J. Synthesis of phalluside-1 and sch II using 1,2-metallate rearrangements. *Org. Biomol. Chem.* **2010**, *8*, 1188–1193.

26. Lu, X.; Zhang, H.; Tonge, P. J.; Tan, D. S. Mechanism-based inhibitors of MenE, an acyl-CoA synthetase involved in bacterial menaquinone biosynthesis. *Bioorg. Med. Chem. Lett.* **2008**, *18*, 5963–5966.

27. Matsuda, A.; Shinozaki, M.; Yamaguchi, T.; Homma, H.; Nomoto, R.; Miyaska, T.; Watanabe, Y.; Abiru, T. Nucleosides and nucleotides. 103. 2-Alkynyladenosines: A novel class of selective adenosine A_2 receptor agonists with potent antihypertensive effects. *J. Med. Chem.* **1992**, *35*, 241–252.

28. Beaumont, K.; Webster, R.; Gardner, I.; Dack, K. Design of ester prodrugs to enhance oral absorption of poorly permeable compounds: Challenges to the discovery scientist. *Curr. Drug Metab.* **2003**, *4*, 461–485.

29. Belanger, P. M.; Lalande, M.; Dore, F. M.; Labrecque, G. Temporal variations in the pharmacokinetics of isoniazid and *N*-acetylisoniazid in rats. *Drug. Metab. Dispos.* **1989**, *17*, 91–97.

30. Isoniazid. *Tuberculosis* **2008**, *88*, 112–116.

31. Ng, K-y.; Zhou, H.; Zhang, Y. L.; Hybertson, B.; Randolph, T.; Christians, U. Quantification of isoniazid and acetylisoniazid in rat plasma and alveolar macrophages by liquid chromatography-tandem mass spectrometry with on-line extraction. *J. Chromatogr. B* **2007**, *847*, 188–198.

32. Baldan, H. M.; De Rosa, H. J.; Brunetti, I. L.; Ximenes, V. F.; Machado, R. G. P. The effect of rifampicin and pyrazinamide on isoniazid pharmacokinetics in rats. *Biopharm. Drug Dispos.* **2007**, *28*, 409–413.

33. Zhou, H.; Zhang, Y.; Biggs, D. L.; Manning, M. C.; Randolph, T. W.; Christians, U.; Hybertson, B. M.; Ng, K-y. Microparticle-based lung delivery of INH decreases INH metabolism and targets alveolar macrophages. *J. Control. Release* **2005**, *107*, 288–299.

34. Palm, K.; Stenber, P.; Luthman, K.; Artursson, P. Polar molecular surface properties predict the intestinal absorption of drugs in humans. *Pharm. Res.* **1997**, *14*, 568–571.

35. Clark, D. E. Rapid calculation of polar molecular surface area and its application to the prediction of transport phenomena. 1. Prediction of intestinal absorption. *J. Pharm. Sci.* **1999**, *88*, 807–814.

36. Navia, M. A.; Chaturvedi, P.R. Design principles for orally bioavailable drugs. *Drug Discovery Today* **1996**, *1*, 179–189.

37. Smith, A. B. III; Hirschmann, R.; Pasternak, A.; Yao, W.; Sprengler, P. A.; Halloway, M. K.; Kuo, L. C.; Chen, Z.; Darke, P. L.; Schleif, W. A. An orally bioavailable pyrrolinone inhibitor of HIV-1 protease: Computation analysis and X-ray crystal structure of the enzyme complex. *J. Med. Chem.* **1997**, *40*, 2440–2444.

38. Veber, D. F.; Johnson, S. R.; Cheng, H-Y.; Smith, B. R.; Ward, K. W.; Kopple, K. D. Molecular properties that influence the oral bioavailability of drug candidates. *J. Med. Chem.* **2002**, *45*, 2615–2623.

39. Schulzke, J. D.; Ploeger, S.; Amasheh, M.; Fromm, A.; Zeissig, S.; Troeger, H.; Richter, J.; Bojarski, C.; Schumann, M.; Fromm, M. Epithelial tight junctions in intestinal inflammation. *Ann. N. Y. Acad. Sci.* **2009**, *1165*, 294–300.

40. Ponferrada, Á.; Caso, J. R.; Alou, L.; Colón, A.; Sevillano, D.; Moro, M. A.; Lizasoain, I.; Menchén, P.; Gómez-Lus, M.; Lorenzo, P.; Cos, E.; Leza, J. C.; Menchén, L. The role of PPARγ on restoration of colonic homeostasis after experimental stress-induced inflammation and dysfunction. *Gastroenterology* **2007**, *132*, 1791–1803.

41. Balimane, P. V.; Sinko, P. J. Involvement of multiple transporters in the oral absorption of nucleoside analogues. *Adv. Drug Deliv. Rev.* **1999**, *39*, 183–209.

42. Li, F.; Maag, H.; Alfredson, T. Prodrugs of nucleoside analogues for improved oral absorption and tissue targeting. *J. Pharm. Sci.* **2008**, *97*, 1109–1134.

43. Strickley, R. G. Solubilizing excipients in oral and injectable formulations. *Pharm. Res.* **2004**, *21*, 201–230.

44. Heacock, D.; Forsyth, C. J.; Shiba, K.; Musier-Forsyth, K. Synthesis and aminoacyl-tRNA synthetase inhibitory activity of prolyl adenylate analogs. *Bioorg. Chem.* **1996**, *24*, 273–289.

45. Smit, C.; Blümer, J.; Eerland, M. F.; Albers, M. F.; Müller, M. P.; Goody, R. S.; Itzen, A.; Hedber, C. Efficient synthesis and applications of peptides containing adenylylated tyrosine residues. *Angew. Chem. Int. Ed.* **2011**, *50*, 9200–9204.

46. Ikeuchi, H.; Meyer, M. E.; Ding, Y.; Hiratake, J.; Richards, N. G. A critical electrostatic interaction mediates inhibitor recognition by human asparagine synthetase. *Bioorg. Med. Chem.* **2009**, *17*, 6641–6650.

47. Kurokawa, T.; Kim, M.; Du Bois, J. Synthesis of 1,3-diamines through rhodium-catalyzed C–H insertion. *Angew. Chem. Int. Ed.* **2009**, *48*, 2777–2779.

48. US Pharmacopeia Test Solution for Simulated Gastric Fluid. http://www.pharmacopeia.cn/v29240/usp29nf24s0_ris1s126.html.

7.3 Chapter 3 References

1. Yuan, L.; Lin, W.; Zheng, K.; Zhu, S. FRET-based small-molecule fluorescent probes: Rational design and bioimaging applications. *Acc. Chem. Res.* **2013**, *ASAP*.

2. Haedke, U.; Küttler, E. V.; Vosyka, O.; Yang, Y.; Verhelst, S. H. L. Tuning probe selectivity for chemical proteomics applications. *Curr. Opin. Chem. Biol.* **2013**, *17*, 102–109.

3. Bunnage, M. E.; Piatnitski Chekler, E. L.; Jones, L. H. Target validation using chemical probes. *Nat. Chem. Biol.* **2013**, *9*, 195–199.

4. Workman, P.; Collins, I. Probing the probes: Fitness factors for small molecule tools. *Chem. Biol.* **2010**, *17*, 561–577.

5. Cohen, P. Guidelines for the effective use of chemical inhibitors of protein function to understand their roles in cell regulation. *Biochem J.* **2010**, *425*, 53–54.

6. Frye, S. V. The art of the chemical probe. *Nat. Chem. Bio.* **2010**, *6*, 159–161.

7. Ferreras, J. A.; Ryu, J. S.; Di Lello, F.; Tan, D. S., Quadri, L. E. Small-molecule inhibition of siderophore biosynthesis in *Mycobacterium tuberculosis* and *Yersinia pestis*. *Nat. Chem. Biol.* **2005**, *1*, 29–32.

8. Somu, R. V.; Boshoff, H.; Qiao, C.; Bennett, E. M.; Barry, C. E., 3rd; Aldrich, C. C. Rationally designed nucleoside antibiotics that inhibit siderophore biosynthesis of *Mycobacterium tuberculosis*. *J. Med. Chem.* **2006**, *49*, 31–34.

9. Quadri, L. E. Strategic paradigm shifts in the antimicrobial drug discovery process of the 21st century. *Infect. Disord. Drug Targets* **2007**, *7*, 230–237.

10. Crosa, J. H.; Walsh, C. T. Genetics and assembly line enzymology of siderophore biosynthesis in bacteria. *Microbiol. Mol. Biol. Rev.* **2002**, *66*, 223–249.

11. Miethke, M.; Marahiel, M. A. Siderophore-based iron acquisition and pathogen

control. *Microbiol. Mol. Biol. Rev.* **2007**, *71*, 413–451.

12. Siegrist, M. S.; Unnikrishnan, M.; McConnell, M. J.; Borowsky, M.; Cheng, T. Y.; Siddiqi, N.; Fortune, S. M.; Moody D. B.; Rubin, E. J. Mycobacterial Esx-3 is required for mycobactin-mediated iron acquisition. *Proc. Natl. Acad. Sci. U.S.A.* **2009**, *106*, 18792–18797.

13. De Voss, J. J.; Rutter, K.; Schroeder, B. G.; Su, H.; Zhu, Y.; Barry, C. E., 3rd. The salicylate-derived mycobactin siderophores of *Mycobacterium tuberculosis* are essential for growth in macrophages. *Proc. Natl. Acad. Sci. U.S.A*. **2000**, *97*, 1252–1257.

14. Timm, J.; Post, F. A.; Bekker, L. G.; Walther, G. B.; Wainwright, H. C.; Manganelli, R.; Chan, W. T.; Tsenova, L.; Gold, B.; Smith, L.; Kaplan, G.; McKinney, J. D. Differential expression of iron-, carbon-, and oxygen-responsive mycobacterial genes in the lungs of chronically infected mice and tuberculosis patients. *Proc. Natl. Acad. Sci. U.S.A*. **2003**, *100*, 14321–14326.

15. Somu, R. V.; Wilson, D. J.; Bennett, E. M.; Boshoff, H. I.; Celia, L.; Beck, B. J.; Barry, C. E., 3rd, Aldrich, C. C. Antitubercular nucleosides that inhibit siderophore biosynthesis: SAR of the glycosyl domain. *J. Med. Chem.* **2006**, *49*, 7623–7635.

16. Miethke, M.; Bisseret, P.; Beckering, C. L.; Vignard, D.; Eustache, J.; Marahiel, M. A. Inhibition of aryl acid adenylation domains involved in bacterial siderophore synthesis. *FEBS J.* **2006**, *273*, 409–419.

17. Vannada, J.; Bennett, E. M.; Wilson, D. J.; Boshoff, H. I.; Barry, C. E. 3rd; Aldrich, C. C. Design, synthesis, and biological evaluation of beta-ketosulfonamide adenylation inhibitors as potential antitubercular agents. *Org. Lett.* **2006**, *8*, 4707–4710.

18. Duckworth, B. P.; Nelson, K. M.; Aldrich, C. C. Adneylating enzymes in *Mycobacterium tuberculosis* as drug targets. *Curr. Top. Med. Chem.* **2012**, *12*, 766–796.

19. Liu, Y.; Shreder, K. R.; Gai, W.; Corral, S.; Ferris, D. K.; Rosenblum, J. S. Wortmannin, a widely used phosphoinositide 3-kinase inhibitor, also potently inhibits mammalian polo-like kinase. *Chem. Biol.* **2005**, *12*, 99–107.

20. MacKinnon, A. L.; Garrison, J. L.; Hegde, R. S.; Tauton, J. Photo-leucine incorporation reveals the target of a cyclodepsipeptide inhibitor of cotranslational translocation. *J. Am. Chem. Soc.* **2007**, *129*, 14560–14561.

21. Puri, A. W., Bogyo, M. Using small molecules to dissect mechanisms of microbial

pathogenesis. *ACS Chem. Biol.* **2009**, *4*, 603–616.

22. Eirich, J.; Orth, R.; Sieber, S. A. Unraveling the protein targets of vancomycin in living *S. aureus* and *E. faecalis* cells. *J. Am. Chem. Soc.* **2011**, *133*, 12144–12153.

23. Duckworth, B. P.; Wilson, D. J.; Nelson, K. M.; Boshoff, H. I.; Barry, C. E. 3rd; Aldrich, C. C. Development of a selective activity-based probe for adenylating enzymes: Profiling MbtA involved in siderophore biosynthesis from *Mycobacterium tuberculosis*. *ACS Chem. Biol.* **2012**, *7*, 1653–1658.

24. Neres, J.; Labello, N. P.; Somu, R. V.; Boshoff, H. I.; Wilson, D. J.; Vannada, J.; Chen, L.; Barry, C. E. 3rd; Bennett, E. M.; Aldrich, C. C. Inhibition of siderophore biosynthesis in *Mycobacterium tuberculosis* with nucleoside bisubstrate analogues: Structure activity relationships of the nucleobase domain of 5′-*O*-[*N*-(salicyl)sulfamoyl]-adenosine. *J. Med. Chem.* **2008**, *51*, 5349–5370.

25. Saghatelian, A.; Jessani, N.; Joseph, A.; Humphrey, M.; Cravatt, B. F. Activity-based probes for the proteomic profiling of metalloproteases. *Proc. Natl. Acad. Sci. U.S.A.* **2004**, *101*, 10000–10005.

26. Leslie, B. J.; Hergenrother, P. J. Identification of the cellular targets of bioactive small organic molecules using affinity reagents. *Chem. Soc. Rev.* **2008**, *37*, 1347–1360.

27. Geurink, P. P.; Prely, L. M.; van der Marel, G. A.; Bischoff, R.; Overkleeft, H. S. Photoaffinity labeling in activity-based protein profiling. *Top. Curr. Chem.* **2012**, *324*, 85–113.

28. Speers, A. E.; Cravatt, B. F. Profiling enzyme activities in vivo using click chemistry methods. *Chem. Biol.* **2004**, *11*, 535–546.

29. Dunetz, J. R.; Danheiser, R. L. Synthesis of highly substituted indolines and indoles via intramolecular [4 + 2] cycloaddition of ynamides and conjugated enynes. *J. Am. Chem. Soc.* **2005**, *127*, 5776–5777.

30. Sikora, A. L.; Wilson, D. J.; Aldrich, C. C.; Blanchard, J. S. Kinetic and inhibition studies of dihydroxybenoate-AMP ligase from *Escherichia coli*. *Biochemistry* **2010**, *49*, 3648–3657.

31. Weerapana, E.; Speers, A. E.; Cravatt, B. F. Tandem orthogonal proteolysis-activity-based protein profiling (TOP-ABPP)–A general method for mapping sites of probe modification in proteomes. *Nat. Protoc.* **2007**, *2*, 1414–1425.

32. Jones, C. M.; Niederweis, M. *Mycobacterium tuberculosis* can utilize heme as an

iron source. *J. Bacteriol.* **2011**, *193*, 1767–1770.

33. Tullius, M. V.; Harmston, C. A.; Owens, C. P.; Chim, N.; Morse, R. P.; McMath, L. M.; Iniguez, A.; Kimmey, J. M.; Sawaya, M. R.; Whitelegge, J. P.; Horwitz, M. A.; Goulding, C. W. Discovery and characterization of a unique mycobacterial heme acquisition system. *Proc. Natl. Acad. Sci. U.S.A.* **2011**, *108*, 5051–5056.

34. Wells, R. M.; Jones, C. M.; Xi, Z.; Speer, A.; Danilchanka, O.; Doornbos, K. S.; Sun, P.; Wu, F.; Tian, C.; Niederweis, M. Discovery of a siderophore export system essential for virulence of *Mycobacterium tuberculosis*. *PLoS Pathog.* **2013**, *9*, e1003120.

35. Heacock, D.; Forsyth, C. J.; Shiba, K.; Musier-Forsyth, K. Synthesis and aminoacyl-tRNA synthetase inhibitory activity of prolyl adenylate analogs. *Bioorg. Chem.* **1996**, *24*, 273–289.

7.4 Chapter 4 References

1. Schatz, A.; Bugie, E.; Waksman, S. Streptomycin, a substance exhibiting antibiotic activity against Gram-positive and Gram-negative bacteria. *Proc. Soc. Exp. Biol. Med.* **1944**, *55*, 66–69.

2. Aldrich, C. C.; Boshoff, H. I.; Remmel, R. P. Antitubercular Agents. In *Burger's Medicinal Chemistry, Drug Discovery and Development, 7th Edition*, Abraham, D. J.; Rotella, D. P., Eds. John Wiley and Sons, Inc.: **2010**; pp 713–813.

3. Umezawa, H.; Ueda, M.; Maeda, K.; Yagishita, K.; Kondo, S.; Okami, Y.; Utahara, R.; Osato, Y.; Nitta, K.; Takeuchi, T. Production and isolation of a new antibiotic: Kanamycin. *J. Antibiot.* **1957**, *10*, 181–188.

4. Kawaguchi, H. Discovery, chemistry, and activity of amikacin. *J. Infect. Dis.* **1976**, *134(Suppl)*, S242–S248.

5. Rifampin. *Tuberculosis (Edinb)* **2008**, *88*, 151–154.

6. Mukai, A.; Fukai, T.; Matsumoto, Y.; Ishikawa, J.; Hoshino, Y.; Yazawa, K.; Harada, K.-i.; Mikami, Y., Transvalencin Z, a new antimicrobial compound with salicylic acid residue from *Nocardia transvalensis* IFM 10065. *J. Antibiot.* **2006**, *59*, 366–369.

7. Miethke, M.; Marahiel, M. A. Siderophore-based iron acquisition and pathogen

control. *Microbiol. Mol. Biol. Rev.* **2007**, *71*, 413–51.

8. Snow, G. A. Mycobactins: Iron-chelating growth factors from mycobacteria. *Bacteriol. Rev.* **1970**, *34*, 99–125.

9. Posey, J. E.; Gherardini, F. C. Lack of a role in the lyme disease pathogen. *Science* **2000**, *288*, 1651–1653.

10. Ratledge, C.; Dover, L. G. Iron metabolism in pathogenic bacteria. *Annu. Rev. Microbiol.* **2000**, *54*, 881–941.

11. Chavadi, S. S.; Stirrett, K. L.; Edupuganti, U. R.; Vergnolle, O.; Sadhanandan, G.; Marchiano, E.; Martin, C.; Qiu, W-G.; Soll, C. E.; Quadri, L. E. N. Mutational and phylogenetic analyses of the mycobacterial *mbt* gene cluster. *J. Bacteriol.* **2011***, 193*, 5905–5913.

12. Vergne, A. F.; Walz, A. J.; Miller, M. J. Iron chelators from mycobacteria (1954–1999) and potential therapeutic applications. *Nat. Prod. Rep.* **2000**, *17*, 99–116.

13. Hu, J.; Miller, M. J. Total Synthesis of a mycobactin S, a siderophore and growth promoter of *Mycobacterium smegmatis*, and determination of its growth inhibitory activity against *Mycobacterium tuberculosis*. *J. Am. Chem. Soc.* **1997**, *119*, 3462–3468.

14. Xu, Y.; Miller, M. J. Total syntheses of mycobactin analogues as potent antimycobacterial agents using a minimal protecting group strategy. *J. Org. Chem.* **1998**, *63*, 4314–4322.

15. Ferreras J. A.; Ryu J. S.; Di Lello F.; Tan D. S.; Quadri L. E. Small-molecule inhibition of siderophore biosynthesis in *Mycobacterium tuberculosis* and *Yersinia pestis*. *Nat. Chem. Biol.* **2005**, *1*, 26–32.

16. Stirrett, K. L.; Ferreras, J. A.; Jayaprakash, V.; Sinha, B. N.; Ren, T.; Quadri, L. E. N. Small molecules with structural similarities to siderophores as novel antimicrobials against *Mycobacterium tuberculosis* and *Yersinia pestis*. *Bioorg. Med. Chem. Lett.* **2008**, *18*, 2662–2668.

17. Tse, B.; Kishi, Y. Conformationally rigid tricyclic tripods: Synthesis and application to preparation of enterobactin analogs. *J. Org. Chem.* **1994**, *59*, 7807–7814.

18. Sakakura, A.; Kondo, R.; Umemura, S.; Ishihara, K. Dehydrative cyclization of serine, threonine, and cysteine residues catalyzed by molybdenum(VI) oxo compounds. *Tetrahedron* **2009**, *65*, 2102–2109.

19. Sattely, E. S.; Walsh, C. T. A latent oxazoline electrophile for N-O-C bond formation in pseudomonine biosynthesis. *J. Am. Chem. Soc.* **2008**, *130*, 12282–12284.

20. Wuest, W. M.; Sattely, E. S.; Walsh, C. T. Three siderophores from one bacterial enzymatic assembly line. *J. Am. Chem. Soc.* **2009**, *131*, 5056–5057.

21. Yamamoto, S.; Okujo, N.; Sakakibara, Y. Isolation and structure elucidation of acinetobactin, a novel siderophore from *Acinetobacter baumannii*. *Arch. Microbiol.* **1994**, *162*, 249–254.

22. Hughes, R. M.; Waters, M. L. Effects of lysine acetylation in a β-hairpin peptide: Comparison of an amide-π and a cation-π interaction. *J. Am. Chem. Soc.* **2006**, *128*, 13586–13591.

23. The reported conditions require overnight heating and a large excess (14 equivalents) of formic acid, however transformation was achieved in 3 hours at room temperature using only 7 equivalents of formic acid.

24. Wuts, P. G. M.; Greene, T. W. *Greene's Protecting Groups in Organic Synthesis*. 4th ed.; John Wiley & Sons, Inc.: Hoboken, NJ, 2007.

25. Li, H.; Jiang, X.; Ye, Y.-h.; Fan, C.; Romoff, T.; Goodman, M. 3-(Diethoxyphosphoryloxy)-1,2,3-benzotriazin-4(3*H*)-one (DEPBT): A new coupling reagent with remarkable resistance to racemization. *Org. Lett.* **1999**, *1*, 91–93

.

26. Field, L. D.; Sternhell, S.; Kalman, J. R. *Organic Structures From Spectra*. 4th Edition ed.; John Wiley & Sons Ltd: West Sussex, England, 2008.

27. Schneider, K.; Rose, I.; Vikineswary, S.; Jones, A. L.; Goodfellow, M.; Nicholson, G.; Beil, W.; Süssmuch, R. D.; Fiedler, H.-P. Nocardichelins A and B, siderophores from *Nocardia* strain acta 3026. *J. Nat. Prod.* **2007**, *70*, 932–935.

28. Young, D. C.; Kasmar, A.; Moraski, G.; Cheng, T. Y.; Walz, A. J.; Hu, J.; Xu, Y.; Endres, G. W.; Uzieblo, A.; Zajonc, D.; Costello, C. E.; Miller, M. J.; Moody, D. B. Synthesis of dideoxymycobactin antigens presented by CD1a reveals T cell fine specificity for natural lipopeptide structures. *J. Biol. Chem.* **2009**, *284*, 25087–25096.

29. Mitchell, J. M.; Shaw, J. T. Synthesis and stereochemical assignment of brasilibactin A. *Org. Lett.* **2007**, *9*, 1679–1681.

30. Fennell, K. A.; Möllmann, U.; Miller, M. J. Syntheses and biological activity of

amamistatin B and analogs. *J. Org. Chem.* **2008**, *73*, 1018–1024.

31. Hoshino, Y.; Mukai, A.; Yazawa, K.; Uno, J.; Ando, A.; Mikami, Y.; Fukai, T.; Ishikawa, J.; Yamaguchi, K. Transvalencin A, a thiazolidine zinc complex antibiotic produced by a clinical isolate of *Nocardia transvalensis* II. Structure elucidation. *J. Antibiot.* **2004**, *57*, 803–807.

32. Williams, K. J.; Boshoff, H. I.; Krishnan, N.; Gonzales, J.; Schnappinger, D.; Robertson, B. D. The *Mycobacterium tuberculosis* β-oxidation genes echA5 and fadB3 are dispensable for growth in vitro and in vivo. *Tuberculosis (Edinb)* **2011**, *91*, 549–555.

33. Mosmann, T. Rapid colorimetric assay for cellular growth and survival: Application to proliferation and cytotoxicity assays. *J. Immunol. Methods* **1983**, *65*, 55–63.

34. Denizot, F.; Lang, R. Rapid colorimetric assay for cell growth and survival: Modifications to the tetrazolium dye procedure giving improved sensitivity and reliability. *J. Immunol. Methods* **1986**, *89*, 271–277.

7.5 Chapter 5 References

1. Cane, D. E.; Walsh, C. T.; Khosla, C. Harnessing the biosynthetic code: Combinations, permutations, and mutations. *Science* **1998**, *282*, 63–68.

2. Clardy, J.; Walsh, C. T. Lessons from natural molecules. *Nature* **2004**, *432*, 829–837.

3. Fischbach, M. A.; Walsh, C. T. Assembly-line enzymology for polyketide and nonribosomal peptide antibiotics: Logic, machinery, and mechanisms. *Chem. Rev.* **2006**, *106*, 3468–3496.

4. Sieber, S. A.; Marahiel, M. A. Molecular mechanisms underlying nonribosomal peptide synthesis: Approaches to new antibiotics. *Chem. Rev.* **2005**, *105*, 715–738.

5. May, J. J.; Kessler, N.; Marahiel, M. A.; Stubbs, M. T. Crystal structure of DhbE, an archetype for aryl acid activating domains of modular nonribosomal peptide synthetases. *Proc. Natl. Acad. Sci. U.S.A.* **2002**, *99*, 12120–12125.

6. Gulick, A. M. Conformational dynamics in the acyl-CoA synthetases, adenylation domains of non-ribosomal peptide synthetases, and firefly luciferase. *ACS Chem. Biol.* **2009**, *4*, 811–827.

7. Challis, G. L.; Ravel, J.; Townsend, C. A. Predictive, structure-based model of amino acid recognition by nonribosomal peptide synthetase adenylation domains. *Chem. Biol.* **2000**, *7*, 211–224.

8. Stachelhous, T.; Mootz, H. D.; Marahiel, M. A. The specificity-conferring code of adenylation domains in nonribosomal peptide synthetases. *Chem. Biol.* **1999**, *6*, 493–505.

9. von Döhren, H.; Dieckmann, R.; Pavela-Vrancic, M. The nonribosomal code. *Chem. Biol.* **1999**, *6*, R273–R279.

10. Sikora, A. L.; Wilson, D. J.; Aldrich, C. C.; Blanchard, J. S. Kinetic inhibition studies of dihydroxybenzoate-AMP ligase from *Escherichia coli*. *Biochemistry* **2010**, *49*, 3648–3657.

11. Fischbach, M. A.; Lai, J. R.; Roche, E. D.; Walsh, C. T.; Liu, D. R. Directed evolution can rapidly improve the activity of chimeric assembly-line enzymes. *Proc. Natl. Acad. Sci. U.S.A.* **2007**, *104*, 11951–11956.

12. Robbel, L.; Marahiel, M. A. Daptomycin, a bacterial lipopeptide synthesized by a nonribosomal machinery. *J. Biol. Chem.* **2010**, *285*, 27501–27508.

13. Chen, C. Y.; Georgiev, I.; Anderson, A. C.; Donald, B. R. Computational structure-based redesign of enzyme activity. *Proc. Natl. Acad. Sci. U.S.A.* **2009**, *106*, 3764–3769.

14. Thirlway, J.; Lewis, R.; Nunns, L.; Al Nakeeb, M.; Styles, M.; Struck, A. W.; Smith, C. P.; Micklefield, J. Introduction of a non-natural amino acid into a nonribosomal peptide antibiotic by modification of adenylation domain specificity. *Angew. Chem. Int. Ed.* **2012**, *51*, 7181–7184.

15. Miethke, M.; Bisseret, P.; Beckering, C. L.; Vignard, D.; Eustache, J.; Marahiel, M. A. Inhibition of aryl acid adenylation domains involved in bacterial siderophore synthesis. *FEBS J.* **2006**, *273*, 409–419.

16. Neres, J.; Labello, N. P.; Somu, R. V.; Boshoff, H. I.; Wilson, D. J.; Vannada, J.; Chen, L.; Barry, C. E. 3rd; Bennett, E. M.; Aldrich, C. C. Inhibition of siderophore biosynthesis in *Mycobacterium tuberculosis* with nucleoside bisubstrate analogues: Structure activity relationships of the nucleobase domain of 5′-*O*-[*N*-(salicyl)sulfamoyl]-adenosine. *J. Med. Chem.* **2008**, *51*, 5349–5370.

17. Chao, G.; Lau, W. L.; Hackel, B. J.; Sazinsky, S. L.; Lippow, S. M.; Wittrup, K. D. Isolating and engineering human antibodies using yeast surface display. *Nat.*

Protoc. **2006**, *1*, 755–768.

18. Miller, K. D.; Pefaur, N. B.; Baird, C. L. Construction and screening of antigen targeted immune yeast surface display antibody libraries. *Curr. Protoc. Cytom.* **2008**, *4*, Unit 4.7.

19. Zhang, K.; Nelson, K. M.; Bhuripanyo, K.; Grimes, K. D.; Zhao, B.; Aldrich, C. C.; Yin, J. Engineering the substrate specificity of the DhbE adenylation domain by yeast cell surface display. *Chem. Biol.* **2013**, *20*, 92–101.

20. Baca, M.; Scanlan, T. S.; Stephenson, R. C.; Wells J. A. Phage display of a catalytic antibody to optimize affinity for transition-state analog binding. *Proc. Natl. Acad. Sci. U.S.A* **1997**, *94*, 10063–10068.

21. Ames, B. D.; Walsh, C. T. Anthranilate-activating modules from fungal nonribosomal peptide assembly lines. *Biochemistry* **2010**, *49*, 3351–3365.

22. Eppelmann, K.; Stachelhous, T.; Marahiel, M. A. Exploitation of the selectivity-conferring code of nonribosomal peptide synthetases for the rational design of novel peptide antibiotics. *Biochemistry* **2002**, *41*, 9718–9726.

23. Heacock, D.; Forsyth, C. J.; Shiba, K.; Musier-Forsyth, K. Synthesis and aminoacyl-tRNA synthetase inhibitory activity of prolyl adenylate analogs. *Bioorg. Chem.* **1996**, *24*, 273–289.

24. Grimes, K. D.; Aldrich, C. C. A high-throughput screening fluorescence polarization assay for fatty acid adenylating enzymes in *Mycobacterium tuberculosis*. *Anal. Biochem.* **2011**, *417*, 264–273.

25. Winkle, M. R.; Ronald, R. C. Regioselective metalation reactions of some substituted (methoxymethoxy)arenes. *J. Org. Chem.* **1982**, *47*, 2101–2108.